



Terms and Conditions of Use of Digitised Theses from Trinity College Library Dublin

Copyright statement

All material supplied by Trinity College Library is protected by copyright (under the Copyright and Related Rights Act, 2000 as amended) and other relevant Intellectual Property Rights. By accessing and using a Digitised Thesis from Trinity College Library you acknowledge that all Intellectual Property Rights in any Works supplied are the sole and exclusive property of the copyright and/or other IPR holder. Specific copyright holders may not be explicitly identified. Use of materials from other sources within a thesis should not be construed as a claim over them.

A non-exclusive, non-transferable licence is hereby granted to those using or reproducing, in whole or in part, the material for valid purposes, providing the copyright owners are acknowledged using the normal conventions. Where specific permission to use material is required, this is identified and such permission must be sought from the copyright holder or agency cited.

Liability statement

By using a Digitised Thesis, I accept that Trinity College Dublin bears no legal responsibility for the accuracy, legality or comprehensiveness of materials contained within the thesis, and that Trinity College Dublin accepts no liability for indirect, consequential, or incidental, damages or losses arising from use of the thesis for whatever reason. Information located in a thesis may be subject to specific use constraints, details of which may not be explicitly described. It is the responsibility of potential and actual users to be aware of such constraints and to abide by them. By making use of material from a digitised thesis, you accept these copyright and disclaimer provisions. Where it is brought to the attention of Trinity College Library that there may be a breach of copyright or other restraint, it is the policy to withdraw or take down access to a thesis while the issue is being resolved.

Access Agreement

By using a Digitised Thesis from Trinity College Library you are bound by the following Terms & Conditions. Please read them carefully.

I have read and I understand the following statement: All material supplied via a Digitised Thesis from Trinity College Library is protected by copyright and other intellectual property rights, and duplication or sale of all or part of any of a thesis is not permitted, except that material may be duplicated by you for your research use or for educational purposes in electronic or print form providing the copyright owners are acknowledged using the normal conventions. You must obtain permission for any other use. Electronic or print copies may not be offered, whether for sale or otherwise to anyone. This copy has been supplied on the understanding that it is copyright material and that no quotation from the thesis may be published without proper acknowledgement.

Early and Late Transition Metal Complexes Incorporating *p*-Block Oxo-Anions.

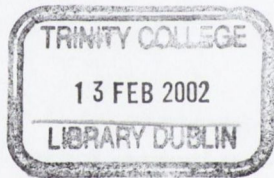
Robert P. Doyle
B.A(Mod), P.Grad.Dip (Stat.)

**A thesis submitted for the Degree
of Doctor of Philosophy.**



**Department Of Chemistry,
University of Dublin,**

2001

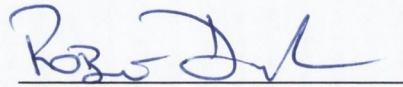


THESIS 6560



Declaration

This thesis has not been submitted as an exercise for a degree at any other University. Except where otherwise indicated, the work described herein has been carried out by the author alone. I, the undersigned, do always give permission to the libraries of the University of Dublin, Trinity College, to lend or copy this work upon request.



**To my Parents,
Paul and Catherine.**

Acknowledgements

I would like to express my sincerest gratitude to Dr. Paul Kruger, for his supervision, friendship and constant encouragement. This thesis is a result of his faith. I would like to especially mention also, Dr Mark (Woody) Nieuwenhuyzen and Profs. Miguel Julve and Francesc Lloret. The former, for looking after me during my time in Belfast and for all his help with the crystallography, and the latter for looking after me on my visits to Valencia, Spain and for carrying out the variable temperature magnetic measurements. Thanks too to the entire academic staff in the chemistry department for helping me to get to this point.

I am also indebted to the technical and secretarial staff in Trinity College, namely Dr. Martin Feeney, Patsy Greene, Teresa, Seamas, Kieron, Peggy, Dorothy, Brendan and Mark, Colm, Tess, Corinne, Helen, Paul, Brendan and John.

Thanks also to the post-docs, Phil Mackie (now Avecia, Manchester) and Noreen Martin (now Royal College of Surgeons), from whom I learned so much.

My friends over the past number of years here in Trinity have made my time so enjoyable and they all deserve mention, so to Brian Conerney, Gar Curran, Tom McDonald, Dan Gregg, Claire Nolan, Caroline Phelan, Michelle Higgins, Yvonne Kavanagh, Mark Glynn, Joe Leonard, Aoife O'Brien, Michael Seery, Karen O'Donohoe, Tito, Paulser, Suresh, Murray, Eithne, Anto, Ronan O'Connor, James Hayes and C.J. Heeney, I say cheers! Thanks to 'the lads' back home, Dunny, Joycie, Doyler, Gerry, Deco, Macker, Johnny and Kenny B for everything over the past 15 years!

Finally, I would like to say thanks to Niamh, who has always been there for me over the past 3½ years. Thanks Babe. This thesis is dedicated to my family, my grandparents (Paddy, Chrisie, John and Mabel) and my baby sister, Leanne and most of all to my parents Paul and Reneé, who made sure I had all the opportunities they never had and ensured I never missed out.

Thanks,

Rob

9/11/2001

Summary

The research presented in this thesis lies within the general area of supramolecular and coordination chemistry. More specifically, this project involved the synthesis of early and late transition metal complexes incorporating group 14 and 15 oxo-anions, with chelating polypyridyl ligands. The primary aim of the project was to construct complexes whereby paramagnetic metal centres were bridged by oxo-anions such as carbonate (CO_3^{2-}), phosphate and pyrophosphate (PO_4^{3-} , $\text{P}_2\text{O}_7^{4-}$ respectively), arsenate (AsO_4^{3-}) and hydroxide (OH^-). The ability of these anions to mediate electronic exchange in multimetallic systems was studied. A secondary aim of the project was to study the oxo-anions with an aim to understanding further their coordinating ability and their capacity to act as part of a donor/acceptor synthon through hydrophilic/hydrophobic interaction and H-bonding. Finally, the ability of water to influence both the structure and function of the complexes was of major interest to us

Chapter two describes results obtained using the trianionic oxo-anion phosphate (PO_4^{3-}), which was successfully utilised in the preparation of tetranuclear copper(II) complexes. The evidence for phosphate being a poor mediator of magnetic exchange has been increased with overall character dependent not on the trianionic PO_4^{3-} but rather on the nature of the additional carbonate or hydroxide bridges also incorporated. The phosphate is however of great importance in the synthesis of the tetranuclear complexes and as a hydrophilic component in the extended pseudo-clathrate structures. Some degree of control over magnetic behaviour has also been obtained through this study with the deliberate synthesis of a ferromagnetic complex, by careful manipulation of reaction conditions, using information gleaned from previous results. Replacing bipyridine with 1,10-phenanthroline also served to disrupt formation of the 3-D water pseudo-clathrate network. This is a result of phenanthroline's larger size relative to bipy, which has the effect of 'pushing' the tetranuclear cores further apart. These factors have the effect of isolating the water molecules between sheets of the complex producing a 2-D structure.

Chapter three describes a series of reactions using the pyrophosphate oxo-anion ($\text{P}_2\text{O}_7^{4-}$) and produced dinuclear (Cu(II) and VO(II)) or tetranuclear (Zn(II)) complexes. The copper(II) complex displays magnetic behaviour that is dependant on degree of hydration, with a ~ five-fold increase in the antiferromagnetic coupling observed on complete dehydration. The vanadyl(II) complex is insoluble and probably polymeric in nature. This

is likely a result of the formation of 'infinity chains' of V=O group within the complex. The ability of pyrophosphate to undergo different coordination modes is demonstrated by the formation of a tetranuclear complex with Zn(II). ^{31}P NMR shows a large shift on coordination in respect to 'free' pyrophosphate.

Chapter four describes results using sodium hydrogen arsenate (Na_2HAsO_4). This returns complexes containing a diprotonated form of the oxo-anion, namely H_2AsO_4^- . The system utilises a network of π - π and H-bonding interactions and displays weak antiferromagnetic exchange coupling through the \sim tetrahedral H_2AsO_4^- bridges. In an effort to generate completely deprotonated inorganic arsenate (AsO_4^{3-}), the pH was increased from 11 to 14. This had the effect of completely removing arsenate, of any form, from the complex recovered. Alternating carbonate/hydroxy bridged copper(II) polymeric species was obtained. Magnetically the complex exists as an isolated spin doublet with two non-interacting spin triplets returning overall ferromagnetic behaviour. The synthesis of a similar hydroxy-bridged copper(II) complex, and its anhydrous analogue, incorporating pendant protonated phosphate was achieved by hydrothermal synthesis and controlled dehydration respectively. The complex exhibits the strongest ferromagnetic exchange coupling yet seen in this family of di- μ -hydroxy copper(II) complexes and exhibits varied intermolecular interactions depending on degree of hydration.

A kinetically metastable complex possessing a 2-D extended structure, is formed on reaction of $\text{Cu}(\text{OH})_2$, 1,10'-phenanthroline and particular group 15 oxo-anions. This species readily converts into a thermodynamically stable product through concomitant loss of lattice water molecules. The phen ligands pack to produce a 3-dimensional complex with entropy loss compensated by loss of water molecules. The trigger of the process is this loss of water, evident by the fact that in solution the process is much slower.

A common theme throughout is the role played by supramolecular interactions in the overall structure, stability and dimensionality of each system and the ability of oxo-anions to act as both facilitators of magnetic super-exchange and as potent H-bond donor-acceptors. The influence of water on both structure and function also plays a vital role in the systems described herein.

TABLE OF CONTENTS

	Page
Title	(i)
Declaration	(ii)
Acknowledgements	(iii)
Summary	(v)
Table of contents	(vii)
Abbreviations	(xiv)

Chapter 1. General Introduction

1.1. Metallosupramolecular Chemistry.	1
1.2. Polynuclear transition metal complexes.	2
1.2.1. Polynuclear complexes of Copper(II): An Introduction.	3
1.2.2. Dinuclear Copper(II) complexes.	4
1.2.3. Trinuclear Copper(II) complexes.	5
1.2.4. Tetranuclear Copper(II) complexes.	6
1.2.5. Higher Nuclearity Cu(II) complexes.	6
1.3. Oxo-anions of Phosphorous, Arsenic and Carbon.	7
1.3.1. Phosphates.	7
1.3.2. Arsenates.	12
1.3.3. Carbonates.	14
1.3.4. Fixation of CO₂.	15
1.4. Molecular Magnetism.	16
1.4.1. Magnetically Dilute Systems.	18
1.4.2. Magnetic Interactions in Polynuclear Systems.	18

1.4.3. Design strategy used in the preparation of exchange-coupled magnetic complexes.	20
1.6. Supramolecular chemistry.	22
1.6.1. Hydrogen bonds.	22
1.6. Clathrate Hydrate Structures.	25
1.7. Present Study.	28
References	28

Chapter 2. Preparation and magneto-structural correlations in polynuclear copper(II) complexes incorporating trianionic phosphate (PO_4^{3-}),
 $\{[(\text{bipy})_4\text{Cu}_4(\mu\text{-PO}_4)_2(\mu\text{-CO}_3)(\text{H}_2\text{O})_2]\cdot 26\text{H}_2\text{O}\}$ (1),
 $\{[(\text{bipy})_4\text{Cu}_4(\mu\text{-PO}_4)_2(\mu\text{-OH})(\text{H}_2\text{O})_2]^{2/3}\text{PO}_4\cdot 15^{1/3}\text{H}_2\text{O}\}$ (2)
and $\{[(\text{phen})_4(\text{Cu})_4(\mu\text{-PO}_4)_2(\mu\text{-CO}_3)(\text{H}_2\text{O})_2]\cdot 40\text{H}_2\text{O}\}$ (3).

Introduction	34
2.1. Preparation and Characterisation of the Tetranuclear copper(II) complex: $\{[(\text{bipy})_4(\text{Cu})_4(\mu\text{-PO}_4)_2(\mu\text{-CO}_3)(\text{H}_2\text{O})_2]\cdot 26\text{H}_2\text{O}\}$; (1)	36
2.2. Description of the Molecular Structure of the Tetranuclear copper(II) complex: $\{[(\text{bipy})_4(\text{Cu})_4(\mu\text{-PO}_4)_2(\mu\text{-CO}_3)(\text{H}_2\text{O})_2]\cdot 26\text{H}_2\text{O}\}$ (1)	38
2.3. The effect of pH and stoichiometry on the synthesis of (1)	48
2.4. Thermal Analysis of (1)	50
2.5. Preparation and Characterisation of the Tetranuclear copper(II) complex: $\{[(\text{bipy})_4(\text{Cu})_4(\mu\text{-PO}_4)_2(\mu\text{-OH})(\text{H}_2\text{O})_2]^{2/3}\text{PO}_4\cdot 15^{1/3}\text{H}_2\text{O}\}$; (2)	52
2.6. Description of the Molecular Structure of the Tetranuclear copper(II) complex: $\{[(\text{bipy})_4(\text{Cu})_4(\mu\text{-PO}_4)_2(\mu\text{-OH})(\text{H}_2\text{O})_2]^{2/3}\text{PO}_4\cdot 15^{1/3}\text{H}_2\text{O}\}$; (2)	54
2.7. Magnetic Behaviour of the Tetranuclear copper(II) complex;	59

	$\{[(\text{bipy})_4(\text{Cu})_4(\mu\text{-PO}_4)_2(\mu\text{-OH})(\text{H}_2\text{O})_2] \cdot \frac{2}{3}\text{PO}_4 \cdot 15\frac{1}{3}\text{H}_2\text{O}\}; (2)$	
2.8.	Preparation and Characterisation of the Tetranuclear copper(II) complex: $\{[(\text{phen})_4(\text{Cu})_4(\mu\text{-PO}_4)_2(\mu\text{-CO}_3)(\text{H}_2\text{O})_2] \cdot 40\text{H}_2\text{O}\}; (3)$	62
2.9.	Description of the molecular structure of the Tetranuclear copper(II) complex: $\{[(\text{phen})_4(\text{Cu})_4(\mu\text{-PO}_4)_2(\mu\text{-CO}_3)(\text{H}_2\text{O})_2] \cdot 40\text{H}_2\text{O}\}; (3)$	64
	Conclusion	69
	References	69

Chapter 3. Preparation of Copper(II), Zinc(II) and Vanadyl(II) complexes incorporating pyrophosphate ($\text{P}_2\text{O}_7^{4-}$). Influence of water on structure and magnetic behaviour.

	Introduction	73
3.1.	Preparation and Characterisation of the Dinuclear copper(II) complex $\{[\text{Cu}(\text{bipy})(\text{H}_2\text{O})]_2(\mu\text{-P}_2\text{O}_7) \cdot 7\text{H}_2\text{O}\}; (4)$	75
3.2.	Description of the Molecular Structure of the Dinuclear copper(II) complex $\{[\text{Cu}(\text{bipy})(\text{H}_2\text{O})]_2(\mu\text{-P}_2\text{O}_7) \cdot 7\text{H}_2\text{O}\}; (4)$	76
	3.2.1. Thermal analysis of complex (4). Formation of stable intermediates (5) and (6) of various degrees of hydration.	79
	3.2.2. Magnetic behaviour of the dinuclear complex $\{[\text{Cu}(\text{bipy})(\text{H}_2\text{O})]_2(\mu\text{-P}_2\text{O}_7) \cdot 7\text{H}_2\text{O}\}; (4)$ and it's dehydrated phases $\{[\text{Cu}(\text{bipy})(\text{H}_2\text{O})]_2(\mu\text{-P}_2\text{O}_7)\}; (5)$ and $\{[\text{Cu}(\text{bipy})]_2(\mu\text{-P}_2\text{O}_7)\}; (6)$	80
3.3.	Preparation, Characterisation and Structural Description of the mononuclear copper(II) complex; $\{[\text{Cu}(\text{bipy})(\text{H}_2\text{O})(\text{Na}_2\text{P}_2\text{O}_7) \cdot 11\text{H}_2\text{O}\}; (7)$	85
3.4.	Preparation and Characterisation of the Tetranuclear Zinc(II) complex $\{[(\text{Zn}(\text{bipy}))_4(\mu\text{-P}_2\text{O}_7)_2(\text{H}_2\text{O})_2] \cdot 6\text{H}_2\text{O}\}; (8)$	89
3.5.	Description of the Molecular Structure of the Tetranuclear Zinc(II) complex $\{[(\text{Zn}(\text{bipy}))_4(\mu\text{-P}_2\text{O}_7)_2(\text{H}_2\text{O})_2] \cdot 6\text{H}_2\text{O}\}; (8)$	90
	3.5.1. Nuclear Magnetic Resonance Studies of (8)	93

3.6. Synthesis and Characterisation of a Vanadyl(II) complex postulated as $\{[(VO)(bipy)]_2(\mu-P_2O_7).5H_2O\};(9)$	95
3.6.1. Infrared analysis of $\{[(VO)(bipy)]_2(\mu-P_2O_7).5H_2O\};(9)$	96
3.6.2. Thermal analysis of complex $\{[(VO)(bipy)]_2(\mu-P_2O_7).5H_2O\};(9)$.	99
3.6.3. Magnetic behaviour of $\{[(VO)(bipy)]_2(\mu-P_2O_7).5H_2O\};(9)$ at room temperature.	100
Conclusion	100
References	102

Chapter 4. Preparation and magnetic behaviour of the dinuclear copper(II) complexes: $[(bipy)Cu(\mu-H_2AsO_4)(H_2AsO_4)]_2$ (10), $\{[(bipy)_3Cu_3(\mu-OH)_2(\mu-CO_3)_2].11H_2O\}_n$ (11) and $\{[(bipy)_2Cu_2(\mu OH)_2(HPO_4)(H_2O)].4H_2O\}$ (12).

Introduction.	104
4.1. Preparation and Characterisation of the Dinuclear copper (II) complex $[bipy(Cu)(H_2AsO_4)(\mu-H_2AsO_4)]_2$; (10)	105
4.2. Structural Characterisation of the Dinuclear Copper (II) complex $[(bipy)Cu(\mu-H_2AsO_4)(H_2AsO_4)]_2$; (10)	106
4.2.1. Magnetic behaviour of $[(bipy)Cu(H_2AsO_4)(\mu-H_2AsO_4)]_2$; (10).	110
4.3. Preparation and Characterisation of the Polymeric Chain complex $\{[Cu_3(bipy)_3(\mu-OH)_2(\mu-CO_3)_2].10H_2O\}_n$; (11)	111
4.4. Structural Characterisation of $\{[Cu_3(bipy)_3(\mu-OH)_2(\mu-CO_3)_2].11H_2O\}_n$; (11)	111
4.4.1. Thermal Analysis of (11).	115
4.4.2. Magnetic Properties of $\{[Cu_3(bipy)_3(\mu-OH)_2(\mu-CO_3)_2].11H_2O\}_n$; (11).	116

4.5.	Hydrothermal Synthesis and Characterisation of the dinuclear copper(II) complex $\{[(bipy)_2Cu_2(\mu-OH)_2(HPO_4)(H_2O)].4H_2O\}$; (12)	119
4.6	Structural Description of $\{[(bipy)_2Cu_2(\mu-OH)_2(HPO_4)(H_2O)].4H_2O\}$; (12)	120
	4.6.1 Thermal analysis (TGA) of (12).	124
	4.6.2. Magnetic properties of (12).	124
	Conclusion	128
	References	129

Chapter 5: The Preparation, Characterisation and Thermal analysis of $[Cu(phen)_2(CO_3).11H_2O]$ (15) and $[Cu(phen)_2(CO_3).7H_2O]$ (16).

	Introduction	131
5.1.	Preparation and Characterisation of the Mononuclear copper(II) complex: $\{[Cu(phen)_2(CO_3)].11H_2O\}$ (15)	132
5.2.	Description of the Molecular Structure of the copper(II) complex $\{[Cu(phen)_2(CO_3)].11H_2O\}$ (15)	133
	5.2.1. Thermal analysis of (15) and (16).	143
	5.2.2. Effect of pH on the formation of (15) and (16).	144
	Conclusion	146
	References	146

Chapter 6. Materials and Methods.

Experimental

6.1.	Materials and methods.	148
	6.1.1. Reagents.	148
	6.1.2. Elemental Analysis.	148

6.1.3. Nuclear Magnetic Resonance.	148
6.1.4. Infrared spectroscopy.	148
6.1.5. Electrospray mass spectroscopy.	149
6.1.6. Ultraviolet-visible spectroscopy.	149
6.1.7. Magnetic measurements.	149
6.1.8. Thermal Gravimetric analysis (TGA).	150
6.1.9. Differential Scanning Calorimetry (DSC).	150
6.1.10. X-ray Powder Diffraction.	150
6.1.11. Single Crystal X-ray Diffraction.	151
6.1.12. Acid digestion Bomb – Hydrothermal Synthesis.	151
6.2. Experimental.	152
$\{[(\text{bipy})_4\text{Cu}_4(\mu\text{-PO}_4)_2(\mu\text{-CO}_3)(\text{H}_2\text{O})_2].26\text{H}_2\text{O}\}.$ (1)	152
$\{[(\text{bipy})_4\text{Cu}_4(\mu\text{-PO}_4)_2(\mu\text{-OH})(\text{H}_2\text{O})_2]^{2/3}\text{PO}_4.15^{1/3}\text{H}_2\text{O}\}.$ (2)	152
$\{[(\text{phen})_4\text{Cu}_4(\mu\text{-PO}_4)_2(\mu\text{-CO}_3)(\text{H}_2\text{O})_2].40\text{H}_2\text{O}\}.$ (3)	153
$\{[\text{Cu}(\text{bipy})(\text{H}_2\text{O})]_2(\mu\text{-P}_2\text{O}_7)\}.$ 7H ₂ O.(4)	154
$[\text{Cu}(\text{bipy})(\text{H}_2\text{O})]_2(\mu\text{-P}_2\text{O}_7).$ (5)	154
$[\text{Cu}(\text{bipy})]_2(\mu\text{-P}_2\text{O}_7).$ (6)	154
$\{[\text{Cu}(\text{bipy})(\text{H}_2\text{O})(\text{Na}_2\text{P}_2\text{O}_7).10\text{H}_2\text{O}\}.$ (7)	155
$\{[(\text{Zn}(\text{bipy}))_4(\mu\text{-P}_2\text{O}_7)_2(\text{H}_2\text{O})_2].7\text{H}_2\text{O}\}.$ (8)	155
$\{[(\text{VO})(\text{bipy})]_2(\mu\text{-P}_2\text{O}_7).5\text{H}_2\text{O}\}.$ (9)	156
$[(\text{bipy})\text{Cu}(\text{H}_2\text{AsO}_4)(\mu\text{-H}_2\text{AsO}_4)]_2.$ (10)	156
$\{[(\text{bipy})_3\text{Cu}_3(\mu\text{-OH})_2(\mu\text{-CO}_3)_2].11\text{H}_2\text{O}\}_n.$ (11)	157
$\{[(\text{bipy})_2\text{Cu}_2(\mu\text{-OH})_2(\text{HPO}_4)(\text{H}_2\text{O})].4\text{H}_2\text{O}\}.$ (12)	157
$\{[(\text{bipy})_2\text{Cu}_2(\mu\text{-OH})_2(\text{HPO}_4)(\text{H}_2\text{O})]\}.$ (13)	158
$[(\text{bipy})_2\text{Cu}_2(\mu\text{-OH})_2(\text{HPO}_4)].$ (14)	158

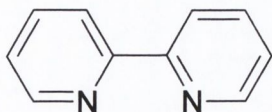
$\{[\text{Cu}(\text{phen})_2(\text{CO}_3)] \cdot 11\text{H}_2\text{O}\} \cdot (15)$	158
$\{[\text{Cu}(\text{phen})_2(\text{CO}_3)] \cdot 7\text{H}_2\text{O}\} \cdot (16)$	159
6.3. References.	159
Chapter 7. Future Work.	160
Appendix A Solvothermal Synthesis	165
Appendix B Naturally Occurring Clathrate Structures	168
Appendix C Crystal Structure Metric Parameters	169
Publications	180

Abbreviations and symbols.

Symbol	Definition
BM	Bohr magneton
C	Curie constant
E	energy of a system
H	magnetic field
J	exchange coupling constant
K	Boltzmann's constant
L	ligand
g	Lande factor
m_L	magnetic quantum number
M	metal
N	Avogadro's number
s	spin quantum number
S-T	singlet-triplet
T	temperature
T_c	Curie or critical temperature
T_N	Neel temperature
V	molar volume
W	weight
α	an alternating parameter
ρ	temperature independent paramagnetism
Γ	irreducible representation of a point group
χ	magnetic susceptibility
κ	volume magnetic susceptibility
μ -	"bridging"
μ	magnetic moment (in BM)

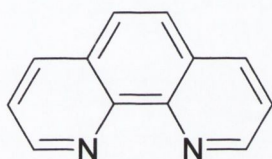
bipy

2,2'-bipyridine



phen

1,10-phenanthroline



FTIR

Fourier-transform infrared

ESMS

electro-spray mass spectroscopy

UV-vis

ultraviolet-visible spectroscopy

DSC

differential scanning calorimetry

TGA

thermal gravimetric analysis

SQUID

superconducting quantum interference device

NMR

nuclear magnetic resonance

ppm

parts per million

M_r

molecular weight

br

broad

m

medium

s

sharp

w

weak

D/A

donor/acceptor

MHz

megahertz

CSD

Cambridge Structural Database

Chapter One

General Introduction

1.1. Metallosupramolecular Chemistry.

Given the diversity of photochemical, photophysical and electrochemical possibilities offered by metal complexes, it is clear that the inclusion of metals into predominantly organic supramolecular structures increases the scope of this field tremendously. At the simplest level, the controlled geometry around a metal centre allows metals to be used as building blocks, responsible for connecting subunits in a controlled fashion. The metal therefore serves as 'cement' holding the ligands together and as centre orienting them in a given direction. The formation of any complex species from an organic ligand and a metal ion is in principle an assembly process that occurs spontaneously. The emphasis here lies in the choice of ligand and the choice of metal ions in order to produce defined architectures in a controlled fashion from multiple subunits. Metal ions have properties of special interest as components of supramolecular systems and linkers for self-assembly.

They provide: -

- (i) a set of coordination geometries,
- (ii) a range of binding strengths, from weak to very strong, and of formation and dissociation kinetics, from labile to inert, and
- (iii) a variety of photochemical, electrochemical and magnetic and properties.

A great diversity of polynuclear metal clusters have been obtained by self-assembly with increasing ability to direct the process. For example, the synthesis of catenanes¹ and rotaxanes², cryptands and azacryptands,³ double and triple helices⁴ and rosettes and ribbons⁵ make use of the directional nature and special characteristics of hydrogen bonding to generate complex supramolecular entities. Numerous metallo-complexes have been 'self-assembled' giving species possessing various structures, for instance: triangular,⁶ square,⁷ star-like,⁸ wheel-shaped,⁹ octameric and decameric,¹⁰ to species containing cavities, which may include a guest molecules.¹¹ These supermolecules are often of biological significance or of interest to materials science (Fig 1.1).

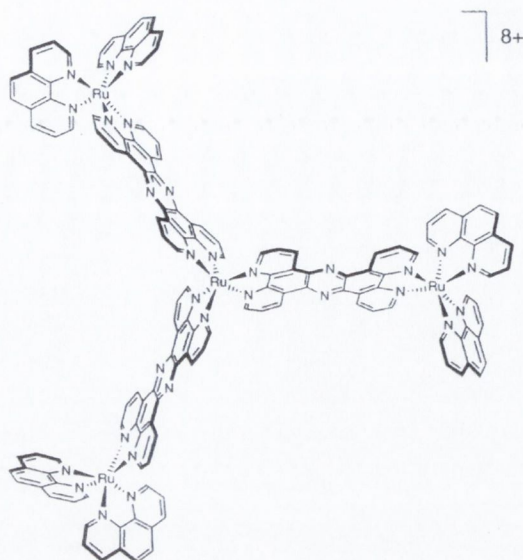


Fig 1.1. Complexes such as this tetranuclear ruthenium complex are predicted to be components in solar cells of the future, a result of their ability to 'harvest light'.¹²

1.2. Polynuclear transition metal complexes.

The study of polynuclear transition metal complexes encompasses an extensive and extremely diverse range of modern coordination chemistry. A current driving force behind this field of research is the quest to develop improved molecular magnetic materials¹³ for use in traditional areas such as information storage or opto-electronic devices (data storage and telecommunications). The quest to reproduce the physico-chemical (structural and functional) aspects of multimetallic sites of metalloproteins also inspires much current interest.¹⁴ Transition metal ions are known to be present at the active sites of many metalloproteins and enzymes and they actively participate in the varied biological functions performed by these biomolecules, which include substrate binding, fixation, activation, storage and transport. Metal ions can mediate facile electron transfer and bind small molecules such as carbon dioxide. Whilst it is recognised that model compounds will never fully mimic the structural and functional properties of the metallo-proteins, since they lack the protein assemblage, there are now sufficient examples of model studies which have aided considerably in a molecular understanding of the parent bio-systems.¹⁵

1.2.1. Polynuclear complexes of Copper(II): An Introduction.

In the current study we will initially concentrate on polynuclear complexes of Cu(II) as the chemistry of copper(II) compounds has been extensively investigated,¹⁶ and the relationship between structure and reactivity ranging from industrial catalysis to biomedical activity is of major importance. In addition to mimicking aspects of protein active sites, investigations into polynuclear copper(II) complexes continues to attract much attention from a magnetostructural point of view. Investigations into such complexes has aided in the development and understanding of the factors responsible for the different modes of spin-spin coupling that occurs between paramagnetic centres. The overwhelming majority of single crystal X-ray crystallographic studies of transition metal compounds are of copper compounds.²³ Complexes of the d^9 Cu(II) ion are intrinsically flexible, displaying a wide range of coordination numbers, but they generally deviate significantly from ideal structures due to the Jahn-Teller effect.¹⁷ Both angular and bond distortions are common. Thus the copper-ligand distance may vary over a wide range depending on the site of coordination. Pentacoordinate complexes are the most common copper(II) species and may exist in two extreme geometries of trigonal bipyramidal and square pyramidal or distortions between these, as often there is only a small energy barrier preventing interconversion.

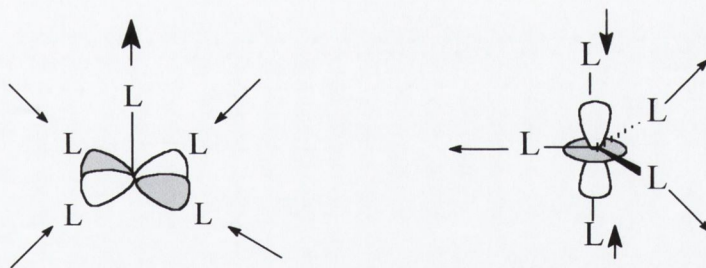


Fig 1.2. In square-pyramidal geometry (left), for Cu(II), there is only one electron in the $d_{x^2-y^2}$ orbital, which encourages short equatorial bonds and long apical bonds. In trigonal-bipyramidal symmetry (right) the 'hole' is in the d_z^2 orbital and encourages short axial and long equatorial bonds.

In nature, copper containing biomolecules are usually associated with oxygen transport and electron transfer reactions.¹⁸ A human adult contains around 100 mg of copper, mostly attached to proteins, an amount exceeded only by iron and zinc among d-block metals, and requiring a daily intake of 3-5 mg. The blue copper proteins such as plastocyanin are involved in long range electron transfer, the multicopper oxidases, such as laccase, couple substrate oxidation at a T1 copper site to the four electron reduction of water to oxygen in the blood of arthropods.²¹ Copper containing bio-enzymes are also associated with the two-electron reduction of nitrous oxide (N_2O) to N_2 . Nitrous oxide is a greenhouse gas, the third most significant contributor to global warming. A key process in the elimination of N_2O from the biosphere is that of nitrous oxide reductases. These copper containing enzymes have caused much recent controversy over their structural make-up but are now thought to contain the first example of a tetra-copper cluster ligated by histidine nitrogens.¹⁹ There also exists an intricate network of H-bonds thought to maintain the imidazole rings of the histidine residues in the appropriate orientation for coordinating the copper ions. As in nitrous oxide reductase, many copper containing bioenzymes such as ascorbate oxidase can accommodate peroxo or hydroxy bridges between copper(II) centres. Attempts to generate models of these enzymes have proved difficult but gained momentum over the past ten years.²⁰ With new bio-structures postulated from X-ray analysis all the time, the need to generate biomimetic complexes becomes more critical.

In addition to mimicking aspects of protein active sites,²¹ investigations into polynuclear copper complexes have continued to attract much attention from a magnetostructural point of view.²² Investigations into such complexes have aided the development and understanding of the factors responsible for the different modes of spin-spin coupling that occur between paramagnetic centres.

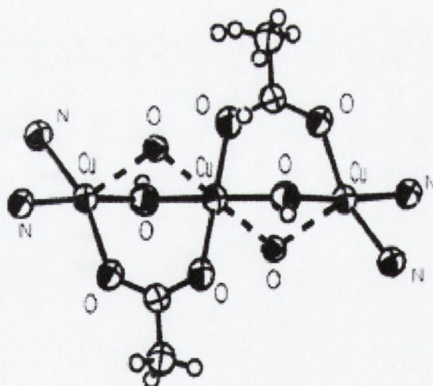
1.2.2. Dinuclear Copper(II) complexes.

These form a major group of copper(II) complexes for three reasons: (i) they are readily prepared by the normal methods used in preparing monomeric complexes;²³ (ii) they provide useful simple models for the study of magnetic interaction of two unpaired d electrons;²⁴ (iii) they are useful models of type III-IV biological copper systems.²⁵ In the past twenty years it

is probably (ii) and (iii) above that have provided the major incentive in the synthesis of novel dimeric copper(II) systems.²⁶ Dinuclear copper(II) complexes have been formed with a diverse range of mono- and poly-dentate, acyclic, macrocyclic and macrobicyclic ligand types and can be structurally symmetrical or unsymmetrical relative to the Cu-Cu axis or end groups. The metals may be linked by one, two, three or four bridging groups, the degree of bridging pre-determined by the metals coordination capacity [usually 4 or 5 for copper (II)].

1.2.3. Trinuclear Copper(II) complexes.

Trinuclear complexes have, over the past ten years, gained prominence through the recognition of a trinuclear copper site within several copper oxidases.²⁷ Three metal atoms can arrange themselves in either a triangular or linear array, and complexes possessing trinuclear Cu(II) centres in both geometries have been structurally characterised.²⁸ Recently Karlin *et al.*²⁹ developed trinuclear copper(II) complexes to model the dioxygen reactivity of trinuclear Cu(II) oxidases. The same group have also used trinuclear Cu(II) complexes to cause site specific scission of DNA³⁰. Thompson *et al.*³¹ and Chakravarty *et al.*³² have reported trinuclear Cu(II) complexes displaying both strong anti-ferromagnetic and ferromagnetic properties. The latter's complexes are presented as first generation models of the active site of ascorbate oxidase.



1.3. A linear trinuclear Cu(II) complex reported by Cano *et al.*³³ Neighbouring Coppers are connected by a hydroxo bridge and a bidentate *syn-syn* carboxylate group. The terminal ligand (N-(2-methylpyridyl)toluenesulfonylamide) is omitted for clarity.

1.2.4. Tetranuclear Copper(II) complexes.

These complexes are much less common than the dinuclear complexes, but slightly more extensive than trinuclear complexes. Four main structural types arise, namely linear, zigzag or stepped, planar and tetrahedral (as a cubane). The linear systems are the least common, but do occur in the linear chain of $\{(\text{Me}_3\text{NH})_2[\text{Cu}_4\text{Cl}_{10}]\}$ involving four coplanar CuCl_4 chromophores,³⁴ or the polyfluoro-*tert*-butoxide complex, $\{\text{Cu}_4(\mu\text{-OCMe}_3)_6[\text{OC}(\text{CF}_3)_2]_2\}$, isolated by Purdy *et al.*³⁵ In $[\text{Cu}(\text{salen})\text{CuCl}_2]_2$, where salen = N,N'-ethylenebis(salicylaldimine), a zigzag Cu_4 unit is present, with a co-planar Cu_2Cl_2 central unit and two terminal CuO_2Cu bridges.³⁶ An essentially planar Cu_4 unit occurs in $[\text{Cu}_2(\text{bpim})(\text{im})]_2(\text{NO}_3)_4$,³⁷ where bpim = 4,5-bis{(2-pyridyl) ethyliminomethylimidazolate}. All four copper atoms are bridged by imidazole ligands and further coordinated by two nitrogens of the bpim ligands coplanar with the CuN_4 chromophore. Another pertinent example of planar disposition is that of the macrocyclic complex synthesised by McKee *et al.*³⁸ using the template reaction of 2,6-diformyl-4-*tert*-butyl-phenol and 1,5-diaminopentan-3-ol in the presence of copper(II) nitrate.

The most regular type of tetrahedral Cu_4 unit is involved in the $[\text{Cu}_4\text{OX}_6\text{L}_4]$ structure, where X = Cl^- or Br^- and L may be Cl^- or OH^- or an organic ligand such as triphenyl phosphine oxide. In all of these structures, the tetrahedron is nearly regular with a central oxygen atom.³⁹

1.2.5. Higher Nuclearity Cu(II) complexes.

Hexanuclear and higher nuclearity copper(II) complexes are far smaller in number. Among some pertinent examples however, of hexanuclear copper(II) systems are the $[\text{Cu}_3\text{O}(\text{dpeo})_3(\text{ClO}_4)]_2$ complex⁴⁰, where dpeo is 1,2-diphenyl-2-(methylimino)ethane-1-oxime, and the $\text{Cu}_6(\mu\text{-OCMe}_3)_6((\mu\text{-O}_2\text{CMe})_4(\mu_4\text{-O}_2\text{CMe})_2)$ complex,⁴¹ where the six copper atoms are linked together by six alkoxo ligands to form a hexagon. Karlin *et al.*⁴² have isolated a hexanuclear complex, through the reaction of a tri-copper(I) species with dioxygen. More recently, Murray *et al.*⁴³ isolated the strongly ferromagnetic hexanuclear Cu(II)

complexes, $\{[(\text{Cubpy})_2(\mu\text{-CO}_3)\text{Cubpy}]_2(\mu\text{-OH})_2\}(\text{X})_6 \cdot y\text{H}_2\text{O}$, where $\text{X} = \text{ClO}_4^-$, $y = 2$, or $\text{X} = \text{PF}_6^-$, $y = 6$. Thompson *et al.*⁴⁴ have reported, not only a macrocyclic hexanuclear Cu(II) complex, but also a dodecanuclear macrocyclic Cu(II) complex with an almost planar, 'benzene-like' metal array. The inherent difficulty and complexity of these complexes has hindered the synthesis, characterisation and theoretical understanding of these systems and explains the relative dearth of examples in respect to mono, di, tri and tetranuclear copper(II) compounds.

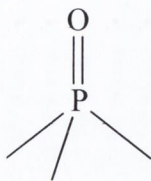
In theory several methods may be employed in the synthesis of polymetallic coordination compounds and include, amongst others, the self-assembly or aggregation of metal centres and ligand species, both coordinating and bridging, into polymetallic arrays; or the direct incorporation of metal ions into preformed polydentate ligands. This second approach offers many potential advantages over the self-assembly route in that it enables more stringent control over the reaction and thus upon the products that form. Nevertheless, self assembly may allow access to a myriad of structural types and complex nuclearities. This is the approach that we will adopt in the current study. We will employ chelating ligands that may enforce certain constraints upon the complexes formed (*i.e.* prevent polymer formation), but still allow substantial freedom. We will also employ bridging ligands that will not only allow the build up of aggregates, but also compensate for charge. To this end, we intend to employ group 14 and 15 oxo-anions, which are ubiquitous throughout nature.

1.3. Oxo-anions of phosphorous, arsenic and carbon.

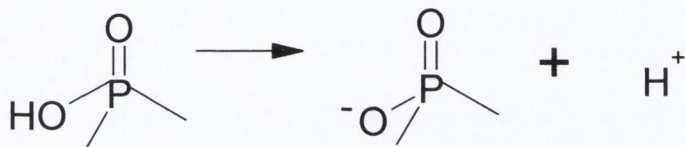
1.3.1. Phosphates.

The oxo-acids of phosphorous are more numerous than those of any other element, and only those of silicon probably exceed the number of oxo-anions and oxo-salts. Many are of great importance technologically and their derivatives are vitally involved in many biological processes. The structural principles covering this extensive array of compounds are very simple with the most important points to note being:

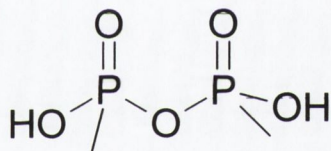
- (i) all P atoms in the oxo-acids and oxo-anions are 4-coordinate and contain at least one P=O unit



- (ii) most oxo-anions contain at least one P-OH group that is ionizable as a proton donor.



- (iii) catenation is by P-O-P links or via direct P-P bonds; with the former, both open chain (“linear”) and cyclic species are known but only corner sharing of tetrahedra occurs, never edge- or face- sharing.



Some examples of phosphorous oxo-acids are listed in Table 1.1.

Phosphates are used in an astonishing array of domestic and industrial applications. Phosphoric acid is manufactured on a vast scale and is used in metal treatment for the prevention of rust, or to prevent paint from blistering or peeling. Polyphosphoric acid supported on diatomaceous earth is a petrochemicals catalyst for the polymerisation, alkylation, dehydrogenation, and low temperature isomerisation of hydrocarbons. This is all in addition to its massive use in the fertiliser industry with a staggering 110 million tonnes of phosphate rock produced per annum for 1995. Phosphates are also used in the food industry, in the hygiene industry (e.g. Toothpaste and laxatives) and as flame-retardants in cellulose material. They are even used in submarine sonar devices as the piezoelectric KH_2PO_4 .⁴⁵

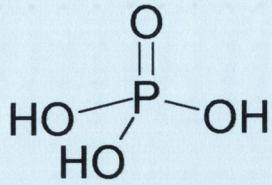
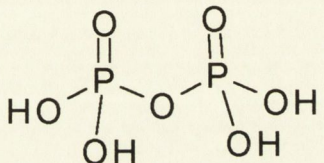
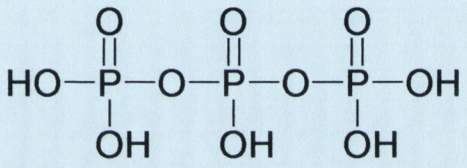
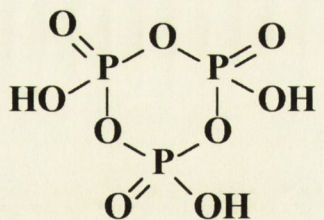
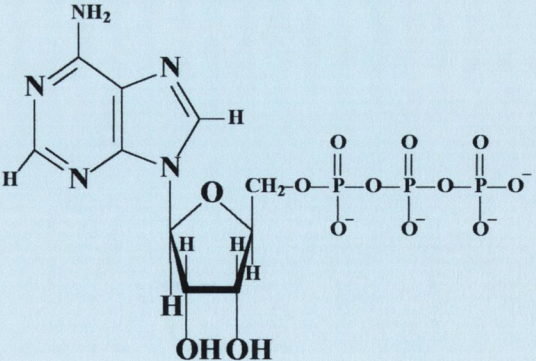
FORMULA	NAME	STRUCTURE
H_3PO_4	(ORTHO)PHOSPHORIC ACID	
$H_4P_2O_7$	DIPHOSPHORIC ACID (PYROPHOSPHORIC ACID)	
$H_5P_3O_{10}$	TRIPHOSPHORIC ACID	
$(HPO_3)_3$	CYCLO-TRIMETA-PHOSPHORIC ACID	
ATP	ADENOSINE TRIPHOSPHATE	

Table 1.1. Examples of some important phosphorous oxo-acids.

Since the discovery of microporous aluminophosphates (ALPO_{4-n}) in 1982,⁴⁶ great attention has been paid to the exploration of new microporous phosphate containing materials because of their potential applications in the fields of catalysis, ion-exchange, adsorption and host-guest assembly.⁴⁷ In fact, along with aluminosilicates (Zeolites), the majority of research aimed at open-framework inorganic materials has been carried out on aluminophosphates. Feray has stated that in the area of three-dimensional open-framework materials “most are based upon oxygen containing materials, especially phosphates...”.⁴⁸ The synthetic procedure used in the formation of these complexes generally involves that of thermal (classic solid state) or hydrothermal conditions. More recently the successful introduction of transition metals into zeolitic aluminophosphates has greatly expanded the scope of this field. Initial interest in the vanadium phosphates for example, stemmed from the catalytic applications of vanadyl pyrophosphate in the selective oxidation of butane to maleic anhydride.⁴⁹ The scope of this field continues to grow with the number of hypothetical topologies reckoned to be infinite⁵⁰.

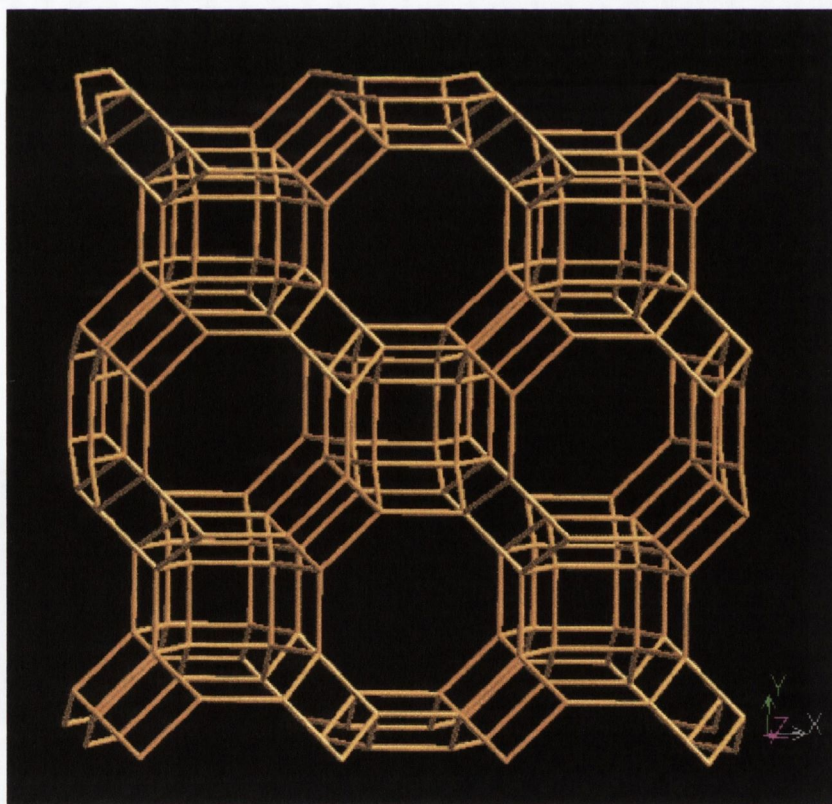


Fig 1.4. The zeolitic aluminophosphate structure $\{(C_7H_{14}N^+)_4(HPO_4^{2-})_2[Al_{24}P_{24}O_{96}]\}$.⁵¹

In living matter phosphate esters play a vital role in many life processes such as protein synthesis, genetic coding, photosynthesis, nitrogen fixation, and innumerable other metabolic pathways.⁵⁹ The bio-phosphorous compound on which all life depends is adenosine triphosphate (ATP) (Table 1.1). Hydrolysis of the ionic form of the triphosphate ester forming adenosine diphosphate (ADP) or adenosine monophosphate (AMP) releases the energy required to power many biochemical processes. The transfer of genetic information occurs by means of deoxyribonucleic acids, which are polymeric phosphate diesters of nucleosides formed from the sugar 2'-deoxyribose and the 4 bases adenine, cytosine, guanine, and thymine. Some other biochemically important phosphates include phosphocreatine used to regenerate ATP, uridine triphosphate used in the synthesis of the polysaccharide molecule glycogen from surplus carbohydrate and nicotinamide-adenine dinucleotide-2-phosphate (NADP⁺) for the photosynthesis of carbohydrates from CO₂.⁵² The phosphate anion itself has the potential to produce a large number of coordination modes, (some of which are listed below), which is why it has so many industrial uses.

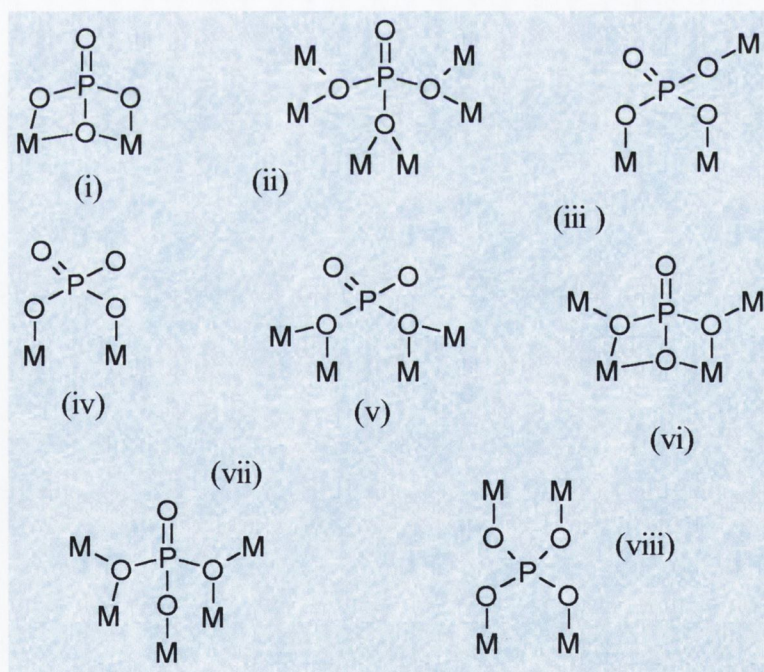


Fig 1.5. Some possible coordination modes of the phosphate group. (ii), (iii), (iv) and (viii) have precedent in the CSD.⁶⁰

We choose to study it however, not from a solid state/polymeric point of view, but rather to develop a better understanding of its coordination chemistry. To this end, we employed a synthetic strategy of incorporating ‘capping’ aromatic ligands such as bipy or phen. This has not been done to any great extent as evidenced by a review of the literature⁵³. Indeed the majority of work published on metal-phosphate coordination complexes has been confined to studies of ATP. Vahrenkamp *et al.*⁵⁴ have made a systematic study of zinc(II) complexes with condensed phosphate and tridentate ligands such as 2,2'-dipyridylamine. The aqueous chemistry of high-valent manganese complexes containing terminal phosphate and 2,2'-bipyridine has been reported by Sarneski *et al.*⁵⁵ Tomlinson *et al.*⁵⁶ have produced coordination complexes containing phosphate or hydrogenphosphate with Co(II), Ni(II) and Cu(II) and zirconium, by diffusion of the M(II) solution with phen or bipy into $Zr(HPO_4)_2$, producing (P-O)M(N-N) moieties. More recently however Lii *et al.*⁵⁷ and Lightfoot *et al.*⁵⁸ have synthesised coordination complexes containing transition metal centres with terminal or bridging ligands and phosphate. This is work in the rapidly expanding area of inorganic-organic open-framework materials, where phosphate is considered to be a vital component because of its ability to adopt varied coordination modes, its hydrophilicity, oxidation resistance and ability to stabilise high oxidation states.

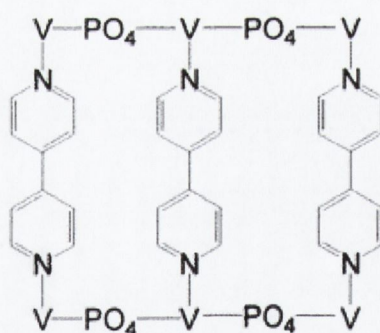


Fig 1.6. Core of the 2-D network compound reported by Lii *et al.*

1.3.2. Arsenates.

Arsenic as an element was amongst the earliest to be discovered being known before nitrogen (1772) or phosphorous (1669) had been obtained as the free elements. Like phosphorous,

arsenic has only one stable isotope and this occurs with 100% abundance in all natural sources of the elements. In relation to life arsenic has until recently, always been considered as extremely toxic. However, with the discovery of a new class of essential elements, the ultra-trace elements, it has been demonstrated that deficiency in arsenic (in microtrace amounts ~50 ppb by weight) can lead to impairment of growth, reproductive and heart function.⁵⁹ In the form of arsenates, the element finds extensive use, for example, in agriculture as herbicides for weed and pest control, e.g. MSMA (monosodium methyl arsenate). Arsenic acid itself is used as a desiccant and as a wood preservative. Medicinal and veterinary uses are declining, as most arsenicals in general are considered poisonous. World production of “white arsenic”, *i.e.* As_2O_3 has been steady over the past 25 years at about 50,000 tonnes per annum. A table of the principal uses of arsenate is given below (Table 1.2).

USE		<i>PESTICIDES</i>	<i>WOOD PRESERVATIVE</i>	<i>GLASS</i>	<i>ALLOYS/ ELECTRONICS</i>
ARSENATE	%	65	18	10	3
TONNES		34 000	9500	5000	1500

Table 1.2. Industrial uses of arsenate compounds.

Work in the present study centred on the use of AsO_4^{3-} synthesised by dissolution of As_2O_5 in water or as the disodium salt. Arsenic acid H_3AsO_4 is a strongly H-bonding material being both water-soluble and, like the phosphate analogue, tribasic. There is also a certain structural similarity between arsenates and phosphates with the tetrahedral $\text{As}^{\text{V}}\text{O}_4$ group resembling the PO_4 group in forming the central unit in several heteropolyacid anions. Arsenates however show less tendency than phosphates to catenation. Another striking difference between arsenates and phosphates is the appreciable oxidising tendency of the former. This is a trend continued down group 15 resulting in the $\text{Bi}^{\text{V}}/\text{Bi}^{\text{III}}$ couple being capable of oxidising water to molecular oxygen. We wished to compare the structures and properties of polynuclear complexes of AsO_4^{3-} with PO_4^{3-} .

1.3.3. Carbonates.

Carbonates are the most common forms of naturally occurring sources of carbon (along with natural allotropes of carbon such as diamond and graphite). The carbonates are found combined with electropositive elements such as Ca and Mg. The study of carbonate as a ligand species has proved to be both a popular and rewarding one with the anion displaying many diverse characteristics, for example, in the area of coordination chemistry where carbonate has been observed in approximately twelve different coordination modes.⁶⁰

(Figure 1.9).

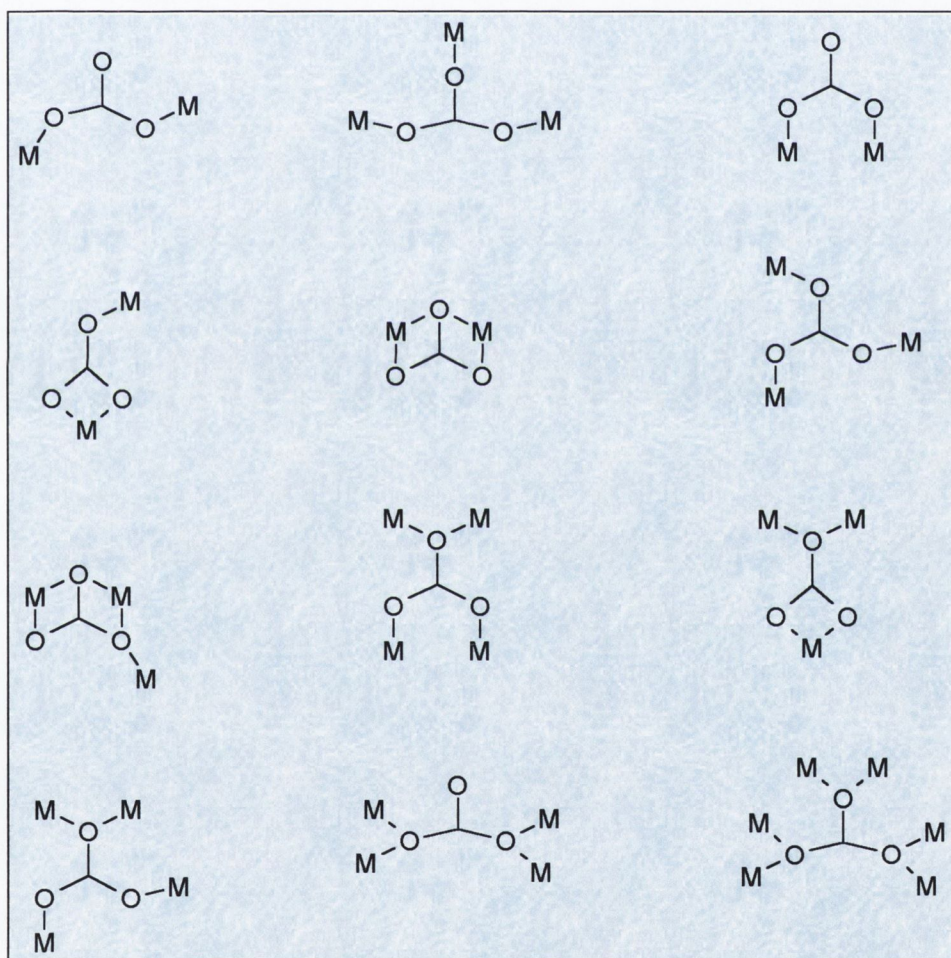


Figure 1.7. Possible coordination modes of the carbonate ligand (Source - CSD).⁶⁰

Due to this high number of possible coordination modes many types of copper(II) carbonate complexes have been obtained including mono-nuclear, dinuclear, trinuclear, tetranuclear, hexanuclear in 1-, 2- and 3- dimensional systems.⁶¹ From a magnetic viewpoint, the range of behaviour observed by copper carbonate complexes is varied. Diamagnetism, weak anti-ferromagnetism and ferromagnetism have all been observed in these complexes.

1.3.4. Fixation of CO₂.

The reduction of atmospheric carbon dioxide has been receiving increasing attention because of the serious environmental problems resulting from the increased concentration of CO₂ in air. The fixation of CO₂ by transition metal complexes have been known for several decades,⁶² and is expected to be effective for the development of such a process. Most of the complexes reported in the literature so far are air-sensitive and not suitable for CO₂ fixation under atmospheric conditions. A second difficulty is caused by the low concentrations of carbon dioxide in air. Most of the transition metal complexes are not reactive enough to fix CO₂ at such a low concentration. Several copper(II) compounds have, however, been synthesised by means of fixation of CO₂ from the air. The carbonate anion that results is a versatile ligand, which can bind in a large variety of modes as mentioned above. Absorption of CO₂ into transition metal complexes is often initiated by nucleophilic attack of the ligand anion on the electropositive carbon of the CO₂. When the ligand is oxo or hydroxo however, the reaction results in the formation of a carbonate or bicarbonate complex.⁶³ This type of reaction is known for Co, Ni, Cu and Zn. This nucleophilic fixation of carbon dioxide, by hydroxo metal complexes, to afford the metal bicarbonate or carbonate species is also relevant to the structures and functions of some metalloenzymes.⁶⁴ D-Ribulose 1,5-bisphosphate carboxylase/oxygenase, designated Rubisco, the single most abundant enzyme on Earth, is a magnesium-containing protein that is responsible for CO₂ fixation in the photosynthetic reaction operating in plants. The enzyme responsible for this fixation in mammals is carbonic anhydrase, which catalyses the physiologically important hydration of CO₂ to bicarbonate and so onto carbonate.

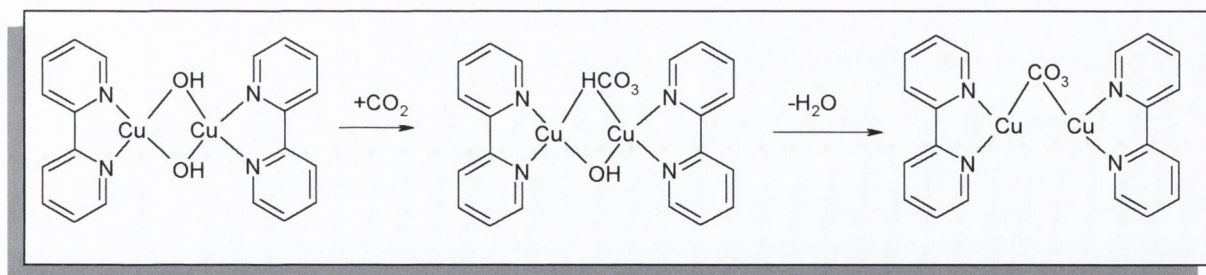


Fig 1.8. Proposed general mechanism of CO_2 fixation for a dinuclear $\text{L}_2\text{Cu}_2\text{OH}_2$ system.⁶⁵

The active site of carbonic anhydrase consists of a monomeric zinc ion, which is coordinated to histidyl nitrogen atoms and a water molecule. The zinc itself is easily replaced by other divalent metals ions such as Co(II) and Cu(II) .

1.4. Molecular Magnetism.

“I have worked in the field of molecular magnetism for almost two decades and I have been more and more fascinated by the beauty of this area and by the diversity it presents”

Prof. Olivier Kahn.

The present study is concerned with the way in which the unpaired spins within complexes interact. This is best ascertained by investigating their magnetic properties.

Molecular magnetism has emerged as a novel field of research over the last two decades. As a field, it is essentially multidisciplinary. It involves synthetic chemistry: one of its challenges is to design systems that exhibit predictable magnetic properties. To achieve this aim, novel compounds have been synthesized containing several kinds of metallic ions, organic radicals and novel bridging ligands.⁶⁶ Secondly, it uses ideas from theoretical chemistry. To design compounds with expected magnetic behaviour it is necessary to use strategies that derive from an understanding of the underlying mechanism of the phenomena.

Molecular based magnets possessing interesting behaviour may have the spin localized on

- (i) *p*-atomic orbitals (organic radicals). These are purely organic magnets and will not be referred to again in the course of this report. e.g. dinitronyl nitroxide.⁶⁷
- (ii) Some of the electrons arise from d and some from p orbitals. e.g. $V(\text{TCNE})_2 \cdot x\text{CH}_2\text{Cl}_2$. where $\text{TCNE} = \{\text{C}_2(\text{CN})_4\}$ ⁶⁸, and finally,
- (iii) all the magnetic electrons arise from d orbitals. e.g. $[\text{Mn}_{12}\text{O}_{12}(\text{OAc})_{16}(\text{H}_2\text{O})_4] \cdot 2\text{AcOH} \cdot 4\text{H}_2\text{O}$.⁶⁹

Irrespective of the nature of the spin carrier, T_C (below which spontaneous magnetization occurs) is directly dependent on dimensionality as magnetic ordering is generally a 3-D phenomenon. There lies within this knowledge the problem that as dimensionality is increased some specificity of the molecular chemistry such as solubility is affected, with polymer formation returning insoluble compounds which are difficult to analyse.

Intramolecular interactions (through bonds) are much more efficient at exchange than the intermolecular interactions (through space). Therefore, a polymeric lattice will most often lead to a higher critical temperature than an assembly of separated units of the same dimensionality. The interactions are generally considered to be mediated in two different ways. It may involve a direct interaction of orbitals containing the unpaired electrons and/or a super-exchange pathway involving interaction of the d-magnetic orbitals on the metal ions via intermediate diamagnetic bridging orbitals.

The strength of coupling is directly related to the degree of favourable orbital overlap and is therefore highly dependent on several geometric variations including: -

- Dihedral angles between coordination planes
- Bridging angles
- Metal-metal separations
- Peripheral ligands

The net sign of the coupling depends on the nature of the metal to ligand, ligand to metal orbital overlap in the contributing pathway.

In summary, when two paramagnetic transition metal ions are present in the same molecular entity, the magnetic properties can be totally different from the sum of the magnetic properties of each ion surrounded by its nearest neighbours. These new properties depend on the nature and the magnitude of the interaction between the metal ions through the bridging ligands.

This field has attracted the attention of a very large number of research workers, the main reason being probably that the phenomenon of interaction between metal centres lies at the crossover point of two widely separated areas, namely the physics/chemistry of magnetic materials and the role of polynuclear reaction sites in biological processes.

1.4.1. Magnetically Dilute systems.

The magnetic susceptibility of a substance is given the symbol χ and from this comes two fundamental classifications in magneto-chemistry: -

- (i) if χ is negative the substance is then said to be diamagnetic *i.e.* it causes a reduction in the density of the lines of force equivalent to the substance producing a flux opposed to the field causing it. χ values tend to be both small and generally independent of field strength and temperature.
- (ii) if χ is positive then the substance is paramagnetic and, though generally independent of field strength, is markedly dependent on temperature (Values in the area of $10^{-5} \text{cm}^3 \text{mol}^{-1}$). Paramagnetic effects are caused by permanent magnetic dipoles within an atom or molecule whereas diamagnetism is a purely induced effect so is a universal feature of all matter and is present even when masked by overlying paramagnetism.

1.4.2. Magnetic interactions in polynuclear systems.

Ferromagnetism and anti-ferromagnetism are two important types of paramagnetism, differing from normal paramagnetism as described below:

- ferromagnetic substances can have χ values as high as $10^4 \text{ cm}^3 \text{ mol}^{-1}$, being both temperature and field dependent.
- in the case of anti-ferromagnetism χ is also T dependent and sometimes field dependent.
- both are the result of spins experiencing a parallel (ferro) or anti-parallel (antiferro) exchange field due to co-operative interactions with neighbouring spins which increase (ferro = $+J$ values) or decrease (antiferro = $-J$) values predicted by the Curie law.

Both these latter phenomena are therefore examples of “co-operative phenomena”. That is to say, they arise when the paramagnetic centres within a sample interact magnetically with each other. At the end of the nineteenth century Curie, while investigating the effects of temperature on magnetic properties, found that for paramagnetic substances χ and T are inversely proportional:

$$\chi_m = C/T$$

This is the Curie law and C is the Curie constant for the substance in question. Curie also discovered that for a ferromagnetic substance (*i.e.* a non-dilute system) there is a temperature above which normal paramagnetic behaviour occurs.

For an antiferromagnetically coupled system, the magnetic susceptibility increases with decreasing temperature until the Neel temperature (T_N) is reached, at which point it rapidly decreases with temperature. This characteristic behaviour is a result of thermal energy being sufficient to overcome aligning forces above T_N , whereas below this point the forces aligning the spins in an antiparallel fashion dominate.

For a ferromagnetic system, as the temperature is lowered the susceptibility shows a steady increase until it reaches the Curie-temperature T_C , at which point an abrupt and rapid increase in susceptibility results. The μ versus T plot shows an increase in μ as T decreases.

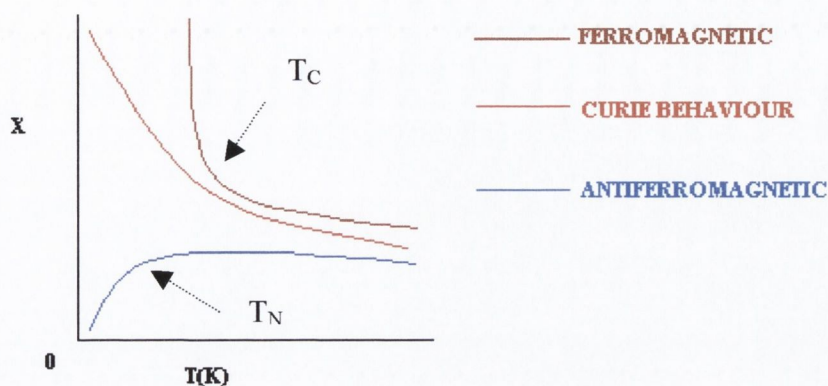


Fig 1.9. Characteristic variation of susceptibility with temperature for dilute (Curie behaviour) and interacting (Ferro and antiferromagnetic) paramagnetic materials.

1.4.3. Design strategy used in the preparation of exchange-coupled magnetic complexes.

Multimetallic species occupy an important position in modern inorganic chemistry. They are ubiquitous in nature as active sites in a variety of metalloenzymes and play a significant role from industrial chemical catalysis through to molecular magnetism. The experimental study of multimetallic complexes dates back to the discovery of Prussian blue in 1704. The traditional approach ever since has been to synthesise complexes containing two or more metal ions with their complement of terminal ligands and one or more shared entities referred to as bridging ligands (See B, Fig 1.12). The most studied of these include the simple oxo- and hydroxo- groups through to multi-atomic species such (1) oxalates⁷⁰; (2) oxamates⁷¹; (3) oxamides⁷²; azide (N₃) and thiocyanate(NCS).⁷³

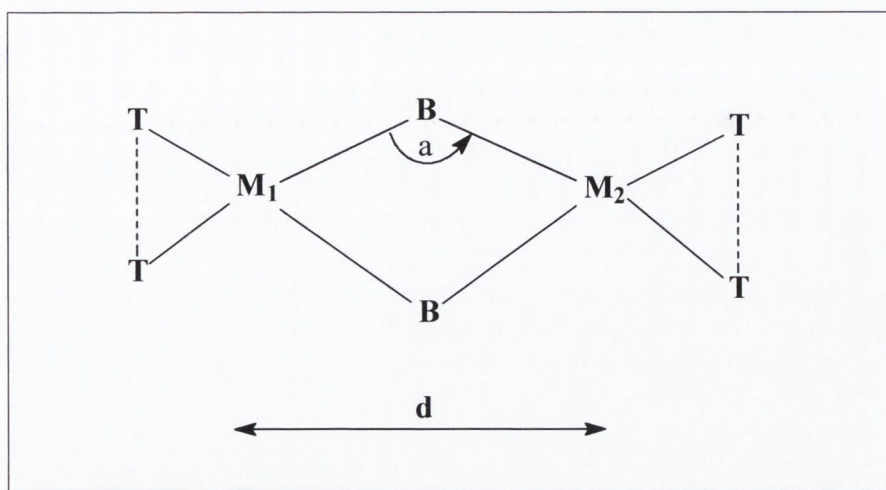


Fig 1.10. Model system used by groups such as Kahn et al and Julve et al.⁷⁴

B is bridging group, M is metal and T is terminal ligand(s). a is bridging angle and d metal-metal distance.

Seemingly slight variations in bridging angle were shown by Hodgson to cause a switch from ferro- to antiferromagnetism in the copper(II) dimeric species $[(bipyCuOH)_2]^{2+}$.⁷⁵ Kahn *et al.*⁷⁶ have made a systematic study over the past two decades of the bridging ligands (1-3) as noted above. They have illustrated the effect, not only of bridging angle, but also of terminal ligands and even the effect the electronegativities of atoms within the bridge itself have on the electronic interaction. An understanding of all the factors in Fig 1.12 is essential for the synthesis of compounds with predictable properties. For example, by systematically varying the bridging group and holding the metals and non-bridging ligands constant, the nature and extent of metal-metal communication has been studied. Also by careful choice of particular bridge properties, 2-D and 3-D networks around multimetallic complexes have been built.⁷⁷ This latter idea is an example where, by the careful selection of molecular building blocks, it is possible to influence the self-assembly processes.

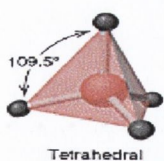
In the areas of solid state and materials chemistry much work has been carried out on group 15 oxo-anions. To date however, little work has been carried out on these anions in the field of coordination, supramolecular chemistry and magnetochemistry. With this in mind, we set about initially synthesising and characterising polynuclear Cu-phosphate complexes purely from aqueous media. Atwood *et al.* recently demonstrated that H-bonded water “clusters”

can play a role in stabilising some supramolecular species, both natural and synthetic⁷⁸ and in the formation of clathrate hydrate structures. It has also been shown that the presence of water within the lattice can have a profound influence on structure and therefore function, particularly magnetic.⁷⁹

1.5. Supramolecular chemistry.

In the past twenty years, a new discipline known as supramolecular chemistry has come to the fore. Lehn,⁸⁰ defines the field as “the chemistry of molecular assemblies and the intermolecular bond”, concerning interactions *between* rather than *within* molecules. The very word *supramolecular* means “beyond the molecule”. In this it distinguishes itself from other fields of classical chemistry in which the behaviour and properties of similar molecules of the same kind are explored. Supramolecular chemistry investigates interactions, which are weaker than the covalent bond. These include electrostatic and ion-pairing interactions between oppositely charged ionic species, hydrophobic or hydrophilic association of appropriate functional groups, hydrogen-bonding between complementary substituents, π -stacking between aromatic rings and other donor acceptor interactions between Lewis bases and Lewis acids. Supramolecular, non-covalent, synthesis consists of the generation of supramolecular architectures through the designed assembly of molecular components directed by the physico-chemical features of intermolecular forces. Like molecular, covalent synthesis, it requires strategy, planning and control. Supramolecular chemistry provides a ways and means for chemical science to explore this area of design and control especially through the concept of 'supramolecular self-assembly'.⁸¹ This latter concept concerns the spontaneous association of either a few or many components resulting in the generation of either discrete oligomolecular supermolecules or of extended polymolecular assemblies such as molecular layers, films, membranes, *etc.* Self-assembly requires molecular components containing two or more interaction sites and thus capable of establishing multiple connections.

1.5.1. Hydrogen bonds.



The explanation as to why water boils at such an elevated temperature relative to similar molecules such as hydrogen sulphide or methane was put forward by Pauling⁸² in the 1930's. He proposed that the partial charges found in water give rise to an electrical force of attraction between neighbouring molecules. This attraction is about ten times that of van der Waals forces that hold 'regular' liquids together, but ten times weaker than the bonds that link hydrogen and oxygen, for example, into discrete molecules. This attraction is a hydrogen bond and varies in strength from about 4 kJ/mol to 25 kJ/mol. The bonding is a phenomenon of hydrogen and electronegative elements, as the hydrogen atom has no inner core of electrons, so the side of the atom facing away from the bond represents a virtually naked nucleus. This positive charge is attracted to the negative charge of an electronegative atom in a nearby molecule and because the hydrogen atom in a polar bond is electron-deficient on one side (*i.e.* the side opposite from the covalent polar bond) this side of the hydrogen atom can get quite close to a neighbouring electronegative atom (with a partial negative charge) and interact strongly with it (the closer it gets, the stronger the electrostatic attraction).

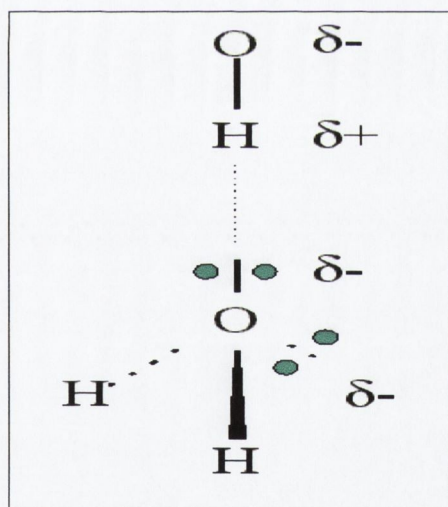


Figure 1.11. Diagrammatical representation of a H-bond.

Water is a distorted tetrahedral structure with two hydrogens and two oxygen lone pairs generating the tetrahedron with a characteristic kink at an angle of 104.5° (distorted from Plato's perfect tetrahedron of 109.5° due to lone pair-lone pair repulsions). As a liquid the

kinetic energy of the molecules prevents an extensive ordered network of hydrogen bonds. When cooled to a solid the water molecules organize into an arrangement, which maximizes the attractive interactions of the hydrogen bonds. Water is unusual in its ability to form an extensive network of hydrogen bonds. In the solid state this arrangement of molecules has greater volume (is less dense) than liquid water, thus water expands when frozen. The arrangement has a hexagonal geometry (involving six molecules in a ring structure), which is the structural basis of the six-sidedness seen in snowflakes.⁸³

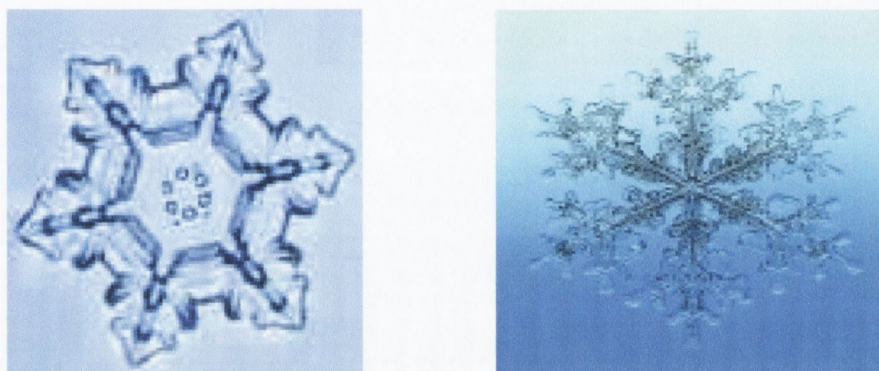


Figure 1.12. Snowflakes showing the distinct hexagonal nature of solid water.

Each water molecule can participate in four hydrogen bonds, one with each non-bonding pair of electrons and one with each H atom. This cooperation of hydrogen bonds is of great importance in biological systems.⁸⁴ They play a role in keeping a highly organised structure and to achieve highly precise biological functions such as sensing and catalyses. In DNA, for example, they provide the 'zipper' that holds the double helix together. They also secure the delicate folds of protein molecules essential to everything from energy production to the structural fabric of soft tissue. The formation of the DNA double helix is an example of a particular kind of supramolecular process known as "self-assembly". Self assembly can be described as the construction of molecular architectures⁸⁵ using molecular recognition. Substituting organic functionalities by metal containing units increases the scope and refines the degree of control over the self-assembly process. In particular the defined characteristics of a metal centre and the lability of ligands are important in the construction of molecular architectures.⁸⁶

The presence of water, during either synthesis or crystallisation, can have quite a profound influence on the resulting structures and therefore their potential functions. A basic tenet of the current study is to monitor this influence; therefore, all synthesis will be conducted in water.

1.6. Clathrate hydrate structures.

The hydrate inclusion compounds have an unusually long scientific history of ~ 170 years, with notable periods of activity in the late nineteenth century, around 1940 and again between 1950 and 1965.⁸⁷ One class of these compounds, the clathrate hydrates have had the most attention and have been examined from several different points of view. In addition to research on their preparation, stoichiometry, thermodynamic properties and crystal structures, these materials have also been studied for their technological interest; in natural gas pipe lines, in marine sediments, and as a methodology for desalination, for the fractionation and storage of gases, for the concentration of aqueous solutions, as low temperature bolometers and as infra-red detectors. There have been hypotheses concerning their role in and existence in biological systems e.g. the respiratory process of deep-sea fish.⁸⁸ There have been speculations concerning their existence in arctic ice, in other parts of the solar system (the "snows" of some planets) and the galaxy (composites in asteroids). Clathrate hydrates are also believed to exist in permafrost and marine sedimentary deposits containing natural gases. Global estimates of the methane in clathrate hydrates may exceed 10^{16} kg, which represents one of the largest sources of hydrocarbons on Earth.

Despite research dating back into the nineteenth century it wasn't until the development of the Lewis-Sedgwick theory of valence was developed that the unusual structure of the hydrates was realised. The octet theory could not predict or explain why stable molecules should combine to form these "molecular compounds". The concept which led to the understanding of the *raison d'être* for the formation and stability of these compounds was brought into focus by the work of Palin and Powell who determined the structure of the molecular compounds formed by quinol in 1947, for which they used the descriptor, *clathrate compound*.⁸⁹

In the field of chemical engineering, the hydrates made their presence known in the 1930's by blocking natural gas pipelines, in the USA and USSR, at temperatures higher than would be expected for normal ice formation. Inclusion hydration is a solid-state phenomenon, which occurs with an extraordinarily wide variety of chemical compounds. The common theme to all these hydrates is the topology of the water structure arising from the tetrahedrally coordinated oxygen atoms of the water molecules. As in the ices, each water molecule donates two and accepts two hydrogen bonds. This permits a rationalization of these hydrate structures in terms of the packing of polyhedra, which requires the sharing of each polyhedra face and at least four edges meeting at every vertex (See appendix B).

The analogy between these hydrate structures and that of ice is a consequence of the topological property that H_2O can form three-dimensional four-connected nets. Indeed the ability to form these solid crystalline compounds is a characteristic property of water.⁹⁰ It is not a unique property, however. Analogous crystal structures to these $(\text{H}_2\text{O})_n$ lattices are not only found in some silicates but are also formed by arsenide, and phosphide with the halide as the included species.⁹¹ In principle therefore, similar inclusion lattices could be formed with carbon or any combination of elements, which form tetrahedral four-connected network structures.

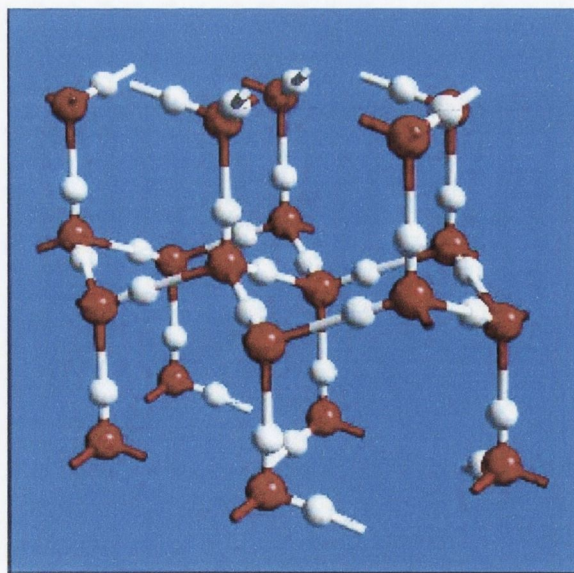


Figure 1.13. Hexagonal ice showing four-connected network.

From the point of view of the structural chemist, clathrate hydrates exist because water molecules can crystallize in such a way as to form a *host* lattice which can physically enclose, on an atomic scale, other molecules, appropriately referred to as guests. The water structure of the clathrate hydrate has much in common with the ice, *i.e.* it is "ice-like". As in ice, each water oxygen is four-coordinated. It has four nearest neighbour oxygen to which it is linked by four hydrogen bonds, two donor and two acceptor. For normal hexagonal ice, I_h , and cubic ice, I_c , this coordination is tetrahedral. In the clathrate hydrates, the oxygen is also tetrahedral, but not as regular as in hexagonal or cubic ice. Both the ices and the clathrate "ice-like" structures contain polyhedral cavities. These cavities tend to be larger in the clathrate structures than in ice. This is the reason they are not ices since the diameter of these voids are greater than the van der Waals diameter of the non-hydrogen-bonded oxygen atoms. The voids are therefore subject to collapse unless the "guest" molecules occupy them. There are two principal limitations to the chemical nature of the guest molecules. The first is that they do not contain either a strong hydrogen -bond functional group, or a number of moderately strong hydrogen-bonding groups. Thus, amides and carboxylates do not form inclusion compounds, yet amines and ethers do. The clathrates are therefore structures where there are no hydrogen-bonding interactions between the guest species and the host framework. The second limitation is dimensional. Most sufficiently hydrophobic molecules form clathrate hydrates. This dimensional requirement is not as rigid as it is when covalent or ionic-bonded atoms, as in the silicate and silicon clathrates, form the host lattice.

Recent research on clathrate hydrates has focused on how water clusters can play a role in the stabilization of supramolecular systems both in solution and in the solid state with a view to better understanding, how these aggregates influence the overall structure of their surroundings, especially in biological systems.⁹²

If a single molecule were to be selected as the most important chemical entity for life, most people would agree that this is water. Yet, the nature of water-water interactions in diverse environments is still a subject of considerable theoretical and experimental scrutiny.⁹³ A detailed understanding of the numerous possible structures and stabilities of water "cages" is therefore vital to generate these insights. Enclosing the "guest" molecules that contain

bio-mimetic properties (e.g. transition metal complexes relating to bio-enzymes) can be of great value in understanding waters role in the organization of biological species.

1.7. Present Study.

Our inspiration comes from a desire to develop magnetic materials and to build systems of biomimetic interest involving d-block metal ions. Of particular interest to the current presentation is the synthesis, structural and magnetic characterisation, of various polynuclear Cu(II) systems. Bridging between the Cu(II) centres is furnished by group 14 (CO_3^{2-}) and 15 (PO_4^{3-} , $\text{P}_2\text{O}_7^{4-}$ and H_2AsO_4^-) and oxo-anions as well as the hydroxo- group (OH^-). By utilizing processes such as spontaneous self-assembly, we have been able to isolate many interesting and diverse structural types, including water 'clathrates' and supra-molecular pseudo-polymorphs. Through the manipulation of solvent pH, we have been able to routinely fix CO_2 (as CO_3^{2-}) in several guises, and to study the impact its coordination mode has, for example, on the resultant structural and magnetic properties. Interesting insights into the role played by the metal ion has been gleaned from replacement of the copper(II) ions with oxovanadium(IV) and Zn(II) especially in regard to obtaining information about the coordinating ability of pyrophosphate and the identity of the compounds in aqueous solution.

References

1. A.C. Benniston, *Chem. Soc. Rev.*, **6**, 427, 1996 and references therein.
2. a) F.G. Gatti, D.A. Leigh, S.A. Nepogodiev, A.M.Z. Slawin, S.J. Teat and J.K.Y. Wong, *J. Am. Chem. Soc.*, **25**, 5983, 2001.
3. J. Nelson, V. Mckee and G. Morgan, *Prog. Inorg. Chem.*, **47**, 167, 1998 and references therein.
4. a) C. Piguet, G. Bernardinelli and G. Hopfgartner, *Chem. Rev.*, **97**, 2005, 1997.; b) A.F. Williams, *Chem. Eur. J.*, **3**, 15, 1997.
5. K.A. Jolliffe, P. Timmerman and D.N. Reinhoudt, *Angew. Chem. Int. Ed.*, **38**, 933, 1999 and references therein.

6. a) M. Schweiger, S.R. Seider, A.M. Arif and P.J. Stang, *Angew. Chem. Int. Ed.*, **40**, 3467, 2001.; b) Z.F. Chen, R.G. Xiong, J. Zhang, J.L. Zuo, X.Z. You, C.M. Che and H.K. Fun, *J. Chem. Soc., Dalton Trans.*, **22**, 4010, 2000.
7. R.W. Saalfrank, I. Bernt and F. Hampel, *Chem. Eur. J.*, **13**, 2770, 2001.
8. a) E.C. Constable, O. Eich, D. Fenske, C.E. Housecroft and L.A. Johnston, *Chem-Eur. J.*, **23**, 4364, 2000.; b) E.C. Constable, O. Eich, C.E. Housecroft and D.C. Rees, *Inorg. Chim. Acta.*, **300**, 158, 2000.
9. a) R.K.R. Jetti, F. Xue, T.C.W. Mak and A. Nangia, *J. Chem. Soc., Perkin Trans 2*, **6**, 1223, 2000.; b) C. Seel and F. Vogtle, *Chem. Eur. J.*, **6**, 21, 2000.
10. a) K.J. Koch, F.C. Gozzo, D.X. Zhang, M.N. Eberlin and R.G. Cooks, *Chem Commun.*, 1854, 2001.; b) B. Salignac, S. Riedel, A. Dolbecq, F. Secheresse and E. Cadot, *J. Am. Chem. Soc.*, **42**, 10389, 2000.
11. *Inclusion Compounds*, J.L. Atwood, J.E.D. Davies and D.D. MacNicol, Academic Press, London, **1984**.
12. V. Balzani, P. Ceroni, A. Juris, M. Venturi, S. Campagna, F. Punteriero and S. Serroni, *Coord. Chem. Rev.*, **219**, 545, 2001.
13. *Molecular Magnetism*, O. Kahn, VCH, New York, **1993**.
14. *Principles of bioinorganic chemistry*, S.J. Lippard and J.M. Berg, USB, California, **1994**.
15. a) M. Fontecave and J.L. Pierre, *Coord. Chem. Rev.*, **170**, 125, 1998 and references therein. b) V.S.I. Sprakel, M.C. Feiters, R.J.M. Nolte and K.D. Karlin, *J. Inorg. Biochem.*, 441, 2001.
16. M. Melnik, M. Kabesova, M. Koman, L. Macaskova and C.E. Holloway, *J. Coord. Chem.*, **3**, 177, 2000.
17. I.B. Bersuker, *Coord. Chem. Rev.*, **14**, 357, 1975.
18. a) M.J. Henson, V. Mahadevan, T.D.P. Stack and E.I. Solomon, *Inorg. Chem.*, **40**, 5068, 2001. b) R.H. Holm, P. Kennepohl and E.I. Solomon, *Chem. Rev.*, **96**, 2239, 1996.
19. K. Brown, M. Tegoni, M. Prudencio, A.S. Pereira, S. Besson, J.J. Moura, I. Moura and C. Cambillau, *Nat. Struct. Biol.*, **3**, 191, 2000.
20. a) S. Ferguson-Miller and G.T. Babcock, *Chem. Rev.*, **96**, 2889, 1996.; b) K.D. Karlin, Z. Tyeklar, A. Farooq, M.S. Haka, P. Ghosh, R.W. Cruse, Y. Gultneh, J.C.

- Hayes, P.F. Toscano and J. Zubieta, *Inorg. Chem.*, **32**, 1436, 1992.; c) C. Harding, V. McKee and J. Nelson, *J. Am. Chem. Soc.*, **113**, 9684, 1991.
21. *Copper Proteins and Enzymes*, R. Lontie (Ed.), CRC Press, Boca Raton, Florida, Vols. 1-3, **1984**.
22. a) R. Ruiz, J. Faus, F. Lloret, M. Julve and Y. Journaux, *Coord. Chem. Rev.*, **193**, 1069, 1999.; b) K.S. Murray, *Adv. Inorg. Chem.*, **43**, 261, 1995.
23. B.J. Hathaway in *Comprehensive Coordination Chemistry*, G. Wilkinson, R.D. Gillard and J.A. McCleverty (Eds.), Pergamon Press, Oxford, **1987**.
24. a) E. Ruiz, P. Alemany, S. Alvarez and J. Cano, *Inorg. Chem.*, **36**, 3683, 1997.; b) E. Ruiz, P. Alemany, S. Alvarez and J. Cano, *J. Am. Chem. Soc.*, **119**, 1297, 1997.
25. *Bioinorganic Chemistry of Copper*, K.D. Karlin and Z. Tyeklar (Eds.), Chapman and Hall, New York, **1993**.
26. a) M. Melnik, M. Kabesova, M. Koman, L. Macaskova and C.E. Holloway, *J. Coord. Chem.*, **48**, 271, 1999. a) U. Casellato, P.A. Vigato and M. Vidali, *Coord. Chem. Rev.*, **23**, 31, 1977.; b) P.A. Vigato, S. Tamburini and D.E. Fenton, *Coord. Chem. Rev.*, **106**, 25, 1990.
27. a) D.E. Fenton and H. Okawa, *J. Chem. Soc., Dalton Trans.*, 1349, **1993**.; b) A. Messerschmidt, *Adv. Inorg. Chem.*, **40**, 121, 1993.
28. F. Akagi, Y. Nakao, K. Matsumoto, S. Takamizawa, W. Mori and S. Suzuki, *Chem. Lett*, **2**, 181, 1997.
29. K.D. Karlin, R.A. Ghiladi, K.M. Kovalski, E.E. Chufan and E.S. Kim, *J. Inorg. Biochem.*, **69**, 60, 2001.
30. K.J. Humphreys, K.D. Karlin and S.E. Rokita, *J. Am. Chem. Soc.*, **123**, 5588, 2001.
31. L. Zhao, L.K. Thompson, Z.Q. Xu, D.O. Miller and D.R. Stirling, *J. Chem. Soc., Dalton Trans.*, **11**, 1706, 2001.
32. S. Meenakumari, S.K. Tiwary and A.K. Chakravarty, *Inorg. Chem.*, **33**, 2085, 1994.
33. L. Gutierrez, G. Alzuet, J. A. Real, J. Cano, J. Borrás and A. Castiñeiras, *Inorg. Chem.*, **39**, 3608, 2000.
34. R.E. Caputo, M.J. Vukosavovich and R.D. Willett, *Acta Crystallogr., Sect. B*, **32**, 2516, 1976.
35. A.P. Purdy, C.F. George and G.A. Brewer, *Inorg. Chem.*, **31**, 2633, 1992.
36. C.A. Bear, J.M. Waters and T.N. Waters, *J. Chem. Soc., Dalton Trans.*, 1059, 1974.

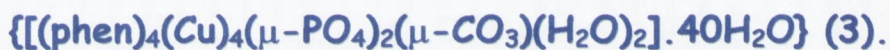
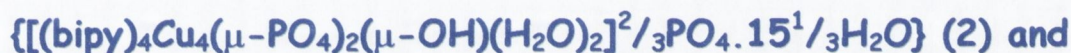
37. G. Kolks and S.J. Lippard, *Acta Cryst.*, Sect. C, **40**, 261, 1984.
38. V. McKee and S.S. Tandon, *J. Chem. Soc., Chem. Comm.*, 385, 1988.
39. R. Belford, D.E. Fenton and M.R. Truter, *J. Chem. Soc., Dalton Trans.*, 2345, 1972.
40. C.J. O'Connor, R.J. Butcher and E. Sinn, *Inorg. Chem.*, **20**, 537, 1981.
41. W.J. Evans and J.H. Hain, *Mater. Res. Soc. Symp. Proc.*, **180**, 39, 1990.
42. K.D. Karlin, Q-F. Gan, H. Farooq, S. Liu and J. Zubieta, *Inorg. Chem.*, **29**, 2549, 1990.
43. P.E. Kruger, G.D. Fallon, B. Moubaraki, K.J. Berry and K.S. Murray, *Inorg. Chem.*, **34**, 4808, 1995.
44. S.S. Tandon, L.K. Thompson and J.N. Bridson, *J. Chem. Soc., Chem. Comm.*, 911, 1992.
45. *Chemistry of the Elements*, N.N. Greenwood and A. Earnshaw, Butterworth-Heinemann, Oxford, p600-601, **1984**.
46. S.T. Wilson, B.M. Lok, C.A. Messian, T.R. Cannon and E.M. Flanigen, *J. Am. Chem. Soc.*, **104**, 1146, 1982.
47. a) J.M. Thomas, *Angew. Chem. Int. Ed.*, **106**, 963, 1994.; b) M. Hartmann and L. Kevan, *Chem. Mater.*, **99**, 635, 1999.
48. G. Feray, T. Loiseau and A.K. Cheetham, *Angew. Chem. Int. Ed.*, **38**, 326, 1999.
49. a) E. Bordes and P. Courtine, *J. Chem. Soc., Chem. Comm.*, 294, 1985.; b) N. Herron, D.L. Thorn, R.L. Harlow and G.W. Coulston, *J. Am. Chem. Soc.*, **119**, 7149, 1997.
50. J. Klinowski, *Curr. Opin. Solid State Mater. Sci.*, **3**, 79, 1998.
51. J. W. Richardson Jr, J.J. Pluth and J.V. Smith, *Naturwiss.*, **76**, 467, 1989.
52. *The Biochemistry of Inorganic Polyphosphates*, I.S. Kulaer, Wiley, Chichester, **1980**.
53. Cambridge Structural Database, Cambridge, U.K, Version 5.22, Oct. **2001**.
54. A. Muller-Hartman and H. Vahrenkamp, *Eur. J. Inorg. Chem.*, 2355, 2000.
55. J.E. Sarneski, M. Didiuk, H.G. Thorp, R.H. Craptree, G. W. Brudvig, J.W. Fallar and G.K. Schulte, *Inorg. Chem.*, **30**, 2833, 1991.
56. C. Ferragina, M. Massucci, A. La Ginestra, P. Patrono and A.A.G. Tomlinson, *J. Chem. Soc., Chem. Comm.*, 1024, 1984.
57. C.H. Huang, L.H. Huang and K.H. Lii, *Inorg. Chem.*, **40**, 2645, 2001.
58. Z.A.D. Lethbridge, A.D. Hillier, R. Cywinski and P. Lightfoot, *J. Chem. Soc., Dalton Trans.*, 1595, **2000**.

59. F.H. Nielsen in *The Cambridge World History of Food*, Vol. 1., K.F. Kiple, K.C. Ornelas, (Eds.), Cambridge University Press, Madrid, 856, **2000**.
60. E.P. Marina, PhD Thesis, University of Barcelona, **1997**.
61. a) K. V. Krishnamurty, G. M. Harris and V. S. Sastri, *Chem. Rev.*, **2**, 171, 1970.; b) A. Escuer, R. Vicente, S. B. Kumar, X. Solans and M. Font-Bardia, *J. Chem. Soc., Dalton Trans.*, 403, 1997 and references therein.
62. J.E. Coleman, *Nature*, **214**, 193, 1967.
63. D.A. Palmer and R. van Eldik, *Chem. Rev.*, **83**, 651, 1983.
64. N. Kitajima, S. Hikichi, M. Tanaka and Y. Moro-oka, *J. Am. Chem. Soc.*, **115**, 5496, 1993.
65. N. Kitajima, K. Fujisawa, T. Koda, S. Hikichi and Y. Moro-oka, *J. Chem. Soc., Chem. Comm.*, 1357, **1990**.
66. a) Research Frontiers in *Magnetochemistry*, C.J. O'Connor (Ed.), World Scientific, Singapore, **1993**.; b) P. Day, *Science*, **261**, 431, 1993.;
67. J. A. Crayson, J. N. Devine and J.C. Walton, *Tetrahedron*, **56**, 7829, 2000 and references therein.
68. J.M. Manriquez, G.T. Yee, R.S. McLean, A.J. Epstein and J.S. Miller, *Science*, 252, 1415, **1991**.
69. R. Sessoli, D. Gatteschi, A. Caneschi and M.A. Novak, *Nature*, **365**, 141, 1993.
70. S. Alvarez, M. Julve and M. Verdaguer, *Inorg. Chem.*, **29**, 4500, 1990.
71. O. Kahn, *Acc. Chem. Res.*, **10**, 647, 2000 and references therein.
72. a) R. Ruiz, J. Faus, F. Lloret, M. Julve and Y. Journaux, *Coord. Chem. Rev.*, **193**, 1069, 1999.; b) K. Nakatani, J.Y. Carriat, Y. Journaux, O. Kahn, F. Lloret, J.P. Renard, Y. Pei, J. Sletten and M. Verdaguer, *J. Am. Chem. Soc.*, **111**, 5739, 1989.
73. S. Decurtins, H. Schmalle, G. Francese and S. Ferlay, *Inorg. Chim. Acta.*, **286**, 108, 1999.
74. a) Y. Pei, O. Kahn, K. Nakatani, E. Codjovi, C. Mathoniere and J. Sletten, *J. Am. Chem. Soc.*, **113**, 6558, 1991.; b) F. Lloret, M. Julve, R. Ruiz, Y. Journaux, K. Nakatani, O. Kahn and J. Sletten, *Inorg. Chem.*, **32**, 27, 1993.
75. a) W.E. Hatfield, J.R. Wasson, H.W. Richardson, W.H. Crawford and D.J. Hodgson, *Inorg. Chem.*, **15**, 2107, 1976.; b) *Magneto-Structural Correlations in Exchange*

- Coupled Systems*, R.D. Willet, D. Gatteschi and O. Kahn (Eds.), D. Reidel, Dordrecht, **1984**.
76. O. Kahn, *Angew. Chem. Int. Ed.*, **24**, 834, 1985.
77. J. Hye and P.S. Myungghyun, *J. Am. Chem. Soc.*, **120**, 10622, 1998.
78. J.L. Atwood, G.W. Orr and L.J. Barbour, *Nature*, **393**, 671, 1998.
79. a) P.E. Kruger, R.P. Doyle, M. Julve, P. Lloret and M. Nieuwenhuyzen, *Inorg. Chem.*, **40**, 1726, 2001.; b) O. Kahn, J. Larionova and J.V. Yakhmi, *Chem. Eur. J.*, **12**, 5, 1999.
80. *Supramolecular Chemistry*, Jean-Marie Lehn, VCH, Weinheim, **1995**.
81. J.S. Lindsey, *New J. Chem.*, **15**, 153, 1991.
82. *The Nature of the Chemical Bond*, Linus Pauling, Cornell University Press, **1948**.
83. *Morphology of Crystals Part B*, T. Kobayashi and T. Kuroda, Terra Scientific, **1987**.
84. *Comprehensive Supramolecular Chemistry*, J.L. Atwood, J.E.D. Davies, D.D. MacNicol and F. Vögtle (Eds.), Vol. 9, Elsevier, Oxford, **1996**.
85. J.F. Stoddart, *Angew. Chem. Int. Ed.*, **35**, 1154, 1996.
86. B. Olenyuk, A. FechtenKolter and P.J. Stang, *J. Chem. Soc., Dalton Trans.*, **11**, 1707, 1998.
87. *Inclusion Compounds.*, J.L. Atwood and P. Davies, (Eds.), Vol. 1, p135, **1984**.
88. *Structural Inorganic Chemistry*, A.F. Wells, Clarendon, Oxford, 5th Ed., **1984**.
89. a) D.E. Palin and H.M. Powell, *J. Chem. Soc.*, 208, 1947.; b) D.E. Palin and H.M. Powell, *J. Chem. Soc.*, 815, 1948.
90. G.A. Jeffrey in *Inclusion Compounds*, J.L. Atwood, J.E.D. Davies and D.D. MacNicol (Eds.), Academic Press, London, Chap. 5, **1984**.
91. a) *The Third Dimension in Chemistry*, A.F. Wells, Oxford University Press, New York, **1956**.; b) J.S. Kasper, P. Hagenmuller, M. Pouchard and C. Cros, *Science*, **150**, 1713, 1965.; c) C. Cros, M. Pouchard and P. Hagenmuller, *J. Solid State Chem.*, **2**, 570, 1970.
92. J.L. Atwood, G.W. Orr and L.J. Barbour, *Chem. Commun.*, 859, 2000.
93. R. Ludwig, *Angew. Chem. Int. Ed.*, **40**, 1808, 2001.

Chapter Two

Preparation and magneto-structural correlations in polynuclear copper(II) complexes incorporating trianionic phosphate (PO_4^{3-}),



Introduction

Multimetallic copper(II) species occupy an important position in modern inorganic and materials chemistry. They are ubiquitous in nature as active sites in a variety of metallo-enzymes and this recognition has fuelled the development of numerous low molecular weight model compounds.¹ The active sites are usually associated with enzymes that participate in multi-electron transfer reactions, a pertinent example being that of the tetranuclear copper cluster of the catalytic enzyme 'Nitrous oxide reductase' (N2OR)². The structure of N2OR reveals four Cu(II) ions ligated by seven histidine residues with N₂O binding to the cluster via a single copper ion. This facilitates the two-electron reduction of N₂O to N₂. Copper is also present in one of the most studied of all enzymes namely, Cytochrome C oxidase. This latter enzyme uses copper, as well as Heme iron, to participate in the 4-electron reduction of dioxygen to water. This process is one of the most indispensable components in the biochemical machinery of aerobic lifeforms.^{1c}

Whilst many examples are known of mono- and dinuclear copper complexes³, tetranuclear and hexanuclear species are far less well explored. A pertinent example however has been reported by Julve *et al.*, who have made a study of cubane type tetranuclear copper clusters: the complex [Cu(bipy)(OH)₄(PF₆)₄], for example, contains a hydroxo-bridged [Cu₄OH₄]⁴⁺ tetrameric unit with bipyridine ligands completing the coordination sphere⁴. In agreement with the structure-function relationship of Hatfield and Hodgson⁵ whereby the Cu-OH-Cu bridging angle dictates the sign of J , ($\varphi > 97.5^\circ = -J = \text{Antiferromagnetic}$; $\varphi < 97.5^\circ = +J = \text{Ferromagnetic}$), where J is the singlet-triplet energy gap, they report a bridging angle of $\sim 96.4^\circ$ and therefore predict (and observe) a ferromagnetic exchange interaction between Cu(II) centres. The ferromagnetic hexanuclear copper(II) complex reported by Murray *et al.*⁶ [(Cu)₆(Bipy)₁₀(μ -CO₃)₂(μ -OH)₂](ClO₄)] is also based on this system of hydroxy bridged copper atoms with an average Cu-OH-Cu bridging angle of 95.1° . The deliberate controlled assimilation of this ferromagnetic hydroxy-bridging unit into a tetranuclear metallo-cluster to specifically tailor function, is thus of particular interest for elucidating structure-function relationships in larger systems. Direct replacement of one bridging group with another, may allow the relationship between magnetic behaviour, geometry and electronic structure to be considered. In the areas of solid state and materials chemistry much work has been carried

out on group 15 oxo-anions.⁷ To date, however, little work has been done with these anions in the field of coordination and magneto-chemistry. The trianionic inorganic phosphate anion (PO_4^{3-}) for example, is interesting as a geometrically defined molecular synthon that could be used in the preparation of multimetallic complexes. The ubiquity of phosphate in Nature, (from enzymes such as ATPases and Kinases to the phosphodiester backbone of nucleic acids),⁸ make it an intriguing ligand from a number of standpoints. Phosphate ions are well documented as being capable of bridging metal centres and are of particular interest for modelling the active sites of enzymes such as Uteroferrin.⁹ Combined with this is the knowledge that divalent metal ions play an important role with regard to both the stabilisation of phosphates in the solid state and in solution as well as in the activation of phosphates for hydrolytic cleavage.¹⁰ In fact all known enzymes that transfer phosphate units (e.g. Kinases) require metal ions for their function. It has been suggested that during enzymatic action the phosphate is coordinated to a metal ion or ions in the active centre.¹¹ Phosphate is also a ligand potentially capable of magnetic super-exchange between paramagnetic metal centres. Hendrickson *et al.*¹² postulated in the late 1970's about phosphates tetrahedral geometry facilitating ferromagnetic exchange interactions between copper(II) ions, but little subsequent work has followed. In valence bond terms the phosphorous atom in PO_4^{3-} employs sp^3 hybrid orbitals to bond to each oxygen. Hendrickson proposed that if a PO_4^{3-} ion bridges between two copper(II) ions, with each centre interacting with one oxygen atom, then the orthogonality that could result should precipitate a net ferromagnetic interaction. This is all clear incentive to study the coordination chemistry of phosphates (and polyphosphates) from both a structural and functional viewpoint, especially in combination with divalent metal ions.

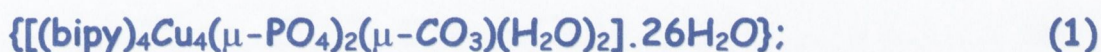
Two ligands that have been well explored in the literature are 2,2'-bipyridine (bipy) and 1,10-phenanthroline (phen).¹³ The use of these versatile ligands has resulted in a myriad of interesting polynuclear systems incorporating many different transition metal ions. Their use as 'terminal ligands' has been well documented and their hydrophobic nature means they make excellent molecular building blocks when used to contrast hydrophilic groups also introduced into the system, so adding to the process of 'informed design'. In fact Christou *et al.*¹⁴, and Hunter *et al.*¹⁵, have postulated that it is the π - π stacking in some complexes that

actually generates and maintains their structural integrity through attractive aromatic ring stacking interactions.

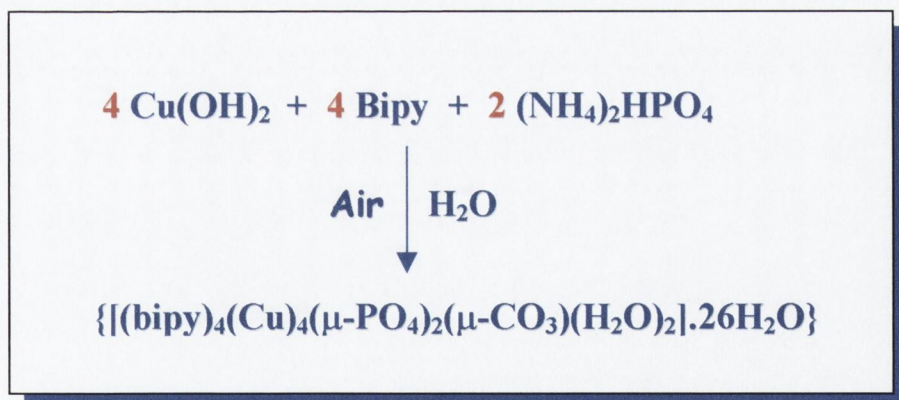
Within the present study we wished to incorporate the aforementioned properties and generate, through 'self-assembly', multinuclear copper complexes through careful control of reaction conditions. The ultimate aim is to produce molecular magnetic materials¹⁶ capable of spontaneous magnetic ordering while studying structure-function correlation at the same time.

2.1. Preparation and Characterisation of the tetranuclear copper

(II) complex :



An aqueous suspension of copper (II) hydroxide ($\text{Cu}(\text{OH})_2$) was reacted with the chelating ligand 2,2'-bipyridine, followed by addition of ammonium hydrogen phosphate ($(\text{NH}_4)_2\text{HPO}_4$) in the overall molar ratio of 2:2:1. A deep blue solution results over ~ 5 minutes and after a period of two weeks deep-royal blue crystals are obtained by slow evaporation.



Scheme 2.1. Direct preparation of the tetranuclear species (1).

Elemental analysis (C:H:N) indicated the structure to be one that had previously reported in a recent doctoral theses¹⁷ and assigned as having the structure recorded as (1) above. The

previously reported structure was structurally of relatively low precision and the precise identity of the bridging 'oxo' species poorly characterised ($R = 0.141$). The current study undertook to definitively assign the bridging 'oxo' species and ensure full characterisation of the complex was ascertained. The infrared spectrum of **(1)** contained two sharp absorption bands at 1524 cm^{-1} and 1316 cm^{-1} , which are consistent with the presence of carbonate.¹⁸ The carbonate having arisen through the fixation of dissolved carbon dioxide within the aqueous solution or already absorbed by exposed copper hydroxide used as starting material. The basic medium (reaction pH is recorded as 10) enhances nucleophilic attack of the $\text{Cu}(\text{OH})_2$ on the electrophilic carbon of CO_2 , which is then followed by water dissociation. Such a reaction is not without precedent in the literature for copper as well as other transition metals.¹⁹ The remainder of the infrared spectrum is dominated by absorption bands from the bipyridine ligands ($1655, 1603, 1569, 783\text{ cm}^{-1}$) and by inorganic phosphate ($\nu(\text{P}=\text{O}) 1166, \nu(\text{P}-\text{O}-\text{M}) 1056, 1029\text{ cm}^{-1}$). The d-d spectrum of an aqueous solution of **(1)** exhibits a very broad and featureless band centred at 687 nm , which is consistent with the presence of a distorted square-pyramidal nature about the $\text{Cu}(\text{II})$ chromophore.²⁰ Electrospray mass spectroscopy of an aqueous solution of **(1)** showed only peaks indicative of fragmentation. The overall coordinate neutrality of the complex means the complex must be ionised in the mass spectrometer to be detected. This process probably results in an unstable ion, which then fragments. Single crystal X-ray diffraction showed the structure to be, as postulated, a complex previously reported.¹⁷ As mentioned earlier conclusive assignment had not been previously achieved however and the current study allows definitive structural assignment. The extensive number of water molecules per asymmetric unit in **(1)** had also not previously been elucidated nor the importance this water has in the overall structure of **(1)**.

2.2. Description of the molecular structure of the tetranuclear copper(II) complex:



A royal-blue plate-like crystal obtained from an aqueous solution was used for a single crystal X-ray diffraction study. Dr. M. Nieuwenhuyzen of the Queens University, Belfast, performed the data collection and structural refinement. Complex (1) is depicted in Figure 2.1, showing the atomic numbering scheme used. The molecule crystallizes in space group Pnna.

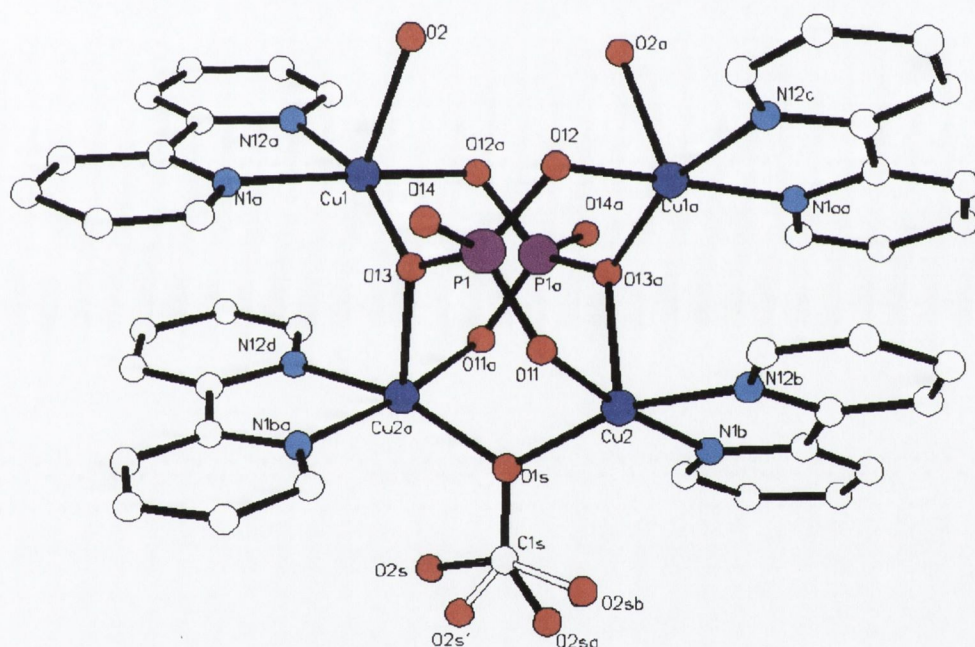


Figure 2.1. $\{[(\text{Cu})_4(\text{bipy})_4(\mu\text{-PO}_4)_2(\mu\text{-CO}_3)(\text{H}_2\text{O})_2]\cdot 26\text{H}_2\text{O}\}$ (1).

Waters of crystallization and hydrogen atoms are omitted for clarity. Carbonate bridge is disordered about the C_2 axis present in (1).

The crystal becomes amorphous through solvent loss upon removal from the mother liquor, so data collection was carried out at low temperature. The structure is of relatively high

precision with $R = 0.0524$. The molecular geometry of the complex consists of four square-pyramidally disposed copper atoms, coordinated by four bipyridyl ligands and bridged by two inorganic tetrahedral phosphate (PO_4^{3-}) groups. Additional bridging between Cu(2) and Cu(2a) is furnished by the carbonate species CO_3^{2-} , which is disordered about the 2-fold axis in **(1)**. A survey of the Cambridge Structural Database (CSD)²¹ indicates that the carbonato- group has been structurally characterised to adopt many coordination modes, most of which are bridging. Coordination around Cu(1) is furnished by two bipyridyl nitrogen donors, namely N(1a) and N(12a). Coordination also occurs with two phosphato-oxygen's, O(12a) from P(1a) and O(13) from P(1). These form the basal plane of the square-pyramid, with bound water (O(2)) occupying the apical position. Cu(2) is coordinated by two bipyridyl nitrogens N(12b) and N(1b) with phosphato-oxygen O(11) and the corner shared μ -carbonato oxygen O(1s) completing the basal plane. Axial coordination to Cu(2) is provided by the bridging phosphate-oxygen, O(13a). These axial bond lengths, as well as those to the apically bound water molecules, are significantly longer than the equatorial bond lengths within **(1)**. This axial elongation is a common feature of copper(II) complexes as a result of Jahn-Teller distortion. The copper centres sit slightly above the basal plane towards the axially coordinated donors (Cu(1) 0.0164, Cu(2) 0.1659 Å). This distortion probably results from a combination of the restricted bite angle of the bipyridine ligands, the tetrahedral nature of the phosphate-bridging group and from the system attempting to optimise π - π stacking interactions between bipyridine ligands. The phosphate groups exhibit both mono- and tri-atomic bridging modes. This results in an intricate array of inter-connected copper atoms, such that Cu(1) and Cu(1a) are doubly tri-atomically bridged to each other, and Cu(2) and Cu(2a), and further linked mono-atomically to Cu(2) and Cu(2a). In addition, Cu(2a) is triply bridged to Cu(2) by two tri-atomic phosphate linkages and mono-atomically by the carbonate group. As a consequence Cu(1) and Cu(1a) are participating in six bridging interaction, whilst Cu(2) and Cu(2a), as a result of the additional carbonate-bridge between them, partake in seven such interactions.

Table 2.1. Selected bond distances (Å) and angles (°) for (1).

Cu(1)-O2	2.322(4)	O(12a)-Cu(1)-O(13)#1	93.3(1)
Cu(1)-O12a	1.938(3)#1	O(13)-Cu(1)-N(1a)	91.9(2)
Cu(1)-O13	1.937(3)	Cu(1)-O(13)-Cu(2a)	96.4(3)
Cu(1)-Cu(1a)	4.388(7)#1	N(1a)-Cu(1)-N(12a)	80.2(2)
Cu(1)-Cu(2a)	3.529(7)	O(13)-Cu(1)-N(12A)	161.1(2)
Cu(1)-Cu(2)	5.011(7)		
Cu(2)-O13a	2.413(7)#1	O(11)-Cu(2)-O(1s)	92.0(1)
Cu(2)-O11	1.914(3)	Cu(2)-O(1s)-Cu(2a)	122.7(3)
Cu(2)-O1s	1.952(2)	N(1b)-Cu(2)-O(11)	171.1(2)
Cu(2)-Cu(2a)	3.426(7)		

Estimated standard deviations are given in the parenthesis.

Symmetry operator:

1: $x, -y + \frac{1}{2}, -z + \frac{1}{2}$

The four copper atoms are disposed in a slightly buckled trapezoidal arrangement with respect to each other. The resulting metal-metal separations are listed in table 2.1. Bridging between Cu(1) and Cu(2a), through the phosphato- oxygen O(13) is asymmetric in nature [Cu(1)-O(13) 1.937 Å ; Cu(2a)-O(13) 2.413 Å], reflecting basal versus axial disposition at Cu(1) and Cu(2a), respectively. The Cu(1)-O(13)-Cu(2a) bridging angle is 96.4°.

The bipyridine ligands do not show any significant deviations from the mean planes with average carbon-carbon and carbon-nitrogen bond lengths close to those reported for uncoordinated 2,2'-bipyridine.²² The positioning of the bipy groups facilitates both inter and intramolecular π - π stacking interactions with separations of ~3.4 Å and a dihedral angle of 4.1° between stacked ligands. This attractive interaction of bipyridine groups in this face-to-face conformation is commonly observed in supramolecular motifs,¹⁵ with the arrangement best described as *offset stacking*. This *offset stacking* describes a favourable near-parallel face-to-face arrangement and is more stable since it minimises π -electron repulsion. The flat

π -electron surfaces associated with aromatic molecules in general are non-polar so that solvatophobic forces favour as much stacking as possible. So a balance is met in the form of an *offset* topology. The aromatic stacking generates the shortest Cu-Cu separation, namely between Cu(1)-Cu(2a) Å. For the rings to stay parallel the Cu-Cu separations must also be ~ 3.4 Å and this is achieved by adoption of a bridging angle of 122.7° between Cu(2a)-Cu(2), bridging through oxygen O(1s) of the carbonate moiety. This gives a M-M separation of 3.426 Å. The tetrahedral nature of the bridging phosphate however, combined with a large bite angle, precludes Cu-Cu separation spanning just 3.4 Å. In fact the Cu(1)-Cu(1a) distance is 4.328 Å. This has the effect of tilting the bipy rings away from each other, thereby strengthening the stacking interaction as a result of this *offsetting*. This process is also the cause of the distorted nature of the copper coordination sphere (combined with the restricted bite angle of the bipyridine ligand) and the reason the copper atoms adopt a square-pyramidal geometry with the copper atoms slightly out of the N_2O_2 basal planes.

Complex **(1)** crystallizes with 13 water molecules per asymmetric unit (26 in total per molecule). The combination of hydrophilic (PO_4^{3-} , CO_3^{2-} , Cu^{2+}) and hydrophobic (bipy) groups in **(1)** has a dramatic effect upon the way the molecule packs intermolecularly. In fact a distinct hydrophilic region exists within **(1)** as the lattice waters more closely associate, through H-bonding, with the phosphate, carbonate and apically bound water molecules (See over). An infinite 3-dimensional array is thus formed, held together by an extensive hydrogen-bonding network involving both the coordinated and non-coordinated (lattice) water molecules.²³

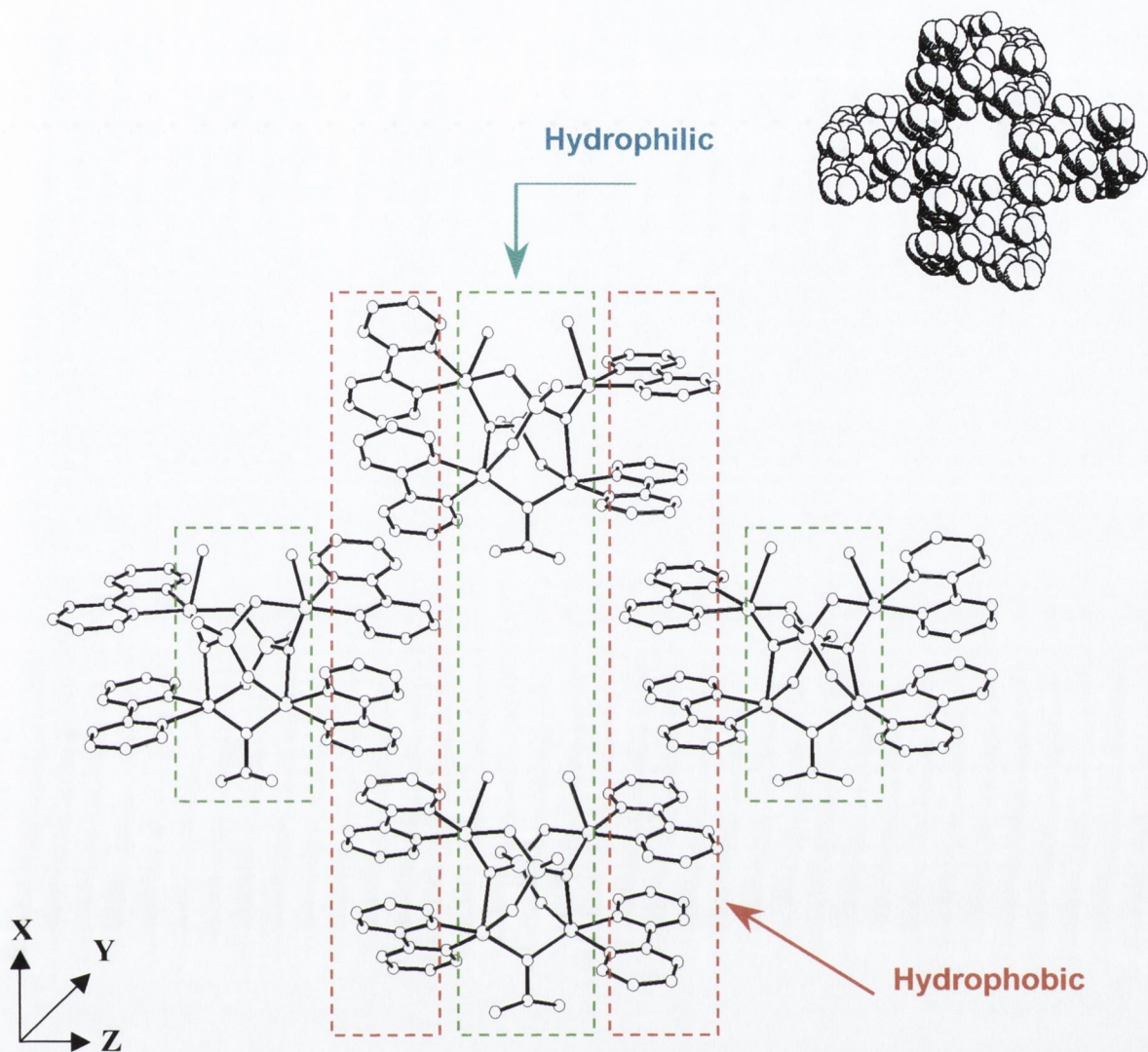


Figure 2.2. Packing and space filling diagrams of (1) showing the hydrophobic exterior and hydrophilic core. Note the apical water molecules align in the x-direction.

This intricate and extensive H-bonded array shows some of the interactions reminiscent of ice phases I_h and I_c .²⁴ Each water oxygen atom is four coordinated. It has four nearest neighbour oxygen atoms to which it is linked by four hydrogen bonds, two donors and two acceptors. As in I_h and I_c the coordination is tetrahedral. Water polyhedra in (1) have pentagonal as well as hexagonal faces. (Figure 2.3-2.6) The ability of water molecules to form a variety of four coordinate networks, which results in the polymorphism of ice, is also well documented for these hydrate inclusion compounds.²⁴

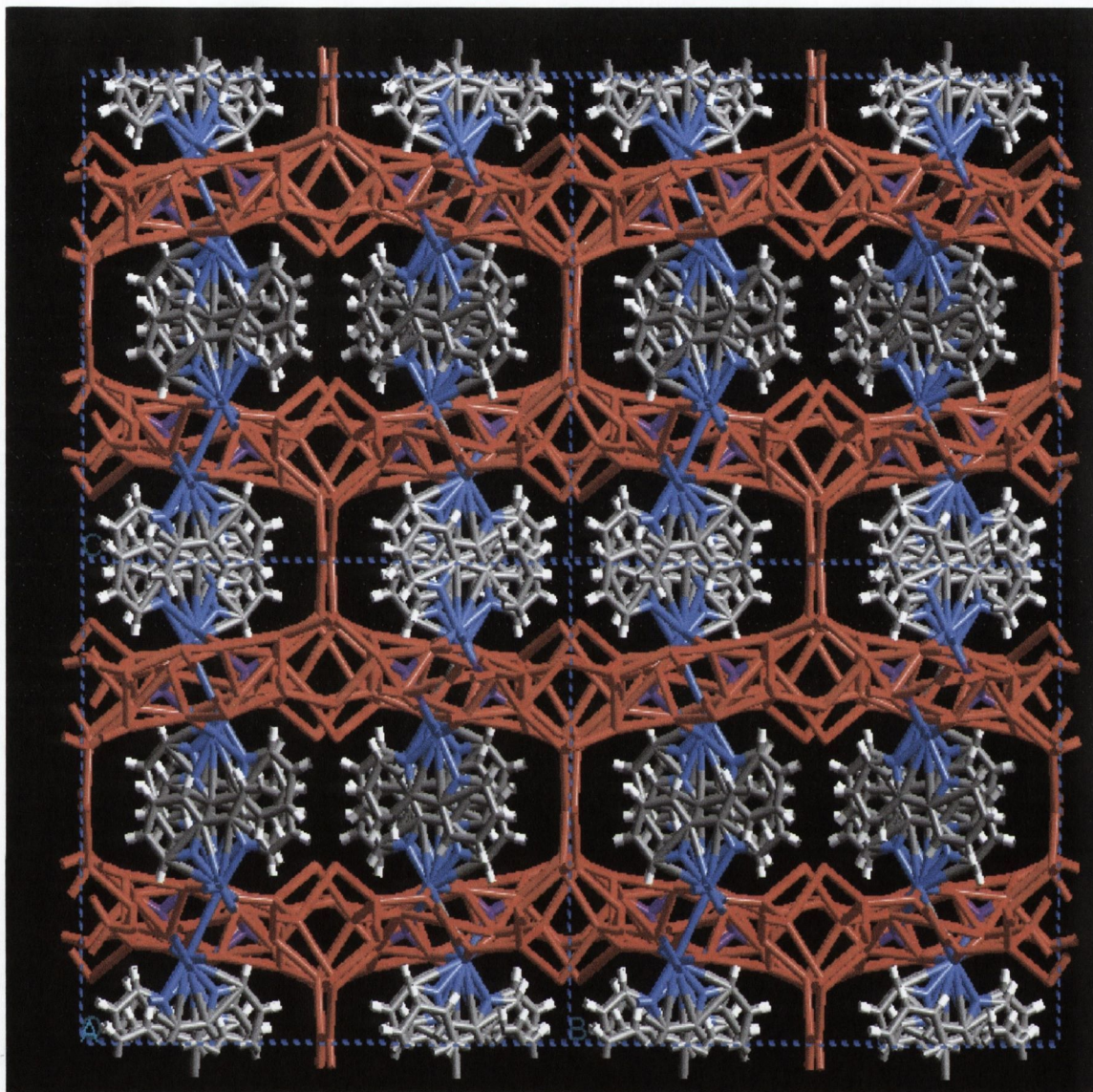


Figure 2.3. H-bonded water array encapsulating complex (1) viewed parallel to the π -stack down the x-axis.

The space occupied by complex (1) (Fig 2.4) is much larger than any void space found in ice, and the H-bonded network is unstable unless occupied by the guest molecule, $[(\text{Cu}_4)(\text{bipy})_4(\mu\text{-PO}_4)_2(\mu\text{-CO}_3)(\text{H}_2\text{O})_2]$. The precise nature of the H-bonded order of water in the liquid phase is still unknown. Calculations predict it's structure to be "random" and to contain many five- and seven-membered rings, as well as the six-membered rings common to ice.²⁵

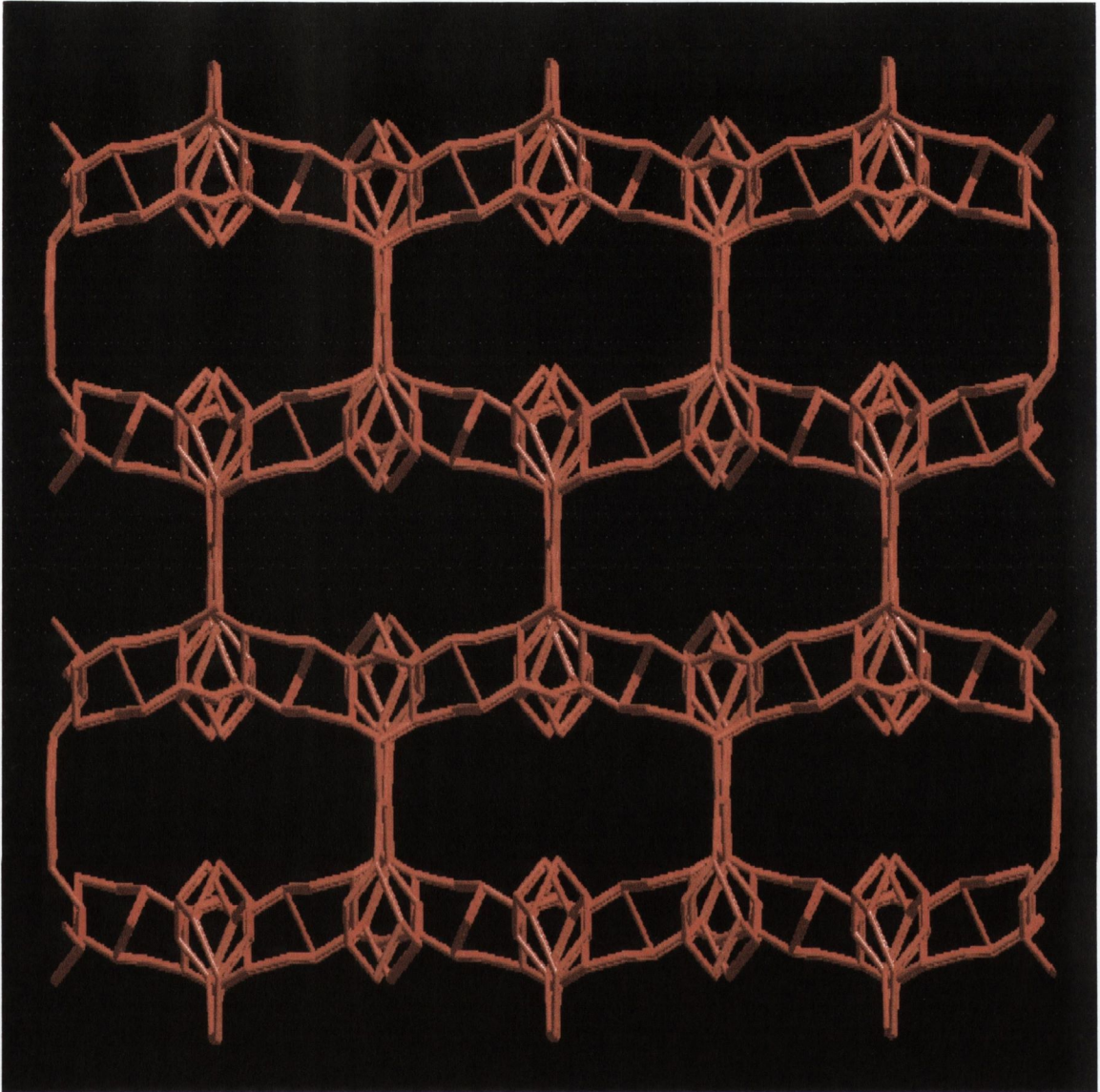


Figure 2.4. Water network viewed down the x-axis showing 'void' occupied by (1). This 'void' measures $2.2 \times 0.8 \times \infty$ nm. Complex is omitted for clarity.

This makes the presence of pentagonal rings in the solid state structure of the water network formed around (1) all the more intriguing as it shows that the solid state structure of water is not confined to six-membered rings but rather that five membered rings also arise in the solid state. (Figures 2.5 and 2.6)

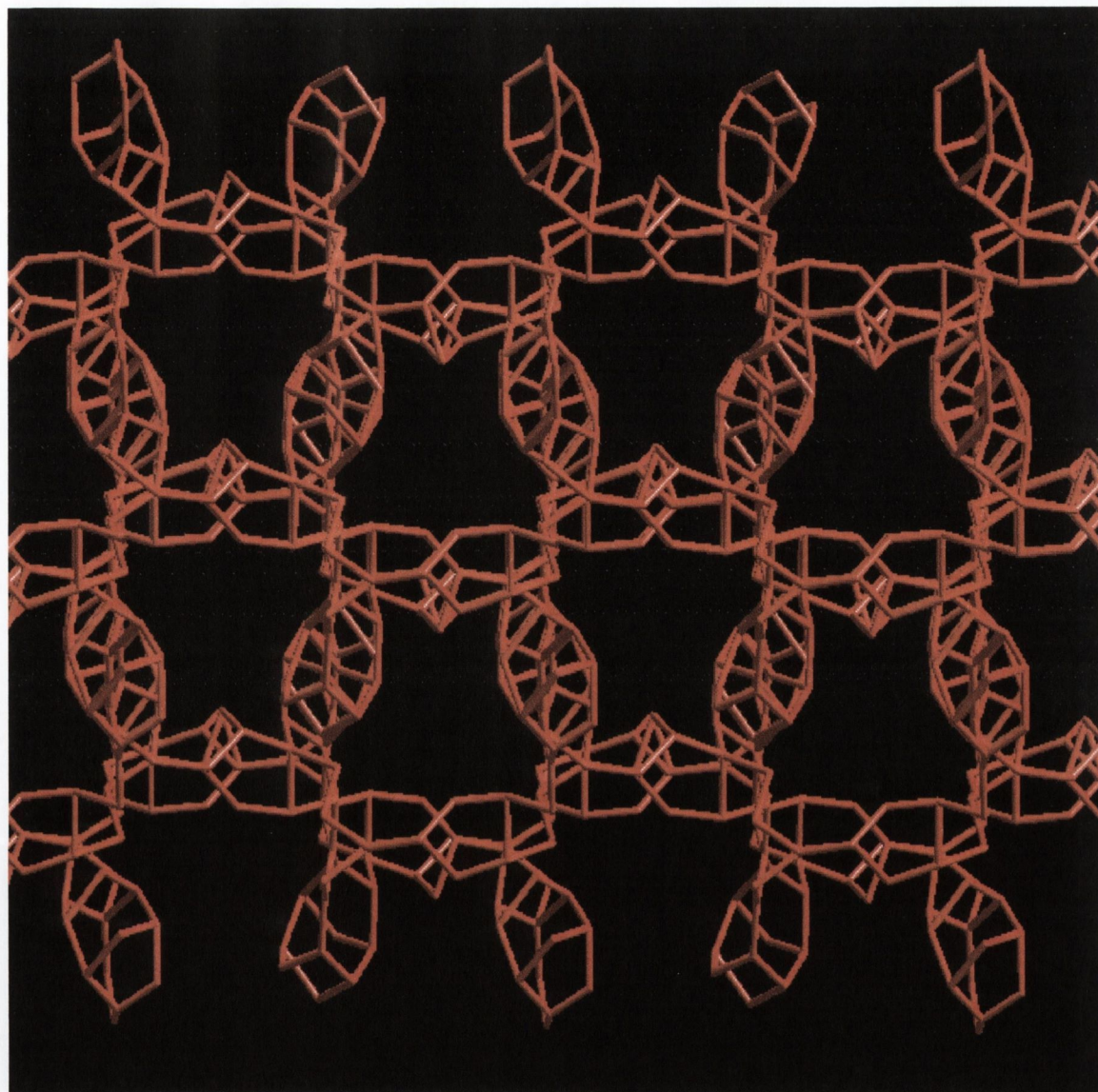


Figure 2.5. The water network, viewed down the y-axis.

The water molecules clearly form a continuous, ordered and dynamic network of hydrogen bonds in which each molecule is linked with up to four others. One aspect of the framework in general is that no interpenetration has occurred. i.e. the independent infinite network does not entangle with itself. Complex (1) omitted for clarity.

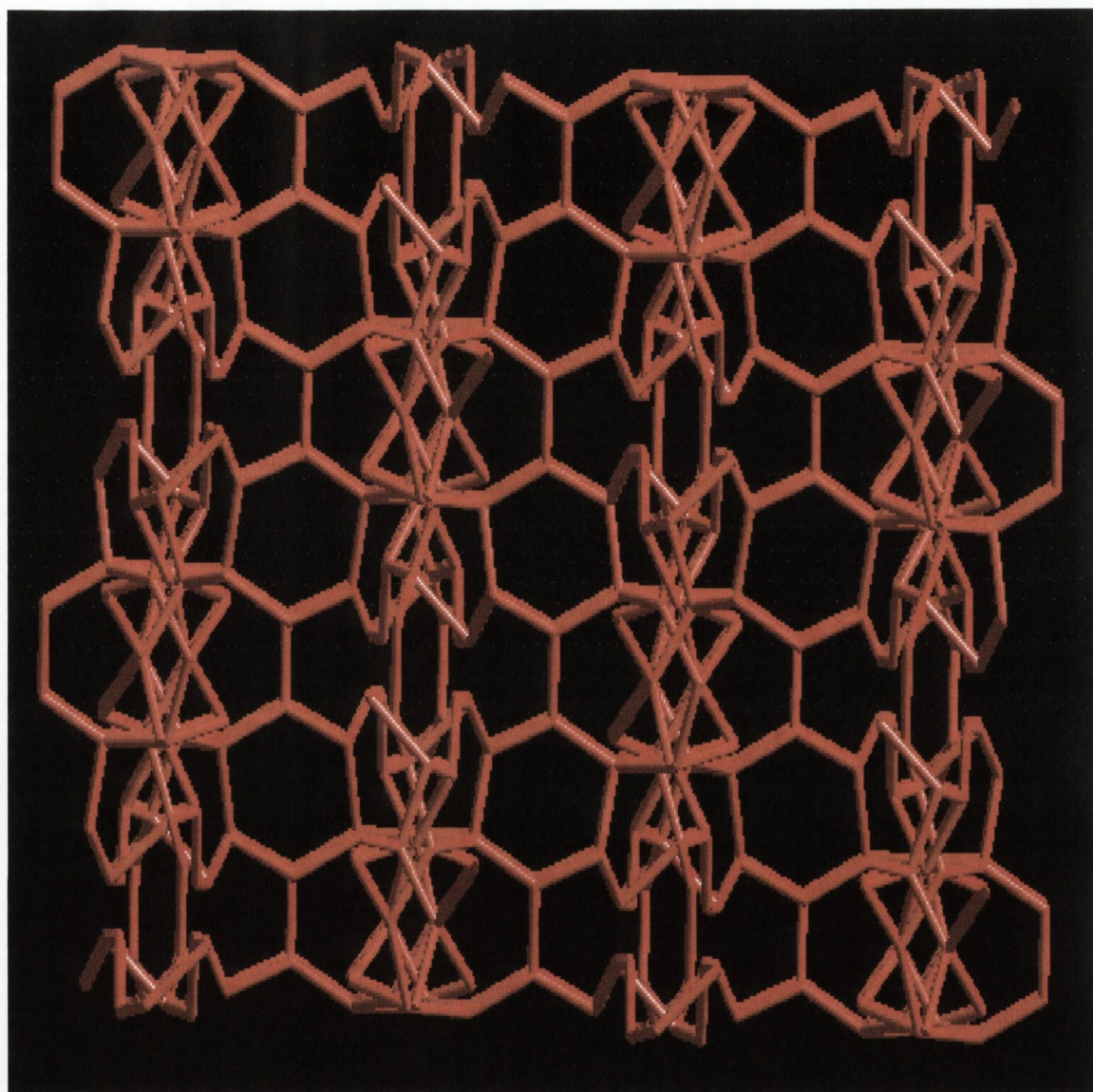


Figure 2.6. Water network viewed down the z-axis. Hexagonal rings formed are clearly illustrated. Complex (1) is omitted for clarity.

The extensive water network goes some way to explaining why the thin plate-like crystals are so mechanically fragile. The complex packs in the x-y plane through π - π interactions between the bipy ligands with each of these sheets separated in the y-direction by the water network. The presence of this 'water' between these sheets allows them to easily glide past one another, thus accounting for the crystal's fragility. After crystals of (1) had been removed from the mother liquor, the clear blue solution was allowed to stand again open to the atmosphere. Further deep royal blue crystals were returned with a slightly different

morphology to the crystals of **(1)**, being more block like. Their behaviour (i.e. unstable out of solution due to solvent loss) was similar to that of **(1)** and they shared near identical infrared spectra. Single crystal X-ray diffraction however showed that a pseudo-polymorph of **(1)**, designated here as **(1a)**, had been formed (They are pseudo-polymorphs because both **(1)** and **(1a)** are iso-structural and differ only in how they aggregate in the solid state and how many water molecules crystallise with them). The space group of this pseudo-polymorph is now $P2/c$ as opposed to $Pnna$ observed for **(1)**. The structure is of relatively high precision with $R = 0.0786$. In **(1)** the apically coordinated water molecules run parallel with each other along the x-axis, whereas in **(1a)** they now H-bond to their nearest neighbour (Fig 2.7). This generates a hydrophilic cavity into which ~ 60 disordered water molecules are trapped. Packing is such that the bipy ligands π -stack in the xy plane forming a 2-D sheet. These sheets then pack in the z-axis but are offset such that the 'supramolecular dimer' sits above the cavity of the sheet above and below.

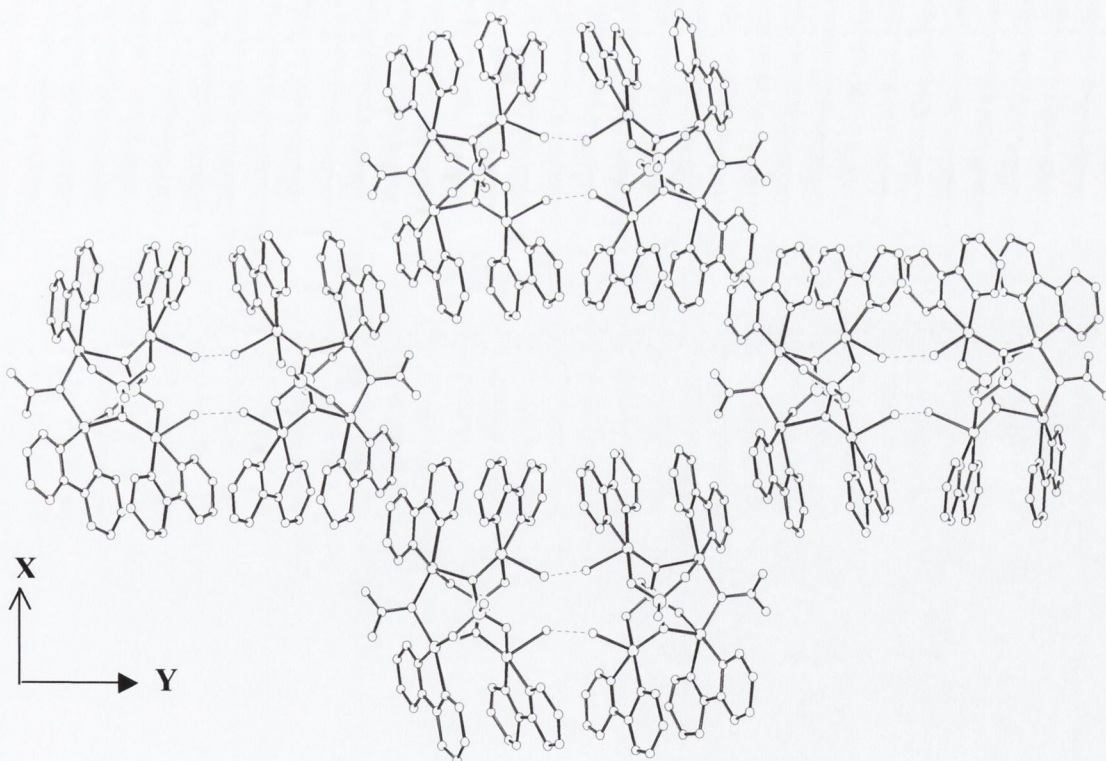


Figure 2.7. Pseudo-polymorphic form of complex **(1)**, designated **(1a)**. Water molecules trapped inside the cavity are omitted for clarity. Viewed along z-axis.

This arrangement then isolates each cavity from each other such that the ~60 water molecules cannot interact with each other throughout the lattice as they do in **(1)**. The pseudo-polymorph has therefore generated a ‘molecular box’ by essentially turning the metallo-aggregate on its head. The core of both **(1)** and **(1a)** are iso-structural with only the core units packing changing. It should be noted that **(1)** was also recovered alongside this new ‘supramolecular dimer’ **(1a)**. After multiple repetitions of this experiment, **(1a)** was never recovered until at least the second and sometimes third batch of crystals were cropped. The only obvious difference in conditions between crystal batches is that as each successive batch is cropped the remaining mother liquor was noted as having a slightly lower pH, from 10 down to a low of 9. This lower pH may play a role in facilitating the dimerisation, through H-bonding, of the apical water molecules of complex **(1)**. Interestingly it was found that changing the solvent system from 100% water to 50:50 ethanol:water had the effect of generating the ‘supramolecular dimer’ pseudo-polymorph. This is most likely a result of ethanol being incorporated into the lattice (observed on single crystal X-ray analysis). This also serves to remove the carbonate disorder by disrupting the C₂ symmetry of the tetranuclear core. Why this subtle change has such a dramatic effect is open to question and the exact reason for this dimerisation to occur remains unclear.

2.3. The effect of pH and stoichiometry on the synthesis of **(1)**.

The fixation of carbon dioxide as carbonate may be a pivotal event in the “self-association” process involved in the complex formation. Since fixation of CO₂ is pH dependant a number of combinatorial experiments with different copper starting materials were tested to check for complex **(1)**/**(1a)** formation, as each different salt results in a different pH in solution. Manipulation of stoichiometry from the product’s usual 4:4:2 was also tried to see if there was a driving force toward formation of the tetranuclear complex. Table 2.2 shows the counter-ions employed and the affect this change has on the outcome of each reaction. The pH recorded for each reaction is also noted above and is recorded to the nearest integer value. The results indicate that only those counter-ions that generated an alkaline environment facilitated the formation of the tetranuclear complex **(1)** and its pseudo-polymorph **(1a)**. In

acidic conditions a thick light blue gelatinous precipitate completely insoluble in all solvents tried (except acid or base) is returned.

Stoichiometry Cu-bipy-(NH ₄) ₂ HPO ₄	pH of solution	Copper salt	Successful formation of both (1) & (1a)
4:4:2	10	a. Cu(OH) ₂	☑
4:4:2	5	b. Cu(ClO ₄) ₂ ·6H ₂ O	☒
4:4:2	12	c. (Cu(OH) ₂ ·CuCO ₃)	☑
4:4:2	3	d. Cu(NO ₃) ₂ ·6H ₂ O	☒

Table 2.2. Counter-ions and pH's in the synthesis of (1). Experiments are in the order they were attempted.

Increasing the pH of these solutions however, to pH 9, using 0.1M ammonium hydroxide, returns the royal blue solution, indicative of the original mother liquor.

These results make plain the requirement for an alkaline environment to facilitate complex formation via carbon dioxide fixation. Further evidence comes from replacing the ammonium hydrogen phosphate starting material with phosphoric acid (H₃PO₄). This results in a pH drop from 10 to 3. The royal blue solution that results returns large block shaped royal blue crystals which were shown by single-crystal X-ray diffraction to be the monomeric copper(II) complex [Cu(bipy)(H₂O)(HPO₄)]. The low pH and presence of divalent phosphate (*i.e.* HPO₄²⁻, the phosphate remains mono-protonated in the acidic environment) facilitates the formation of a simple salt by acting as a divalent counterion for the copper(II). This indicates that generation of the tri-anionic phosphate (PO₄³⁻) is also vital for the formation of the tetranuclear copper core.

A number of different stoichiometries were also tried to test for the formation of (1) or (1a) as shown in Table 2.3. In all cases the product was returned as deep blue parallelepiped shaped unstable crystals indicative of complex (1). In the case of the reaction recorded as

entry **d** (Table 2.3), large, stable, royal blue crystals of formula $\{[(\text{bipy})_2(\text{Cu})(\text{CO}_3)].2\text{H}_2\text{O}\}$ were also recovered. This complex was not recovered in the solid state with reactions **a**, **b**, **c** or **e**.

Reaction	2,2'-bipyridine	$\text{Cu}(\text{OH})_2$	$(\text{NH}_4)_2\text{HPO}_4$	Successful formation of (1)
a	4	4	2	☑
b	2	4	1	☑
c	4	4	4	☑
d	4	4	1	☑
e	2	4	4	☑

Table 2.3. Stoichiometries tried in the synthesis of (1) or (1a). All products were recovered as crystalline solids and were fully characterised by Infrared and UV/vis spectroscopies as well as single crystal XRD.

These results overall, at least in regard to the counterions and stoichiometries attempted, seem to indicate stability inherent in the formation of the tetranuclear complex (1) with a second stable pseudo-polymorph also forming at slightly lower pH. This statement should however be qualified in view of the specific requirement of an alkaline environment, to say inherent stability in a particular window of pH. It is also crucial that the Cu:bipy ratio be maintained as 1:1 to avoid competing synthesis of monomeric $\{[(\text{bipy})_2(\text{Cu})(\text{CO}_3)].2\text{H}_2\text{O}\}$.

2.4. Thermal analysis of (1).

The thermal analysis (TGA) carried out on crystals of (1) showed a gradual weight loss over the temperature range 25-310°C, while at the same time the Differential Thermal Analysis (DTA) trace exhibits multiple features consistent with water evaporation. The large range of T suggests the loss of both coordinated and non-coordinated water molecules.

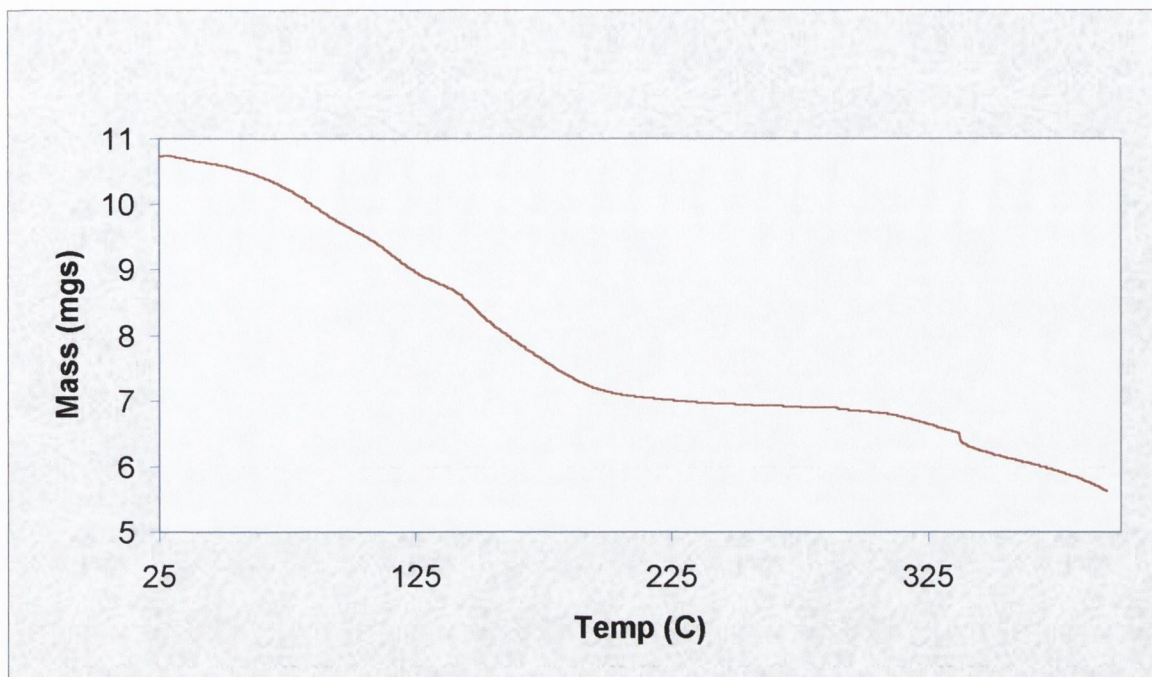


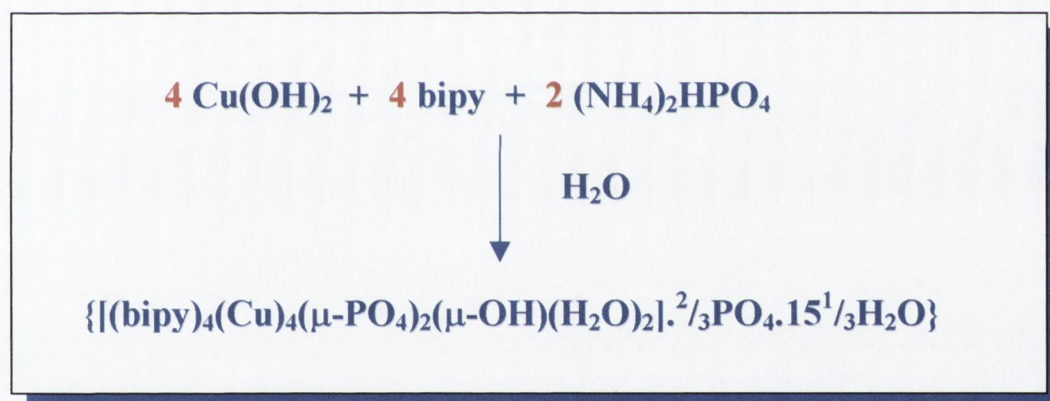
Figure 2.8. TGA curve generated by compound (1).

A stable intermediate is shown by the TG curve to be present in (1). This intermediate corresponds to the completely anhydrous phase of (1), which is then stable to $\sim 300^{\circ}\text{C}$. The fact that the water molecules are not completely removed until temperatures exceeding 175°C indicates the presence of H-bonding within the system.

2.5. Preparation and Characterisation of the Tetranuclear copper (II) complex:



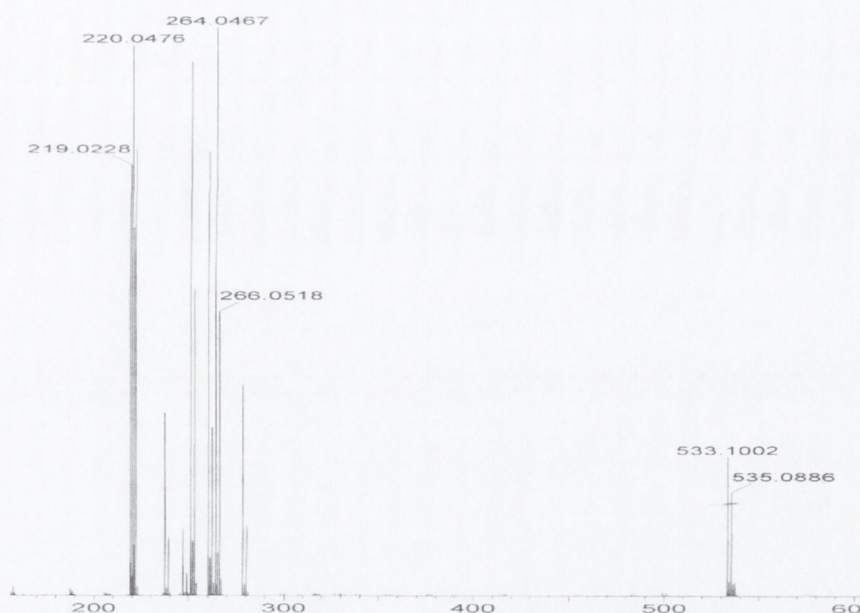
In an endeavour to establish as to whether CO₂ fixation during synthesis is a requirement for the successful formation of the tetranuclear core, we carried out the preparation of '(1)' under inert atmosphere. The alkaline pH of the reaction, a result of both the copper hydroxide and ammonium hydrogen phosphate reactants, meant that unless carbon dioxide was rigorously excluded from the reaction than compound (1) or (1a) would likely be returned. As a result, the reaction was carried out in triply distilled, degassed water prior to use. Freshly prepared copper hydroxide was used to ensure against malachite formation, despite it being stored under vacuum.



Scheme 2.2. Direct preparation of the tetranuclear species (2).

As with complex (1) a deep blue solution is formed after a period of time (< 5 minutes), as the pale blue suspension gradually dissolves with concomitant colour change. This solution was stirred under inert atmosphere over a 24-hour period. Stable diamond shaped crystals were isolated following slow evaporation over a period of approximately twenty days. No precautions were taken during crystal growth to prevent atmospheric CO₂ from entering the system. Initial infrared study indicated an absence of the carbonate absorption bands noted previously for (1) and the introduction of two new sharp bands at 3586 and 3564 cm⁻¹, which

may be assigned to the possible presence of bridging hydroxide.¹⁸ Since the complex is hydrated, this necessarily complicates interpretations made in the 3500 cm⁻¹ region. In addition the water band in this region is extremely strong and broad. However, a shoulder appears on the high frequency side of the water band, and it is this that may be assigned to the OH⁻ stretch. A weak band at 998 cm⁻¹ is tentatively assigned to the bending OH⁻ vibration. As well as the peaks observed in **(1)** for the bridging phosphate groups, an additional phosphate peak is observed for **(2)** at 1166 cm⁻¹ combined with an overall broadening of the phosphate signal. This may be assigned to the possible presence of ionic PO₄³⁻. Sharp bands of medium intensity are observed at 1654, 1507, 1493 and 1444 cm⁻¹. These bands involve the ring C-C and C-N vibrations of 2,2'-bipyridine. Electro-spray mass spectroscopy on an aqueous solution of **(2)** showed peaks at 533/535m/z which are assigned to the isotopic, charged species [(bipy)₄(Cu)₄(μ-PO₄)₂]²⁺ (see below).



A single crystal X-ray diffraction study confirmed the structure to be a tetranuclear complex of similar composition to **(1)**, but with bridging hydroxide replacing the bridging carbonate. The system was left with no other obvious source of anion other than the hydroxide present as reactant.

2.6. Description of the molecular structure of the tetranuclear copper (II) complex:



A representative deep blue diamond shaped crystal was used for data collection. Dr. M. Nieuwenhuyzen of the Queens University, Belfast, performed the data collection and structural refinement. The tetranuclear unit is depicted in Figure 2.9, showing the atomic numbering scheme used. The molecule crystallises in space group P2/c.

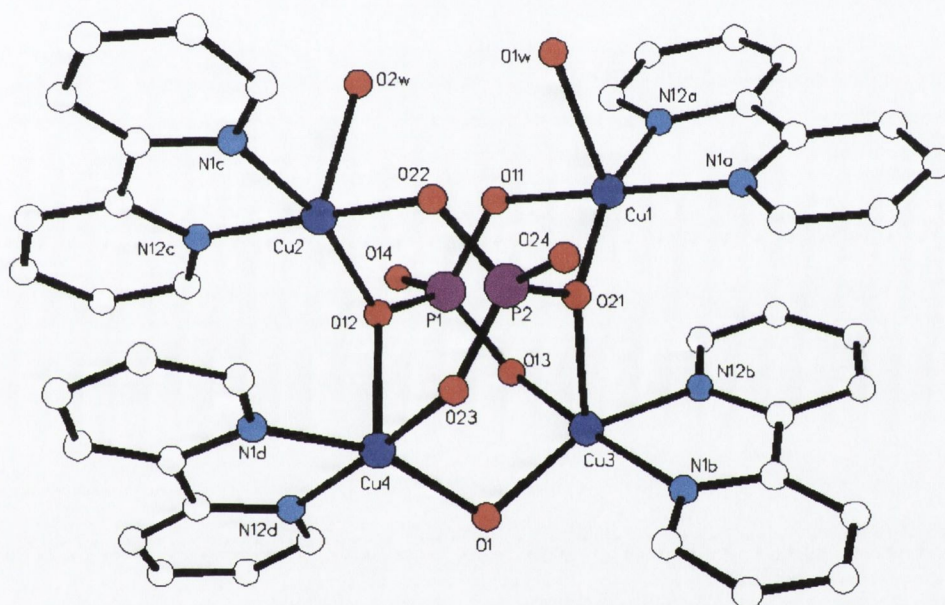


Figure 2.9. $\{[(\text{Cu})_4(\text{bipy})_4(\mu\text{-PO}_4)_3(\mu\text{-OH})(\text{H}_2\text{O})_2] \cdot \frac{2}{3}\text{PO}_4 \cdot 15\frac{1}{3}\text{H}_2\text{O}\} \quad (2)$.

Waters of crystallisation and hydrogen atoms omitted for clarity.

Complex (2), as with (1) and (1a), is built around a trapezoidally displaced tetramer of copper centres. The cluster exhibits coordination furnished by 2,2'-bipyridine groups and bridging tri-anionic phosphate groups. The geometry around each Cu(II) is again best described as being square-based pyramidal with a bound water molecule occupying the apical positions of Cu(1) and Cu(2) and a phosphate oxygen bound axially at Cu(3) and Cu(4). The coordination sphere of Cu(3) and Cu(4) is completed by bridging hydroxide.

There are a number of subtle geometrical changes also associated with the incorporation of the hydroxy group into (2). The bridging angle through the hydroxy group is 109.8° [Cu(3)-O(1)-Cu(4)]. This is significantly smaller than the angle generated through the corner-shared carbonate species found in (1) and (1a) of 122.7°. As a result Cu-Cu separation is also shorter for (2) compared with (1), with a Cu(3)-Cu(4) bond distance of 3.191 Å compared with the equivalent Cu-Cu distance for (1) [Cu(2)-Cu(2a)] of 4.26 Å.

Table 2.4. Selected bond distances (Å) and angles (°) for (2).

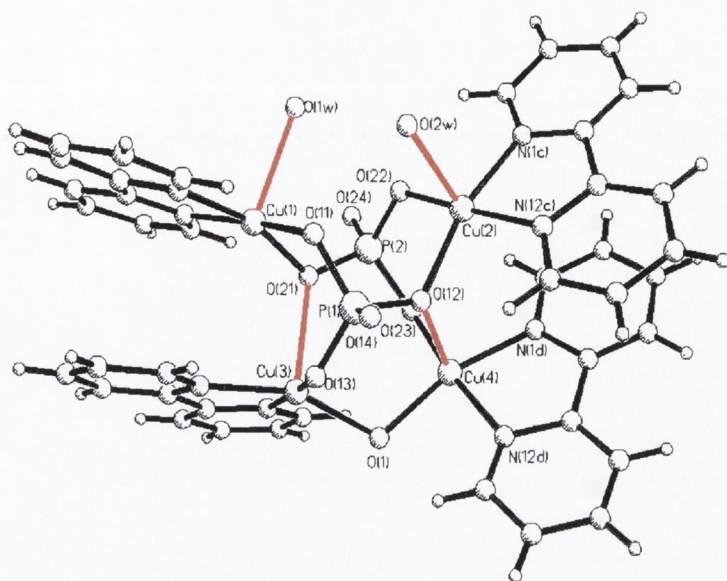
Cu(1)-O11	1.881(7)	O(11)-Cu(1)-N(12a)	91.3(3)
Cu(1)-O21	1.961(7)	Cu(1)-O(21)-Cu(3)	106.1(3)
Cu(1)-Cu(2)	4.219(7)	O(11)-Cu(1)-O(21)	92.3(3)
Cu(1)-Cu(4)	5.004(7)		
Cu(2)-O22	1.910(7)	Cu(2)-O(12)-Cu(4)	104.4(3)
Cu(2)-O12	1.974(7)	O(22)-Cu(2)-O(12)	94.2(3)
Cu(2)-Cu(3)	4.963(7)		
Cu(3)-O13	1.911(7)	Cu(3)-O(1)-Cu(4)	109.8(3)
Cu(3)-O1	1.953(8)	O(13)-Cu(3)-O(1)	108.9(3)
Cu(3)-Cu(4)	3.191(7)	Cu(3)-O(21)	2.316(7)
Cu(4)-O12	2.273(7)	O(21)-P(2)-O(22)	109.7(3)
Cu(4)-O1	1.947(7)	O(23)-Cu(4)-O(1)	93.6(3)

Estimated standard deviations are given in the parenthesis.

Axial bond lengths within (2) are significantly larger than the equatorial bonds found in the N₂O₂ chromophore (*i.e.* the basal plane of each copper atom). These axial bond lengths also differ significantly from one another as demonstrated in Table 2.5.

Cu(1) - O(1w)	2.381(7)
Cu(2) - O(2w)	2.319(7)
Cu(3) - O(21)	2.316(7)
Cu(4) - O(12)	2.273(7)

Table 2.5. Axial bond lengths for (2). Note ~45° twist between each half of the molecule.



These axial bond differences are reflected in the deviations of each copper atom from the equatorial mean planes. Cu(1) is displaced 0.097 Å compared with Cu(2), which is displaced 0.081 Å. Even greater deviation is observed for Cu(3) (0.1750 Å) and Cu(4) 0.1531 Å. This relationship has previously been observed in tetranuclear copper complexes.²⁶ The combination of mean plane deviations and various axial bond lengths results in different intra-nuclear Cu-Cu separations. Indeed, intranuclear Cu-Cu separation is shorter between Cu(2) and Cu(4) (3.36 Å) compared with Cu(1) and Cu(3) 3.425 Å. Compared with (1) intranuclear π - π interactions between bipyridine ligands are at slightly greater distance (3.465(7) in (2) as opposed to 3.399(5) for (1). The bipyridine stacks however, again try to optimise π -stacking, which combined with defined bipyridine bite distance plays a significant role in the distortion of the copper atoms from the mean plane. The dihedral angle between intranuclear stacking bipyridine rings is 6.7°. The tetrahedral nature of the phosphate bridging results in a twist in each half of the molecule of ~45° (Table 2.5).

Despite the 15 waters of crystallisation present per asymmetric unit in (2), no extended H-bonded hydrate network is observed in (2). The reason for this lack of pseudo-clathrate structure is probably the same as that for the pseudo-polymorph (1a), namely supramolecular dimerisation. As in the polymorph (1a), (2) undergoes intermolecular H-bonding between

nearest neighbour apically bound water molecules forming again a 'supramolecular dimer' in the solid state (Figure 2.10). This has the effect, as it did in (1a), of preventing channel formation and so inhibiting long-range ordering of the water molecules into a distinct hydrate network. Instead the water molecules are disordered about the hydrophilic regions of (2).

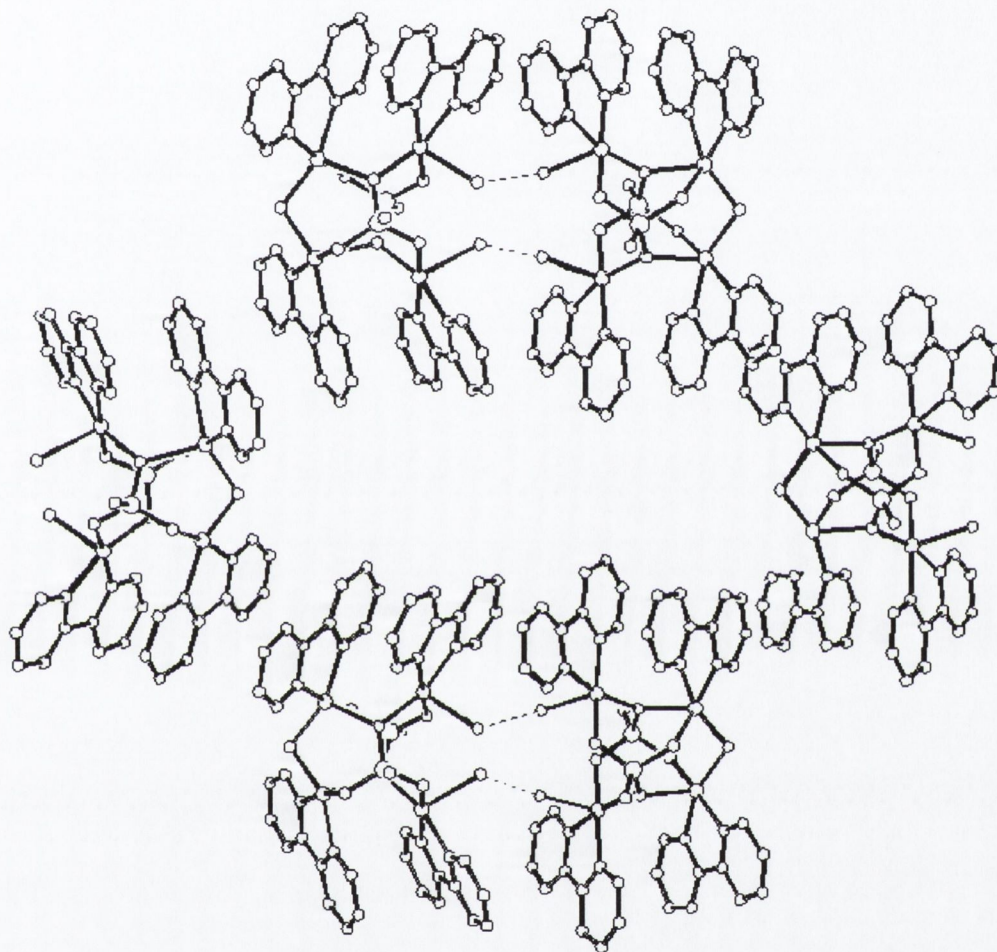


Figure 2.10. Packing diagram showing supramolecular dimerisation in complex (2) through H-bonding of apical water molecules. Waters of crystallisation and lattice phosphate omitted for clarity.

Successful and deliberate incorporation of hydroxide into the tetranuclear core led us to attempt to introduce both sulphate (SO_4^{2-}) and thiocyanate (NCS^-). However in neither case were the analogous tetrameric species generated. The presence of SO_4^{2-} in solution (added by

bubbling sulphur dioxide gas into an aqueous degassed (Ar) solution of $\text{Cu}(\text{OH})_2$, ammonium hydrogen phosphate and 2,2'-bipyridine under inert atmosphere (Ar)) resulted in the formation of a polymeric copper(II) compound $[\text{Cu}(\text{bpy})(\text{H}_2\text{O})_2(\text{SO}_4)]_n$, which was found to have been previously reported in the literature.²⁷

Thiocyanate was introduced as the sodium salt to an aqueous degassed (Ar) solution of copper hydroxide, ammonium hydrogen phosphate and 2,2'-bipyridine under argon. What resulted was the formation of the bridging thiocyanate containing copper(II) compound $[\text{Cu}(\text{bpy})(\text{NCS})_2]_n$. As with the simple mononuclear sulphate complex, this thiocyanate compound was found to have been previously reported in the literature²⁸ although both were synthesised in different manners.

The fact that carbonate could so readily be excluded answers the question as to whether the carbonate anion is necessary to template tetramer formation. This observation suggests that a tetranuclear core is built about trianionic phosphate and then charge is balanced with carbonate or hydroxide depending on what is available.

2.7. Magnetic behaviour of the tetranuclear copper (II)

complex:



A variable temperature magnetic susceptibility study had previously been reported on complex (1) with weak antiferromagnetic behaviour recorded. We therefore undertook to see what effect replacing the carbonate-bridging group with hydroxide might have on overall magnetic behaviour. Variable temperature magnetic susceptibility studies were carried out on a powdered sample of the crystalline complex (2) over the temperature range 300K-1.9K. The magnetic behaviour of (2) is shown in Figure 2.11 in the form of a $\chi_M T$ versus T plot, χ_M being the molar magnetic susceptibility and T the temperature. This increase of $\chi_M T$ upon cooling is the signature of a ferromagnetic exchange coupling between nearest neighbour metal ions.

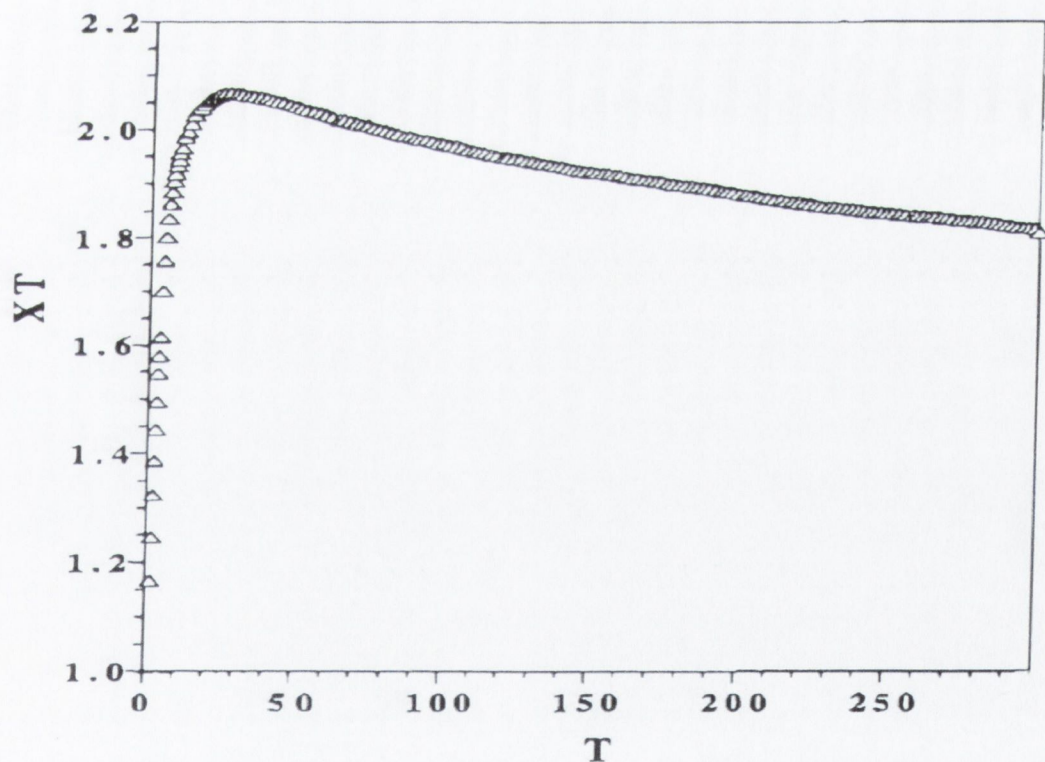


Figure 2.11. $\chi_M T$ versus T plot for (2). T is in degrees Kelvin and $\chi_M T$ is in cm³ K mol⁻¹.

The curve exhibits a rounded maximum at 31K (i.e. $\chi_M T$ tends towards zero approaching absolute zero). Since pure ferromagnetic coupling would result in an increase upon cooling until a plateau was reached corresponding to the temperature range where only the ground triplet state is populated, the maximum reveals deviations due to small effects applicable only at very low temperature. These small effects can be zero-field splitting of the ground state or intermolecular interactions. The latter usually results in antiparallel coupling of the molecular triplet states resulting in an antiferromagnetic coupling. Moreover the presence of some small amount of uncoupled species, which obeys the Curie law, may also affect the overall magnetic behaviour. It is likely in this case however that intermolecular interactions are resulting in a maximum due to the formation of a singlet ground state in (2). Figure 2.12 shows the plot of molar magnetization versus field. The curve is non-linear, reflecting the non-Curie behaviour of the sample and is characteristic of an $S = 1$ ground state (For molecules with a $^{2S+1}\Gamma$ ground state) i.e. the ground state has a spin multiplicity of 3.

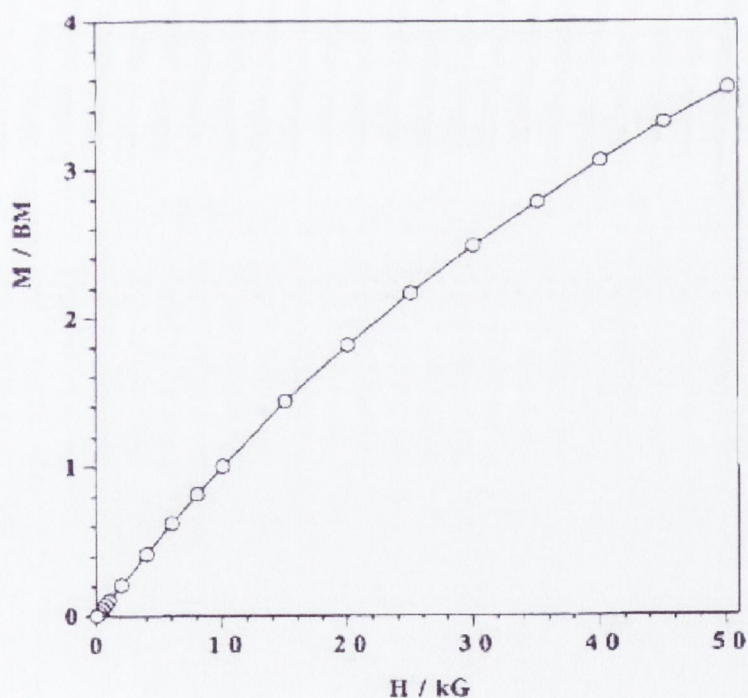


Fig 2.12. Field dependence of (2) below T_c .

It has been shown by Hodgson *et al*²⁹ that an increase in the bridging angle in the Cu-OH-Cu system implies greater s character and that pure *p*-orbitals generate triplet ground states in

Cu-OH-Cu systems with pure *s*-orbitals generating singlet ground states. Therefore there is greater *p*-bond character inherent in the Cu-O-Cu (hydroxide) bridge of **(2)** than the Cu-O-Cu (carbonate) bridge of **(1)** as indicated by the decreased size of the bridging angle in **(2)** *versus* **(1)**. This slight difference in *s* and *p* character as indicated by differences in the bridging angle in **(1)** and **(2)** is probably enough to cause the stark difference in magnetic behaviour of both compounds i.e. Antiferromagnetic vs Ferromagnetic.

Fitting the experimental data to the myriad of possible exchange pathways contained in **(2)** is very complicated and still ongoing, involving the groups of Prof. Miguel Julve at the University of Valencia, Spain and Prof Juan Cano at the University of Barcelona, Spain. The dominant pathway is assumed to be through the hydroxide bridge however the other mono- and tri-atomic pathways that may possibly be acting to strengthen or weaken the exchange interaction within **(2)** require further consideration. An overall exchange coupling constant (*J*) for the system will then be ascertained.

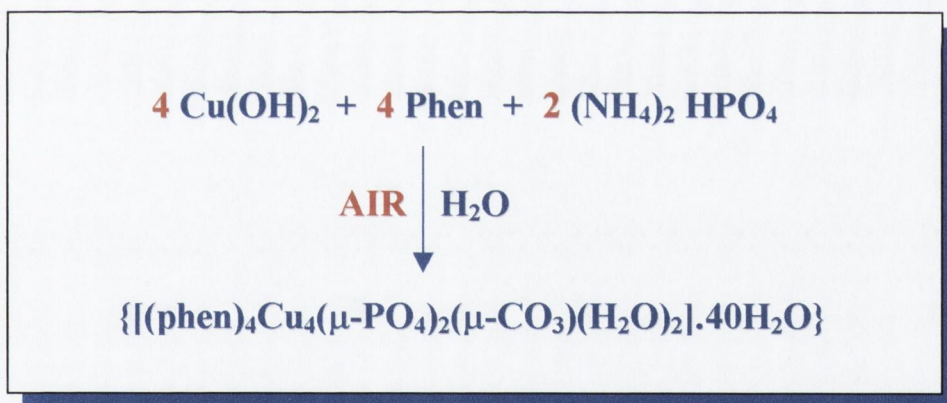
2.8. Preparation and characterisation of the tetranuclear copper

(II) complex:



The 1,10'-phenanthroline (phen) analogue of (1) was prepared in a similar fashion to (1) by replacing 2,2'-bipyridine with anhydrous 1,10'-phenanthroline. The reaction proceeds as for (1) with initial light blue suspension becoming a deep royal blue solution on stirring in water open to air. Greater time is needed for this solution to develop however with an increase from approximately five minutes for (1) to over fifteen minutes for (3). Solubility differences between both aromatic ligands, with phen having poorer solubility in water *c.f.* bipy, being the probable cause. Reactions in both cases were stirred over 24 hrs to ensure completion.

The complex was initially formed as a crystalline product obtained from the aqueous solution of a reaction recorded in Scheme 2.3 below. The diamond shaped royal blue crystals are unstable on removal from the mother liquor.



Scheme 2.3. Direct preparation of the tetranuclear species (3).

Infrared studies indicated the presence of carbonate with peaks at 1520 cm^{-1} and 1333 cm^{-1} . Again, however, the spectrum is dominated by the presence of both the phenanthroline ligand ($1640, 1592, 724 \text{ cm}^{-1}$) and the inorganic phosphate moiety ($1121, 1060, 1010 \text{ cm}^{-1}$). Infrared spectra of both the crystalline phase and the powder phase, obtained on exposure to air over one hour, were virtually identical with no major shifts recorded in the phosphate,

carbonate or phenanthroline bands. The d-d spectrum of an aqueous solution of **(3)** again exhibits a very broad and featureless band centred at 685 nm, which is consistent with the distorted square-pyramidal nature of the Cu(II) chromophores. Electro-spray mass spectroscopy of an aqueous solution of **(3)** also shows no parent ion peaks but rather a pattern of peaks indicative of fragmentation, the neutral complex not surviving ionisation. Peaks are assigned to $[\text{Cu}(\text{bipy})]^{2+}$ and $[\text{Cu}(\text{bipy})_2(\text{H}_2\text{PO}_4)]^+$.

As with complex **(1)**, a series of reactions were carried out testing pH, counterion and stoichiometric effects on the formation of **(3)**. These experiments gave similar results to those observed for **(1)**.

Stoichiometry Cu:phen:(NH ₄) ₂ HPO ₄	pH of solution	Copper salt	Successful formation of (3)
a) 4:4:2 b) 4:4:1 c) 4:4:4 d) 4:2:1 e) 4:2:2	10	Cu(OH) ₂	☑
4:4:2	5	Cu(ClO ₄) ₂	☒
4:4:2	12	Cu(OH) ₂ .CuCO ₃	☑
4:4:2	3	Cu(NO ₃) ₂	☒

Table 2.6. Counter-ions and pH's tested in the synthesis of **(3)**. All samples were recovered as crystalline solids and were fully spectroscopically characterised by Infrared, UV/vis, ESMS and XRD.

The complex was recovered in all stoichiometries used with copper hydroxide and again only with those counter-ions that generated an alkaline environment, namely copper hydroxide and malachite. The mononuclear complex $[\text{Cu}(\text{phen})_2\text{CO}_3.11\text{H}_2\text{O}]$ was returned along side the tetramer with Reaction **1d** in Table 2.6, namely with a 4:2:1 stoichiometry using copper hydroxide as copper salt. This complex was amenable to direct synthesis and its final composition was shown to be very sensitive to pH. This work will be described elsewhere in this thesis.

Finally thermal analysis (TGA) showed endothermic weight loss indicative of dehydration (solvent loss) similar to that recorded for the bipyridine analogue (1). No stable intermediates were obvious prior to degradation at temperatures >300°C.

2.9. Description of the molecular structure of the tetranuclear copper (II) complex:



A royal-blue crystal obtained from an aqueous solution was used for a single crystal X-ray diffraction study. Dr. M. Nieuwenhuyzen of the Queens University, Belfast, performed the data collection and structural refinement. The tetranuclear unit is depicted in Figure 2.13, showing the atomic numbering scheme used.

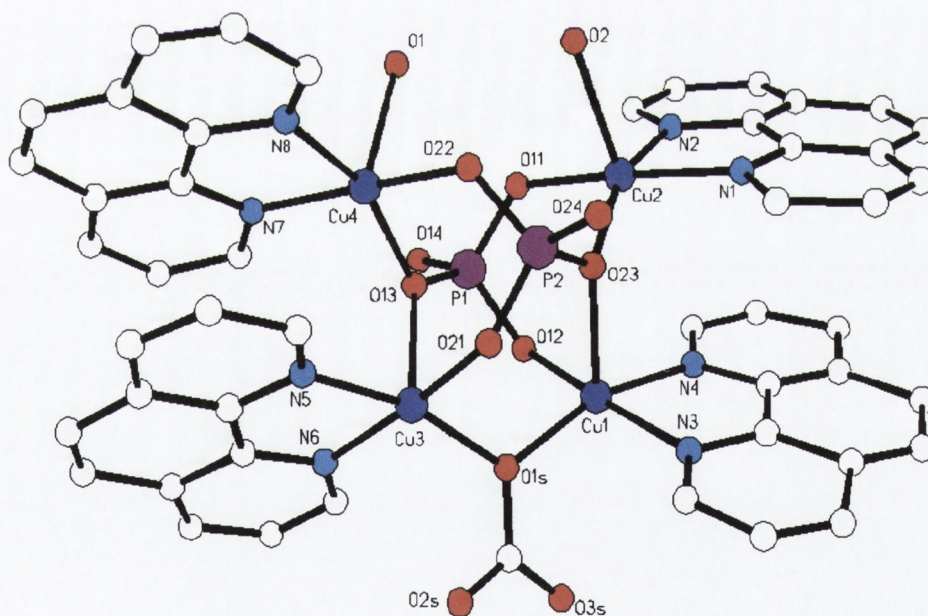


Figure 2.13. $\{[(\text{Cu})_4(\text{phen})_4(\mu\text{-PO}_4)_3(\mu\text{-CO}_3)(\text{H}_2\text{O})_2].40\text{H}_2\text{O}\} (3)$.

Waters of crystallisation omitted for clarity.

Complex **(3)** becomes amorphous through solvent loss upon removal from the mother liquor, so data collection was carried out at low temperature. The structure is of high precision with $R = 0.0756$. The molecular geometry of complex **(3)**, as in **(1)**, consists of four square-pyramidally disposed copper atoms, coordinated by 4 phen ligands and bridged by two inorganic phosphate (PO_4^{3-}) groups. Additional bridging between Cu(1) and Cu(3) is furnished by the carbonate species CO_3^{2-} . Coordination around Cu(2) and Cu(4) is furnished by two phen nitrogen donors, N(1) and N(2) and N(7) and N(8) respectively. Coordination also occurs with two phosphato-oxygens, O(11), O(23) and O(22), O(13) respectively. Combined this forms the basal plane of the square-pyramid, with bound water occupying the apical positions analogous to complex **(1)** for Cu(2) and Cu(4). Cu(1) and Cu(3) are again coordinated by two phen nitrogen's but now by only one phosphato-oxygen (O(12) and O(21) respectively) with corner shared μ -carbonate species completing the basal plane. The bridging phosphato oxygen's, (O(23) and O(13)) provide axial coordination to Cu(1) and Cu(3). The phosphate groups therefore exhibit varied hapticity acting as both mono- and tri-atomic bridging species. This results in an intricate array of inter-connected copper atoms, such that Cu(2) and Cu(4) are doubly tri-atomically bridged to each other, and Cu(1) and Cu(3), and further linked mono-atomically to Cu(1) and Cu(3). In addition, Cu(1) is triply bridged to Cu(3) by two tri-atomic phosphate linkages and mono-atomically by the carbonate group. As a consequence Cu(2) and Cu(4) are participating in six bridging interaction, whilst Cu(1) and Cu(3), as a result of the additional carbonate-bridge between them, partake in seven such interactions. The four copper atoms are disposed in a slightly buckled trapezoidal arrangement with respect to each other. The resulting metal-metal separations are listed in Table 2.7. Bridging between Cu(2) and Cu(1), through the phosphato- oxygen O(23) is asymmetric in nature [Cu(2)-O(23) 1.952 Å; Cu(1)-O(23) 2.307 Å]. This reflects this bridging oxygen's basal versus axial disposition at Cu(2) and Cu(1), respectively. The Cu(1)-O(23)-Cu(2) bridging angle is 101.8° . This angle is almost five degrees larger than that recorded for the bipyridine analogue **(1)**. This is likely the result of the greater surface inherent in phenanthroline, versus bipyridine, and the attempts by the system to optimise π - π stacking interactions. This asymmetric bridging is also evident now, across the carbonate-bridging group [Cu(1)-O(1s)-Cu(3); bridging angle of 119.7°], with actual bond lengths differing by 0.013 Å. [Cu(1) -O(1s) 1.932; Cu(3)-O(1s) 1.945].

As in complex **(1)**, the carbonate group is trigonal planar with no deviation from the mean plane observed. This carbonate-bridging pathway generates a shorter Cu-Cu separation within the cluster between Cu(1)–Cu(3) of 3.354 Å relative to Cu(2)–Cu(4) of 4.229 Å, through the mono-atomic phosphate oxygen bridges. The shortest Cu-Cu separation actually exists between Cu(3) and Cu(4) with a distance of 3.237 Å. This shortest Cu-Cu separation is noticeably smaller than the shortest Cu-Cu separation observed for the bipyridine analogue **(1)** of 3.426 Å. This is again likely a result of a closer approximation of intra-molecular layers due to increased π - π stacking facilitated by the larger 1,10-phenanthroline molecule relative to 2,2'-bipyridine. The \sim parallel positioning of the phen groups facilitates these stacking interactions and defines the inter-phen separation at \sim 3.3 Å. As in **(1)** a compromise of various steric and electronic factors resulting from the incorporation of interleaving *syn* phen ligands in the *yz* plane and the specific geometric nature of the phosphate bridging moieties also exists in **(3)**. This increased approximation is balanced by an increase in the offsetting of the rings with tilting of the aromatic (phenanthroline) rings away from each other occurring so as to optimise the stacking interaction. The dihedral angle between intramolecular stacked phen rings (5.2°) is now greater than that observed for the bipy analogue **(1)**. The influence of the phen-phen stacking interactions therefore plays a key role in determining the overall molecular structure, possibly favouring its formation.

Table 2.7. Selected bond distances (Å) and angles (°) for (3).

Cu(1)-O23	2.307(3)	O(12)-Cu(1)-O(15)	91.6(3)
Cu(1)-O15	1.932(3)	O(12)-Cu(1)-N(4)	92.1(3)
Cu(1)-Cu(3)	3.354(6)	Cu(1)-O(15)-Cu(3)	119.7(3)
Cu(1)-Cu(2)	3.237(6)	Cu(1)-O(23)-Cu(2)	101.8(3)
Cu(2)-O2	2.320(3)	O(11)-Cu(2)-O(23)	94.6(3)
Cu(2)-O11	1.913(3)	N(2)-Cu(2)-O(23)	158.0(3)
Cu(2)-O23	1.952(4)	Cu(2)-Cu(4)	4.229(5)
Cu(3)-O13	2.336(3)	O(15)-Cu(3)-O(21)	92.4(3)
Cu(3)-O21	1.919(3)	Cu(3)-O(13)-Cu(4)	97.8(4)
Cu(3)-O15	1.945(3)	N(5)-Cu(3)-N(6)	81.7(3)
Cu(4)-O1	2.283(3)	O(13)-Cu(4)-O(22)	94.6(6)
Cu(4)-O22	1.958(3)	Cu(2)-Cu(4)	4.229(5)
Cu(4)-O13	1.945(4)	Cu(3)-Cu(4)	3.237(5)

Estimated standard deviations are given in the parenthesis.

The complex crystallises with 40 water molecules per asymmetric unit. The combination of hydrophilic and hydrophobic groups in (3) has a dramatic effect upon the way the molecule packs in the crystal. A distinct hydrophilic region exists within the crystal as the lattice waters more closely associate, through H-bonding, with the phosphate, carbonate and apically bound water molecules, as observed in (1).

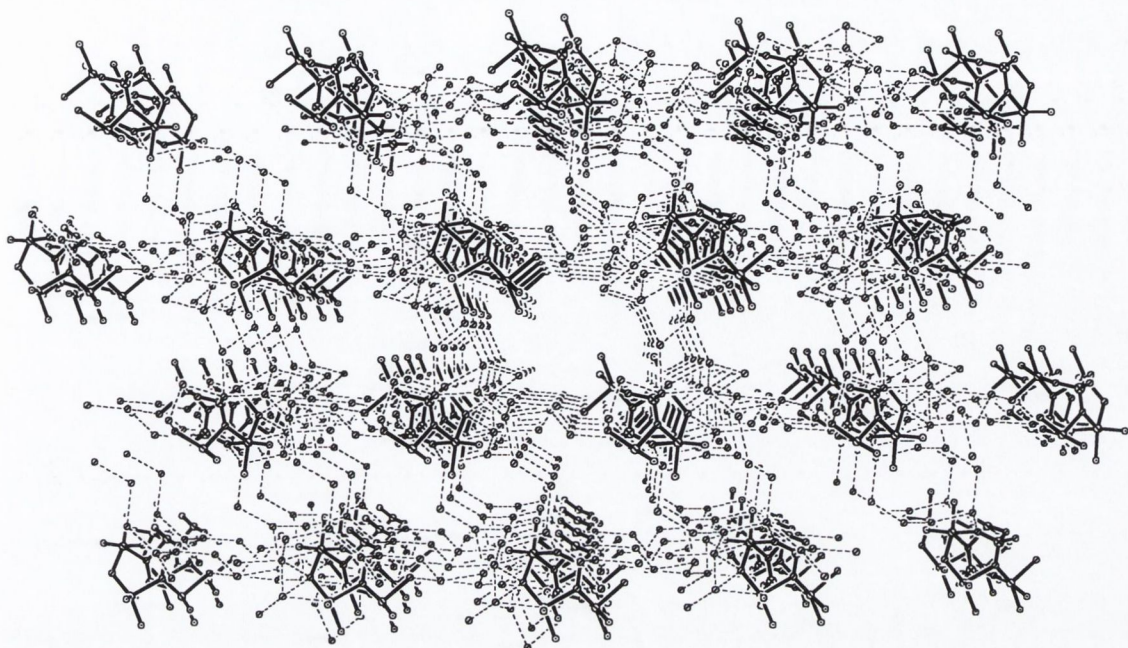


Figure 2.14. Packing diagrams of (3) showing the core unit and extended water network. Viewed along the x-axis. The 'Voids' that can be seen are occupied by the phenanthroline ligand.

A 3-D water network which enclathrates the tetranuclear Cu(II) complex as found in (1) is not generated for (3) due to the increased size of the phen ligand relative to bipy. As a result of this greater size the tetranuclear cores are 'pushed' further apart via π - π stacking. There is also an increase in hydrophobicity. These factors have the effect of isolating the water molecules between sheets of complex (3) producing a 2-D structure. The lattice water molecules do however link through H-bonding with the hydrophilic groups (Cu(II), PO_4^{3-} , CO_3^{2-}) of the complex core generating an overall 3-D hydrate network.

While a pseudo-polymorph (1a) was recovered on lowering of pH for (1), no pseudo-polymorph was observed for (3). There were no visible differences observed in the crystals recovered for (3). This would seem to rule out the possibility that a pseudo-polymorph is present. This may be a result of subtle electronic differences within (3) compared with (1a)

(phen *vs* bipy) or possibly because the specific conditions producing ‘supramolecular dimerisation’ were not exactly met.

Conclusion

A number of multinuclear copper(II) complexes were formed by careful control of pH. Supramolecular non-covalent bonding plays a key role in the overall morphology of the systems with the π -bonding, H-bonding and hydrophilic-hydrophobic interactions vital in the formation of extended water networks or complex supramolecular dimerisation. The framework structures have been accessible by self-assembly under mild conditions and are particularly attractive from both a structural and aesthetic viewpoint. Subtle effects such as increasing ligand size has been shown to have a dramatic effect on the overall structure with a decrease in dimensionality observed on going from bipy to phen.

From a magneto-structural viewpoint the successful incorporation of the hydroxy group (in **(2)**) *in lieu* of the carbonate in **(1)** shows vividly how the character of exchange interaction is dependent on geometric and electronic structure of the compounds in question, and so has a decisive influence on the overall magnetic properties.

The evidence for phosphate being a poor mediator of magnetic exchange has been increased with overall character dependent not on the trianionic PO_4^{3-} but rather on the nature of the additional bridges. The phosphate is however of great importance in the synthesis of the tetranuclear complexes and as a hydrophilic component in the extended pseudo-clathrate structures. Some degree of control over magnetic behaviour has also been obtained through this study with the deliberate synthesis of a ferromagnetic complex, by careful manipulation of reaction conditions, using information gleaned from previous results.

References

1. a) J. Slim, M.A.S. Aquin and A.G. Sykes, *Inorg. Chem.*, **35**, 614, 1991.; b) N. Yoshinori, S. Takao, T. Fumito, T. Yoishimitsu, K. Nabuo and N. Nobuhumi, *J.*

- Inorg. Biochem.*, **83**, 239-246, 2001; c) S.C. Lee and R.H. Holm, *J. Am. Chem. Soc.*, **115**, 5833, 1993.
2. K. Brown, M. Tegoni, M. Prudencio, A.S. Pereira, S. Besson, J.J. Moura, Moura, I. Moura, and C. Cambillau, *Nature. Struct. Biol.*, **7**, 191, 2000.
 3. M. Melnik, M. Kabessora, M. Koman, L. Macaskova and E. Holloway, *J. Coord. Chem.*, **50**, 177, 2000.
 4. J. Sletten, A. Sorensen, M. Julve, and Y. Journaux, *Inorg. Chem.*, **29**, 5054, 1990.
 5. W.H. Crawford, H.W. Richardson, J.R. Wasson, D.J. Hodgson and W.E Hatfield, *Inorg. Chem.*, **15**, 2107, 1976.
 6. P.E. Kruger G.D. Fallon, B. Moubaraki, K.J. Berry and K.S. Murray, *Inorg. Chem.*, **34**, 4808, 1995.
 7. AK. Cheetham, G. Ferey and T. Loiseau, *Angew. Chem. Int. Ed.*, **38**, 3269, 1999 and references therein.
 8. a) *The Biological Chemistry Of The Elements*, J.J.R. Frausto de Silva and R.J.P Williams, Clarendon, Oxford, **1991**.; b) *Chemistry Of The Elements*, N.N. Greenwood and A. Earnshaw, Butterworth-Heinemann Ltd, Oxford, **1984**.
 9. a) T. Klabunde and B. Krebs, *Struct. Bonding*, **89**, 177, 1997.; b) J. B. Vincent, G. L. Olivier-Lilley, B. A. Averill, *Chem. Rev.*, **90**, 1447, 1990.
 10. a) *Crystal Chemistry Of Condensed Phosphates*, A. Durif, Plenum Press, New York, **1995**.; b) A. Muller-Hartmann and H. Vahrenkamp, *Eur. J. Inorg. Chem.*, **11**, 2355, 2000.; c) *Chemistry of Biomolecules*, R.J. Simmons, RSC, **1995**.
 11. A. Muller-Hartmann and H. Vahrenkamp, *Inorg. Chim. Acta.*, **300**, 531, 2000.
 12. S.N. Lambert, T.R. Felthouse and D.N.Hendrickson, *Inorg. Chim. Acta.*, **29**, L223, 1978.

13. C. Kaes, A. Katz and M.W. Hosseini, *Chem. Rev.*, **100**, 3553, 2000.
14. S.P. Perlepes, J.C. Huffman and G. Christou, *Polyhedron*, **11**, 1471, 1992.
15. C.A. Hunter, K.R. Lawson, J. Perkins and P.L. Anelli, *J. Chem. Soc., Perkin. Trans.*, **2**, 651, 2001.
16. a) *Molecular Magnetism*, O. Kahn, VCH, Weinheim, Germany, **1993**.; b) *Research Frontiers in Magnetochemistry*, C.J O'Connor, World Scientific, Singapore, **1993**.
17. P.E. Kruger, Doctoral Thesis, Monash University, **1994**.
18. *Infrared and Raman Spectra of Inorganic and Coordination Compounds*, Part B, Kazuo Nakamoto, John Wiley, New York, **1997**.
19. a) M.J. Young, D. Wahnnon, R.C. Hynes and J. Chin, *J. Am. Chem. Soc.*, **117**, 9441, 1995.; b) S.K. Nair and D.W. Christianson, *J. Am. Chem. Soc.*, **113**, 9455, 1991.; c) F. Toda and Y. Tohi, *J. Chem. Soc., Chem. Comm.*, 1236, 1993.
20. *Inorganic Electronic Spectroscopy*, A.B.P. Lever, Elsevier, New York, p355, **1968**.
21. Cambridge Structural Database, Cambridge, U.K, Version 5.22, Oct., **2001**.
22. L.L. Merrit and E.D. Schroedar, *Acta. Cryst.*, **9**, 801, 1956.
23. a) *Inclusion Compounds*, J.L. Atwood, J.E.D. Davies and D.D. MacNicol, Oxford University Press, **1991**.; b) K.A. Udachin and J.A. Ripmeester, *Angew. Chem. Int. Edit.*, **38**, 1983, 1999.
24. R. Ludwig, *Angew. Chem. Int. Ed.*, **40**, 1808, 2001.
25. I. Dance and M. Scudder, *J. Chem. Soc., Chem. Comm.*, **10**, 1039, 1995.
26. a) R. Boca, L. Dihan, D. Makanova, J. Mrozinski, G. Ondrejovic and M. Tatarko, *Chem. Phys. Lett.*, **344**, 305, 2001.; b) G. Alzuet, J.A Real, J. Borrás, R. Santiago-García and S. García-Granda., *Inorg. Chem.*, **40**, 2420, 2001.

27. S. Ferlay, G. Francese, H. Schmalle and S. Decurtins, *Inorg. Chem. Acta.*, **286**, 108, 1999.
28. P.C. Healy, J.M. Patrick and A.H. White, *Aust. J. Chem.*, **52**, 271, 1999.
29. a) D.J. Hodgson, *Prog. Inorg. Chem.*, **19**, 173, 1975.; b) V.H. Crawford, H.W. Richardson, J.R. Wasson, D.J.Hodgson and W.E.Hatfield, *Inorg. Chem.*,**15**, 2107, 1976.

Chapter Three

Preparation of Copper(II), Zn(II) and Vanadyl(II) complexes incorporating pyrophosphate ($P_2O_7^{4-}$).

Influence of water on structure and magnetic behaviour.

Introduction.

The oligophosphates are the simplest forms of condensed phosphates. Their anions correspond to the general formula $[P_nO_{3n+1}]^{(n+2)-}$. Pyrophosphates, or diphosphates ($n = 2$) as they are also known, were first characterised, as salts, by Berzelius and date back to 1816.¹ Considerable current interest continues to revolve around the chemistry and biochemistry associated with polyphosphate anions because of their importance in biology. They participate in a diverse series of bio-energetic processes ranging from oxidative phosphorylation including ATP (adenosine 5'-triphosphate) production,² through nucleic acid mediated information processing, to energy storage and transduction.³ A pivotal intermediate within this family is the pyrophosphate tetra-anion, $P_2O_7^{4-}$. Nature has produced ubiquitous cytoplasmic enzymes that hydrolyse pyrophosphate. This is essential for maintaining intracellular levels of phosphate and for removing the pyrophosphate product of the nucleotide coupling reactions, thereby favourably affecting the thermodynamics of nucleotide coupling.⁴ In all enzymatic pyrophosphatases, divalent metal ions are required with Mg(II) providing the highest levels of activity, but Zn(II), Mn(II), and Cu(II) all sustaining appreciable rates of hydrolysis. It is somewhat surprising then that the coordination chemistry of this naturally present, biologically vital tetra-anion is practically unexplored, as metal ions are so heavily involved in pyrophosphate metabolism.⁵ This relative dearth may be a consequence of its ready hydrolysis as exemplified by those bioinorganic reactions catalysed by the inorganic pyrophosphatases. A systematic study was therefore under-taken using as precursors metal ions previously bound to chelating ligands in order to minimise hydrolysis of the pyrophosphate and subsequent precipitation of undesired phosphato complexes. This is because simple divalent metal ions have been shown to enhance cleavage of both inorganic and biological pyrophosphates by up to 100-fold at room temperature (298K).⁶ Short chain pyrophosphates have been shown to be usually fairly inert to cleavage in the presence of metal ions that have been previously chelated. Diphosphates are also more stable at alkaline pH. Indeed without the presence of M(II) ions, and in basic solution, cleavage of P-O-P linkages have half-lives measured in years.⁷ Most effort devoted to the study of pyrophosphate is from a kinetic and/or thermodynamic viewpoint.

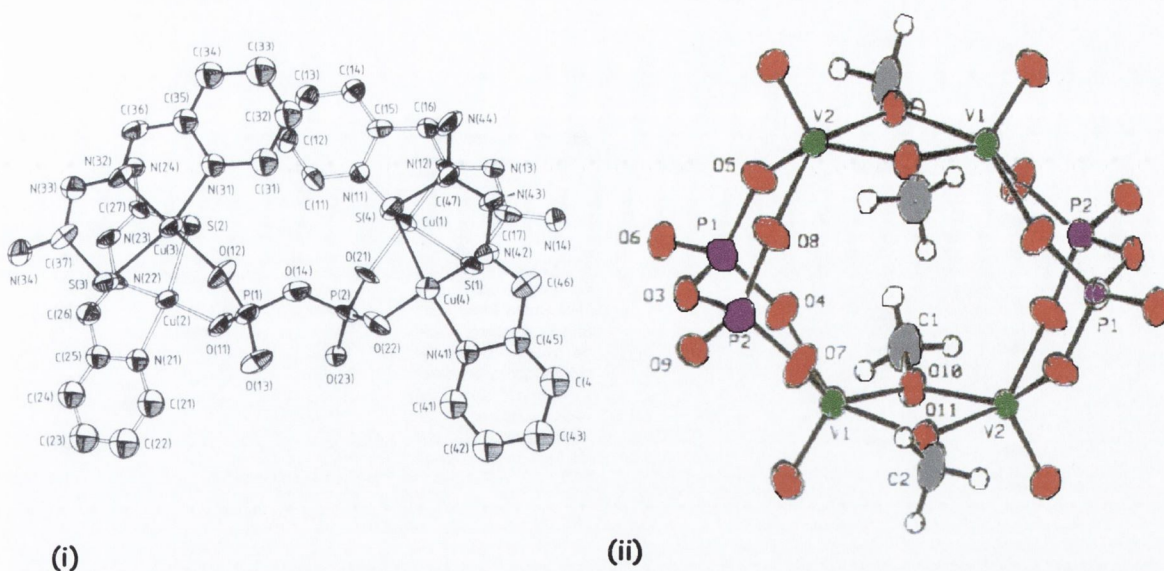
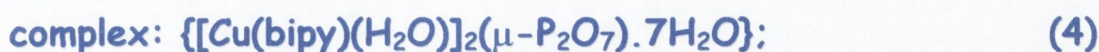


Fig 3.1. Structures of both coordination complexes containing bridging pyrophosphate found on literature review. (i) $[(\text{CuL})_4(\mu\text{-P}_2\text{O}_7)] \cdot n\text{H}_2\text{O}$ (HL = 2-formylpyridinethiosemicarbozone; $n = 9\text{-}12^8$ and (ii) $[\text{C}_8\text{H}_{11}\text{NH}]_4[(\text{VO})_4(\text{P}_2\text{O}_7)_2(\text{OCH}_3)_4]^9$. Waters of crystallisation of (i) and $(\text{C}_8\text{H}_{11}\text{NH})_4$ counterion of (ii) are omitted for clarity.

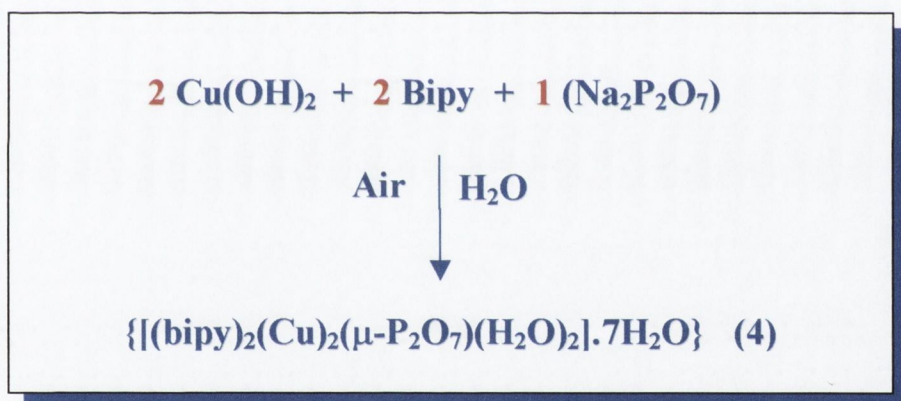
To illustrate the problem of hydrolysis a literature review revealed only two X-ray structures of coordination compounds containing bridging pyrophosphate and transition metals, namely, $[(\text{CuL})_4\text{P}_2\text{O}_7] \cdot n\text{H}_2\text{O}$ (HL = 2-formylpyridinethiosemicarbozone; $n = 9\text{-}12^8$) and $[(\text{C}_8\text{H}_{11}\text{NH})_4[(\text{VO})_4(\text{P}_2\text{O}_7)_2(\text{OCH}_3)_4]^9$ (Figure 3.1). Of these two complexes, the former, reported by Murray *et al.*, was shown to exhibit weak antiferromagnetic coupling between Cu(II) ions with the pyrophosphate in a staggered tetrakis monodentate coordination mode, and the latter complex was employed in the catalytic oxidation of butane to maleic anhydride. In this case the pyrophosphate exhibits a bis-bidentate bridging arrangement between vanadyl ions. While bridging pyrophosphate complexes such as those just mentioned are uncommon it has been demonstrated that pyrophosphate is a good non-bridging ligand for M(II) ions at neutral and alkaline pH and it has been established that the predominant species in solution is a M(II) complex with two $\text{P}_2\text{O}_7^{4-}$ ligands.¹⁰ Our interest was also expanded to incorporate oxovanadium(IV). Oxovanadium phosphate chemistry has grown impressively in recent times initially as a result of industrial interest in the $(\text{VO})_2\text{P}_2\text{O}_7$ catalysts.¹¹ This has resulted

in a rich chemistry, which is associated in part, with the ability of vanadium to adopt different coordination polyhedra and to readily accede to various oxidation states.

3.1. Preparation and Characterisation of the Dinuclear



An aqueous suspension of copper(II) hydroxide (or solution of copper(II) nitrate) was reacted with an aqueous suspension of 2,2'-bipyridine and resulted in the formation of a deep blue solution after ~5 minutes. Solid tetra-sodium pyrophosphate was then added resulting in a slightly darker blue solution. Compound (4) was then obtained in good yield (*ca* 90%) as sky blue parallelepipeds by slow evaporation of the concentrated aqueous solution over approximately four days.



Scheme 3.1. Direct preparation of the dinuclear copper(II) species (4).

Infrared spectra obtained of the crystals confirmed the presence of pyrophosphate and 2,2'-bipyridine. Elemental analysis (C:H:N:P) was consistent with the formation of a complex with the following formula: $\{[(\text{bipy})_2(\text{Cu})_2(\mu\text{-P}_2\text{O}_7)(\text{H}_2\text{O})_2]\cdot 7\text{H}_2\text{O}\}$. The d-d spectrum of an aqueous solution of (4) reveals a broad featureless band with a maximum at 657 nm, which again is consistent with Cu(II) in a distorted square based pyramidal geometry. Electrospray mass spectroscopy reveals a series of peaks consistent with fragmentation of the complex.

3.2. Description of the molecular structure of the dinuclear

copper(II) complex $[[\text{Cu}(\text{bipy})(\text{H}_2\text{O})]_2(\mu\text{-P}_2\text{O}_7)\cdot 7\text{H}_2\text{O}]$: (4)

Crystals were grown by slow evaporation of a concentrated aqueous solution containing stoichiometric amounts of $\text{Cu}(\text{OH})_2$, 2,2'-bipyridine and tetra-sodium pyrophosphate over approximately ten days. The crystals are stable deep blue diamond shaped entities and were used for a single crystal X-ray diffraction study. Dr. M. Nieuwenhuizen of the Queens University, Belfast, performed the data collection and structural refinement. Complex (4) is depicted in Figure 3.2, showing the atomic numbering scheme used.

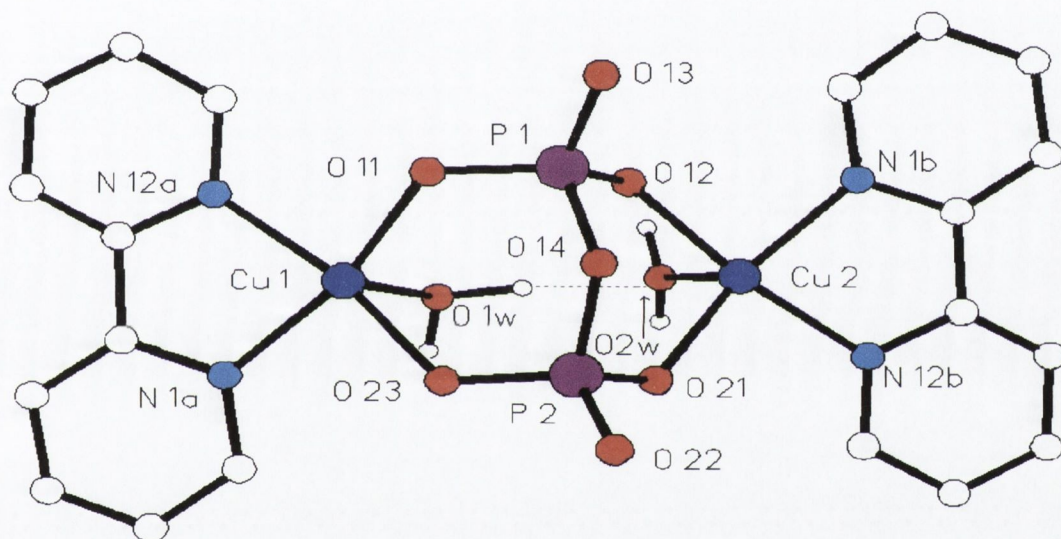


Figure 3.2. $[[\text{Cu}]_2(\text{bipy})_2(\mu\text{-P}_2\text{O}_7)(\text{H}_2\text{O})_2]\cdot 7\text{H}_2\text{O}$ (4).

Bipyridine hydrogen atoms and waters of crystallization omitted for clarity.

The structure of (4) consists of neutral $\{[\text{Cu}(\text{bipy})(\text{H}_2\text{O})]_2(\mu\text{-P}_2\text{O}_7)\}$ dinuclear copper(II) units and seven waters of crystallisation linked by a network of hydrogen bonds. The geometry of the two crystallographically independent copper atoms is distorted square pyramidal with two bipy-nitrogens and two pyrophosphate oxygen atoms building the basal plane with a water molecule occupying the apical position. The copper atoms are shifted 0.226 Å $[[\text{Cu}(1)]$ and 0.190 Å $[[\text{Cu}(2)]$ from the mean basal plane towards the axially

coordinated water molecules O(1w) and O(2w), respectively. The bipyridine ligands are essentially planar with a dihedral angle between the pyridyl rings of 3.9° and 3.7°.

Table 3.1. Selected bond distances (Å) and angles (°) for (4).

Cu(1)-Cu(2)	4.646(4)	O(11)-Cu(1)-O(23)	95.1(2)
Cu(1)-O(23)	1.925(4)	P(1)-O(11)-Cu(1)	128.7(2)
Cu(1)-O(11)	1.978(4)	N(1a)-Cu(1)-N(12a)	80.6(2)
Cu(1)-O(1w)	2.295(4)		
Cu(2)-O(12)	1.967(4)	O(12)-Cu(2)-O(21)	93.3(2)
Cu(2)-O(21)	1.933(4)	P(2)-O(21)-Cu(2)	121.4(2)
Cu(2)-N(1b)	2.017(5)	N(1b)-Cu(2)-N(12b)	80.6(2)
Cu(2)-O(2w)	2.268(4)		

Estimated standard deviations are given in the parenthesis.

Hydrogen bonds involving the coordinated O(1w) and O(2w) water molecules [2.913 Å and 154°, for O(1w)-O(2w) and O(1w)-H(1w1)⋯O(2w), respectively] and O(2w) and O(13p) [2.767 and 169° for O(2w)⋯O(13p) and O(2w)-H(2w2)⋯O(13p); $p = 1-x, 1-y, -z$] can be seen in Figure 3.3.

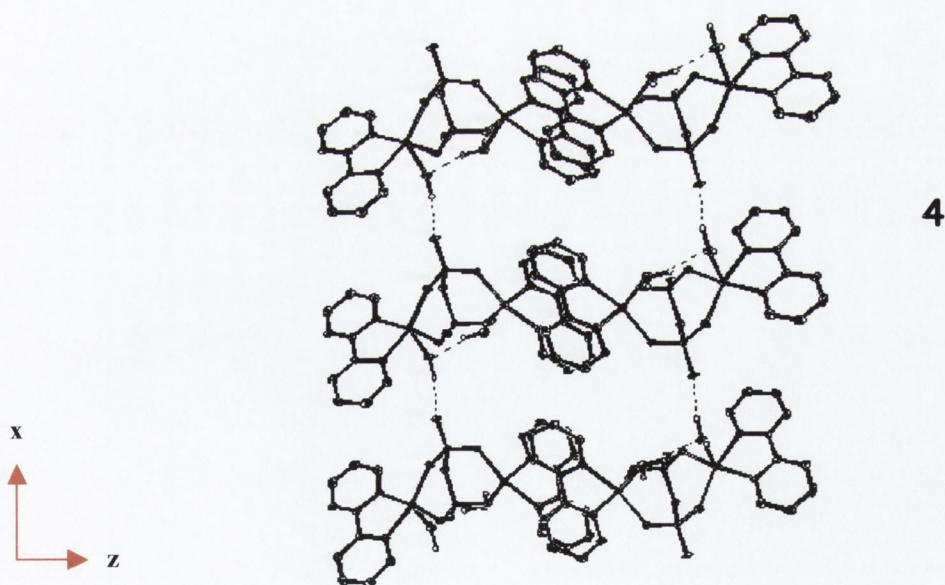


Figure 3.3. Packing diagram of complex (4) showing the intermolecular H-bonding and π - π interactions; Bipyridine H-atoms and waters of crystallization omitted for clarity.

The pyrophosphate group acts as a bis-bidentate ligand forming two six-membered chelate rings with an envelope conformation. The dihedral angle between the P(1)P(2)O(11)O(23) and P(1)P(2)O(12)O(21) mean planes is 115° , a value close to that of perfect tetrahedral (109.5°).

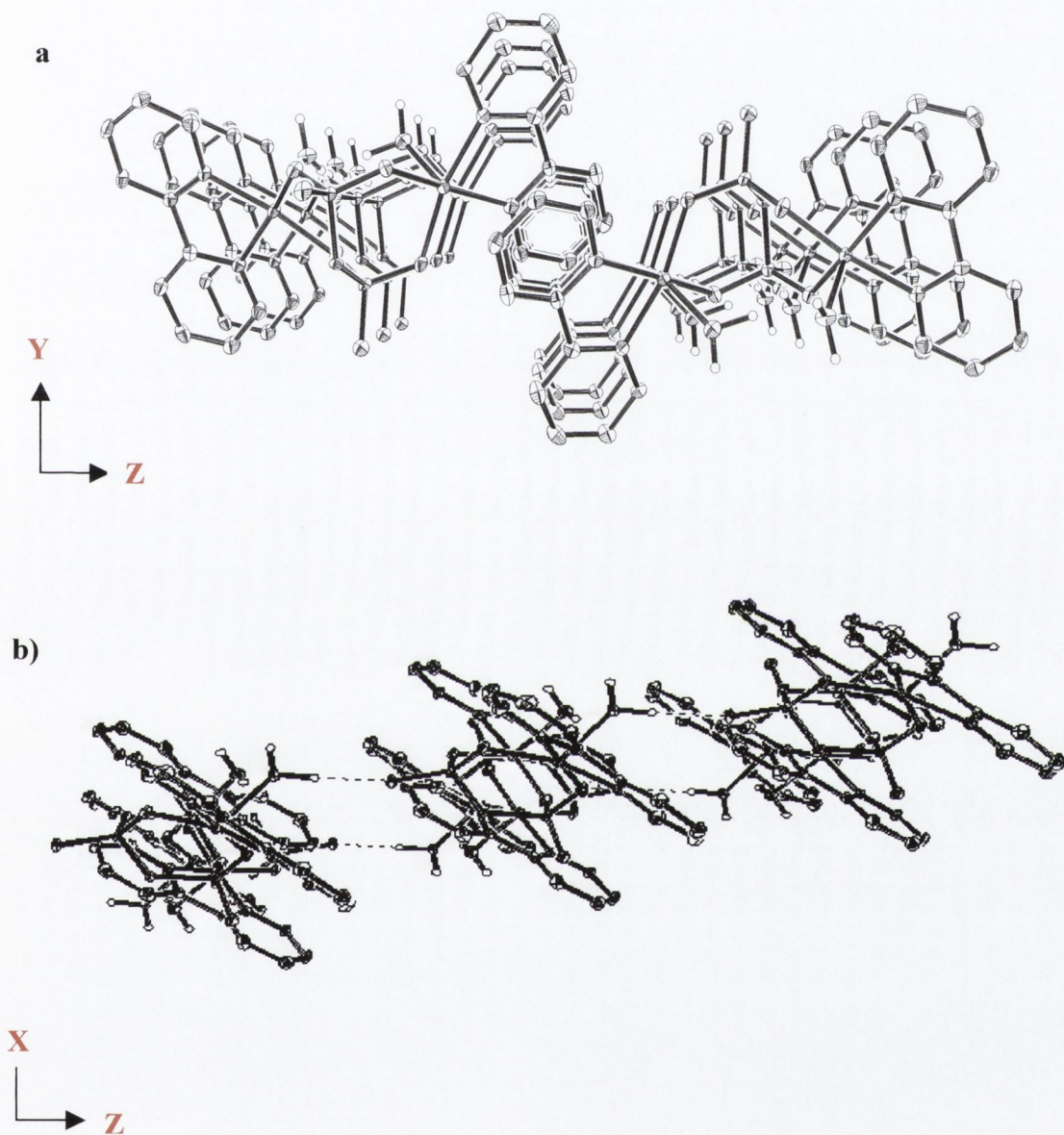


Figure 3.4. Thermal ellipsoid (50%) plots of (4) showing a) the intermolecular π - π interactions in the yz plane i.e. along the x-axis and b) H-bonding interaction in the xz plane i.e. along the z-axis. Waters of crystallization have been omitted for clarity.

The bond lengths of the terminal oxygens of the pyrophosphate ligand [1.498 and 1.500 Å for P(1)-O(13) and P(2)-O(22)] are shorter than those of the inner O(14) atom [1.637 and 1.612 Å for P(1)-O(14) and P(2)-O(14)] in agreement with their single and double bond character, respectively. The Cu(1)-Cu(2) distance is 4.646 Å whereas the shortest interdimer Cu-Cu separations are 5.899 [Cu(2)-Cu(2p)] and 6.057 Å [Cu(1)-Cu(1q); $q = 1-x, 1-y, 1-z$]. Intermolecular π - π interactions from adjacent H-bonded chains (interplanar distance between adjacent bipy's is 3.5 Å) through an interleaving of bipy ligands in the yz plane leads to a layer containing Cu(II) dimers.

3.2.1. Thermal analysis of complex (4). Formation of stable intermediates (5) and (6) of various degrees of hydration.

Thermal analysis (TGA/DTA) of (4) shows that it loses the seven lattice water molecules in the temperature range 25-68°C, the resulting partially dehydrated phase (5) being stable for $68^\circ < T < 86^\circ$. The loss of the two remaining coordinated water molecules starts at 86° giving the fully anhydrous phase (6) at $T > 120^\circ$. This latter species decomposes at temperatures above 325°C.

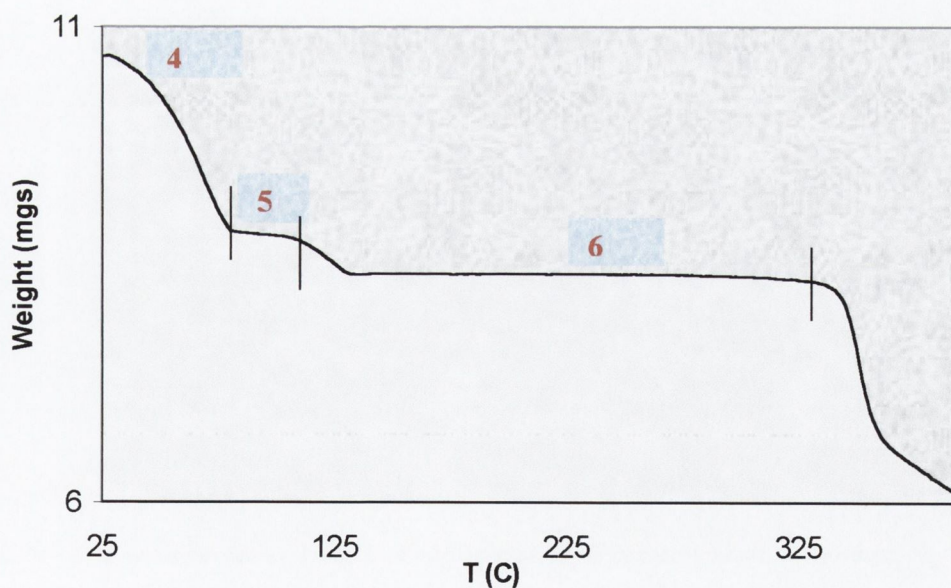


Figure 3.5. Thermogravimetric analysis plot of (4) showing how it gives rise to (5) and (6).

All three stages of various hydration ((4)-(6)), were isolated and characterised by infrared spectra with variable temperature magnetic susceptibility data recorded for each. Washing the fully hydrated crystals with ethanol returns a pale blue powder, the infrared spectra of which exhibits shifts in the infrared consistent with the shifts observed on a sample taken from thermal analysis between 68°C and 86°C indicating that lattice water can be removed by simple washing. Elemental analysis suggests that washing does not remove the coordinated water molecules.

3.2.2. Magnetic behaviour of the dinuclear complex

$\{[\text{Cu}(\text{bipy})(\text{H}_2\text{O})]_2(\mu\text{-P}_2\text{O}_7)\cdot 7\text{H}_2\text{O}\}$ (4) and its dehydrated phases
 $\{[\text{Cu}(\text{bipy})(\text{H}_2\text{O})]_2(\mu\text{-P}_2\text{O}_7)\}$ (5) and $\{[\text{Cu}(\text{bipy})]_2(\mu\text{-P}_2\text{O}_7)\}$ (6)

The room temperature magnetic moment measured on an Evans-modified Guoy balance indicated a moment of 1.93 BM per Cu(II). The magnetic behaviour of the compounds 4-6 ($H = 50 \text{ G}$) is shown in Figure 3.6. The χ_M versus T curves are characteristic of antiferromagnetic coupling with susceptibility maxima at 19 K for (4) and (5), and 90 K for (6). From a magnetic point of view, (4) can be described to a first approximation as a Cu(II) chain with regular alternation of two kinds of bridges, namely pyrophosphato- and hydrogen-bonded pathways. The analysis of the susceptibility data of (4) through the Hamiltonian $H = -J\sum_i(\hat{S}_{i-1}\cdot\hat{S}_i - \alpha\hat{S}_{i-1}\cdot\hat{S}_{i+1})$ (α being the alternating parameter and \hat{S}_i the local spin) leads to a value of α practically equal to zero. In other words, (4) behaves magnetically as an isolated copper(II) dimer with $J = -20\text{cm}^{-1}$, $g = 2.09$, and $R = 1.2 \times 10^{-6}$ (R is the agreement factor defined as $\sum_i [\chi_M^{\text{obs}}(i) - \chi_M^{\text{calc}}(i)]^2 / [\chi_M^{\text{obs}}(i)]^2$). Inspection of the structure shows that the magnetic orbital on each copper atom is most probably of the $d_x^2 - y^2$ type with the x and y axes being roughly defined by the bonds from copper to bipy nitrogen. The poor overlap between the two non-coplanar copper centred magnetic orbitals through the equatorial O(11)-P(1)-O(12) and O(23)-P(2)-O(21) bridging networks accounts for the weak antiferromagnetic coupling observed. Although there is possibly an additional exchange pathway in (4), that involving the axially coordinated waters through hydrogen bonding, it would be expected to

be much less efficient than the bis-chelating pyrophosphate in mediating exchange interactions.

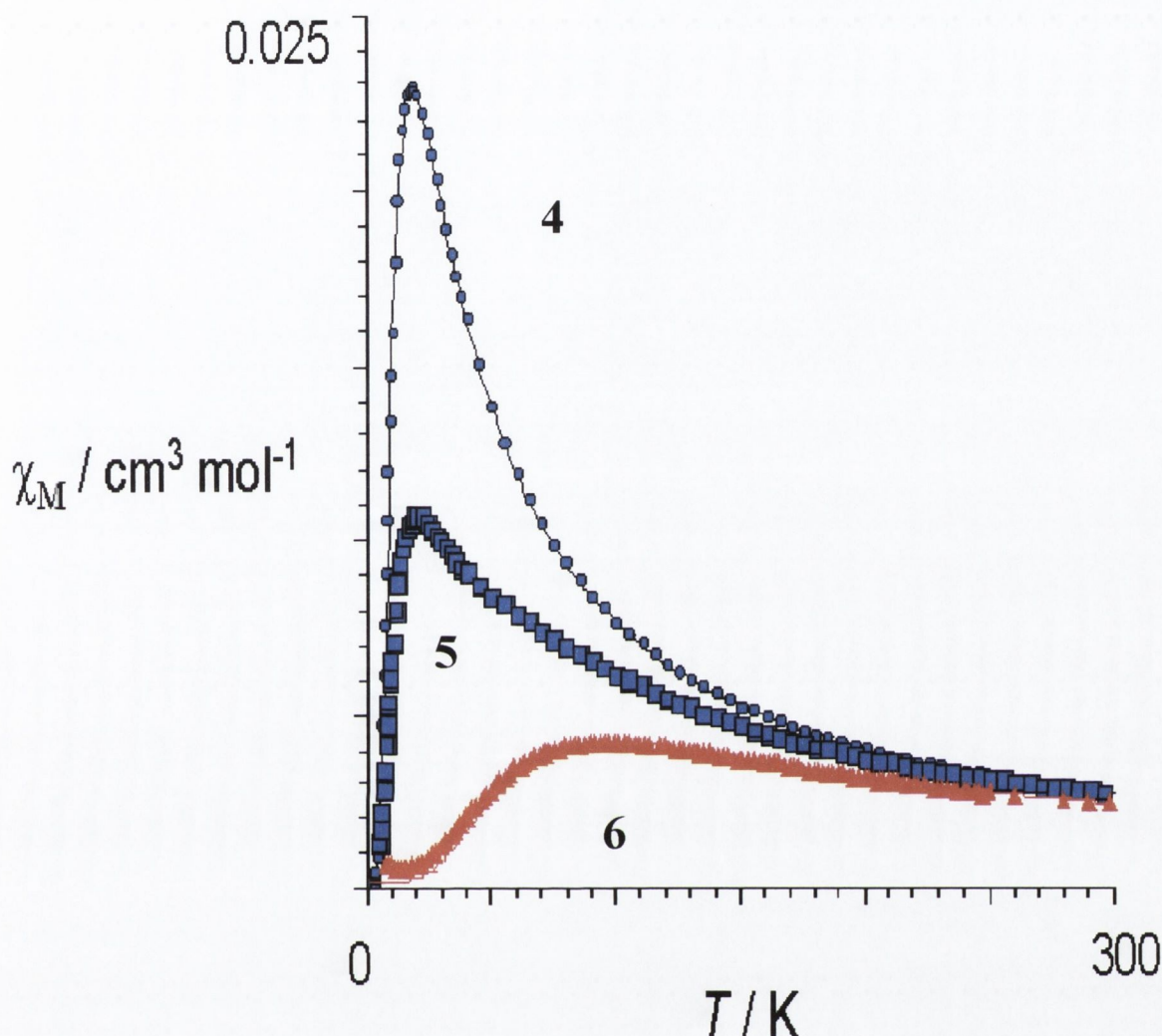


Figure 3.6. Thermal dependence of χ_M for the compounds 4-6 [χ_M being the magnetic susceptibility per two copper (II) ions]. Solid lines indicate the best fit.

The loss of seven water molecules from (4) to yield (5) causes a decrease in the height of the susceptibility curve, while leaving the temperature at which the maximum occurs unchanged. These features are typical of a higher magnetic dimensionality in (5), indicating that α is now non-zero (Figure 3.7).¹²

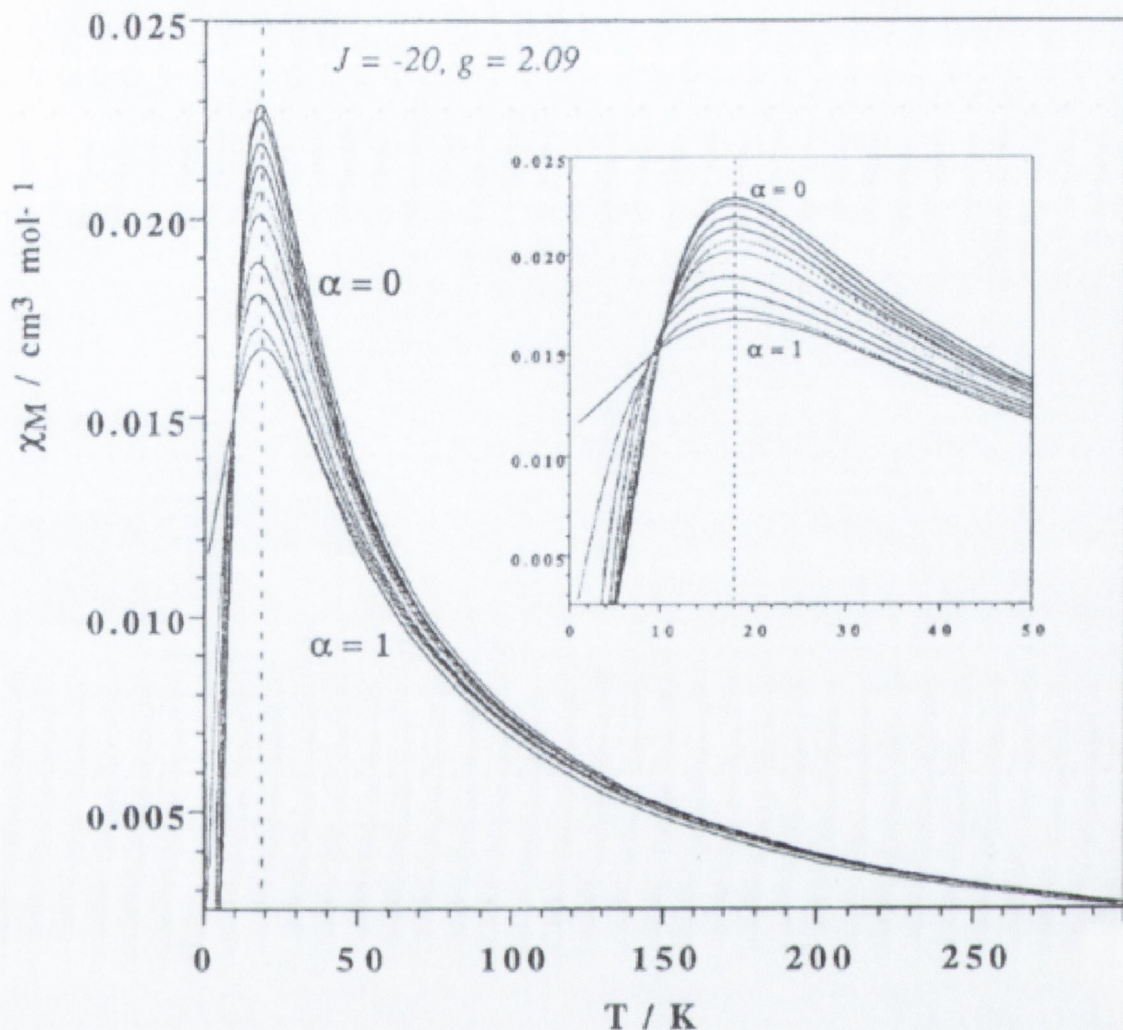
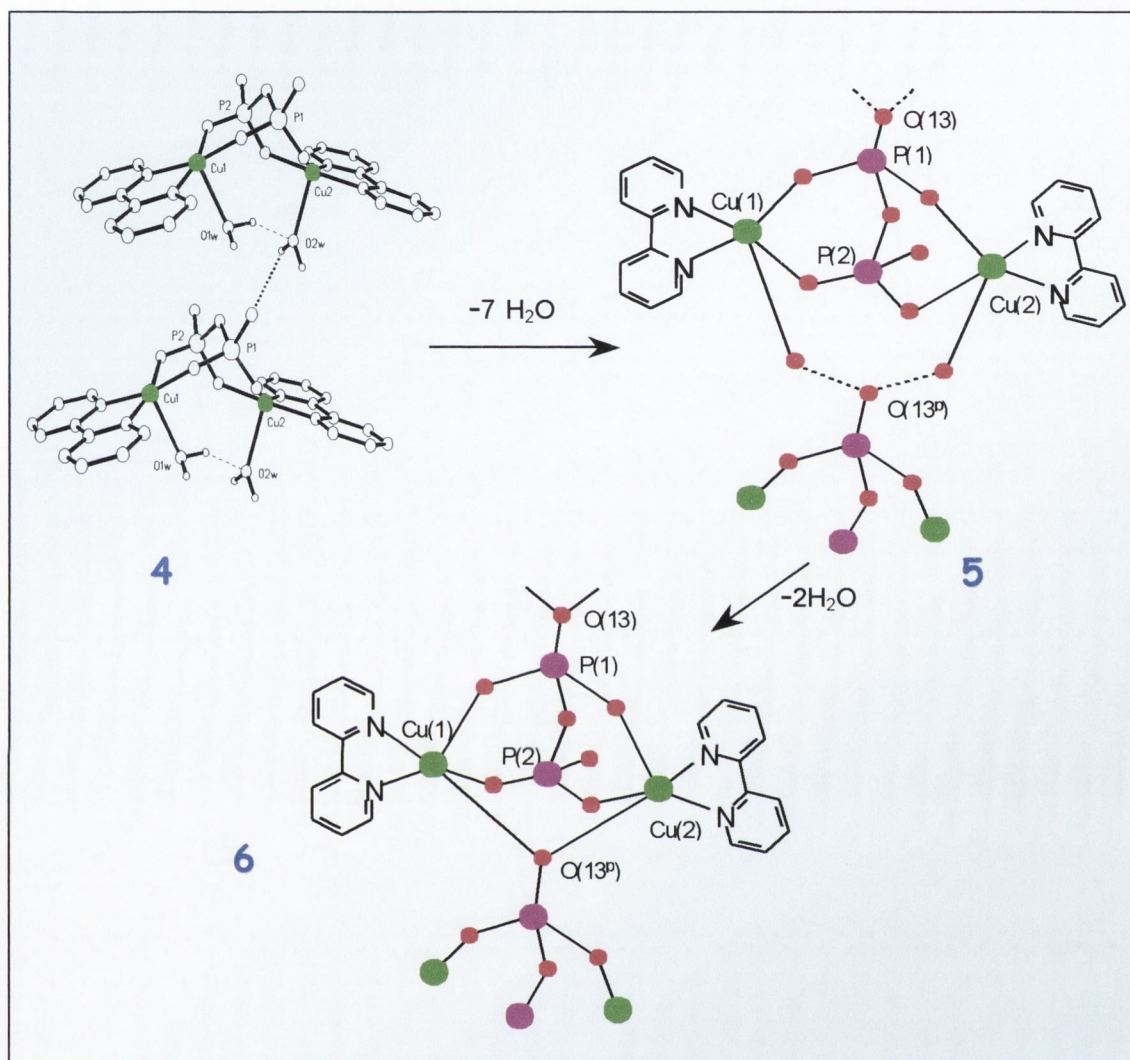


Figure 3.7. Thermal dependence of χ_M as a function of α . Systematic variation of α (between 0 and 1) whilst holding J and g constant resulted in a lowering of the height of the susceptibility curve maximum while at the same time leaving the temperature at which the maximum occurs unchanged.

It is likely the loss of lattice water molecules makes easier the approximation of the adjacent pyrophosphate-bridged dinuclear units, reinforcing the π - π overlap and introducing additional H-bonding to give an alternating two-dimensional magnetic system. The pyrophosphate-bridged copper(II) fragment would remain essentially unchanged (indeed as noted the temperature at which the maximum occurs remains the same), so the additional

weaker magnetic coupling is assigned to the hydrogen-bonded pathway. Further dehydration leads to compound **(6)** (Scheme 3.2).



Scheme 3.2. Proposed dehydration route for (4-6). (4) is a crystal structure whilst compounds 5 and 6 are postulates from Infrared and magnetic susceptibility studies.

Its susceptibility curve exhibits a maximum at 90 K indicating that stronger antiferromagnetic coupling occurs in **(6)** and suggesting the formation of a polymeric compound upon complete dehydration. This conclusion is further supported by a shift toward lower frequencies of the strongest P-O stretching vibration (*ca.* 20 cm^{-1}) in the IR spectrum¹³ when going from (4) to (5) to (6).

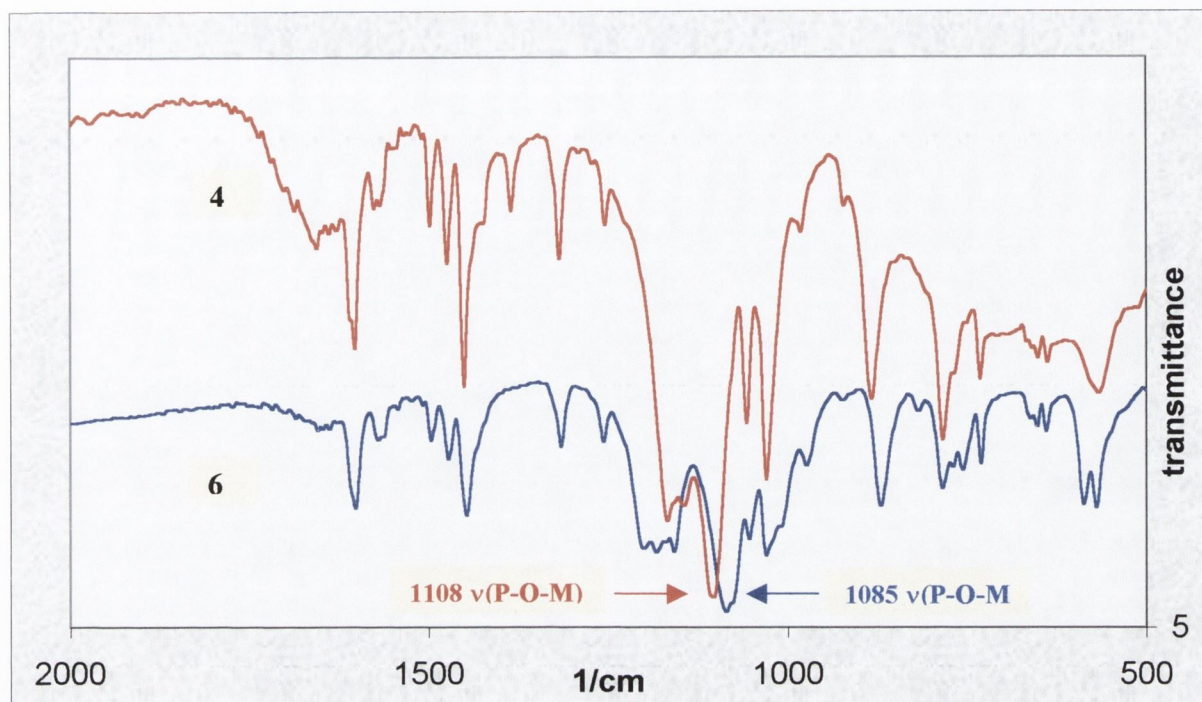


Figure 3.8. Infrared spectra of complex (4) at room temperature and complex (6), formed on heating a sample of (4) for 1hr at 120°.

The exchange coupling through the “oxo” bridge (P-O) would be expected to be dominant and strongly antiferromagnetic in nature. Consequently, the magnetic behaviour of (6) would be typical of a relatively strongly coupled copper(II) dimer, and this is consistent with the shift of the susceptibility maximum from 19 K (4) to 90 K (6). The analysis of the magnetic behaviour of (6) through a simple Bleaney-Bowers expression¹⁴ leads to an excellent fit with $J = -110 \text{ cm}^{-1}$, $g = 2.08$, and $R = 5.0 \times 10^{-5}$. This relatively strong coupling is in agreement with the proposed “oxo” pathway. It should be noted here that strong antiferromagnetic coupling of up to -500 cm^{-1} has been reported for singly hydroxo bridged copper(II) complexes.¹⁵

3.3. Preparation, Characterisation and Structural Description of the mononuclear copper(II) complex



Having successfully formed the dinuclear copper(II) complex it was decided that attempts would be made to generate hetero-bimetallic analogues containing Cu(II). With this in mind we reacted an aqueous suspension of copper(II) hydroxide with 2,2'-bipyridine and tetrasodium pyrophosphate in a 1:1:1 equimolar stoichiometry. The blue solution that results was filtered and allowed to stand. Compound (7) was obtained in good yield (ca 80%) as deep royal blue needles. Infrared spectra confirmed the presence of pyrophosphate with a broad band at 1112 cm^{-1} and shoulders at 1184 and 1022 cm^{-1} . 2,2'-bipyridine bands were recorded at 1608 , 1570 , and 769 cm^{-1} . Elemental analysis (C:H:N) was consistent with the following formulation $\{[\text{Cu}(\text{bipy})(\text{H}_2\text{O})(\text{Na}_2\text{P}_2\text{O}_7)\cdot 10\text{H}_2\text{O}]\}$. Single crystal X-ray crystal diffraction proved conclusively the existence of (7) with pyrophosphate in a bidentate mode. The eleven water molecules calculated (from elemental analysis) to be present were found to be mostly coordinated with one water bound apically to the copper(II) atom and four bound to each of the two sodium atoms. The remaining two water molecules are present in the lattice. Complex (7) is depicted in Figure 3.9, showing the atomic numbering scheme used. The geometry of the copper atom is distorted square pyramidal with bipy-nitrogens and two pyrophosphate oxygen atoms building the basal plane and a water molecule occupying the apical position. The copper atom is shifted 0.096 \AA [(Cu(1))] from the mean basal plane towards the axially coordinated water molecule O(1w). The bipyridine ligand is essentially planar with a dihedral angle between the pyridyl rings of 3.7° . As in (4), the phosphorous-oxygen bond lengths vary within the pyrophosphate ligand, with P(1)-O(23) and P(2)-O(13) [1.517 and 1.507 \AA] being shorter than those of P(1)-O(11) and P(2)-O(21) [1.531 and 1.529 \AA] in agreement with their single and double bond character.

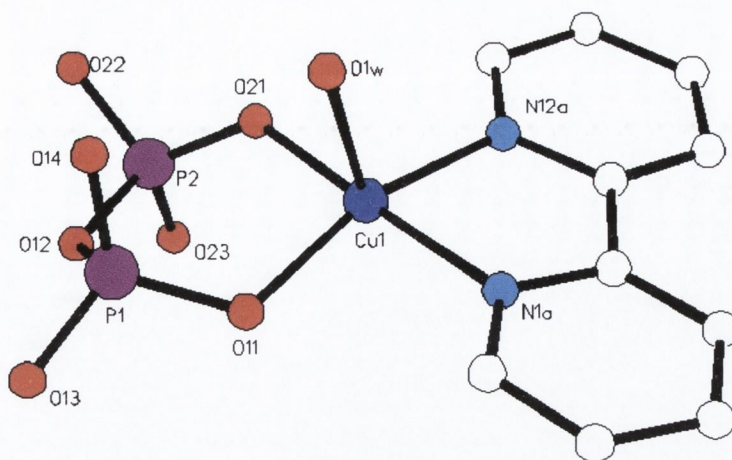


Figure 3.9. Mononuclear copper(II) di-anionic complex (7). Sodium atoms and waters of crystallisation omitted for clarity.

The dihedral angle between the P(1)P(2)O(21)O(11) and P(1)P(2)O(13)O(23) mean planes is 113° , a value closer to that of perfect tetrahedral than that of the dinuclear analogue (**4**) [115°]. This is attributed to greater steric freedom about the phosphorous centres, which are no longer accommodating a second copper(II) atom.

Table 3.2. Selected bond distances (Å) and angles ($^\circ$) for (7).

Cu(1)-O(11)	1.923(3)	O(11)-Cu(1)-O(21)	93.8(5)
Cu(1)-O(21)	1.944(3)	N(1a)-Cu(1)-O(21)	172.4(5)
Cu(1)-N(1a)	1.966(3)	N(1a)-Cu(1)-N(12a)	80.7(3)
Cu(12a)-N(12a)	1.998(2)	O(1w)-Cu(1)-N(1a)	92.1(3)
Cu(1)-O(1w)	2.323(2)		

Estimated standard deviations are given in the parenthesis.

Two sodium atoms are required to balance charge in (**7**). Na(1) is not coordinated directly to (**7**) but resides in the lattice where it is coordinated to six water molecules. Na(2) is bound to pyrophosphate oxygen O(14) and five lattice water molecules, two of which are shared with an adjacent sodium atom acting as bridges between these adjacent sodium atoms (Fig 3.10).

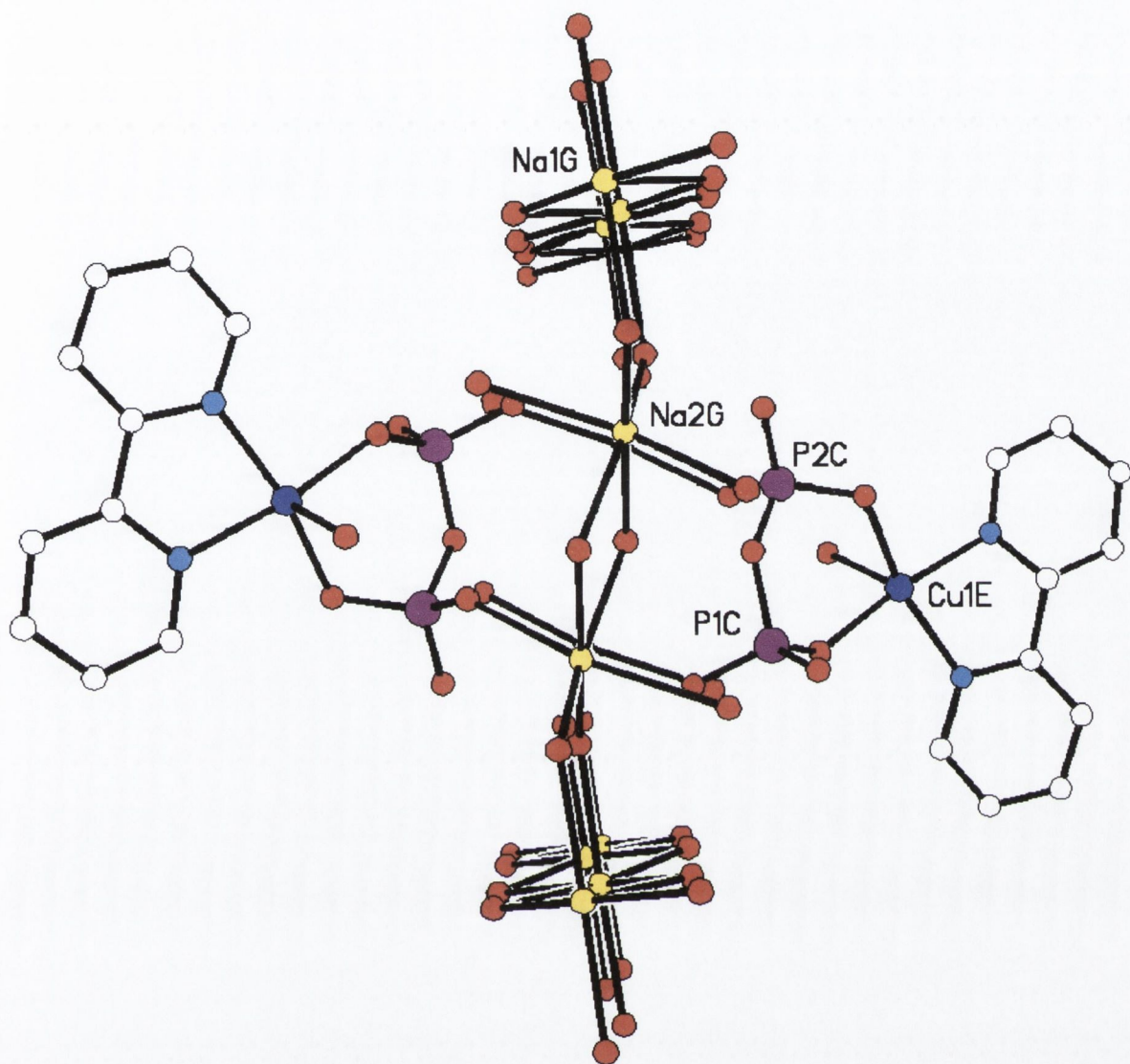


Figure 3.10. Packing diagram of (7) showing extensive sodium and lattice water interactions.

Intermolecular π - π interactions between adjacent 2,2'-bipyridine rings exist along the x-axis, in the yz plane. An extensive array of water and sodium atoms is built up in (7) forming a 2-D layered network.

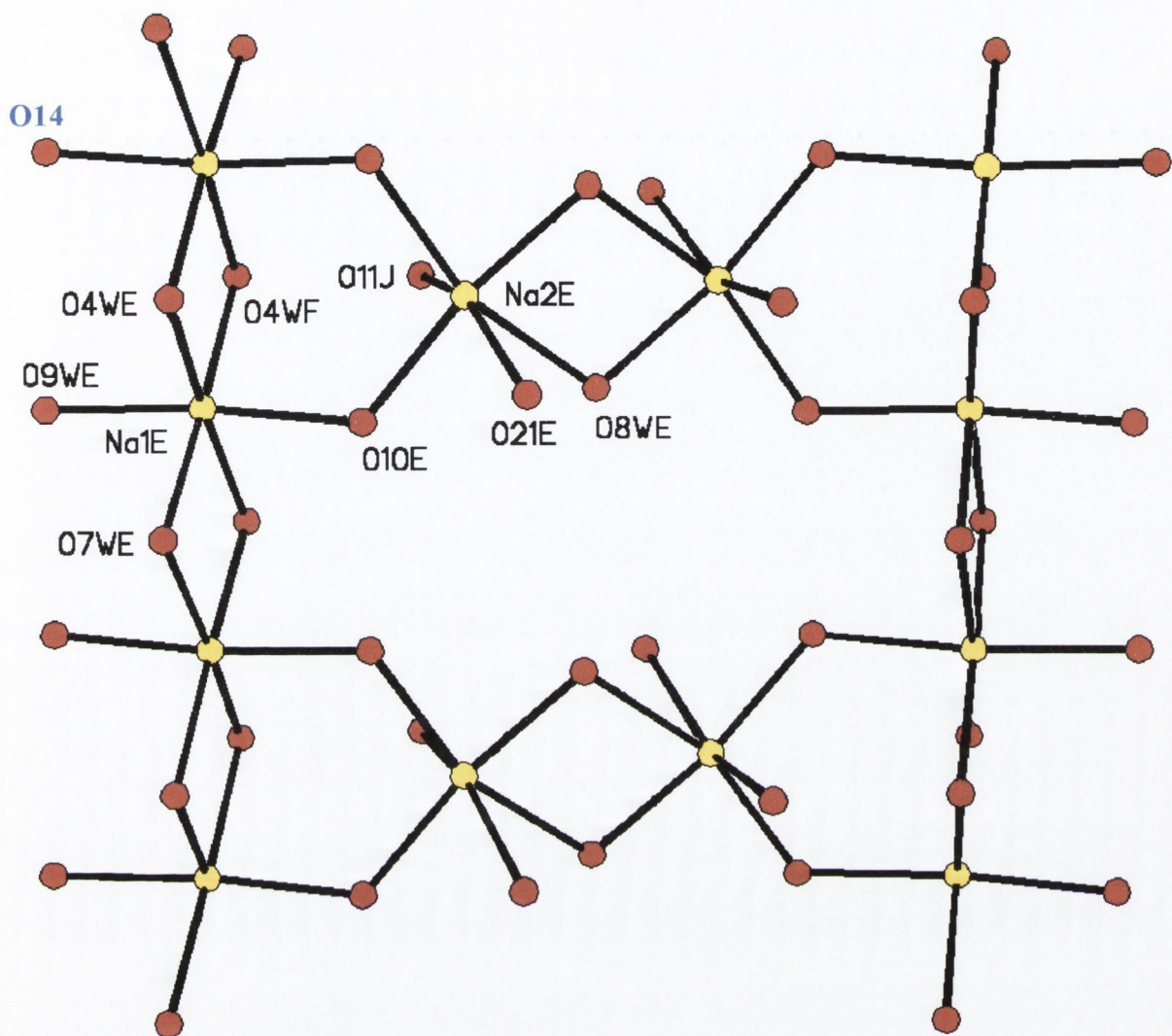


Figure 3.11. Packing diagram showing 2-D network of lattice water and sodium atoms. One of the oxygen atoms present belongs to the complexed pyrophosphate and is marked **O(14)**. The remaining pyrophosphate atoms as well as copper and bipy are omitted for clarity.

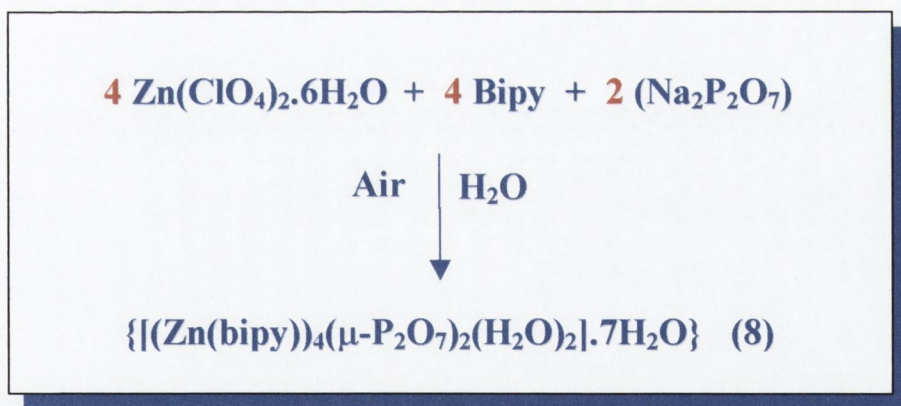
Despite the use of various starting metal salts and utilizing more forcing conditions (*i.e.* refluxing) attempts to further react complex (7) with VO(II) and Co(II) were unsuccessful with the starting materials recovered each time. The reason for this behaviour is unclear. Attempts to generate hetero-bimetallic analogues of (4) containing copper(II) by direct means

(i.e. reacting both Cu(II) and M(II) starting materials with bipy and pyrophosphate simultaneously) only served to return complex (7) and the starting salt of M(II).

3.4. Preparation and Characterisation of the tetranuclear

Zinc(II) complex $\{[(\text{Zn}(\text{bipy}))_4(\mu\text{-P}_2\text{O}_7)_2(\text{H}_2\text{O})_2].7\text{H}_2\text{O}\}$: (8)

In an effort to gain further insights into the coordinating ability of the pyrophosphate ligand and to open the study up to NMR spectroscopy, it was decided to replace paramagnetic copper(II) with diamagnetic zinc(II). An aqueous solution of zinc(II) perchlorate was reacted therefore with an aqueous suspension of 2,2'-bipyridine, resulting in the formation of a clear colourless solution. Solid tetra-sodium pyrophosphate was then added resulting after approximately 2 minutes in the precipitation of a white solid. This precipitate re-dissolved into aqueous solution on increasing pH (0.6N NaOH) from 7.5 to 9. Compound (8) was then obtained in good yield (*ca* 75%) as white needles by slow evaporation of the concentrated aqueous solution over approximately fourteen days.



Scheme 3.3. Direct preparation of the tetranuclear zinc(II) species (8).

Infrared spectra obtained of the crystals confirmed the presence of pyrophosphate and 2,2'-bipyridine. Elemental analysis (C:H:N:P) produced variable percentages of carbon, nitrogen and hydrogen due to weight loss (from solvent evaporation) during the analytical experiment.

However the carbon to nitrogen ratio was maintained for each of the three batches run, being (C : N) 4.27 : 1, 4.28 : 1 and 4.31 : 1. The calculated ratio for the tetranuclear complex $\{[(\text{Zn}(\text{bipy}))_4(\mu\text{-P}_2\text{O}_7)_2(\text{H}_2\text{O})_2]\}$ is 4.28 : 1. Electrospray mass spectroscopy of an aqueous solution of re-dissolved crystals reveals a series of peaks consistent with fragmentation.

3.5. Description of the molecular structure of the tetranuclear Zinc(II) complex $\{[(\text{Zn}(\text{bipy}))_4(\mu\text{-P}_2\text{O}_7)_2(\text{H}_2\text{O})_2].7\text{H}_2\text{O}\}$: (8)

Crystals were grown by slow evaporation of a concentrated aqueous solution containing stoichiometric amounts of $\text{Zn}(\text{ClO}_4)_2$, 2,2'-bipyridine and tetra-sodium pyrophosphate over approximately fourteen days. The crystals are stable, white needle shaped entities and were used for a single crystal X-ray diffraction study. Dr. M. Nieuwenhuyzen of the Queens University, Belfast, performed the data collection and structural refinement. Complex (8) is depicted in Figure 3.12 showing the atomic numbering scheme used.

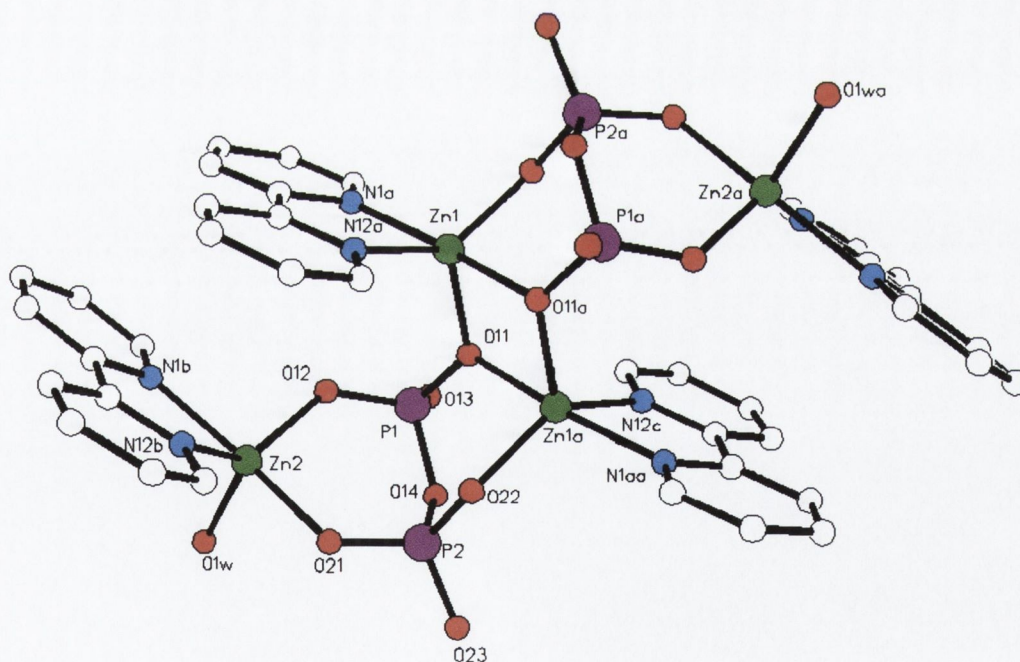


Figure 3.12. Molecular structure of $\{[(\text{Zn})_4(\text{bipy})_4(\mu\text{-P}_2\text{O}_7)_2(\text{H}_2\text{O})_2].7\text{H}_2\text{O}\}$ (8). Bipyridine hydrogen atoms and waters of crystallization omitted for clarity.

The structure of **(8)** consists of neutral $\{[(\text{Zn}(\text{bipy}))_4(\mu\text{-P}_2\text{O}_7)_2(\text{H}_2\text{O})_2]\cdot 7\text{H}_2\text{O}\}$ tetranuclear zinc(II) units and seven waters of crystallisation. The geometry of the two crystallographically independent zinc atoms is distorted square pyramidal with two bipy-nitrogens and two pyrophosphate oxygen atoms building the basal plane with a water molecule (O(1w)) occupying the apical position of Zn(2) and a pyrophosphate oxygen (O(11)) occupying the apical position of Zn(1). The zinc atoms are shifted 0.4878 Å [Zn(1)] and 0.3883 Å [Zn(2)] from the mean basal plane towards the axially coordinated atoms O(11) and O(1w), respectively. The chelating bipyridine ligands are essentially planar with a dihedral angle between the pyridyl rings of the those ligands coordinated to Zn(1) and Zn(1a) of 16.8°.

Table 3.3. Selected bond distances (Å) and angles (°) for (8).

Zn(1)-O(11)	1.970(2)	Zn(1)-O(11)-Zn(1)#1	97.8(8)
Zn(1)-O(22a)#1	1.960(2)	P(1)-O(11)-Zn(1a)#1	122.6(1)
Zn(1)-N(1a)	2.095(3)	N(1a)-Zn(1)-N(12a)	78.6(1)
Zn(1)-N(12a)	2.071(3)	O(22)-Zn(1a)#1-O(11a)	89.8(8)
Zn(1)-O(11a)#1	2.170(2)	O(11)-Zn(1)-N(1a)	104.5(1)
Zn(1)-Zn(1a)#1	3.124(8)	O(12)-P(1)-O(14)	108.8(1)
Zn(1)-Zn(2a)	5.165(8)	O(14)-P(2)-O(21)	107.0(1)
Zn(2)-O(12)	1.948(2)	O(12)-Zn(2)-O(21)	97.1(8)
Zn(2)-O(21)	2.027(2)	O(1w)-Zn(2)-N(1b)	91.8(1)
Zn(2)-N(1b)	2.164(3)	N(1b)-Zn(2)-N(12b)	76.5(3)
Zn(2)-N(12b)	2.106(3)	O(21)-Zn(2)-O(1w)	93.3(1)
Zn(2)-O(1w)	2.021(2)	O(12)-Zn(2)-P(1)	130.1(1)
P(1)-O(11)	1.536(2)	P(2)-O(14)	1.625(2)
P(1)-O(13)	1.496(2)	P(2)-O(22)	1.523(2)
P(1)-O(14)	1.617(2)	P(2)-O(23)	1.495(2)

Estimated standard deviations are given in the parenthesis.

Symmetry operator #

1 : $x, -y - \frac{1}{2}, z - \frac{1}{2}$

It is noticeable that the Zn-O bonds are shorter than the Zn-N bonds, indicating good zinc-pyrophosphate bonding, and that the P=O and P-O(Zn) bonds are dissimilar, pointing to the weakly ionic nature of the zinc-phosphate interactions.¹⁶ The pyrophosphate group acts as a bis-bidentate ligand forming two six-membered chelate rings between Zn(1) and Zn(2a) with an envelope conformation. The pyrophosphate also acts as a mono-dentate ligand, bridging between Zn(1) and Zn(1a) through O(11). This is the main structural difference between the Cu(II) complex **(4)** and **(8)**, namely nuclearity. In fact complex **(8)** resembles two of the Cu(II) dimer complexes **(4)** bridged together through uncoordinated pyrophosphate oxygens in a back-to-back conformation, as indicated by the apically coordinated water molecules, which now face in opposite directions. This mono-atomic bridging shows that pyrophosphate will undergo coordination that can increase dimensionality and is further evidence for the postulate put forward to explain the ~five-fold increase in magnetic coupling observed for the Cu(II) complex **(6)** (see scheme 3.2). The possibility that an additional pathway can be created through available pyrophosphate oxygens is shown to be the case with the zinc tetramer. Intermolecular π - π stacking interactions exist along the x-axis through an interleaving of bipy ligands. Further π - π interactions are also present along the y-axis (Figure 3.13). Interplanar distance between bipy's is 3.5 Å. Hydrogen bonds involving the lattice and coordinated water molecules result in the formation of an overall 3-dimensional network.

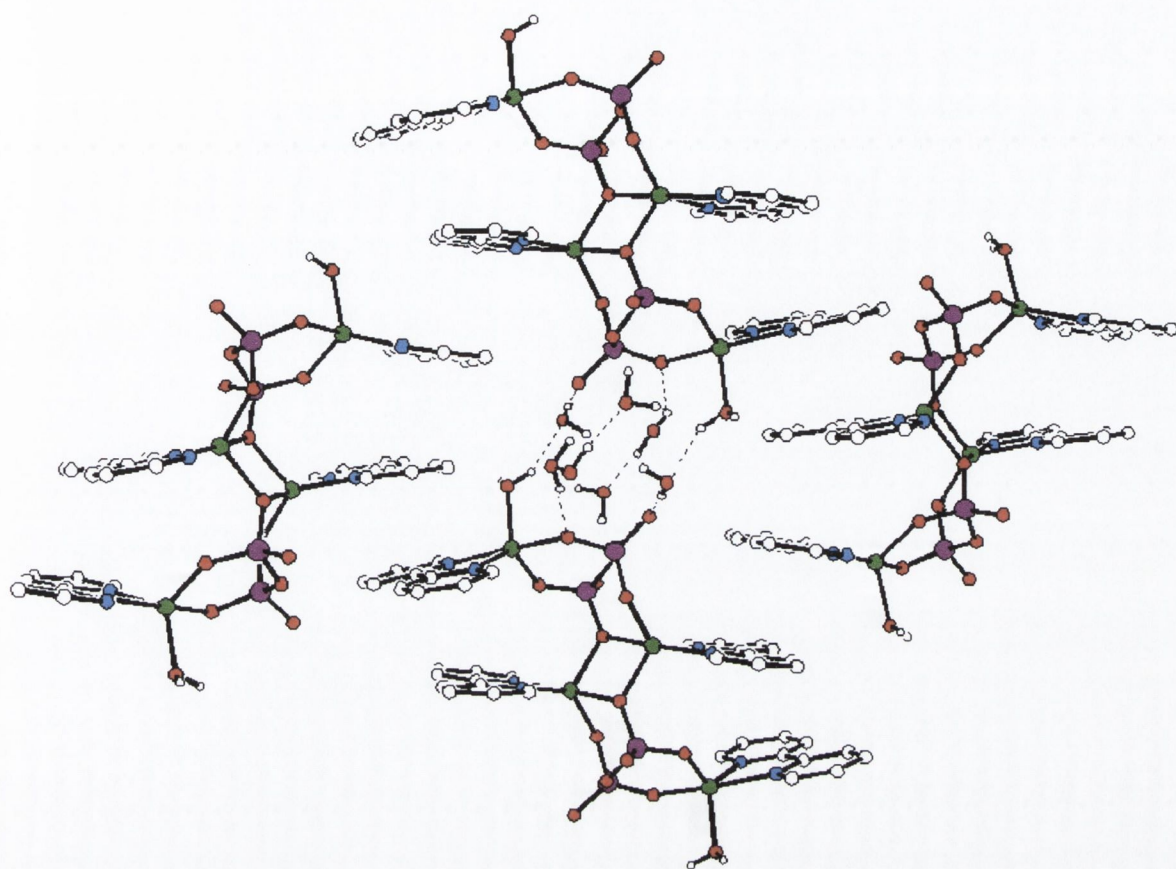


Figure 3.13. Packing diagram of (8) showing H-bonding between phosphate oxygens, coordinated and lattice water molecules. Bipy hydrogens and additional waters of crystallisation omitted for clarity.

3.5.1 Nuclear Magnetic Resonance Studies of (8).

^{31}P NMR experiments were carried out on solutions of (8) in deuterated water. The ^{31}P NMR of sodium pyrophosphate was also conducted and used as reference (Figure 3.14). The ^{31}P NMR spectrum of complex (8) contains two peaks, at -4.42 and -26.63 ppm. The shift to more negative δ values is expected on coordination and is consistent with literature precedent.¹⁷ The fact that there are now two peaks in the NMR is consistent with the known structure.

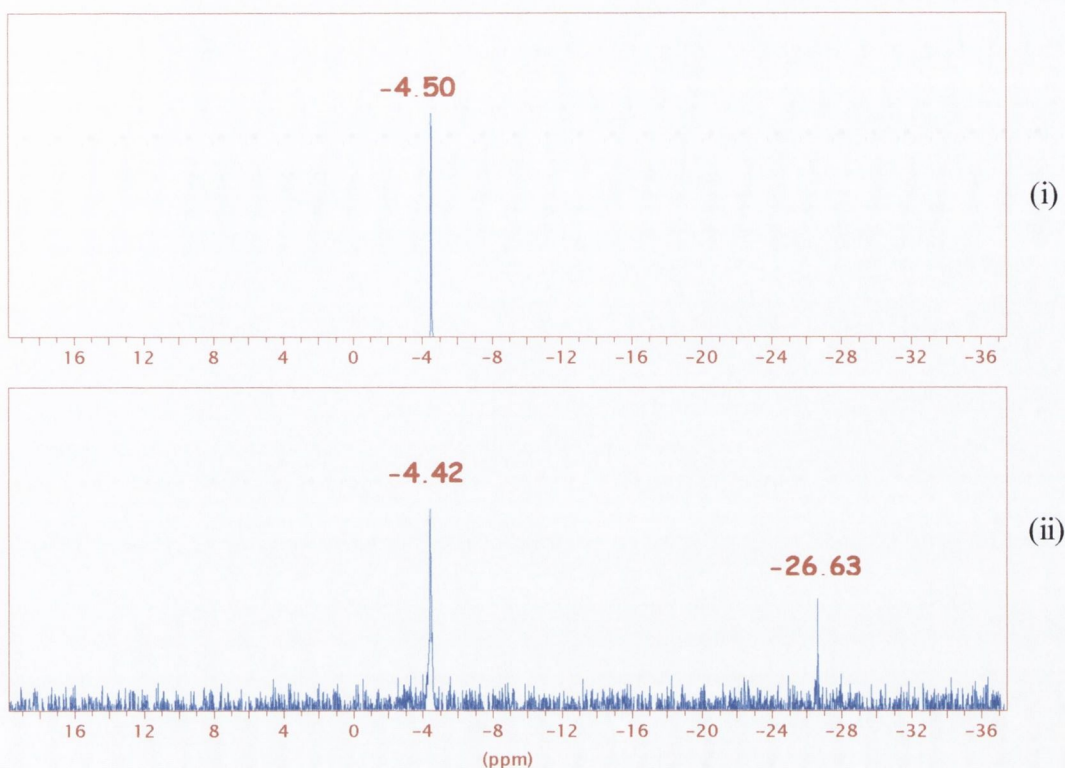


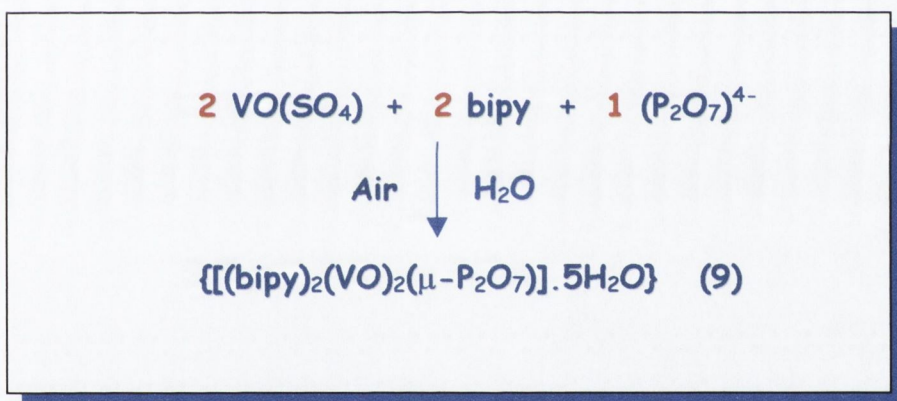
Figure 3.14. ^{31}P NMR spectra of (i) $\text{Na}_4\text{P}_2\text{O}_7$ and (ii) $\{[(\text{Zn}(\text{bipy}))_4(\mu\text{-P}_2\text{O}_7)_2(\text{H}_2\text{O})_2]\cdot 7\text{H}_2\text{O}\}(\mathbf{8})$.

There are clearly two phosphorous environments in **(8)**, namely P(1) and P(2). It is possible that the peak that remains almost identical to that of the uncoordinated pyrophosphate starting material could be assigned to the more ionic of the two P atoms. From the comparison of P=O and P-O(Zn) bond lengths discussed earlier, it is known that the P(2) has a weakly ionic interaction through oxygens O(21) and O(22) with Zn(1a) and Zn(2). If there was a strong ionic interaction, the P=O and P-O(Zn) bond lengths would be similar. Therefore the peak at -4.42 ppm may be tentatively assigned to P(2) and the greater shift, to -26.63 ppm, assigned to P(1). However, while the P environments (P(1) and P(2)) are different in the solid state they are not *that* different. As -4.42 is so close to -4.49 ppm it is more likely to be ‘free’ pyrophosphate resulting from dissociation in solution or present as unreacted starting material. It is suspected that P(1) and P(2) would be very similar in solution and therefore appear as a single peak at -26.63 ppm. The ^1H NMR also showed the

expected multiplet pattern for bipy, with a broadening of the peaks. There is also a slight shift to more positive δ values indicative of coordination.

3.6. Synthesis and Characterisation of a vanadyl(II) complex containing pyrophosphate and 2,2'-bipyridine: (9)

In an attempt to synthesise the vanadyl analogue of complex (4), namely a binuclear vanadyl(II) complex with bridging pyrophosphate and 2,2'-bipyridine, a number of different procedures were attempted. Vanadium was chosen due to the similarities between the d^1 and d^9 configurations.¹⁸ Electronically and magnetically d^9 can be thought of as an inversion of d^1 . The first method tried involved the direct stoichiometric reaction of $\text{VO}(\text{SO}_4)$ with pyrophosphate and 2,2'-bipyridine, in an analogous fashion to that used in the synthesis of (4).



Scheme 3.4 Direct preparation of complex (9).

This resulted in the formation a lime green insoluble powder, which was separated by filtration. The infrared spectrum indicated the presence of the vanadyl functional group, $\nu(\text{V}=\text{O})$ 971 cm^{-1} , as well as the pyrophosphate group at 1157 and 1093 cm^{-1} . Characteristic bipy bands were also present, at 1654 , 1600 , and 772 cm^{-1} . However, as the compound is insoluble in all solvents other than those that decompose it (e.g. nitric acid), solution analysis could not readily be performed. The first method was therefore modified by replacing sulphate as vanadyl counter-ion and synthesising $\text{VO}(\text{acac})_2$.¹⁹ This latter procedure however

also returned the same insoluble lime green powder as before. Attempts to grow crystals through the use of diffusion methods²⁰ or gel permeation crystal growth (Tetramethyl ortho-silicate gel)²¹ also produced the insoluble lime green powder. Microanalytical data (C:H:N:P), carried out for each of the experimental procedures recorded above, indicated the formation of a compound with the probable formulation $\{[\text{VO}(\text{bipy})]_2(\mu\text{-P}_2\text{O}_7)\cdot x\text{H}_2\text{O}\}$, with x varying between 2 and 5 and dependent on how the sample was dried. The carbon to phosphorous ratio however is unaffected by the number of water molecules present and was calculated to be (C:P) 3.90:1. Analysis returned values of, on average, 3.88:1.

3.6.1. Infrared analysis of (9).

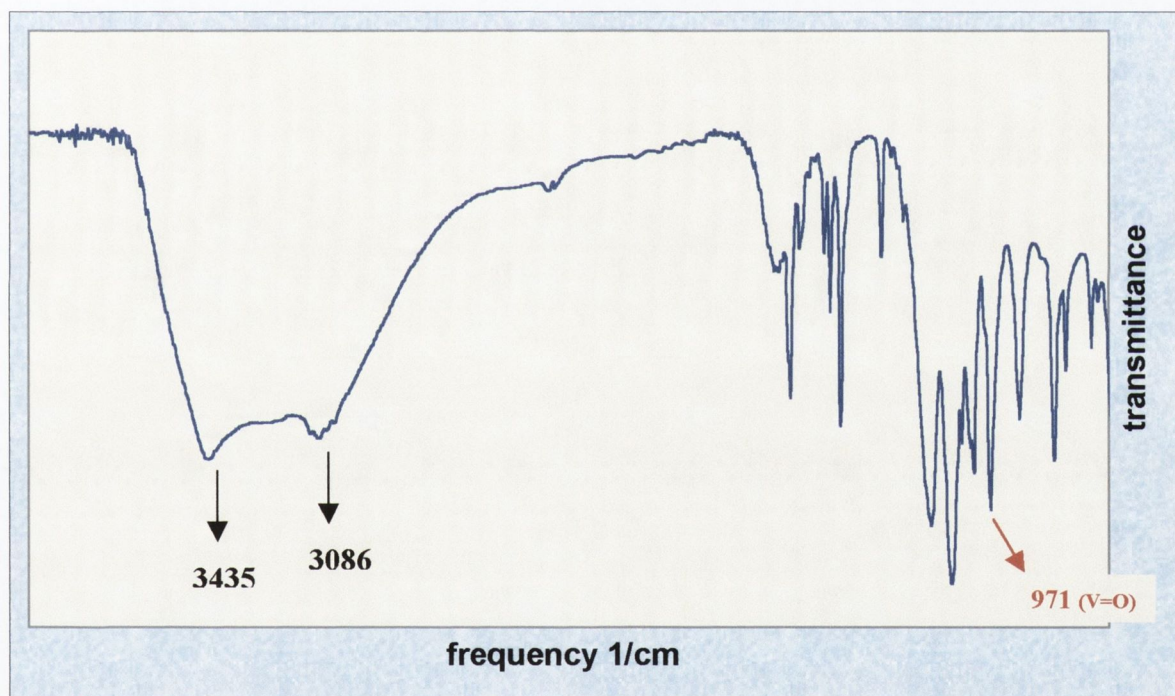


Figure 3.15. Infrared spectrum for complex (9). Water bands in the high-energy range (3435 and 3086 cm^{-1}) are split indicating the existence of Hydrogen-bond interactions.

There is little commonality between the bands recorded for the pyrophosphate in the tetranuclear zinc(II) complex (8) and that shown for (9) in figure 3.15. This may indicate a similar dimer based bis-bidentate arrangement in (9) as witnessed in complex (4). The band

at 971 cm^{-1} for the V=O group tells a lot about the environment of the oxovanadium(IV) group within compound (9). Variation of the frequency of the V=O vibration due to the change in the environment of the VO(II) entity has been extensively studied.²² The V=O stretching frequency range for various oxovanadium (IV) complexes has been reported to be $985 \pm 50\text{ cm}^{-1}$.

Complex	$\nu(\text{Pyrophosphate})\text{ cm}^{-1}$
(4)	1153, 1101, 1029
(8)	1173, 1086, 1018
(9)	1158, 1093, 1024

Table 3.4. Comparison of Infrared frequency values for complexes (4), (8) and (9).

There is very strong π -bonding between the vanadium $3d_{xz}$, $3d_{yz}$ orbitals and the oxygen $2p_x$, $2p_y$ orbitals in the V=O bond and this is largely enhanced when ligand coordination at the sixth axial site (trans to the V=O bond axis) is achieved. The frequency for oxovanadium(IV) complexes having $\text{O}=\text{V}(\text{L}_2)$ composition such as $[\text{VO}(\text{bipy})_2]^{2+}$ is found to be $ca \sim 985\text{ cm}^{-1}$. It has been suggested that the shift to lower frequencies of the V=O stretching vibration is due to the transfer of increasing amounts of charge onto the vanadium by ligands of increasing donor strength. However, if the complex has an intermolecular interaction through $\text{V}=\text{O}\cdots\text{V}=\text{O}$ units, then the V=O band is reported to appear at lower frequency. The insolubility of complex (9) is also best explained by the possible existence of these intermolecular V=O chains, for which there is in a well documented case in the literature,²² resulting in a polymeric species. The configuration adopted by $\text{V}=\text{O}\cdots\text{V}=\text{O}$ interactions in bridged, binuclear oxovanadium(IV) units is arranged according to the orientation of the oxo-groups with respect to the bridging plane (Figure 3.16). The formation of these so called 'infinity chains'²³ is reported to result in $\nu(\text{V}=\text{O})$ stretching frequencies under 900 cm^{-1} . Kim *et al.*²⁴ however, have postulated that the presence of groups capable of sufficiently altering

the vanadium coordination environment might sufficiently weaken the intermolecular interaction of $V=O \cdots V=O$ chains, which would leave the $V=O$ stretching frequency relatively unchanged compared with simple monomeric $V=O$ complexes such as $[(bipy)_2V=O]^{2+}$.

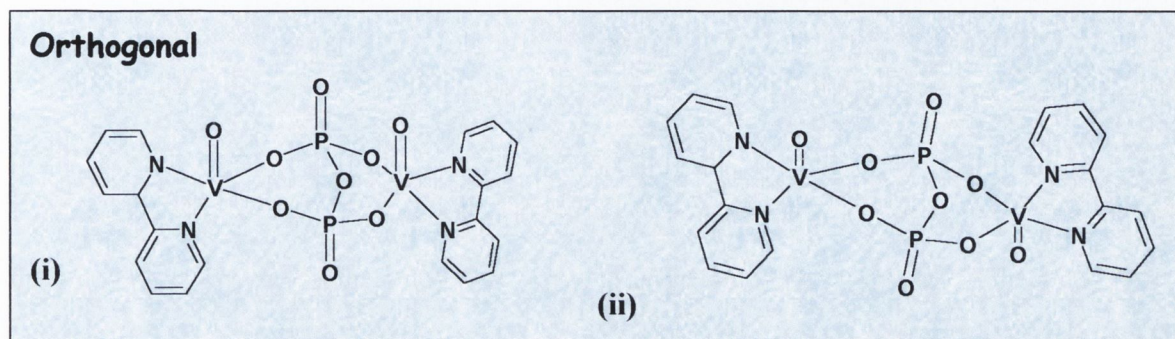


Figure 3.16. Proposed structures for (9). (i) *syn*-orthogonal (ii) *anti*-orthogonal configurations for the two terminal oxo-groups in binuclear vanadyl units. Steric considerations would probably make a co-planar configuration (not shown) unlikely for (9).

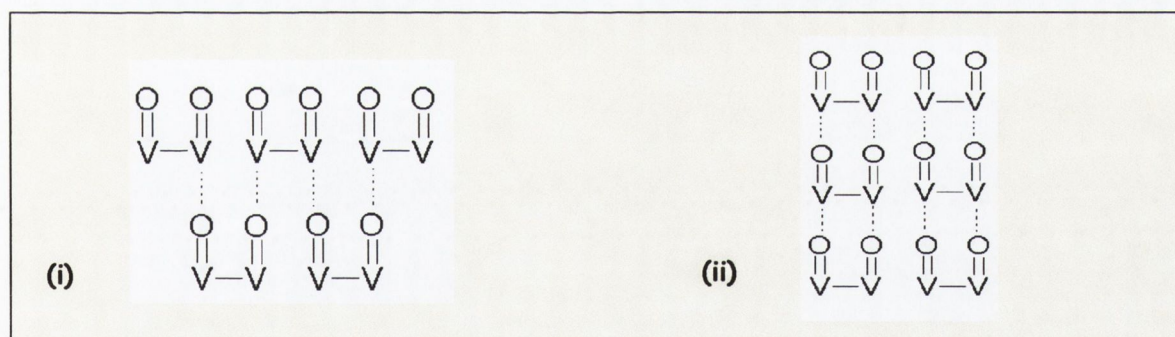


Figure 3.17. Alternating (i) and ladder (ii) stacking possibilities for $V=O$ units in a *syn*-orthogonal arrangement.

Thus it is possible that π -stacking interactions, between the 2,2'-bipyridine ligands could prevent a sufficiently close approximation of $V=O$ entities and so only a slight shift to lower frequencies (*ca.* 15cm^{-1}) is observed in (9). The absence of splitting in the $(V=O)$ band at 971cm^{-1} indicates equivalent vanadyl environments within the molecule, with this value also

consistent with the rather long V=O bond encountered for most square-based pyramidal oxovanadium(IV) complexes.²⁵

3.6.2. Thermal analysis of complex (9).

The variation in the number of water molecules (between 2 and 5) recorded for (9) and the fact that water played such a key role in the magnetic behaviour of the binuclear copper(II) complex (4), led us to carry out thermal analysis on (9). Figure 3.19 shows the TG/DTA curves, which exhibit the thermal behaviour of the material from 25°C to 370°C. From the curves the following observations can be made: (a) there is a stable intermediate in evidence in the course of the thermal evolution from ~160°C to ~270°C (b) a weight loss of 12.6% is observed in the temperature range 25-160°C and can be attributed to the evolution of lattice water molecules.

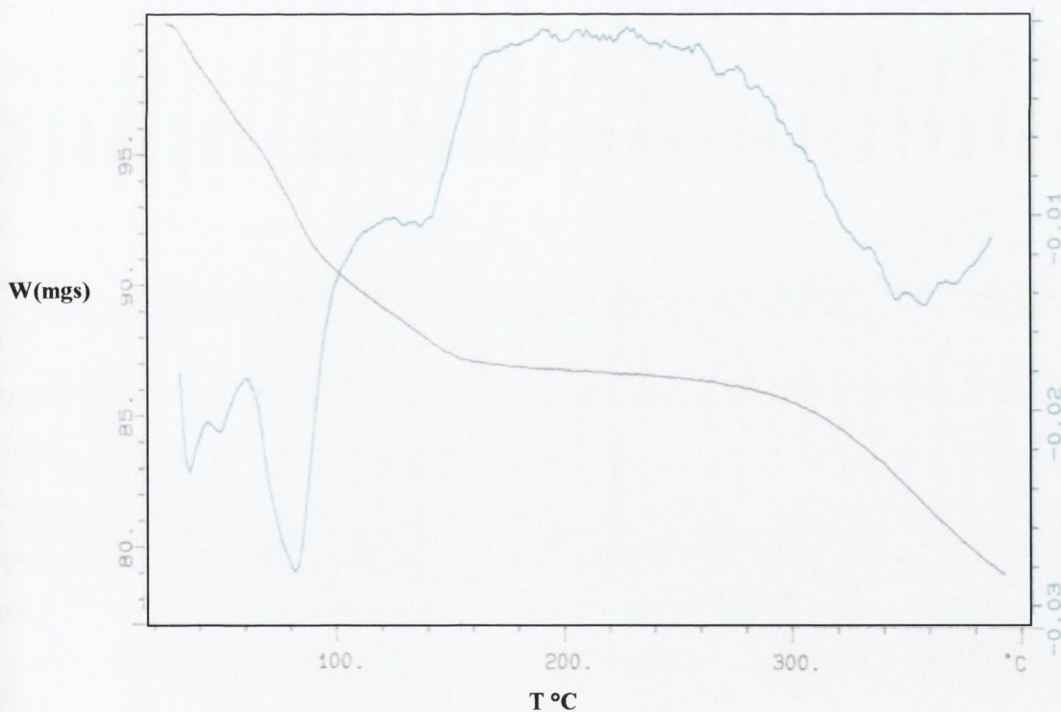


Figure 3.18. Thermogravimetric analysis curve (TGA, black) and differential thermal analysis curve (DTA, green) of compound (9) carried out under a flowing argon atmosphere. DTA curve is indicative of endothermic mass loss consistent with solvent loss.

This indicates that, assuming the correct formulation has been stipulated, there are five waters of crystallisation in the compound, which is consistent with the highest value returned for x by elemental analysis: (c) the weight loss from ~270°C onwards corresponds to the exothermic evolution of organic species and the decomposition of compound (9). There is no evidence from the thermal behaviour of (9) to indicate the presence of coordinated water and this would fit for the structure as it has been postulated. The presence of lattice water molecules up to 160°C suggests a degree of H-bonding between the lattice water molecules.

3.6.3. Magnetic behaviour of (9) at room temperature.

At room temperature (295K) the magnetic moment was found to be 1.59 BM, a value lower than the spin-only value (μ_{eff} 1.73 BM) expected for a $3d^1$ configuration with a d_{xy} based ground state. It is possible that an antiferromagnetic interaction therefore exists in (9). Based on results obtained from the copper(II) analogue (4), a likely scenario is that there is a weak antiferromagnetic exchange pathway present through the pyrophosphate bridge. Intermolecular $V=O \cdots V=O$ bonding may also be sufficient to cause this magnetic interaction through overlap of the d_{xy} magnetic orbital on one oxo-vanadium(IV) with the intermolecular $V=O$ units in the solid state, thus facilitating the reduced magnetic moment observed at 295 K. On the basis of magnetic moments observed for similar complexes between 1.27 and 1.6 BM, Symal²² and Poddar²⁶ *et al.* have proposed binuclear structures with a weak antiferromagnetic interaction through $V=O$ chains. However it would be expected that the pyrophosphate super-exchange would be much stronger than any coupling through $V=O$ chains. Combined then there is good evidence to suggest that the binuclear VO(II) complex comparable to the binuclear Cu(II) complex (4), has been prepared with solid-state spectroscopic methods suggesting complex (9) contains both intermolecular ‘infinity chains’ and also a H-bonded water network.

Conclusion

The original goal of synthesising a pyrophosphate bridged coordination compound and to study its ability to mediate magnetic exchange has been achieved. The results obtained

illustrate for the first time the profound influence of pyrophosphate –assisted water loss on magnetic properties and demonstrates that controlled dehydration may lead to an increase in magnetic dimensionality.²⁷ Similar examples of spectacular magnetostructural effects caused by carboxylate-assisted water loss in polynuclear compounds have been reported previously.²⁸ The ability to generate materials capable of switching from a weak magnetic state to a strongly magnetic one through a simple process such as dehydration can provide new exotic materials based on the concepts of molecular chemistry. The copper-pyrophosphate complex (**4**) is appealing as it combines some physical properties encountered in classical materials with some other properties specific to the molecular state. What is evident overall however is that the pyrophosphate ligand is a poor mediator of super-exchange with weakly coupled systems to be expected. The strong coupling observed in (**6**) is due to an additional *inter* molecular pathway acting in concert with an *intra* molecular pathway, without which low values of T_c are observed.

The successful synthesis of the zinc(II) complex offered interesting insights into pyrophosphates coordinating ability and allowed information to be gleaned about the structure in solution. The move to greater nuclearity for the pyrophosphate anion is also relevant to the postulate put forward to explain the increased magnetic interaction recorded on dehydration of the copper(II) complex (**4**) and subsequent formation of complex (**6**).

The incorporation of oxo-vanadium(IV) returned an insoluble, probably polymeric, species. The formation of a polymer through alternating or ladder orthogonal arrangements of V=O ‘infinity chains’ is well documented in the literature²⁹ and is postulated to be the case here. The room temperature magnetic moment indicates weak antiferromagnetic interactions operating within (**9**) as shown by the reduction in the magnetic moment from the spin-only value for a dilute system of 1.73 BM to a value of 1.59 BM.³⁰

The coordinating ability of pyrophosphate with metal centres such as Ni(II) and Co(II) as well as developing a method to generate hetero-nuclear multi-metallic complexes containing bridging pyrophosphate is considered the avenue of approach for future work in this area within our group.

References

1. E. M. Melado, PhD, Princeton University, **1977**.
2. a) J.E. Walker, *Angew. Chem. Int. Ed.*, **37**, 2308, 1998.; b) P.D. Boyer *Angew. Chem. Int. Ed.*, **37**, 2296, 1998.
3. a) *The Biochemistry of Nucleic Acids*, R.L.P. Adams, J.T. Knowler and D.P. Leader, (Eds.), 10th ed., Chapman and Hall, New York, **1986**.; b) *Nucleic Acids in Chemistry and Biology*, G.M. Blackburn and M.J. Gaits, (Eds.), 2nd ed., Oxford University Press, **1996**.
4. *Metal Ions in Biological Systems*, K. Aoki, Marcel Dekker, Basel, **1996**.
5. W.N. Lipscomb and N. Strater, *Chem. Rev.*, **96**, 2375, 1996 and references therein.
6. a) D.E. Wilcox, *Chem. Rev.*, **96**, 2375, 1996.; b) K.M. Welsh and B.S. Cooperman, *Biochemistry*, **22**, 2243, 1983.
7. a) *Phosphorous and it's Compounds*, J.R. Van Wazer, Vol. 1, Interscience, New York, **1958**.; b) L.M. Engelhardt, E.A. Keegan, G.A. Lawrence and A.H. White, *Aust. J. Chem.*, **42**, 1045, 1989.
8. E.W. Ainscough, A.M Brodie, J.D Ranford, J.M. Waters and K.S. Murray, *Inorg. Chim. Acta.*, **197**, 107, 1992.
9. N. Herron, D.L. Thorn, R.L. Harlow and G.W. Coulston, *J. Am. Chem. Soc.*, **119**, 7149, 1997.
10. D.E. Cabelli, J.F. Wishart, J. Holcman, M. Meier and R. van Eldik, *J. Phys. Chem. A*, **101**, 5131, 1997.
11. a) B.K. Hodnett, *Catal. Today*, **1**, 477, 1987.; b) G.U. Wolf, B. Kubias, B. Jacobi and B. Lucke, *Chem. Commun.*, 1517, **2000**.
12. K.S. Murray, *Adv. Inorg. Chem.*, **43**, 261, 1995.
13. a) *Infrared and Raman Spectra of Inorganic and Coordination Compounds, Part B, Applications in Coordination, Organometallic and Bioinorganic Chemistry*, K. Nakamoto, 5th ed., Wiley, Chichester, **1997**.; b) D.E.C. Corbridge and E.J. Lowe, *J. Chem. Soc.*, 493, **1954**.; c) A. Hezel and S.D. Ross, *Spectrochimica Acta.*, **23A**, 1583, 1967.

14. B. Bleaney and K.D. Bowers, *Proc. R. Soc. London. Ser. A*, **214**, 451, 1952.
15. I. Castro, J. Faus, M. Julve, F. Lloret, M. Verdaguer, O. Kahn, S. Jeannin and J. Vasserman, *J. Chem. Soc., Dalton Trans.*, **7**, 2207, 1990.
16. A. Muller-Hartman and H. Vahrenkamp, *Eur. J. Inorg. Chem.*, 2355, 2000.
17. A. Muller-Hartman and H. Vahrenkamp, *Inorg. Chim. Acta.*, **300**, 531, 2000.
18. *Chemistry of the Elements*, N.N. Greenwood and A. Earnshaw, Butterworth-Heinemann, Oxford, **1984**.
19. S.G. Brand, N. Edelstein, C.J. Hawkins, G. Shalimoff, M.R. Snow, E.R.T. Tiekink, *Inorg. Chem.*, **29**, 434, 1990.
20. *The Growth of Single Crystals*, R.A. Laudise, Prentice-Hall, **1970**.
21. *Crystal Growth and Design*, H.K. Henisch, Dover, New York, **1990**.
22. A. Szymal, *Coord. Chem. Rev.*, **16**, 309, 1975 and references therein.
23. a) F. Bayi, G. Pourroy, M. Balaiche, P. Legoll, M. Drillon and R. Kuentzler, *Eur. J. Sol. State Inor.*, **30**, 55, 1993.; b) M.A.G. Aranda, J.P. Attfield, S. Brugue and M. Martinezlara, *Inorg. Chem.*, **31**, 1045, 1992.
24. Y.J. Kim, Y.I. Kim and S.N. Choi, *Polyhedron*, **19**, 2155, 2000.
25. a) J.K. Money, J.C. Huffman and G. Christou, *Inorg. Chem.*, **24**, 5745, 1985.; b) D.B. McConvill, W.J. Young, P.R. Klich, A.T. Daniher and P.R. Challen, *Inorg. Chem.*, **35**, 347, 1996.
26. S.N. Poddar, K. Dey, J. Halder and S.C. Nath Sarkar, *J. Indian. Chem. Soc.*, **47**, 743, 1970.
27. a) O. Kahn, J. Larionova and J. Yakhmi, *Chem. Eur. J.*, **5**, 3443, 1999.; b) Y. Pei, O. Kahn, K. Nakatani, E. Codjovi, C. Mathoniere and J. Sletten, *J. Am. Chem. Soc.*, **113**, 6558, 1991.
28. a) K. Nkatani, J.Y. Carriat, Y. Journaux, O. Kahn, F. Lloret, J.P. Renard, Y. Pei, O. Kahn, J. Sletten and M. Verdaguer, *J. Am. Chem. Soc.*, **111**, 5739, 1989.; b) F. Lloret, M. Julve, R. Ruiz, Y. Journaux, K. Nakatani, O. Kahn and J. Sletten, *Inorg. Chem.*, **32**, 27, 1993.; c) J. Cano, G. De Munno, J.L. Sanz, R. Ruiz, J. faus, F. Lloret, M. Julve and A. Caneschi, *J. Chem. Soc., Dalton Trans.*, 1915, 1997.
29. W. Plass, *Inorg. Chem.*, **36**, 2200, 1997.
30. *Introduction to Magnetochemistry*, A. Earnshaw, Academic Press, New York, **1968**.

Chapter Four

Preparation and magnetic behaviour of the
dinuclear copper(II) complexes:



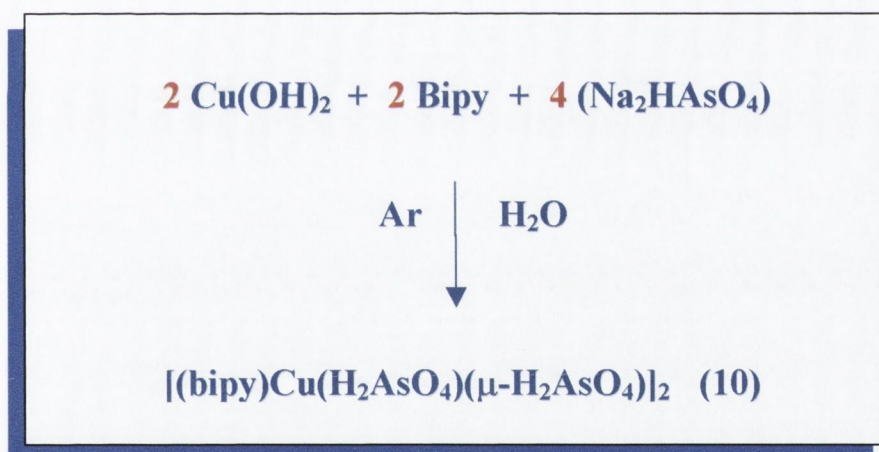
Introduction.

Supramolecular design provides a means to generate a variety of novel inorganic materials with complex unusual structural features in areas such as host-guest chemistry and open-framework structures.¹ In these compounds, one can visualize structures of different dimensionalities with complex structures expected to contain subunits, which not only are structural motifs but also act as building blocks in the construction of complex structures. Such building blocks can be considered to be synthons of complex structures. These synthons are generally simple geometrical shapes such as squares, cubes or polyhedra, their corners acting as linkage points. The polyhedral group 15 oxo-anion H_2AsO_4^- is one such potentially hydrogen bonding supramolecular synthon. Orthoarsenate is a potential multi-dentate bridging ligand and, as with other polyprotic inorganic oxy-acids of the group 15 elements, is a potent hydrogen bond donor and acceptor synthon. These oxo-anions are prevalent throughout nature and have been extensively studied in solid-state and materials chemistry (alumino-phosphates, zeolites *etc*)² and more recently in the hydrothermal synthesis of porous materials.³ To our surprise they have been somewhat neglected in the development of metallo-supramolecular coordination chemistry. Our surprise is fuelled by the recognition that these species, in their various deprotonated states in combination with simple cations, have been shown to form extended network structures in which H-bonding is the main ordering mechanism. This has giving rise to crystalline solids possessing such phenomena as non-linear optical and ferroelectric properties.⁴ The efficacy of employing hydrogen bonding in the development of supramolecular architectures via crystal engineering is well established.⁵ Robust organic and inorganic networks, or composites of them, may be readily generated by taking advantage of these hydrogen bond donor (D) and acceptor (A) interactions. The nature of the association is primarily driven by an electrostatic interaction and thus the charge distribution on the D/A system dictates the strength of the connection. Multiple D/A interactions similarly enhance the stability of the resultant framework. In combination with this we also desired a coordination motif that would not only controllably introduce a transition metal into the superstructure but also would itself promote intermolecular association. To this end we reasoned that a complex containing a flat aromatic ligand (e.g. 2,2'-bipyridine, 1,10-phenanthroline *etc.*) would promote π - π interactions

throughout any resultant crystal lattice. Therefore a combination of supramolecular and coordination chemistry would be employed to hopefully develop topical architectures and novel networks.⁶ In this way we introduce into the superstructures both the versatility, strength and directionality, and hence predictability, of the hydrogen bonding with the chemical and physical properties and predictable bonding nature of transition metals.

4.1. Preparation and Characterisation of the dinuclear copper(II) complex $[(\text{bipy})\text{Cu}(\text{H}_2\text{AsO}_4)(\mu\text{-H}_2\text{AsO}_4)]_2$: (10)

Compound (10) is obtained in good yield (*ca.* 60%) as blue parallelepipeds by slow evaporation of concentrated aqueous solutions containing stoichiometric amounts of $\text{Cu}(\text{OH})_2$, 2,2'-bipyridine and Na_2HAsO_4 . An inert atmosphere of argon was necessary to prevent fixation of carbon dioxide as carbonate.



Scheme 4.1. Direct preparation of the dinuclear species (10).

Infrared analysis indicated the presence of bipy peaks at 1650, 1550, 1473, 1446, 771 with arsenate at 854 cm^{-1} . The complex is typically coloured for a copper(II) complex, being deep royal blue. A d-d band at 647 nm in the visible spectra is broad and featureless and indicative of a distorted square-pyramidal nature of the copper(II) chromophore. Electrospray mass spectroscopy returned a series of peaks indicative of $\{[\text{M}^{2+}].4\text{H}_2\text{O}\}$

4.2. Structural characterisation of the dinuclear copper(II)

complex $[(\text{bipy})\text{Cu}(\mu\text{-H}_2\text{AsO}_4)(\text{H}_2\text{AsO}_4)]_2$:

(10)

The atomic numbering scheme and atom connectivity for **(10)** are shown in Fig. 4.1. The structure of **(10)** consists of a centro-symmetric Cu(II) dimer with tri-atomic bridging between copper centres furnished by dihydrogen arsenate $[\text{Cu}(1)\text{-O}(21)\text{-As}(1)\text{-O}(23)\text{-Cu}(1a)]$.

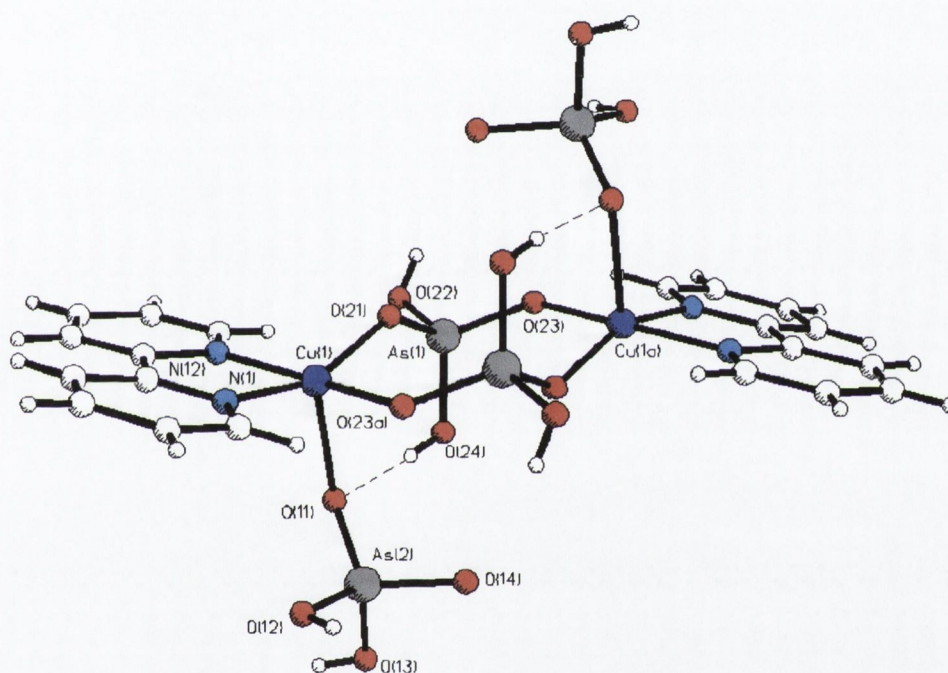


Fig 4.1. Molecular structure and atomic numbering scheme in **(10)**.

Further coordination about copper is provided by bidentate 2,2'-bipy (N(1) and N(12)) and an additional mono-dentate dihydrogen arsenate O(11), resulting in a slightly distorted square pyramidal metal coordination chromophore $[\text{CuN}_2\text{O}_3]$. The distortion is best exemplified by considering the mean planes around Cu(1) that form the base of the pyramid, which shows the plane defined by N(1)-Cu(1)-N(12) inclined by *ca.* 25° to that plane containing O(21)-

Cu(1)-O(23a). There is nothing exceptional about the bonding around either of the dihydrogen-arsenate ligands with bonds and angles similar to reported values (Table 4.1).

Table 4.1. Selected bond distances (Å) and angles (°) for (10).

Cu(1)-Cu(1a)#1	5.287(3)	N(12)-Cu(1)-N(1)	81.0(1)
Cu(1)-O(23a)#1	1.917(3)	O(21)-Cu(1)-O(11)	97.5(1)
Cu(1)-O(11)	2.326(3)	N(12)-Cu(1)-O(11)	93.0(1)
Cu(1)-O(21)	1.943(3)	O(23)-Cu(1a)#1-O(21)	92.4(1)
As(1)-O(23)	1.658(3)	As(2)-O(11)-Cu(1)	118.1(2)
As(1)-O(22)	1.711(3)	O(21)-As(1)-O(23)	117.8(2)

Estimated standard deviations are given in the parenthesis.

Symmetry operators used to generate equivalent atoms:

1: -x, -y, -z

The copper centres [Cu(1)-Cu(1a)] are separated by 5.287 Å, whilst the copper to arsenic [Cu(1)-As(1)] and [Cu(1)-As(2)] separations are 3.312 and 3.447 Å, respectively. Extensive H-bonding exists within the dinuclear unit and throughout the crystal lattice. Firstly, intramolecular H-bonding through O(24)-H(24)···O(11), and intermolecular H-bonding via O(22)-H(22)···O(12), link the bridging dihydrogen arsenate, centred around As(1), to apically bound ones, centred around As(2). Secondly, these apically bound dihydrogen arsenates interact with themselves intermolecularly through self-complementary ‘head-to-tail’ hydrogen bonding. This generates a $R_2^2(8)$ chain that continues along the *x*-axis which, through linking with As(1), propagates a two-dimensional dihydrogen arsenate sheet in the *xy*-plane containing a $R_4^6(20)$ motif, Fig. 4.2. The nomenclature used here is that devised by Etter and Bernstein⁷ to categorise H-bonding interactions. For example, $R_2^2(8)$ means that an 8-membered ring has been formed by the interaction of 2 H-bond donors with 2 H-bond acceptors.

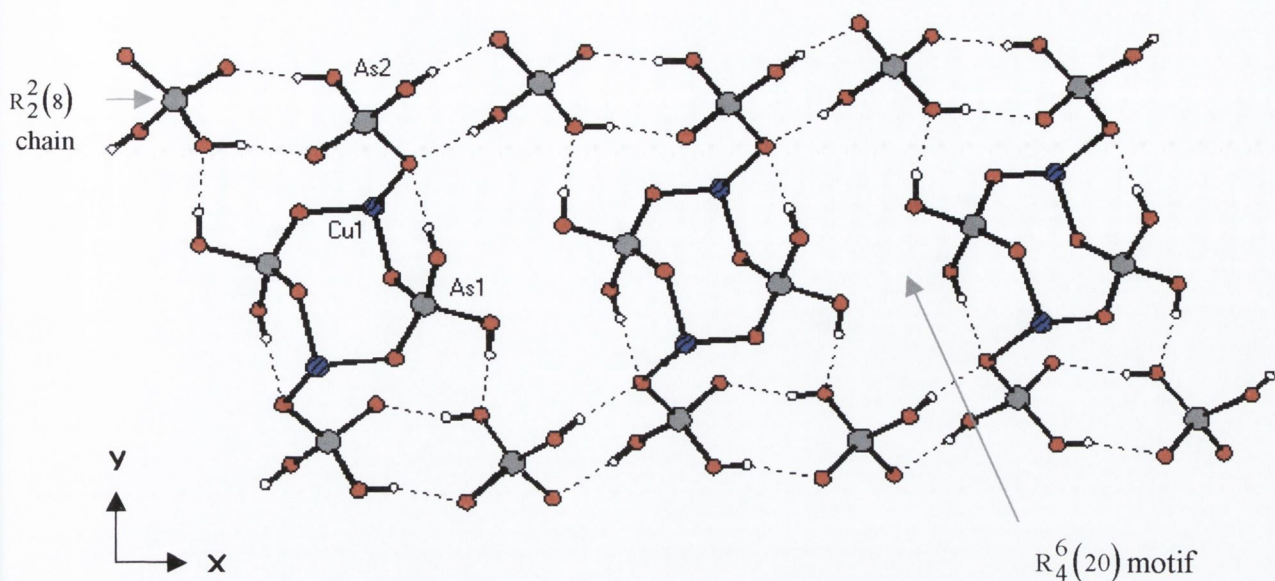


Fig 4.2. H-bonded network formed by intra- and inter-molecular self-association of dihydrogen arsenate groups showing the $R_2^2(8)$ chain and the $R_4^6(20)$ motif. 2,2'-bipyridine omitted for clarity.

The copper atoms are situated slightly above and below this sheet such that the 2,2'-bipy ligands project into the space between sheets. The 2,2'-bipy ligands themselves form a π - π stack down the y -axis which serves not only to separate sheets but also to link them into three dimensions.

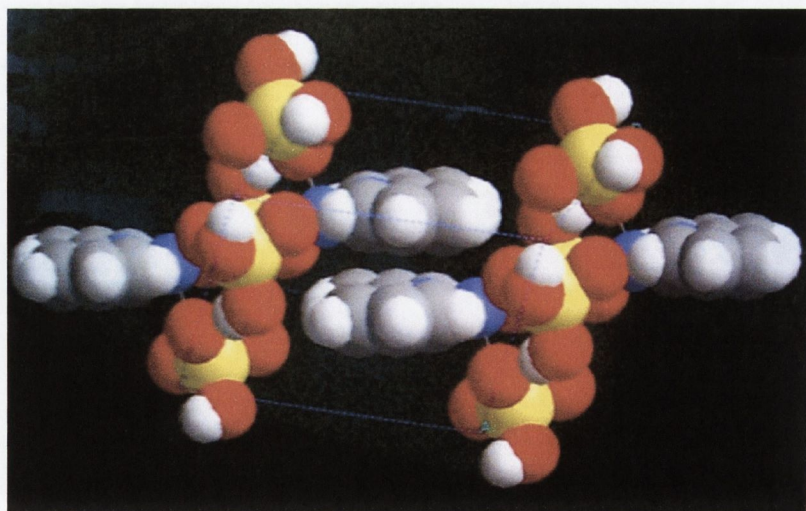


Fig 4.3. Space filled diagram showing π - π stacking through aromatic bipyridine rings in (10).

Additional interactions are also evident between the 2,2'-bipy hydrogens H(5) and H(8) and the oxygen atoms O(12) and O(14), respectively, from an adjacent dihydrogen arsenate sheet. It is interesting to note that the efficacy of packing within **(10)** is at the total exclusion of water from which it crystallised. This is somewhat unusual considering the hydrophilicity of dihydrogen-arsenate and the strong precedent that exists for complexes such as this to incorporate water, if not directly bound, then in the lattice. This may be explained by firstly the fact that at pH ~ 11 , the arsenate is diprotonated, which forces the copper(II) species to coordinate H_2AsO_4^- in the axial position to satisfy charge in the dinuclear complex. This arrangement of equatorially bridging dihydrogen-arsenate and axially bound dihydrogen-arsenate, combined with terminal bidentate 2,2'-bipyridine furnishes the square-based pyramidal geometry preferred by copper(II). Combined with dihydrogen-arsenates strong self-association and generation of a 2-dimensional sheet probably accounts for the absence of water in complex **(10)**.

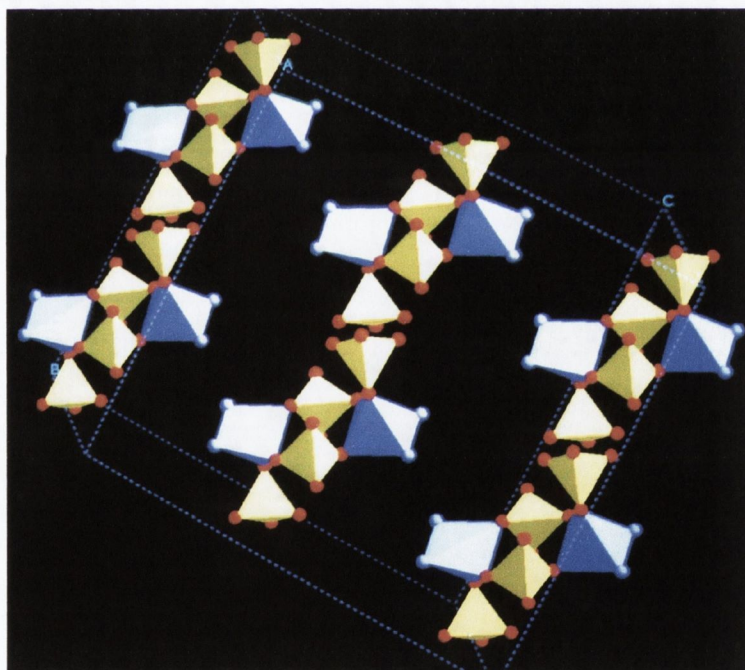


Fig 4.4. Polyhedral view of the structure of compound **(10)**. When packed the molecules exists as a chain of copper centred square based pyramids connected via 4 arsenic centred tetrahedra (yellow) per pair of square-based pyramids (blue). Bipy carbon atoms omitted for clarity.

4.2.1 Magnetic behaviour of $[(\text{bipy})\text{Cu}(\text{H}_2\text{AsO}_4)(\mu\text{-H}_2\text{AsO}_4)]_2$; (10).

The variable temperature magnetic behaviour of complex (10) in the form of a $\chi_m T$ versus T plot (χ_m is the magnetic susceptibility per copper(II) ion) is shown in Fig. 4.5.

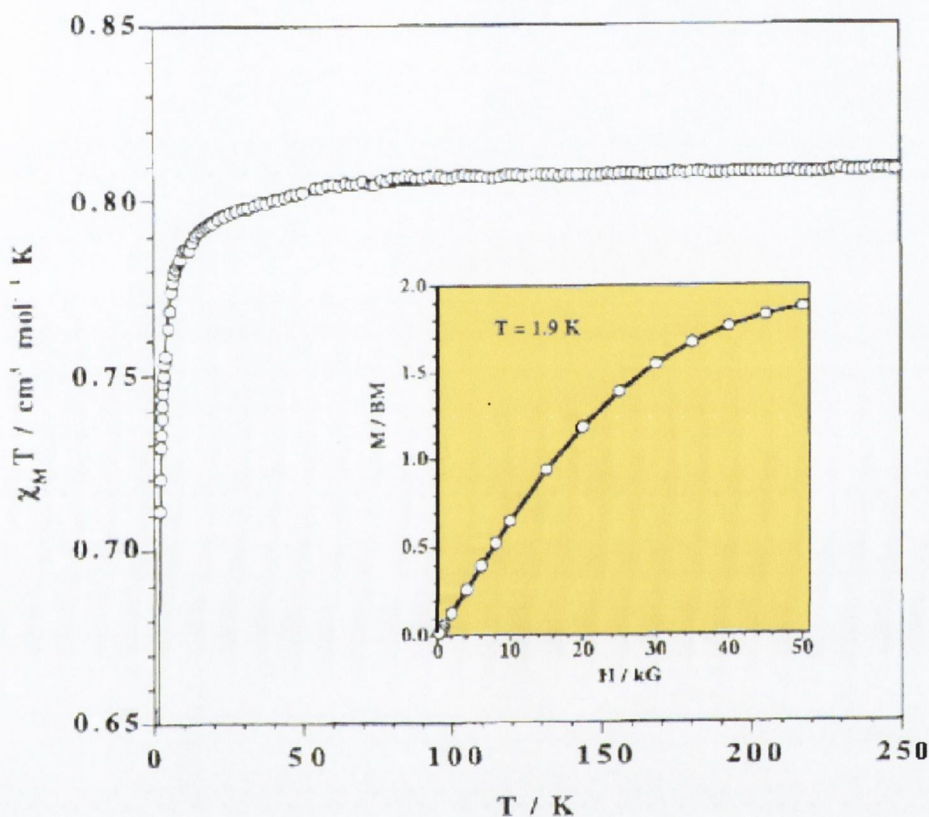
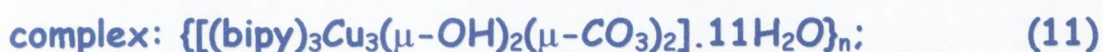


Fig 4.5. Thermal variation of $\chi_m T$ for compound (10) at $H = 0.1\text{T}$. The solid line represents the best fit through the theoretical expression for a dinuclear copper(II) complex. The inset shows the field dependence for complex (10) below T_c .

The value of $\chi_m T$ at 290 K is $0.81\text{ cm}^3\text{ mol}^{-1}\text{ K}$, which is as expected for a magnetically isolated spin doublet.⁸ This value remains practically constant upon cooling (Curie law behaviour- each molecule contains a unique magnetic centre with no first-order angular momentum) and then decreases sharply in the low temperature region attaining a value of $0.71\text{ cm}^3\text{ mol}^{-1}\text{ K}$ at 1.9 K. The results of the fit are $J = -0.58\text{ cm}^{-1}$ with $g = 2.07$ and $R = 4.3 \times 10^{-6}$. These features are characteristic of very weak antiferromagnetic interactions between

the copper(II) ions. The field dependence of the first magnetization below T_c is indicative of an $S = 1$ ground state with a spin multiplicity of 3.⁹

4.3. Preparation and Characterisation of the polymeric chain



Attempts were made to remove the remaining two protons of the dihydrogen-arsenate moiety in an effort to synthesise the direct tetranuclear Cu(II) analogue of the phosphate complex described in chapter 2. This was done by careful variation of the pH (from 11 to 14) of the solution using 5% NaOH. The complex was therefore prepared serendipitously at first through this increase in pH of an aqueous solution of Cu(OH)₂, 2,2'-bipyridine and sodium dihydrogen arsenate but could be directly prepared by simply allowing Cu(OH)₂ to react with 2,2'-bipyridine in 1:1 stoichiometry at pH 14. The pH increase resulted in a slight darkening of the originally royal blue solution. No precipitate was observed. On standing, open to the atmosphere, violet-blue prismatic single crystals were obtained in 60% yield based on copper. Infrared analysis of the crystals indicated the absence of arsenate in the complex with the loss of the broad peak at 854 cm⁻¹. The spectrum now indicated the presence of carbonate peaks at 1544 and 1383 cm⁻¹, indicative of bidentate coordination. Distinguished from the broad aquo peak at 3392 cm⁻¹ were two sharp peaks at 3111 and 3060 cm⁻¹, which is the signature of a bridging hydroxy group. Sharp bands of medium intensity at 1654, 1603, 1474, and 771 cm⁻¹ were assigned to the bipyridine ligand. A d-d spectrum of an aqueous solution of (11) showed a broad featureless band at 637 nm (blue-shifted with respect to the arsenate predecessor (10)) indicative of a square-pyramidal geometry of the Cu(II) chromophore.

4.4. Structural characterisation of



A representative violet-blue crystal was used for a single crystal X-ray diffraction study from which the molecular structure was unambiguously determined. The structure was solved by Dr Mark Nieuwenheuzen, of the Queens University, Belfast. X-ray crystal analysis

confirmed both the presence of bidentate carbonate and bridging hydroxide and characterised the prisms as the title complex $\{[(\text{Cu})_3(\text{bipy})_3(\mu\text{-OH})_2(\mu\text{-CO}_3)_2] \cdot 11\text{H}_2\text{O}\}_n$ (**11**) with 11 waters of crystallisation per asymmetric unit.

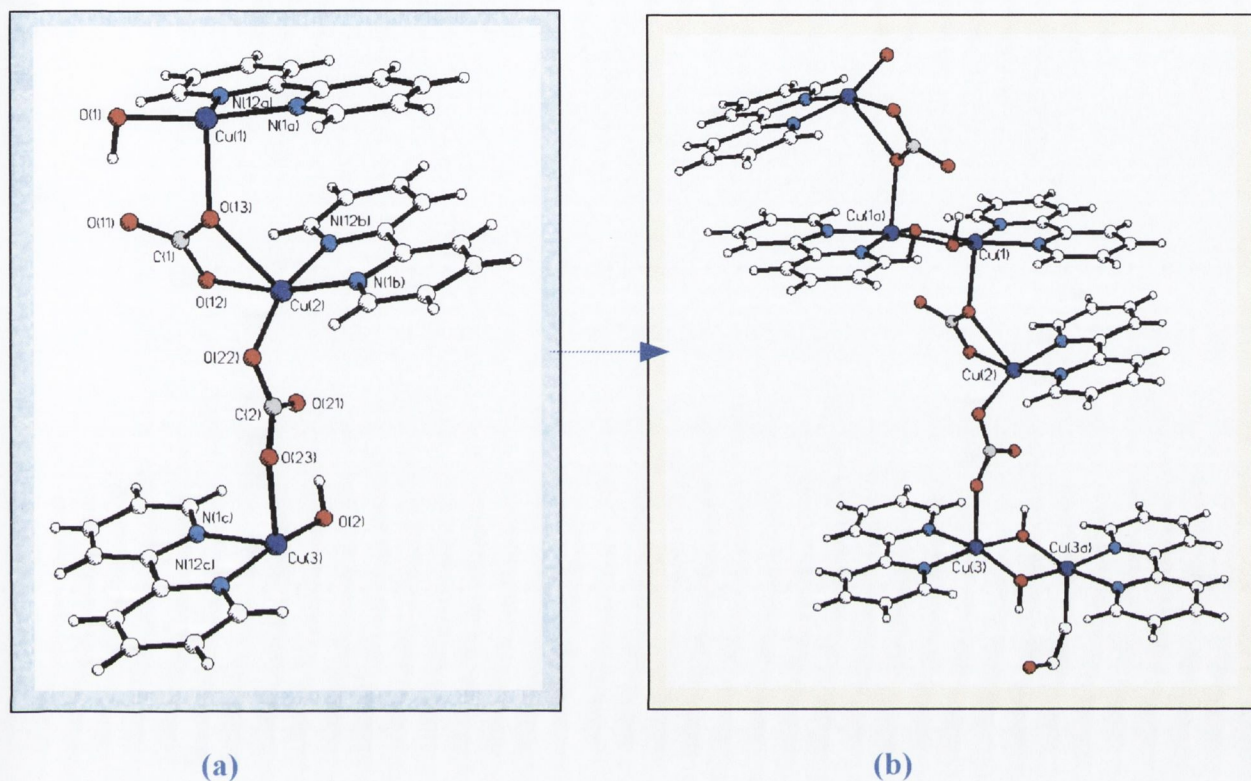


Fig 4.6. Molecular structures of the asymmetrical unit (a) of (11) and a 'dimer' repeat structure (b) obtained from symmetry. Note formation in (b) of an alternating series of copper(II) monomers and dimers, connected through carbonate and hydroxide bridges. Waters of crystallization omitted for clarity.

The polymeric nature of the complex was not expected especially since the crystals re-dissolve in both water and methanol. The crystal structure of the title compound consists of repeat units of $\{[\text{Cu}_3(\text{bipy})_3(\mu\text{-OH})_2(\mu\text{-CO}_3)_2]\}$ each with 11 waters of crystallization. The overall geometry then consists of the classical di- μ -hydroxy-bis[bipyridyl copper(II)] species, ligated trans-axially at each copper by μ -carbonato-mono[bipyridyl copper(II)] moieties. The three crystallographically unique copper(II) centres in (**11**) have square-pyramidal, five-coordinate geometry. The equatorial bonds of each copper(II) centre consist of 2 oxygen

atoms (carbonate oxygens for the monomer units, Cu(2) and bridging hydroxyl oxygens in the case of Cu(1) and Cu(3)) and 2 bipyridine nitrogens, generating an N₂O₂ basal plane. Oxygen from the adjacent copper unit occupies the apical position. Cu-Cu distances vary from a minimum of 2.871 Å for Cu(1)-Cu(1a) to a maximum of 6.469 Å between Cu(2)-Cu(3a). Cu(1)-Cu(2) distance is 4.292 Å. Further pertinent bond lengths and angles are given in Table 4.2.

Table 4.2. Selected bond distances (Å) and angles (°) for (11).

Cu(1)-O(1)	1.949(2)	Cu(1)-Cu(1a)#1	2.871(8)
Cu(1)-N(12A)	2.025(3)	Cu(3)-Cu(3a)#1	2.923(8)
Cu(1)-N(1a)	1.988(3)	Cu(1)-Cu(2)	4.292(8)
Cu(1)-O(13)	2.211(2)	Cu(2)-Cu(3)	5.687(8)
Cu(2)-O(13)	2.351(2)	Cu(1)-O(1)-Cu(1a)#1	94.55(7)
Cu(2)-O(12)	1.975(2)	Cu(3)-O(2)-Cu(3a)#1	96.54(6)
Cu(2)-O(22)	1.931(2)	Cu(1)-O(13)-Cu(2)	138.1(1)
Cu(2)-N(1b)	2.008(3)	O(1)-Cu(1)-O(13)	92.6(1)
Cu(2)-N(12b)	2.000(3)	O(12)-Cu(2)-O(22)	95.0(1)
Cu(3)-O(23)	2.179(2)	O(2)-Cu(3)-O(23)	98.1(1)
Cu(3)-O(2)	1.951(2)	C(2)-O(22)-Cu(2)	108.3(2)
Cu(3)-N(1c)	2.027(3)	O(23)-C(2)-O(22)	118.1(3)
Cu(3)-N(12c)	1.997(3)	C(2)-O(23)-Cu(3)	124.7(2)

Estimated standard deviations are given in the parenthesis.

Symmetry operators:

#1: -x, -y, -z

Distortion from square-pyramidal geometry is most pronounced about Cu(2) with a mean plane deviation (O(22), O(12), N(12b), N(1b)) of 0.2387 Å. Mean plane deviations for Cu(1) and Cu(3) are 0.0516 Å and 0.0445 Å, respectively. The dihedral angle between the bipy rings attached to Cu(1) and Cu(2) in the asymmetric unit (Fig 4.6a) is 10.7°. The copper atom array and carbonate bridging disposition resembles the copper containing minerals malachite [Cu₂(OH)₂(CO₃)] and azurite [Cu₃(OH)₂(CO₃)₂], although within these compounds all the

oxygen atoms from the carbonate group are involved in coordination. Overall there is an interwoven pattern of bipyridine rings throughout complex **(11)** generating 2-D layers from which the waters of crystallisation are 'squeezed' out, existing in the hydrophilic regions between those layers (Figure 4.7).

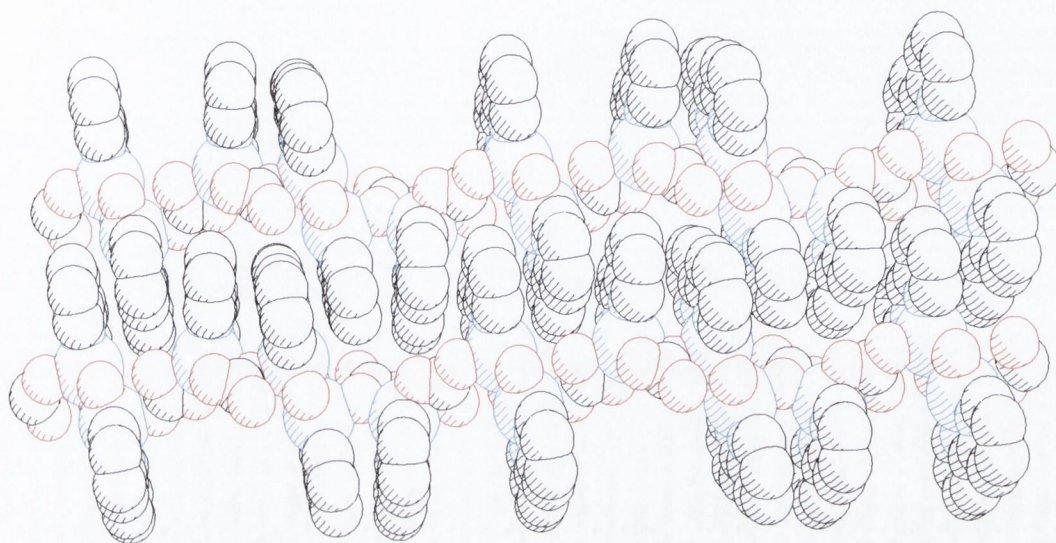


Fig 4.7. Space-filling representation showing 2-D packing in (11).

The presence of bpy-bpy π - π stacking interactions is considered to play a role in determining the overall molecular structure. Inspection of the bipyridyl rings incorporating N(12a)-N(1a) and N(1b)-N(12b) and coordinated to Cu(1) and Cu(2) shows that they are *offset* face-to-face stacked in an attempt to maximise stabilising π -interactions while minimising electrostatic repulsion.¹⁰ The separation between bipyridine rings at closest contact is 3.449 Å. The cohesiveness of the crystal structure is ensured by the extensive 3-dimensional H-bonding interactions in **(11)** with H-bonds linking the 2-D chains together as well as H-bonding to other lattice water molecules.

4.4.1. Thermal analysis of (11).

Thermal analysis (TGA) of a small amount (11.73mgs) of powdered sample of complex (11) showed gradual, continuous mass loss from slightly above room temperature ($\sim 30^{\circ}\text{C}$) to 220°C with no stable intermediates.

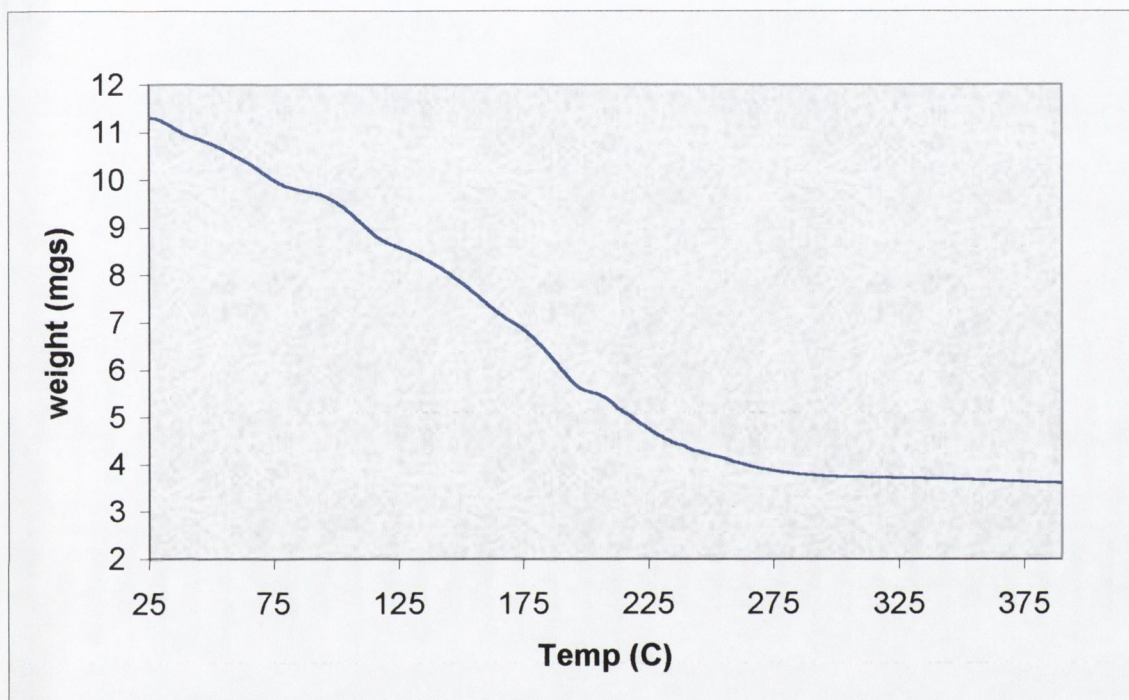


Figure 4.8. Thermal Gravimetric analysis curve for complex (11). Curve is indicative of gradual mass loss with no stable intermediates.

The differential thermal gravimetric (DTG) curve showed the mass loss was endothermic and characteristic of dehydration. It is likely therefore that all 11 water molecules are lost by 220°C . The total mass lost however ($\sim 35\%$ by 220°C) indicates that carbonate is also being eliminated, as CO_2 , from the system. Above 220°C oxidation occurs probably resulting in black copper oxide. The loss of the lattice water molecules over a large and relatively high temperature range is indicative of the presence of a H-bonding network within complex (11).

4.4.2. Magnetic properties of $\{[(\text{bipy})_3\text{Cu}_3(\mu\text{-OH})_2(\mu\text{-CO}_3)_2]\cdot 11\text{H}_2\text{O}\}_n$; (11).

Variable temperature magnetic susceptibility measurements (300-1.9K) on a polycrystalline sample of (11) under an applied magnetic field $H = 50\text{G}$ shows the occurrence of complex ferromagnetic coupling. The $\chi_m T$ value (χ_m being the magnetic susceptibility per copper(II) ion) increases continuously from $0.40\text{ cm}^3\text{ mol}^{-1}$ at room temperature to a maximum value of $1.15\text{ cm}^3\text{ mol}^{-1}$ at low temperature (Figure 4.9).

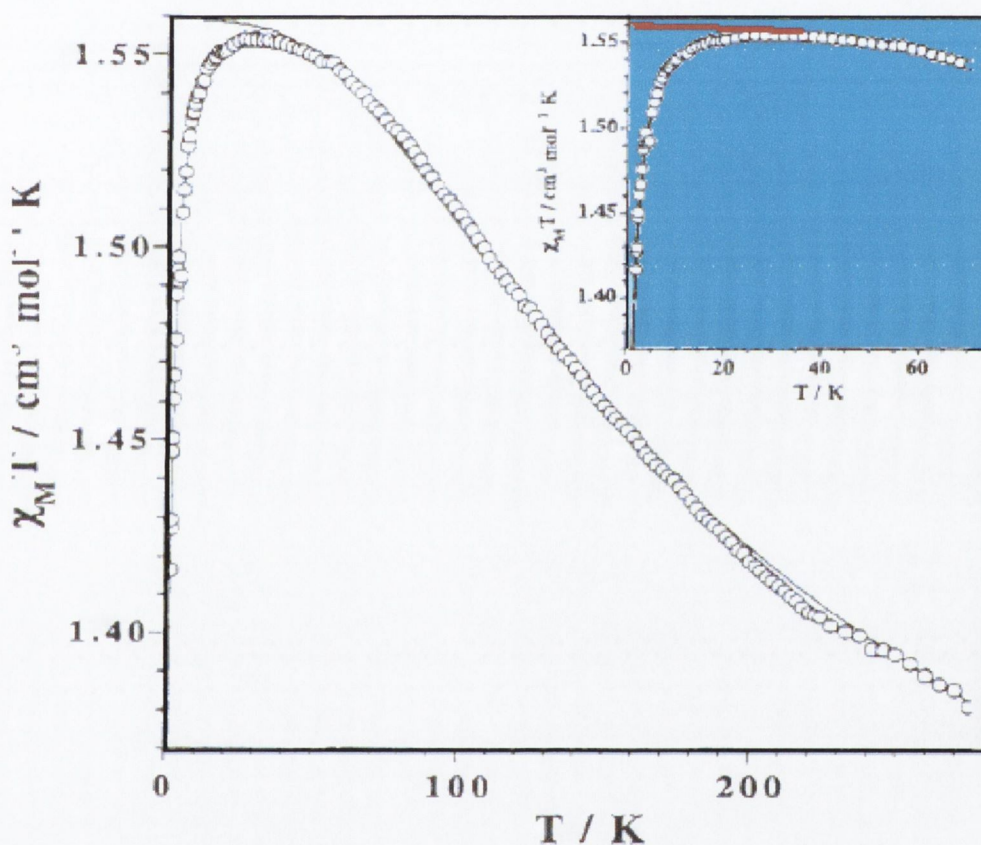
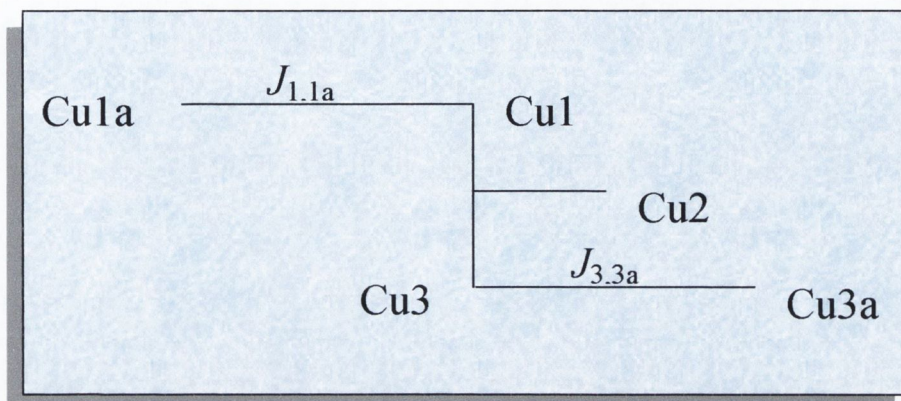


Fig 4.9. $\chi_m T$ versus T plot for (11). Solid line indicates line of best fit. Curve is characteristic of ferromagnetism with a maximum indicating the presence of weak anti-ferromagnetism at low T . Note red solid line marked clearly in inset (blue) box.

The shape of the curve is as expected for the occurrence of ferromagnetic coupling. In the periodicity observed in the chain compound (Scheme 4.2) two important magnetic pathways

($J_{1,1a}$, $J_{3,3a}$) are distinguished. ($J_{1,1a} = J_{1a,1}$; $J_{3,3a} = J_{3a,3}$). The pathways between $J_{1,2}$ and $J_{2,3}$ are considered to be extremely weak and are therefore neglected from the final fit.



Scheme 4.2. Exchange coupling pathways in complex (11). Horizontal lines represent hydroxy bridges while vertical lines represent carbonate bridges.

Magnetically the system contains therefore, an isolated spin doublet and two non-interacting spin-triplets giving overall ferromagnetism. The two different triplets have exchange coupling constants (J defined by the Hamiltonian $H = -2JS_1S_2$) of $J_{1,1a} = 154 \text{ cm}^{-1}$ ($\theta = 94.6^\circ$, that is for Cu(1)-O(1)-Cu(1a)) and $J_{3,3a} = 135 \text{ cm}^{-1}$ ($\theta = 96.5^\circ$, that is for Cu(3)-O(1)-Cu(3a)) with an average Lande factor of $g = 2.45$. The positive J values verify the presence of a triplet ground state. The monomer (with spin = $1/2$) is a doublet with $g' = 2.07$. The red solid line in the low temperature range marked in the inset box in Figure 4.9 above, corresponds to the consideration of only the two non-interacting triplets plus an isolated spin doublet. This does not account however for the experimentally observed low Temperature anti-ferromagnetism. The addition of a Weiss parameter¹¹ of $\theta = -0.19 \text{ K}$ accounts for this decrease, a result of long-range weak antiferromagnetic intermolecular interactions through the axial carbonate groups. The equation for the overall $\chi_m T$ value obtained is:

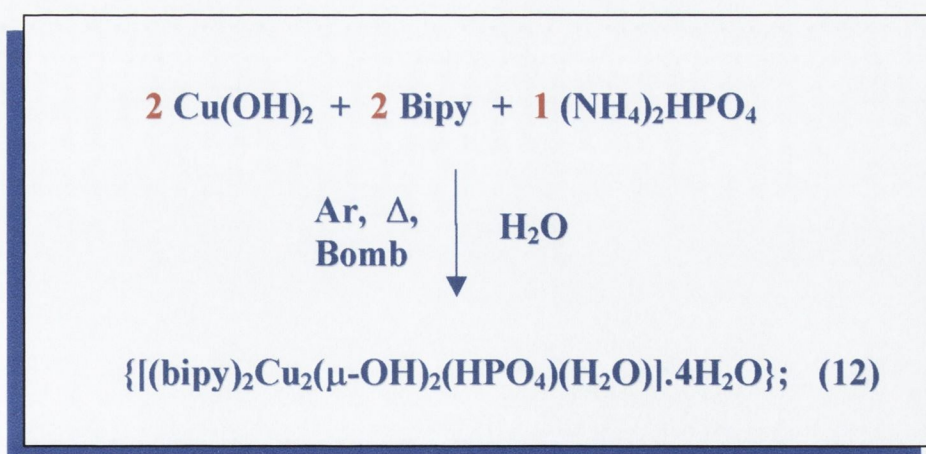
$$\chi_m T = \frac{1}{2} (\chi_{\text{dimer}}) + \frac{1}{2} (\chi_{\text{dimer}})' + (\chi_{\text{monomer}}) \times T^2 / (T - \theta)$$

The fit is excellent with $R = 3.0 \times 10^{-6}$. The two non-interacting triplets co-existing in complex **(11)** allow a correlation between structural and magnetic features to be attempted. A seminal work in this area, published by Hodgson and Hatfield,¹² noted that an examination of the relevant structural and magnetic data for a series of hydroxo-bridged copper(II) dimer complexes, revealed a monotonic decrease in the value of J as the value of the Cu-O-Cu angle ϕ increased. Since the principal path for the magnetic interaction is through the bridging hydroxy ligands the trend is explained in terms of super-exchange. If the orbitals used by the bridging oxygen atoms are pure p orbitals, the bond angle is expected to be 90° and the ground state is predicted to be a triplet. (*i.e.* $J > 0$). If the orbitals are purely s , the ground state is predicted to be a singlet (*i.e.* $J < 0$). Hence, since an increased value of the bridging angle implies greater s character in the bridging orbitals, a decrease in J values is expected as the bridging angle increases from 90° . In the case of complex **(11)** this exact trend is observed. For the exchange coupling between Cu(1)-O(1)-Cu(1a) a J value of 154 cm^{-1} is observed. The second J value for Cu(3)-O(1)-Cu(3a) is 135 cm^{-1} , a drop of 19 cm^{-1} . This decrease coincides with an increased bridging angle for Cu(3)-O(1)-Cu(3a) of $\theta = 96.5^\circ$ compared to the bridging angle for Cu(1)-O(1)-Cu(1a) of $\theta = 94.6^\circ$. While this correlation between structural and magnetic features is of great significance it should be noted that such large positive J values are known to only limited precision since the Van Vleck equation¹³ for exchange-coupled pairs of copper(II) ions is extremely insensitive to variations in large positive J values. It is virtually impossible to distinguish between J values as disparate as $+100$ and $+200 \text{ cm}^{-1}$ on the basis of low temperature susceptibility measurements.

4.5. Hydrothermal synthesis and Characterisation of the dinuclear copper(II) complex



During the course of our investigations into the coordination and magneto-chemistry of Cu(II) phosphate complexes it was decided to see what effect hydrothermal conditions would have on any final product. The reaction conditions utilized in the synthesis of complex (2), namely the tetranuclear hydroxy-bridged Cu(II) complex containing the $[(\text{bipy})_4(\text{Cu})_4(\mu\text{-PO}_4)_2(\mu\text{-OH})(\text{H}_2\text{O})_2]$ core, were repeated except now under high temperature and pressure. The effect this change had on the identity of the final product was profound and warrants discussion here. The title complex (12) was prepared hydrothermally by reacting a mixture containing $\text{Cu}(\text{OH})_2$, 2,2'-bipyridine and ammonium hydrogen phosphate in 15 mls of degassed water. The suspension was further degassed over 40 minutes under argon and then added to a Teflon bomb insert that had previously been flushed with argon. The insert was then sealed and placed in a temperature programmable oven at 180°C over 6 hours. On removal from the bomb a deep royal blue solution containing slight traces of un-reacted starting material was observed. The filtrate was allowed to stand (in air) over the course of two weeks and large blue block crystals formed.



Scheme 4.3. Direct preparation of the dinuclear species (12).

Infrared analysis of the crystals indicated the presence of both 2,2'-bipyridine and a phosphate species. The presence of hydroxide in the complex could not be ascertained due to the broad aquo peak at 3396 cm^{-1} . No carbonate peaks were observed in (12). A d-d spectrum of an aqueous solution of (12) revealed a broad featureless band at 667 nm, characteristic of a square-pyramidal geometry about the copper(II) ions.

4.6. Structural characterisation of



A representative dark blue block crystal was used for the data collection from which the molecular structure was determined. The molecule is monoclinic with space group $P2(1)/c$. The overall molecular geometry of the dinuclear complex again consists of the classical di- μ -hydroxy-bis[bipyridyl copper(II)] species, ligated axially by HPO_4^{2-} at Cu(1) and by H_2O at Cu(2) in a trans configuration.

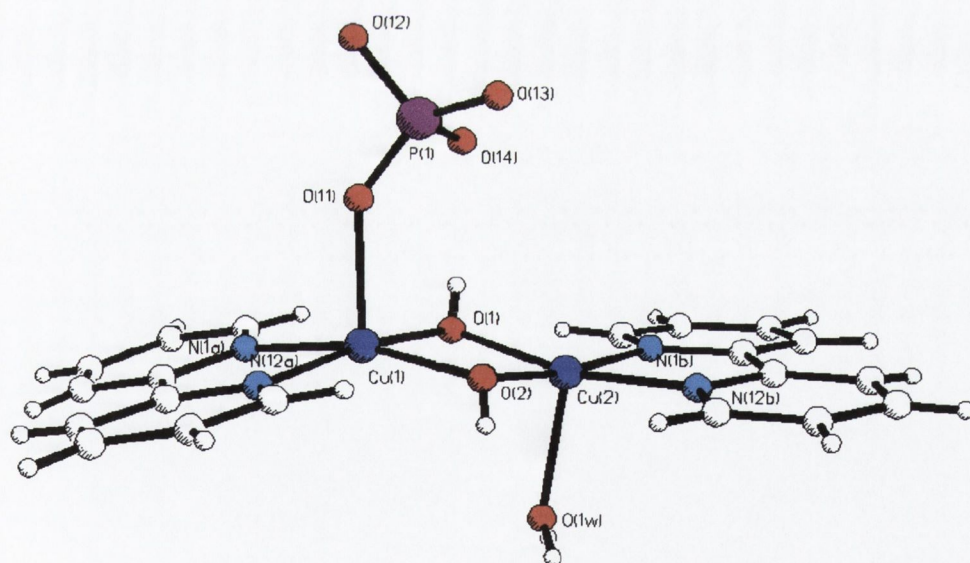


Fig. 4.10. Molecular structure of $\{[\text{Cu}_2(\text{bipy})_2(\mu\text{-OH})_2(\text{HPO}_4)(\text{H}_2\text{O})].4\text{H}_2\text{O}\}$ (12), looking along the xy plane. Waters of crystallization omitted for clarity. The proton from the HPO_4^{2-} group could not be directly located but is inferred from charge considerations.

The Cu(1)-Cu(2) separation is 2.906 Å with a Cu(1)-O(1)-Cu(2) bridging angle of 95.44°. Both values fall within the range found for similarly coordinated di- μ -hydroxo-copper(II) dimers.¹⁴ Square pyramidal geometry about the copper atoms is furnished by two nitrogen donors from the coordinated bipyridyl ligand and two oxygen atoms from the bridging hydroxy groups, forming the N₂O₂ basal plane, and axially by oxygen from either the HPO₄²⁻ group (to Cu(1)) or water (to Cu(2)). Cu(1) experiences a slightly more pronounced distortion than does Cu(2) with Cu(1) displaced 0.0724 Å towards the apical oxygen atom from the mean basal plane. Cu(2) in comparison is displaced 0.06 Å from the mean plane of its basal atoms. This deviation is a reflection of the difference in apically bound ligands, with the HPO₄²⁻ group causing a greater deviation than does the coordinated, neutral water. The complex has an average Cu-OH distance ~1.95 Å with a separation of 2.846 Å between the two hydroxyl oxygens. These values agree well with the average Cu-OH distance of ~1.96 Å and OH-OH distance ~2.65 Å found in other similar copper(II) dimers.¹⁵

Table 4.3. Selected bond distances (Å) and angles (°) for (12).

Cu(1)-Cu(2)	2.906(5)	Cu(1)-O(1)-Cu(2)	95.44(5)
Cu(1)-N(1a)	2.029(2)	Cu(1)-O(2)-Cu(2)	96.53(5)
Cu(1)-N(12a)	1.997(2)	O(11)-Cu(1)-O(1)	97.33(8)
Cu(1)-O(1)	1.962(2)	N(1a)-Cu(1)-N(12a)	80.03(8)
Cu(1)-O(11)	2.191(2)		
Cu(2)-N(1b)	2.005(2)	N(1b)-Cu(2)-N(12b)	80.93(8)
Cu(2)-N(12b)	2.016(2)	O(1w)-Cu(2)-O(1)	95.91(8)
Cu(2)-O(1)	1.965(2)		
Cu(2)-O(2)	1.936(2)		
Cu(2)-O(1w)	2.205(2)		

Estimated standard deviations are given in the parenthesis

The hydrogen phosphate group exhibits near ideal tetrahedral geometry with only slight deviations from 109.5° observed. [e.g. O(11)-P(1)-O(14) 109.37° , O(12)-P(1)-O(13) 109.55°]. Phosphorous-oxygen bonds are in the range 1.46 to 1.91 Å. Within the crystal there is an extensive interleaving of the bipyridine rings, producing 2-D layers through π - π interactions (See Figure 4.11).

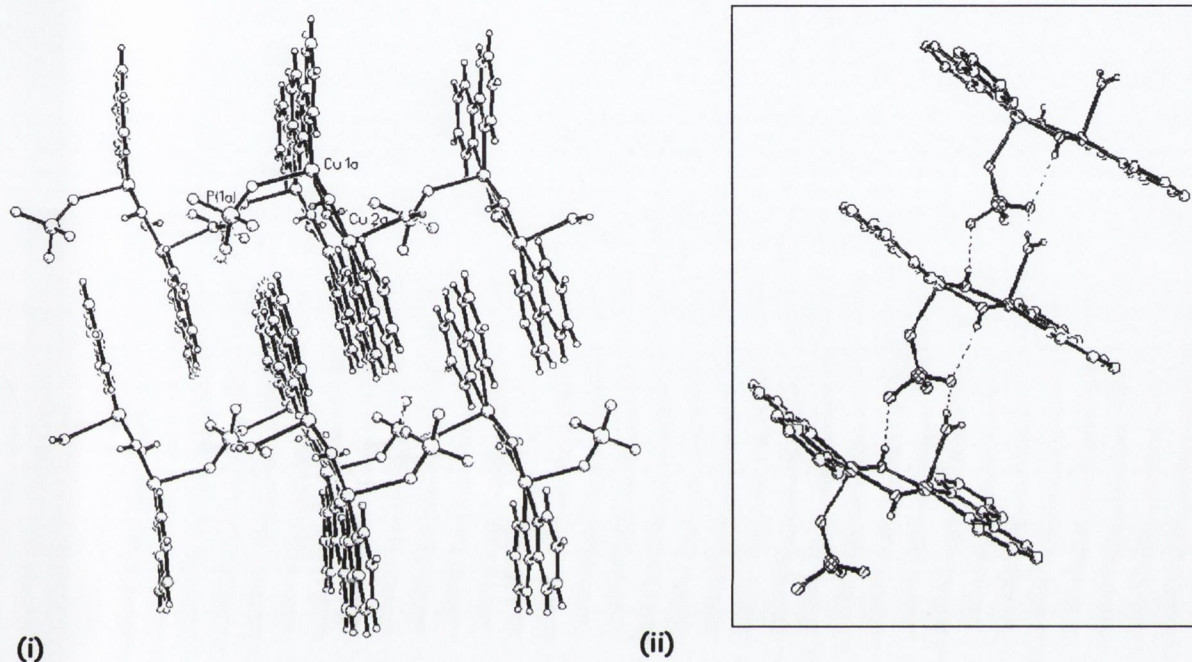


Fig 4.11. Packing diagrams showing (i) an alternating interleaving of the 2,2'-bipyridine ligands and (ii) extensive H-bonding between the apically bound hydrogen-phosphate moieties, bridging OH and bound water molecules. Average bpy-bpy distance is ~ 3.4 Å. Waters of crystallization omitted for clarity.

The formation of π -stacks in **(12)** is not the only supramolecular interactions in which the bipy ligand is involved. H-bonding between peripheral bipy-hydrogens and an apically bound phosphate from the adjacent layer, serve to bridge together the sheets formed by complex **(12)**. There is now also a distinct hydrophilic region existing within the molecule and it is within this region that the lattice water molecules reside. An extensive water array forms from H-bonding not only between the water molecules and the apical phosphate groups but

also between the water molecules and the bridging hydroxide groups. H-bonds of the type O-H \cdots Ow, P-O \cdots Hw, and Hw \cdots Ow serve to form a 3-D network as illustrated by Figure 4.12.

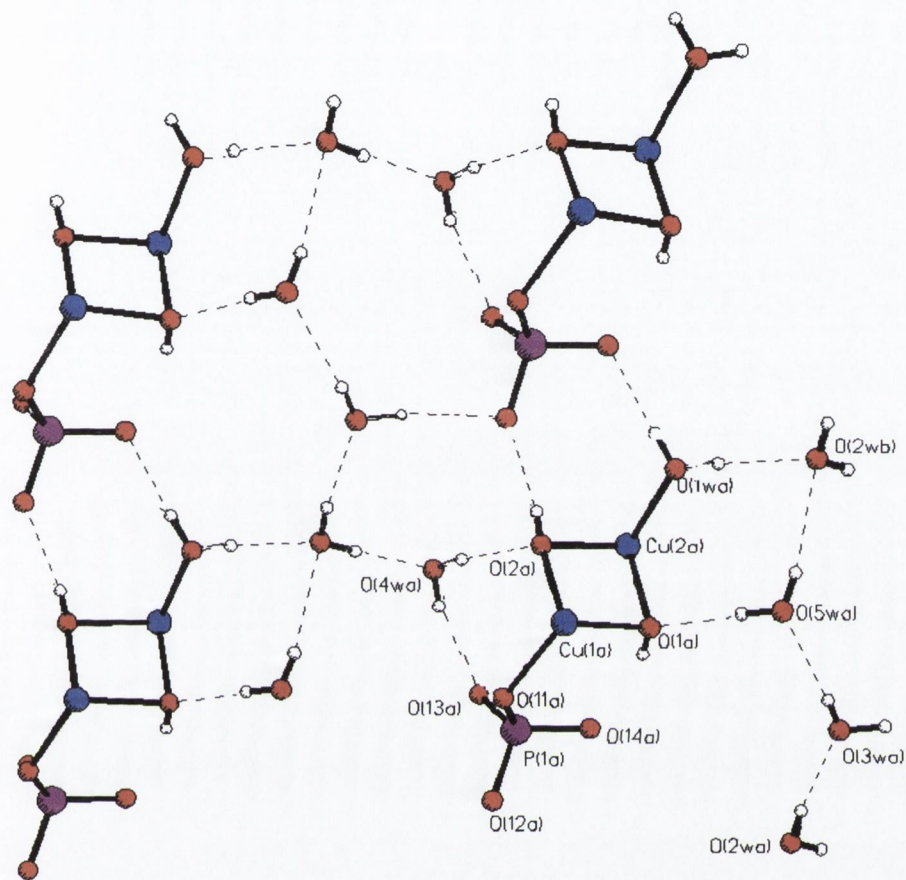


Fig 4.12. Packing diagram showing H-bonds between bound hydroxy and phosphate groups and lattice water molecules. An infinite array of H-bonding also exists between the lattice waters. 2,2'-bipyridine ligands omitted for clarity, but would project above and below this sheet.

The lattice water molecules also serve to maintain an effective interchain intermolecular distance (Cu(1)-Cu(1a) 10.913 Å). Removal of this loosely bound lattice water has been shown previously by ourselves¹⁶ and others¹⁷ to have potential effects on not only the resulting structure but also the magnetic behaviour of the system.

4.6.1. Thermal Gravimetric Analysis (TGA) of (12).

Thermal gravimetric analysis carried out on a sample of $\{[(\text{bipy})_2\text{Cu}_2(\mu\text{-OH})_2(\text{HPO}_4)(\text{H}_2\text{O})].4\text{H}_2\text{O}\}$ showed a two stage decomposition with two stable intermediates (13) and (14). The first step occurs between 25° and $\sim 78^\circ$ and corresponds to the loss of the four non-coordinated lattice water molecules generating (13). The second step, between $\sim 79^\circ$ and $\sim 120^\circ$, is due to the loss of the coordinated water molecule giving (14) (Figure 4.13).

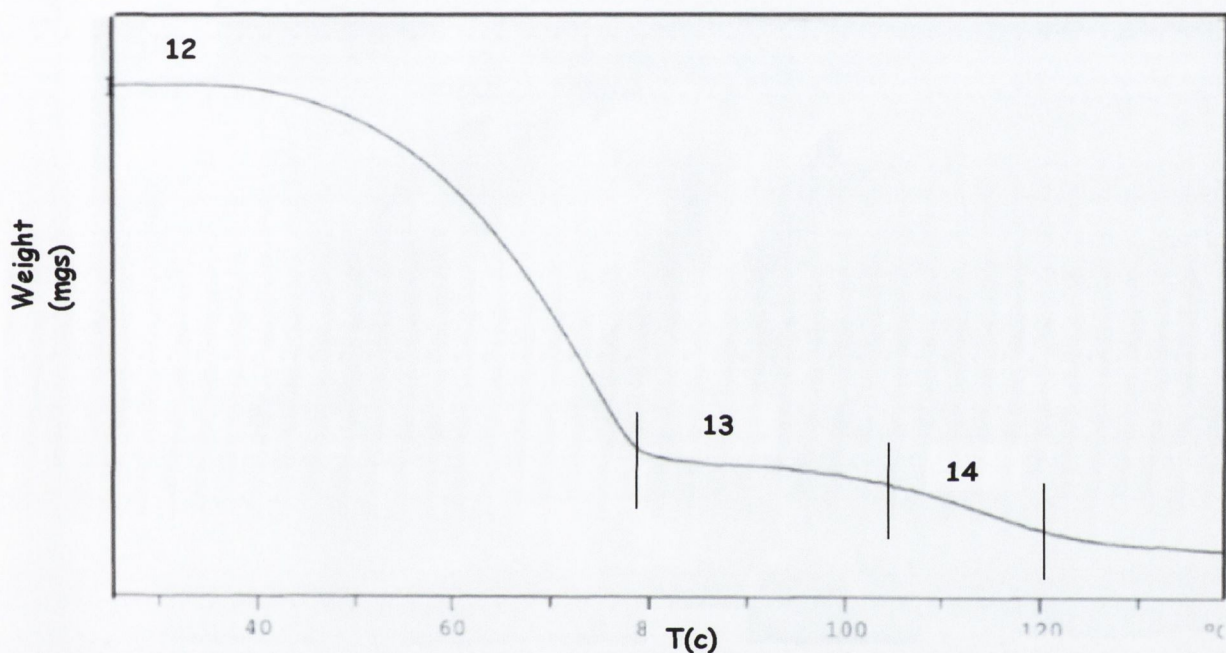


Fig 4.13. TGA curve for complex (12).

This results in three distinct phases of varied degree of hydration.

4.6.2. Magnetic properties of $[(\text{bipy})_2\text{Cu}_2(\mu\text{-OH})_2(\text{HPO}_4)(\text{H}_2\text{O})].4\text{H}_2\text{O}$ (12) and $[(\text{bipy})_2\text{Cu}_2(\mu\text{OH})_2(\text{HPO}_4)]$ (14).

While three phases of different degrees of hydration were indicated by thermal analysis, variable temperature magnetic susceptibility measurements (300-1.9K) were only carried out on the completely hydrated phase (all 5 water molecules, (12)) and the completely

dehydrated phase $[(\text{bipy})_2\text{Cu}_2(\mu\text{-OH})_2(\text{HPO}_4)]$ (**14**). The exchange coupling constants were evaluated by calculating the energy difference between the singlet (S) and triplet (T) states using the dimer law $H = -2JS_1S_2$.

1. Hydrated Phase (**12**); Under an applied magnetic field $H = 50\text{G}$, the hydrated phase $\{[\text{Cu}_2(\text{bipy})_2(\mu\text{-OH})_2(\text{HPO}_4)(\text{H}_2\text{O})].4\text{H}_2\text{O}$ (**12**) shows intramolecular ferromagnetic coupling through the di- μ -hydroxo bridge, as predicted by the reduced values of the $\text{Cu}(1)\text{-O}(x)\text{-Cu}(2)$ angles in (**12**) of $x = 1, 95.44^\circ$ and $x = 2, 96.53^\circ$.¹⁸

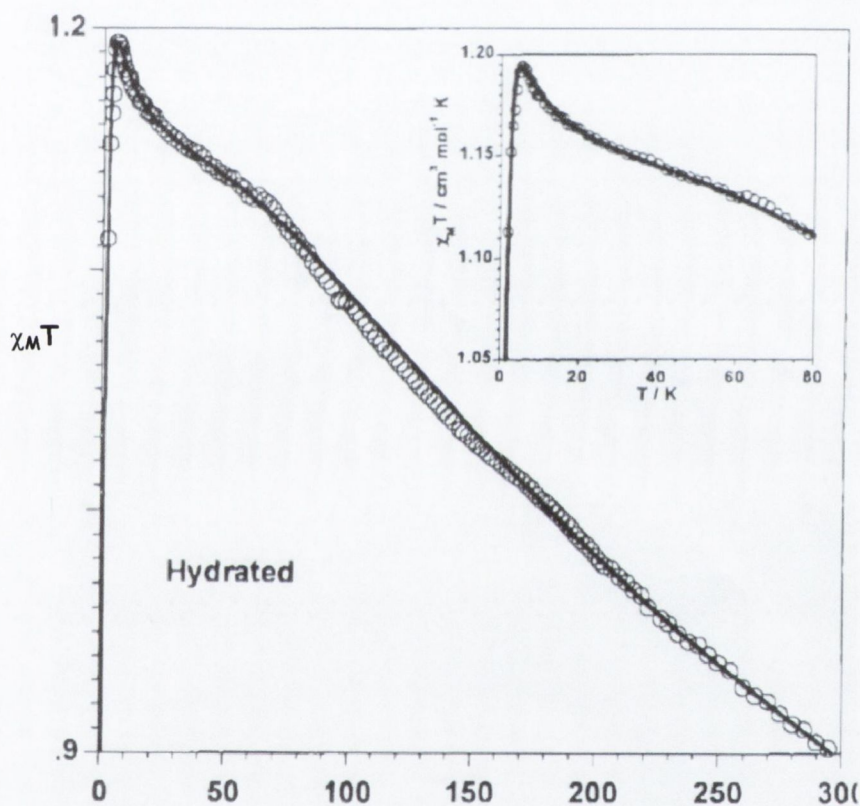


Fig 4.14. Plot of $\chi_m T \text{ cm}^3 \text{ mol}^{-1} \text{ K}$ against $T \text{ (K)}$ for (**12**). Calculated fit is shown by the solid line and is obtained with $J = +184 \text{ cm}^{-1}$, $g = 2.12$, $\theta = +0.38^\circ$, $D = 2.8 \text{ cm}^{-1}$ and $R = 8 \times 10^{-6}$.

There also exists an intermolecular ferromagnetic interaction between dimers in (**12**) as indicated by the positive Weiss constant (θ) of $+0.38$. Finally zero-field splitting ($D = 2.8 \text{ cm}^{-1}$) occurs in (**12**) at very low temperatures, which forces the $\chi_m T$ product to vanish.

2. Anhydrous phase (**14**); The magnetic coupling exhibited by the anhydrous phase (**14**) is shown in Fig 4.15. Again strong intramolecular ferromagnetic exchange ($J = 197 \text{ cm}^{-1}$) occurs through the di- μ -hydroxo bridge of the Cu(II) dimer but now the interdimer interaction is slightly antiferromagnetic ($\theta = -0.06^\circ$). As in the hydrated phase, zero-field splitting forces the $\chi_m T$ product to vanish at very low temperatures.

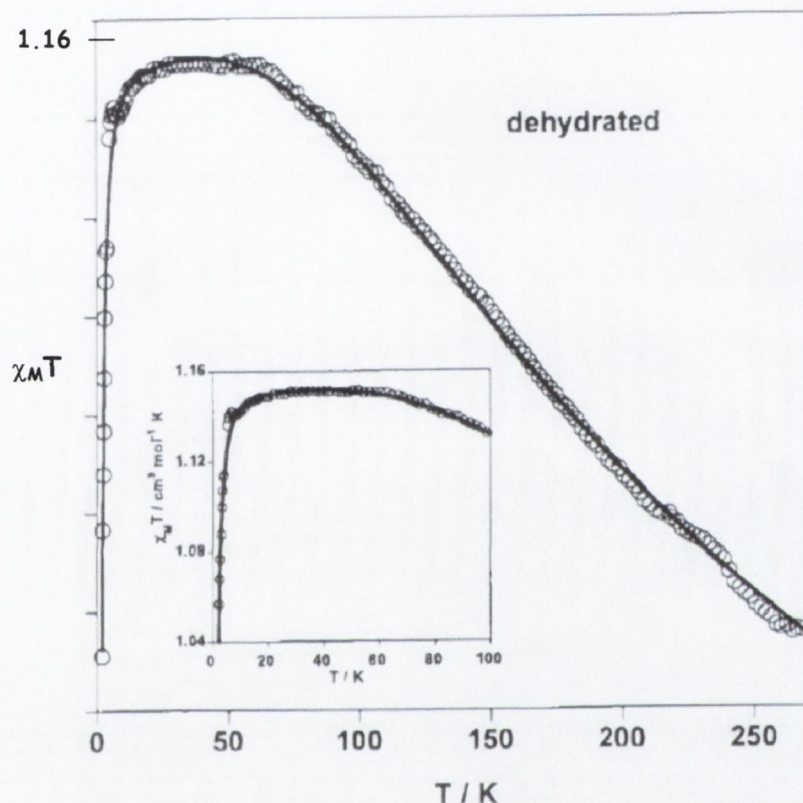


Fig 4.15. Plot of $\chi_m T \text{ cm}^3 \text{ mol}^{-1} \text{ K}$ against $T \text{ (K)}$ for (**14**). Calculated fit is shown by the solid line and is obtained with $J = +197 \text{ cm}^{-1}$, $g = 2.11$, $\theta = -0.06^\circ$, $D = 1.6 \text{ cm}^{-1}$ and $R = 7 \times 10^{-6}$.

The values of J obtained for (**12**) and (**14**) are larger than any reported previously in the literature for this particular family of complexes. The complex $[\text{Cu}(\text{bipy})\text{OH}]_2(\text{NO}_3)_2$ with a bridging angle of 95.5° is one of the highest previously reported for this group of complexes with a J value of $+172 \text{ cm}^{-1}$.¹⁹ The slightly smaller bridging angles found in (**12**) of 95.44° ,

through Cu(1)-O(1)-Cu(2) resulting in a value for J of 184 cm^{-1} , agrees with the correlation of Hatfield and Hodgson, where for every change of one degree in bridging angle there results a variation of $\sim 74 \text{ cm}^{-1}$ in S-T separation (J).¹² Since there is asymmetry in (12), it should be noted here that an average Cu-OH-Cu angle (of 95.9°) was used, in an approach validated by Ruiz *et al.*¹⁸

Finally, magnetisation curves of the hydrated and anhydrous phases at 2K show the effect the intermolecular interactions have on the complexes. The solid line in Figure 4.17 is the theoretical curve for an $S = 1$ system without any intermolecular interactions. It can be seen that the behaviour of the hydrated phase (12) is above this line, whereas that of the anhydrous phase (14) is below it, in accord with θ values of $+0.38$ and -0.06° , respectively.

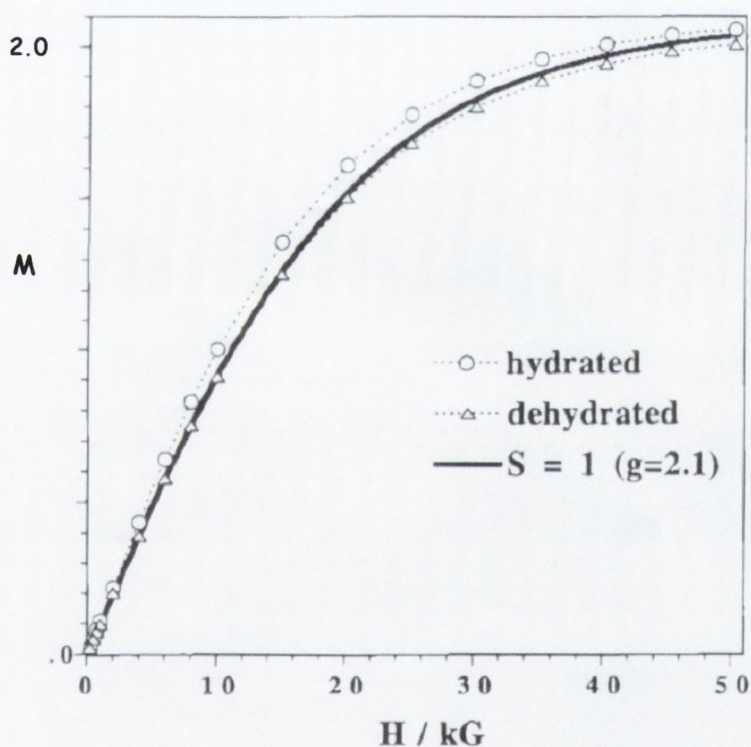


Fig 4.16. Magnetisation M (BM) against Field H (kG).

This occurs for the hydrated phase (12) because of ferromagnetic intermolecular interactions and for the anhydrous phase (14) because of slight anti-ferromagnetic intermolecular inter-

actions. These intermolecular interactions are most probably through the apically bound HPO_4^{2-} group. This interaction would be expected to be weak as it interacts with d_z^2 orbital of Cu(II). The change from ferromagnetic to antiferromagnetic coupling on dehydration is likely a result of slight variations in bridging angles and Cu-Cu inter-dimer distances through the hydrogen-phosphate moiety.

Conclusion

A dinuclear copper(II) complex (**10**) was synthesised containing both bridging and apical dihydrogen-arsenate groups. The system utilises a network of π - π and H-bonding interactions and displays weak antiferromagnetic exchange coupling through the \sim tetrahedral H_2AsO_4^- bridges. In an effort to generate completely deprotonated inorganic arsenate (AsO_4^{3-}), the pH was increased from 11 to 14. This had the effect of completely removing arsenate, of any form, from the complex recovered (**11**). Now an alternating carbonate/hydroxy bridged copper(II) polymeric species was obtained. Magnetically the complex exists as an isolated spin doublet with two non-interacting spin triplets returning overall ferromagnetic behaviour. The synthesis of a similar hydroxy-bridged copper(II) complex (**12**), and its anhydrous analogue (**14**), incorporating pendant protonated phosphate was achieved by hydrothermal synthesis and controlled dehydration respectively. The complex exhibits the strongest ferromagnetic exchange coupling yet seen in this family of di- μ -hydroxy copper(II) complexes and exhibits varied intermolecular interactions depending on degree of hydration. A common theme throughout is the role played by supramolecular interactions in the overall structure, stability and dimensionality of each system and the ability of oxo-anions to act as both facilitators of magnetic super-exchange and as potent H-bond donor-acceptors.

References

1. a) *Supramolecular Materials and Technologies*, D.N. Reinhoudt, Wiley, Chichester, **1999**.; b) *Supramolecular Control of Structure and Reactivity*, A.D. Hamilton, Wiley, Chichester, **1996**.
2. M.E. Davis, *Chem. Eur. J.*, **3**, 1745, 1997.
3. B. Bazan, J.L. Pizarro, L. Lezama, M.I. Arriortua and T. Rojo, *Inorg. Chem.*, **39**, 6056, 2000.
4. a) U. Kumar, J.M.J. Frechet, T. Kato, S. Ujiie and K. Timura, *Angew. Chem. Int. Ed.*, **31**, 1531, 1992 and references therein.; b) E.K. Fan, J. Yang, S.J. Keib, T.C Stoner, M.D. Hopkins and A.D. Hamilton, *J. Chem. Soc., Chem. Comm.*, 1251, 1995.
5. *Supramolecular Chemistry*, J.M. Lehn, VCH, Weinheim, **1995**.
6. P.J. Stang and B. Olenyuk, *Acc. Chem. Res.*, **30**, 502, 1997.
7. J. Bernstein, M.C. Etter and J.C. Macdonald, *J. Chem. Soc., Perkin Trans. 2*, **5**, 695, 1990.
8. K.S. Murray, *Advances in Inorganic Chemistry*, **43**, 261, 1995.
9. *Molecular Magnetism*, O. Kahn, VCH, New York, p11, **1993**.
10. C.A. Hunter, K.R. Lawson, J. Perkins and C.J. Urch, *J. Chem. Soc., Perkin Trans. 2*, **2**, 651, 2001.
11. *Introduction to Magnetochemistry*, A. Earnshaw, Academic Press, London, **1968**.
12. D.J. Hodgson, W.H. Crawford, H.W. Richardson, J.R. Wasson, D.J. Hodgson and W.E. Hatfield, *Inorg. Chem.*, **15**, 2107, 1976.

13. *The Theory of Electric and Magnetic Susceptibilities*, J.H. van Vleck, Oxford University Press, Oxford, **1932**.
14. a) J.A. Barnes, W.E. Hatfield and D.J. Hodgson, *J. Chem. Soc., Chem. Comm.*, 1593, 1970; b) R.J. Majeste and E.A. Meyers, *J. Phys. Chem.*, **74**, 3497, 1970; c) K.T. McGregor, N.T. Watkins, D.L. Lewis, D.J. Hodgson and W.E. Hatfield, *Inorg. Nucl. Chem. Lett.*, **9**, 423, 1973. d) B.J. Cole and W.H. Brumage, *J. Phys. Chem.*, **53**, 4718, 1970.
15. a) J.A. Barnes, D.J. Hodgson and W.E. Hatfield, *Inorg. Chem.*, **11**, 144, 1972.; b) A.T. Casey, B.F. Hoskins and F.D. Whillans, *J. Chem. Soc., Chem. Comm.*, 904, 1970.; c) D.L. Lewis, W.E. Hatfield and D.J. Hodgson, *Inorg. Chem.*, **11**, 2246, 1972.
16. a) P.E. Kruger, R.P. Doyle, M. Julve, F. Lloret and M. Nieuwenhuyzen, *Inorg. Chem.*, **40**, 1726, 2001.
17. K. Nakatani, P. Bergerat, E. Codjovi, C. Mathoniere, Y. Pei and O. Kahn, *Inorg. Chem.*, **30**, 3978, 1991.
18. a) E. Ruiz, P. Alemany, S. Alvarez and J. Cano, *Inorg. Chem.*, **36**, 3683, 1997.; b) E. Ruiz, P. Alemany, S. Alvarez and J. Cano, *J. Am. Chem. Soc.*, **119**, 1297, 1997.
19. R.J. Majeste and E.A. Meyers, *J. Phys. Chem.*, **74**, 3497, 1970.

Chapter Five

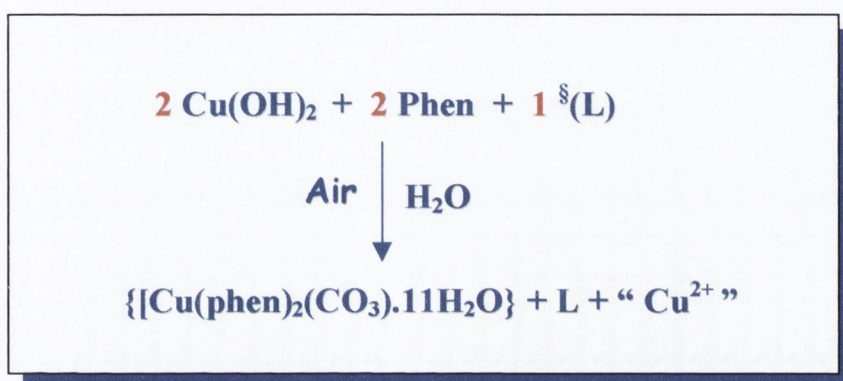
The Preparation, Characterisation and Thermal analysis of $[\text{Cu}(\text{phen})_2(\text{CO}_3)\cdot 11\text{H}_2\text{O}]$ (15) and $[\text{Cu}(\text{phen})_2(\text{CO}_3)\cdot 7\text{H}_2\text{O}]$ (16).

Introduction

One of the most important acid-base systems in water is that of carbonate.¹ The chemical species that make up this system, namely CO_2 (aq), carbonic acid H_2CO_3 , bicarbonate HCO_3^- and carbonate CO_3^{2-} , comprise one of the major acid-conjugate base systems in water. The coordination ability of the carbonate anion (CO_3^{2-}) has been widely investigated over the past number of decades.² Considerable attention has been devoted to the carbonate ligand as a structural unit in the preparation of ordered polymetallic complexes in the context of low dimensional electronic and magnetic systems.³ The use of potent species well documented in their ability to fix carbon dioxide has also generated much current interest due to its environmental implications. The presence of carbon dioxide in the atmosphere, hydrosphere, geosphere and biosphere is well known⁴ and over the years much effort has been made in the search for compounds that can act as a CO_2 catcher i.e. insertion of atmospheric CO_2 into coordination compounds. As a naturally occurring ligand carbonate is quite fascinating exhibiting both monodentate, bidentate and even tridentate characteristics.⁵ The ability of synthetic compounds to essentially mimic this process of atmospheric CO_2 capture, as carbon dioxide, carbonate CO_3^{2-} or oxalate $\text{C}_2\text{O}_4^{2-}$, has as mentioned environmental application and this has been realised outside of the obvious scientific community. In 1999, a conference attended by world leaders began negotiating a new global treaty that would lead to the reduction of greenhouse gas emissions to less hazardous levels. The fixation of carbon dioxide by transition metal complexes has been expressly cited as a means to develop a global process. We have however, quite frequently observed this fixation process in the course of our work on polynuclear Cu(II) complexes and so we undertook to investigate the process further using a more facile approach based around copper(II) hydroxide. A simple system based on readily accessible cheap materials that is a highly effective chemical method for CO_2 elimination would be highly desirable and there have been numerous studies that have demonstrated the efficiency of simple metal hydroxides for hydrating carbon dioxide.⁶ Metal (Zinc) hydroxides have also been implicated in carbonic anhydrase hydration of CO_2 .⁷

5.1 Preparation and Characterisation of the mononuclear copper(II) complex: $\{[\text{Cu}(\text{phen})_2(\text{CO}_3)].11\text{H}_2\text{O}\}$: (15)

An aqueous suspension of copper(II) hydroxide ($\text{Cu}(\text{OH})_2$) was reacted with the chelating ligand 1,10-phenanthroline, followed by addition of either tetrasodium pyrophosphate or sodium hydrogen arsenate in the overall molar ratio of 2:2:1. A deep blue solution results and after a period of two weeks block shaped deep-royal blue crystals are obtained by slow evaporation.



$^{\S}\text{L} = \text{Na}_4\text{P}_2\text{O}_7$ or Na_2HAsO_4

Scheme 5.1. Direct preparation of the mononuclear species (15).

The infrared spectrum of (15) indicated that there was no oxo-anion present for either reaction using arsenate or pyrophosphate. Instead two sharp absorption bands at 1474 cm^{-1} and 1383 cm^{-1} were observed, which were consistent with the presence of carbonate,⁸ which presumably arises from the fixation of dissolved carbon dioxide within the aqueous solution or already absorbed by exposed copper hydroxide used as starting material. The basic medium (reaction pH is recorded as 12.2) enhances nucleophilic attack of the $\text{Cu}(\text{OH})_2$ on the electrophilic carbon of CO_2 , which is then followed by water dissociation. Such a reaction is not, as mentioned, without precedent in the literature for copper as well as other transition metals,⁹ and indeed has been reported previously in this report. The remainder of the infrared spectrum is dominated by absorption bands from the phenanthroline ligands ($1655, 1517, 783 \text{ cm}^{-1}$). It was noted that the originally blue KBr disk used to carry out the infrared experiment was now green on removal from the spectrometer.

The d-d spectrum of an aqueous solution of **(15)** exhibits a very broad and featureless band centred at 670 nm, which is consistent with the presence of a distorted square-pyramidal nature about the Cu(II) chromophore. Electrospray mass spectroscopy of an aqueous solution of **(15)** showed one set of peaks indicative of $[\text{Cu}(\text{phen})_2]^{2+}$. This is as expected, from literature precedent for complexes of the type $[\text{M}(\text{L})_x\text{CO}_3]$ as it has been shown that CO_3^{2-} may decompose on introduction into a mass spectrometer with evolution of gaseous CO_2 ¹⁰ or with formation of H_2CO_3 . Single crystal X-ray diffraction confirmed the presence of carbonate (and absence of oxo-anion) with the structure being, $\{\text{Cu}(\text{phen})_2(\text{CO}_3)\cdot 11\text{H}_2\text{O}\}$ (**15**).

5.2 Description of the molecular structure of the copper(II) complex $\{\text{Cu}(\text{phen})_2(\text{CO}_3)\cdot 11\text{H}_2\text{O}\}$: **(15)**

The complex is obtained by reaction of stoichiometric amounts of copper(II) hydroxide with 1,10'-phenanthroline and either sodium hydrogen arsenate or tetrasodium pyrophosphate. In both cases, a deep royal blue solution is returned. Royal-blue block shaped crystals were obtained from this aqueous solution and used for a single crystal X-ray diffraction study. Dr. M. Nieuwenhuyzen of the Queens University, Belfast, performed the data collection and structural refinement. Complex **(15)** is depicted in Figure 5.1, showing the atomic numbering scheme used.

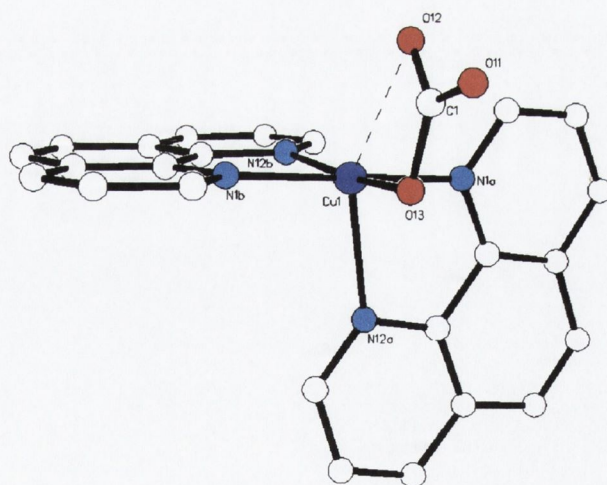


Figure 5.1. Crystal structure of $\{\text{Cu}(\text{phen})_2(\text{CO}_3)\cdot 11\text{H}_2\text{O}\}$ (**15**). Hydrogen atoms and waters of crystallisation omitted for clarity.

The molecule crystallises in space group P1. The crystal is unstable through solvent loss upon removal from the mother liquor, so data collection was carried out at low temperature. The structure is of relatively high precision with R = 6.25%. The molecular geometry of the complex consists of one square pyramidally disposed copper(II) atom, coordinated by two phenanthroline ligands and mono-dentate carbonate. Table 5.1 contains pertinent bonds and angles for (15).

Table 5.1. Selected bond distances (Å) and angles (°) for (15).

Cu(1)-O(13)	1.968(3)	O(13)-Cu(1)-N(12a)	94.2(1)
Cu(1)-N(1a)	2.005(4)	N(1b)-Cu(1)-N(12a)	101.0(1)
Cu(1)-N(12a)	2.251(3)	N(1a)-Cu(1)-N(12a)	78.9(1)
Cu(1)-N(1b)	2.002(3)	N(1a)-Cu(1)-N(1b)	173.5(1)
Cu(1)-N(12b)	2.038(3)	O(13)-Cu(1)-N(1a)	94.3(1)
Cu(1)-O(12)	2.516(3)	C(1)-O(13)	1.308(4)
C(1)-O(12)	1.280(5)	C(1)-O(11)	1.266(6)

Estimated standard deviations are given in the parenthesis.

Coordination around Cu(1) is furnished by four phenanthroline nitrogen donors, namely N(1a), N(12a) and N(1b), N(12b). Three of these nitrogen atoms, namely N(1a), N(1b) and N(12b) along with carbonate-oxygen O(13) form the basal plane of the complex, with phenanthroline nitrogen N(12a) occupying the apical position. This axial bond length is significantly longer than the equatorial bond lengths within (15). This axial elongation is a common feature of copper(II) complexes as a result of Jahn-Teller distortion. N(12b) is also longer than N(1a) and N(1b) because of its position *trans* to O(13). The copper centre sits 0.0375 Å above the basal plane toward the apical nitrogen. This distortion probably results from the restricted bite angle of the phenanthroline ligands. The phen ligands themselves do not show any significant deviations from the mean planes with average carbon-carbon and carbon-nitrogen bond lengths close to those reported for uncoordinated 1,10-phenanthroline.¹¹ The two planar ligands are also fixed approximately 90° with respect to one another. This produces a 1D chain made up of π - π 'face-to-face' stacking and 'edge-to-face (T-bonding) interactions along the x-axis (Fig 5.2). These 1-D

chains are linked into 2-dimensions through further π - π stacking interactions along the z-axis.

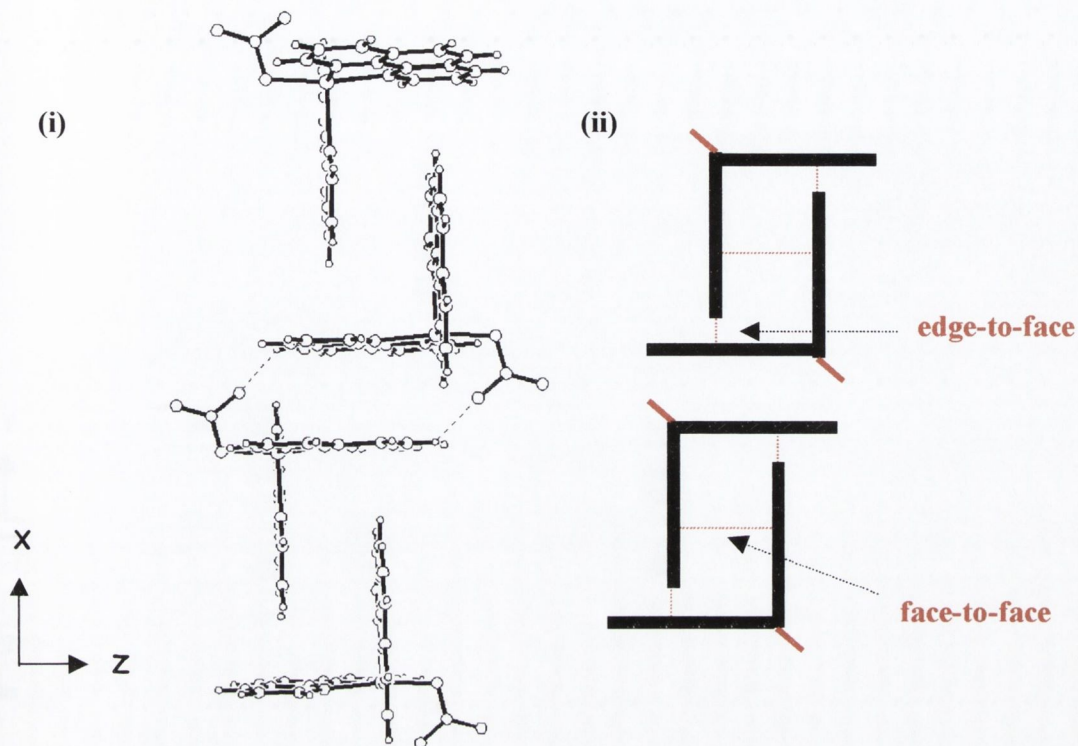


Figure 5.2. The 2-dimensional structure of (15) (i) and its schematic representation (ii). Note the complex packs as a series of 'pairs' with the carbonate moieties in an *anti* configuration within those 'pairs'. The 'edge-to-face' and 'face-to-face' stacking of phenanthroline ligands are indicated, as is the H-bonding between carbonate-oxygens and phen-hydrogens. Waters of crystallisation are omitted for clarity.

The 11 waters of crystallisation are orientationally disordered and concentrated about the carbonate moieties. There is a 3-D network of oxygen contacts (from the water and carbonate) within (15) (Fig 5.3). There is also disorder evident in the water molecules indicating that they are 'free' to move within the lattice.

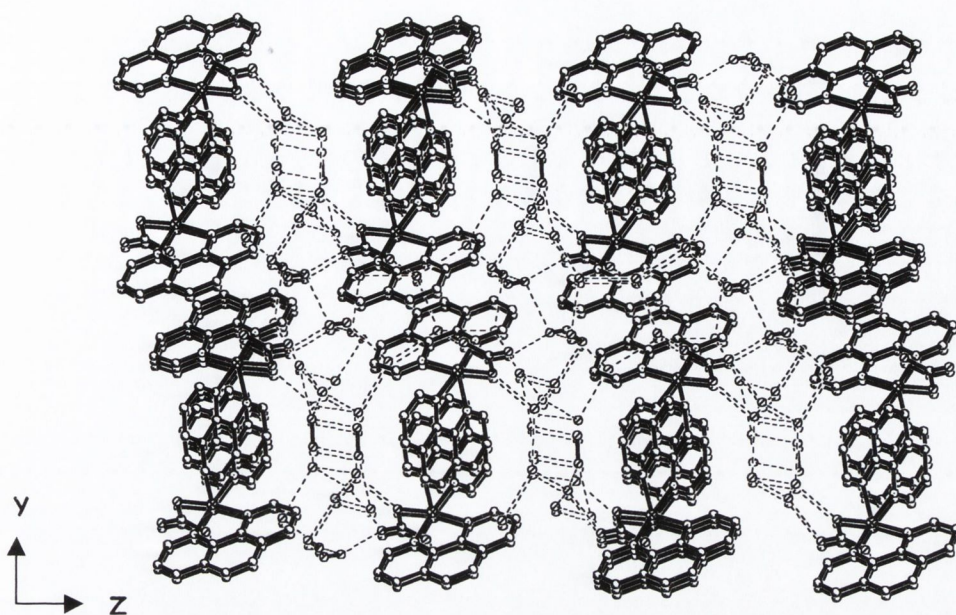


Figure 5.3. 3-D network formed between water molecules and carbonate groups. Note the presence of disordered water molecules (Marked as bonds between oxygen atoms).

During analysis of the blue crystals of **(15)** it was observed that upon removal from their mother liquor and when allowed to equilibrate with the atmosphere, they underwent a solid-state transition. The relatively large, block royal, blue crystals began almost immediately to fracture and change colour. Within approximately one minute, a green crystalline phase was recovered **(16)**. This green phase was stable and infrared analysis showed a virtually identical spectrum to that of the blue crystals **(15)**. The relatively small splitting of the degenerate vibrations obtained for both **(15)** and **(16)** in the infra-red (1474 cm^{-1} and 1383 cm^{-1}) is in fact indicative of mono-dentate carbonate coordination.¹² Elemental analysis indicated that the structure was now $\{[(\text{Cu}(\text{phen})_2(\text{CO}_3)].7\text{H}_2\text{O})\}$, *i.e.* there had been a loss of four water molecules. Remarkably, this new phase still displayed X-ray diffraction. A structural determination of the daughter crystal¹³ **(16)** indicated retention of an essentially iso-structural mononuclear copper(II) unit compared with **(15)** with only the loss of four lattice water molecules, *i.e.* $\{[(\text{Cu}(\text{phen})_2(\text{CO}_3)].7\text{H}_2\text{O}$ **(16)** (Figure 5.4).

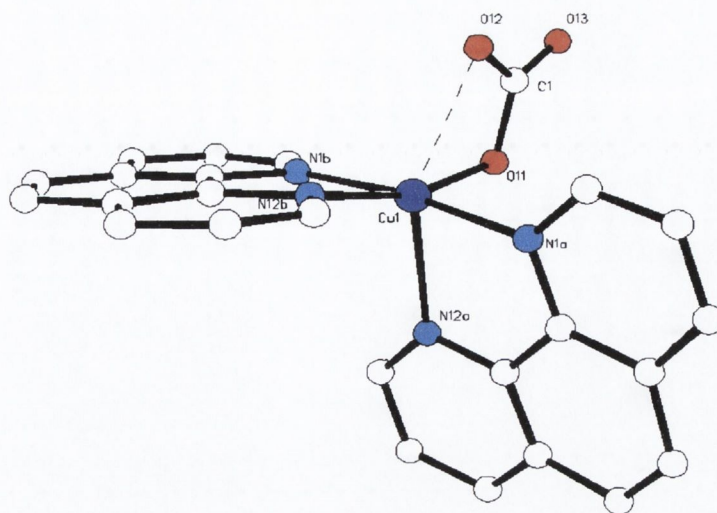


Figure 5.4. Crystal structure of $\{[\text{Cu}(\text{phen})_2(\text{CO}_3)] \cdot 7\text{H}_2\text{O}\}$ (16). Hydrogen atoms and water of crystallisation omitted for clarity.

Both phenanthroline ligands chelate in a bidentate fashion to the metal centre, at 90° with respect to one another. The carbonate group is again bound in a mono-dentate mode, although the ‘non-coordinated’ oxygen, O(12), is now somewhat closer (2.432 vs 2.516 Å). Secondary interactions are evident between O(12) and Cu(1) generating a square-pyramidal, (possibly pseudo-octahedral) copper(II) centre.

Table 5.2. Selected bond distances (Å) and angles ($^\circ$) for (16).

Cu(1)-O(12)	2.432(9)	O(11)-Cu(1)-N(12a)	88.8(3)
Cu(1)-O(11)	1.975(7)	N(1b)-Cu(1)-N(12a)	95.4(3)
Cu(1)-N(12a)	2.240(9)	N(1a)-Cu(1)-N(12a)	78.9(3)
Cu(1)-N(1b)	2.009(8)	N(1a)-Cu(1)-N(1b)	171.1(3)
Cu(1)-N(12b)	2.034(8)	O(11)-Cu(1)-N(1a)	94.5(3)
C(1)-O(12)-Cu(1)	84.9(7)	O(11)-C(1)-O(12)	114.0(1)
Cu(1)-N(1a)	2.002(8)	C(1)-O(13)	1.240(1)

Estimated standard deviations are given in the parenthesis.

What was immediately evident was that a major transition had taken place between (15) and (16). The first obvious difference is the way in which the pack throughout the crystal with the complex 'pairs' now changed considerably, as demonstrated by (Figure 5.5).

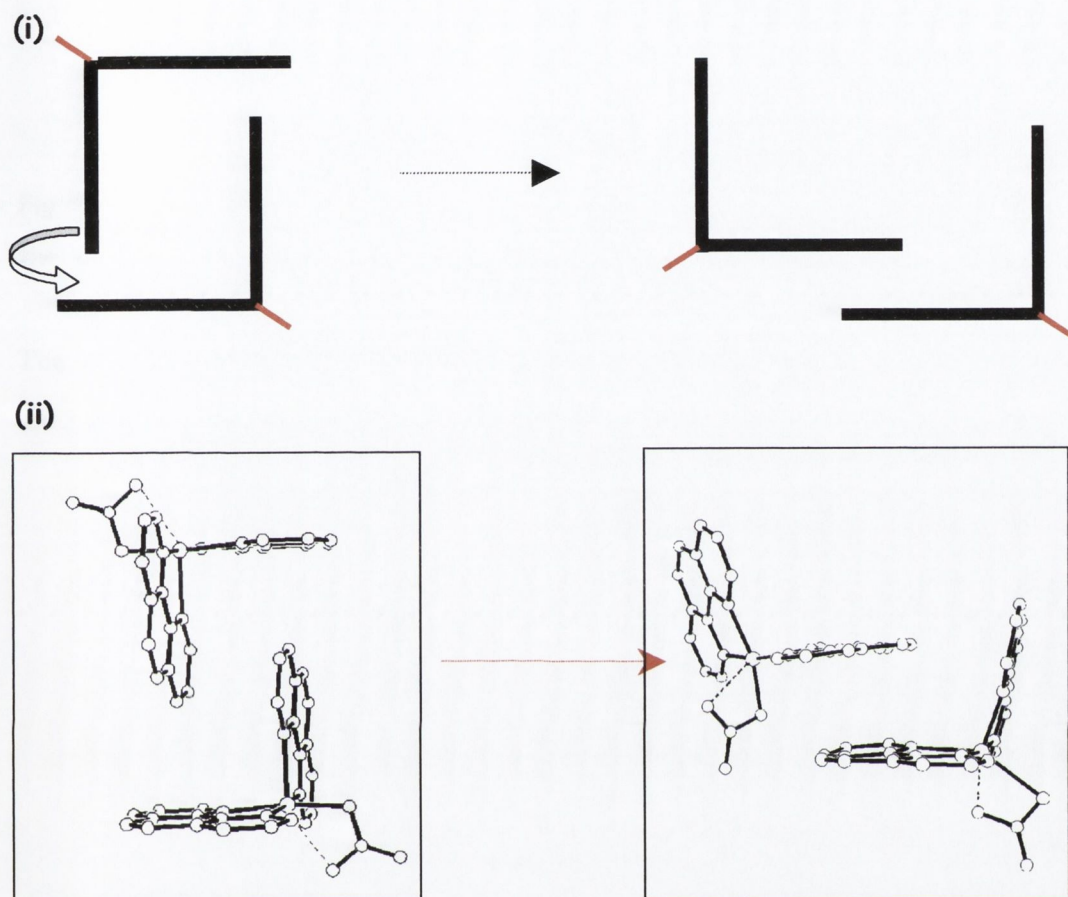


Figure 5.5. (i) Schematic and (ii) crystal structure images showing rearrangement of the central core 'pairing' in complexes (15) and (16). Waters of crystallisation and phenanthroline-hydrogens omitted for clarity.

The carbonate groups in (16) are now on the same side of the pair, although facing in opposite directions (Essentially they have switched from *anti* in (15) to *syn* in (16)). Complex (16) is now also 3-dimensional with each dimension clearly shown in the following figure. Note also that where there were two 'edge-to-face' interactions in (15), there is now only one such T-bonding interaction in (16).

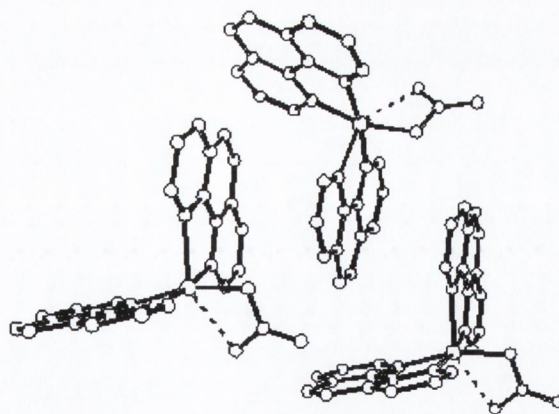


Fig 5.6. 1-D linear chain within (16). The chain resides in the yz plane and packs along the x-axis.

The second dimension is generated by a series of π - π stacking interactions running along the z-axis forming a linear sheet of 'I' units.

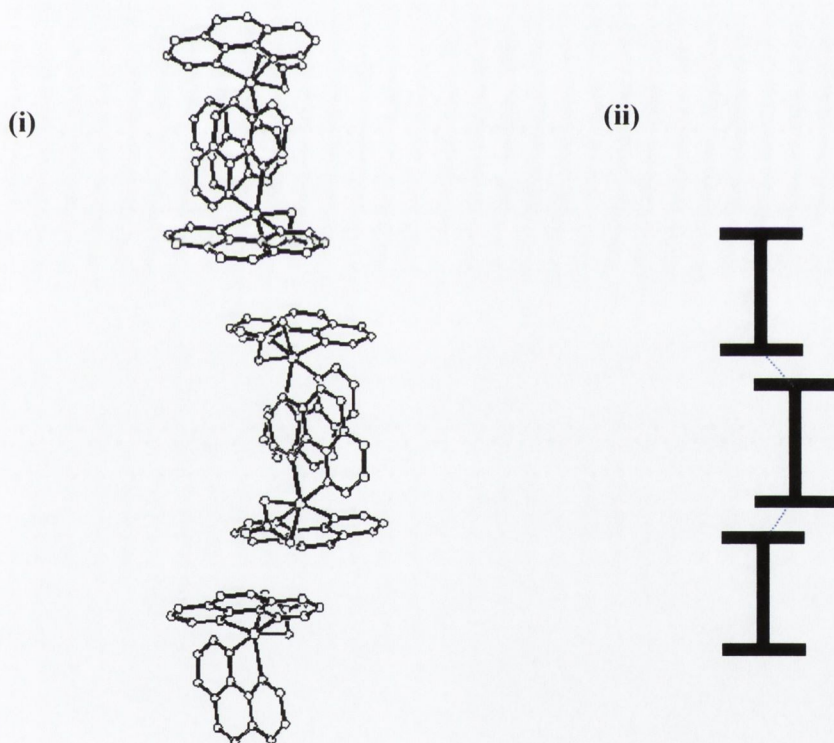


Figure 5.7. Crystal structure image (i) (and Schematic (ii)) indicating the second dimension in (16). Water of crystallisation and phen hydrogens are omitted for clarity.

Finally, the third dimension is generated as a result of the ABABAB π - π stacking arrangements of the 'I' units of (16).

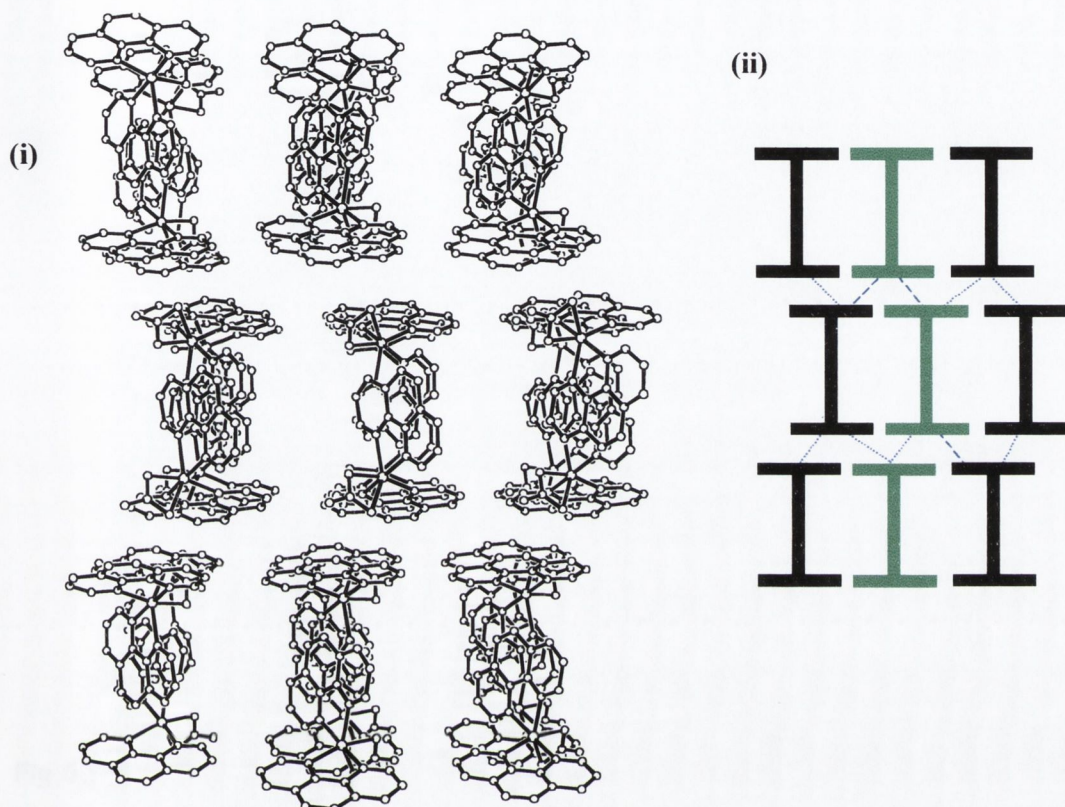


Fig 5.8. (i) 3-D sheet formed by joining of the 2-D sheets through π - π stacking interactions (Noted in the schematic (ii) by blue dotted lines). Waters of crystallisation and phenanthroline hydrogens are omitted for clarity.

As in (15), there is a 3-D network of oxygen contacts between water and carbonate in (16), as shown in figure 5.9. The carbonate group serves to join the 2-D water 'columns' together, thus generating an overall 3-dimensional array.

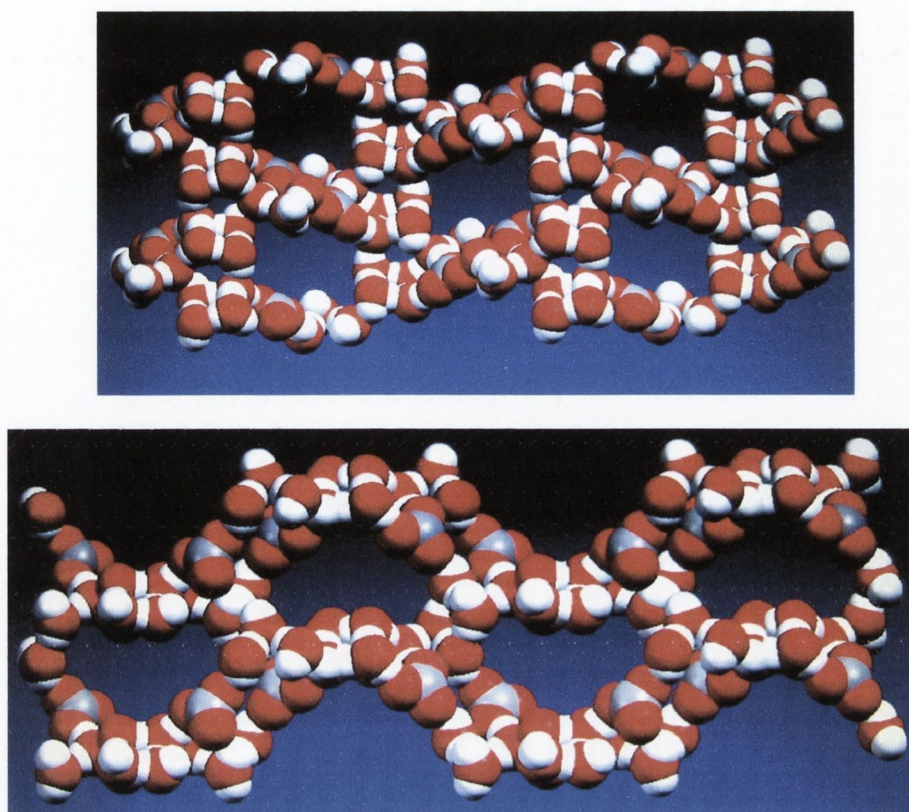


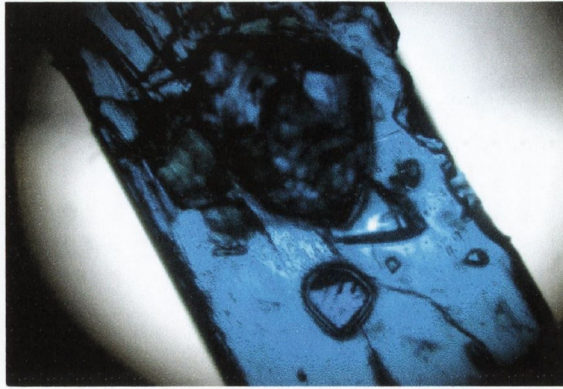
Fig 5.9. Array of oxygen contacts in (16). As in (15), the water is concentrated about the carbonate moieties and there are distinct hydrophilic/hydrophobic regions. The 'channels' are occupied by phenanthroline ligands, which have been omitted for clarity.

Further comparisons revealed substantial differences in the unit cell dimensions between (15) and (16). The y-axis has now doubled in length, a result of the greater dimensionality now present in (16) (Table 5.3), which is reflected by the higher symmetry space group of P2(1)/c for (16) compared with P1 for (15).

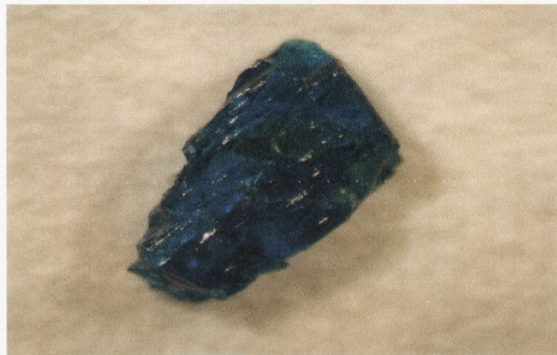
Mother (15) (Å)	Daughter (16) (Å)	Mother (15) (°)	Daughter (16) (°)
10.87	9.86	77.73	90.00
11.59	26.15	77.63	105.95
13.39	10.47	70.03	90.00

Table 5.3. Comparison of unit cell parameters between complexes (15) and (16).

(i)



(ii)



(iii)



Fig 5.10. Photographic images of the transformation from (15) to (16). Note in (ii) initial loss of translucence and appearance of fracture planes before (iii) complete colour change and fragmentation (For entire process see video on CD attached to this Thesis).

Following this second data collection, the same green crystal was re-immersed in water returning a blue solution. Uv-vis of this solution returned a broad peak at 670 nm as was observed for the original blue solution that had returned crystals of (15). Re-dissolving large amounts of the green crystals in water and allowing the resulting blue solution to evaporate over time yielded blue crystals of (15), confirmed by single crystal X-ray analysis. Room temperature magnetic moment obtained for complexes (15) and (16) returned values of 1.91 and 1.93 BM, which is consistent with a copper(II) monomer with a distorted pseudo-octahedral environment.

5.2.1. Thermal analysis of (15) and (16).

The obvious structural difference between the two complexes (15) and (16) is the number of lattice water molecules. This begs the question of whether the lattice water molecules are lost or whether, on rearrangement from 2-dimensions into 3-dimensions, the unit cell only incorporates seven water molecules. Due to the inherent loss of entropy in going from 2-dimensions into three we postulated that it was the former, i.e. water loss, as this is favoured entropically. Differential scanning calorimetry (DSC) was carried out on a crystalline sample of (15) from 25° to 100° (Figure 5.11).

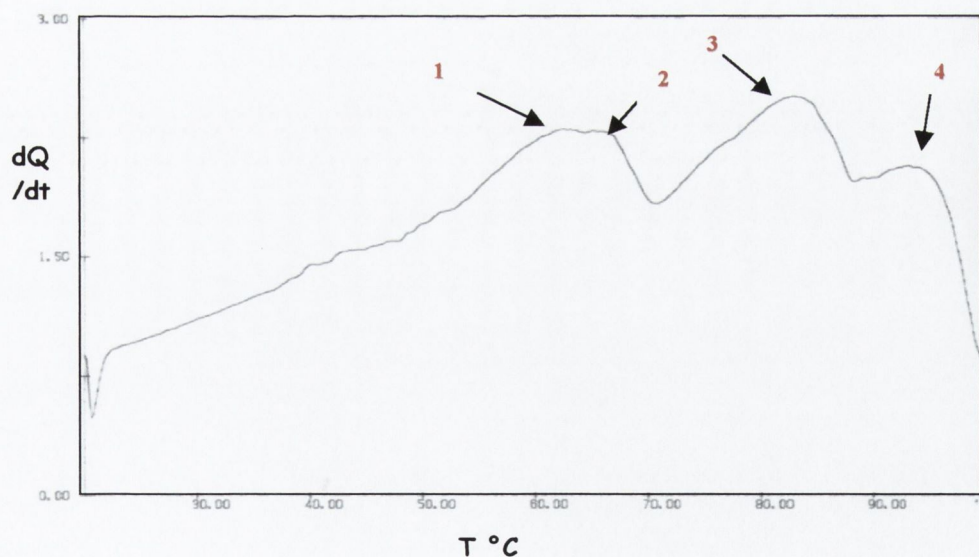


Fig 5.11. DSC curve for (15) showing the endothermic deviation from the baseline due to the vaporization of water from the sample forming complex (16).¹⁴

The peaks involve the absorption of more power by the sample compared with the reference, indicating endothermic events. These are assigned to the loss of the four lattice water molecules.

Thermo-gravimetric analysis (TGA) was also carried out on a sample of (16) from 25° to 475°.

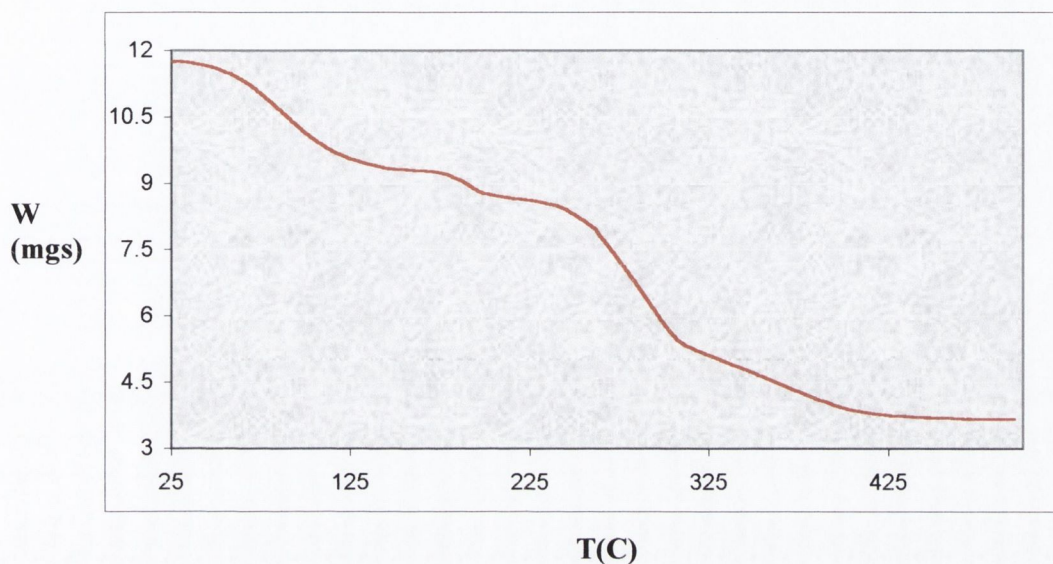


Fig 5.12. TGA curve for (16).

The curve is characteristic of multi-stage decomposition with no stable intermediates formed. The estimated weight loss within the range 25° to ~105° was 22.2% corresponding to the loss of the seven lattice water molecules, with the carbonate and phenanthroline ligands then lost gradually at temperatures over 105°. A black solid is returned at the end of the experiment.

5.2.2. Effect of pH on the formation of (15) and (16).

A series of experiments were carried to understand why and when the complex behaved as it does in undergoing the 2-D to 3-D transition. Using a pH meter accurate to two decimal places and triply distilled water (pH 7.78), the pH of each reaction was measured. Firstly it was found that on direct reaction of $\text{Cu}(\text{OH})_2$ with 1,10'-phenanthroline that a blue solution was returned. The pH of this solution was 8.68. On evaporation, green crystals were returned, which on analysis were shown to be complex (16). At no point were blue crystals recovered from this direct preparation. The reaction between $\text{Cu}(\text{OH})_2$,

1,10'-phenanthroline and tetra-sodium pyrophosphate was repeated with crystals of (15) recovered. These again underwent the phase change noted previously. The pH of this solution was recorded as 12.20. Replacing the pyrophosphate with sodium hydrogen arsenate returned the blue solution and then blue crystals of (15) (and from these the green crystals of (16)). The pH was noted here as 11.23. Replacing the arsenate with phosphate produced a blue solution, which returned, as shown previously in chapter 2, the tetranuclear copper(II) complex $\{[(\text{phen})_4(\text{Cu})_4(\mu\text{-PO}_4)_2(\mu\text{-CO}_3)(\text{H}_2\text{O})_2].40\text{H}_2\text{O}\}$ (3). The pH of this solution was 8.19. A summary of these results is given in Table 5.4.

$\text{Cu}(\text{OH})_2 + 1,10'$ - phen +	PH of solution	Complex Formed:
(i) Phosphate	8.19	(3)
(ii) Pyrophosphate	12.16	(15)
(iii) Arsenate	11.23	(15)
(iv) No oxo-anion	12.82	(16)

Table 5.4. Table showing the exact pH produced by reaction of copper(II) hydroxide with 1,10'-phen either with or without the presence of a particular group 15 oxo-anion.

From Table 5.4 it can be seen that the highly unstable (15) is returned only in a pH window of ~ 11- 12.5. The arsenate and pyrophosphate are acting as buffers stabilizing formation of (15), which is essentially the kinetically labile metastable intermediate of the more thermodynamically stable (16). This is supported by the fact that the blue crystals of (15), over a period of ~ four weeks, eventually become (16) even if left undisturbed in the solution from which they grow. The solution itself becomes a green colour over a greater period of time (months).

Conclusion

A kinetically metastable complex (**15**), possessing a 2-D extended structure, is formed on reaction of $\text{Cu}(\text{OH})_2$, 1,10'-phenanthroline and particular group 15 oxo-anions. This species readily converts into the thermodynamically stable product (**16**) through concomitant loss of lattice water molecules. The phen ligands now pack to produce a 3-dimensional complex with entropy loss compensated by loss of the four water molecules. The trigger of the process is loss of water, evident by the fact that in solution the process is much slower. The loss of water from between the layers in (**15**) is less likely to occur in an aqueous environment. While crystal-crystal phase transitions are not unknown,¹⁵ they are uncommon as solvent loss usually results in the formation of an amorphous phase and typically, steps need to be taken to prevent this from occurring.

References

1. *A Biologist's Physical Chemistry*, J.G. Morris, Edward Arnold Press, London, 2nd ed., 1974.
2. a) K.V. Krishnamurty, G.M. Harris and V.S. Sastri, *Chem. Rev.*, **2**, 171, 1970.; b) C. Fernandez, A. Neves, A.J. Bertoluzzui, B. Szpoganicz and E. Schwingel, *Inorg. Chem. Comm.*, **7**, 354, 2001.
3. a) G. Kolks, S.J. Lippard and J.V. Waszcak, *J. Am. Chem. Soc.*, **102**, 4832, 1980.; b) A. Schrodtt, A. Neubrand and R. vanEldik, *Inorg. Chem.*, **36**, 4570, 1997.; c) A.R. Davies and F.W.B. Einstein, *Inorg. Chem.*, **19**, 1203, 1980.
4. *Carbon Dioxide Review*, W.C. Clark (Ed.), Oxford University Press, New York, 1982.
5. a) A.Escuer, F. A. Mautner, E. Penalba and R. Vicente, *Inorg. Chem.*, **37**, 4191, 1998.; b) P. Chaudhuri, D. Ventur, K. Wiegardt, E.M. Peters, K. Paters and A. Simon, *Angew. Chem. Int. Ed.*, **1**, 57, 1985.
6. N. Kitajima, K. Fujisawa, T. Koda, S. Hikichi and Y. Moro-Oka, *J. Chem. Soc., Chem. Comm.*, 1357, 1990.
7. N. N. Murthy and K. D. Karlin, *J. Chem. Soc., Chem. Comm.*, 1236, 1993.
8. *Carbon Dioxide Activation by Metal Complexes*, A. Behr, VCH, Weinheim, 1988.
9. *Infrared and Raman Spectra of Inorganic and Coordination Compounds*, K. Nakamoto, Wiley, 1963.

10. D.J. Darensbourg, M.L.M. Jones and J.H. Reibenspies, *Inorg. Chem.*, **35**, 4406, 1996.
11. M. Julve, personal communication.
12. *Pyridine and its Derivatives*, E. Klingsberg, Wiley, New York, **1974**.
13. *Tables of Characteristic Group Frequencies for the Interpretation of Infrared and Raman Spectra*, I. A. Degen, Harrow, **1997**.
14. B. F. Abrahams, P. A. Jackson and R. Robson, *Angew. Chem. Int. Ed.*, **37**, 2656, 1998.
15. a) *Thermal Methods of Analysis*, P.J. Haines, Chapman and Hall, London, **1995**.;
b) *Handbook of Thermal Analysis*, T. Hatakeyama and Z. Liu, Wiley, **1998**.
16. D. Braga, G. Cojazzi, D. Paolucci and F. Grepioni, *Cryst. Eng. Comm.*, **38**, 2001.

Chapter Six

Materials and Methods.

Experimental.

6.1. Materials and methods.

6.1.1. Reagents.

All chemicals and solvents were of reagent grade and purchased from either Aldrich Chem. Co. Ltd. or Fluka Chemika-Biochemica (United Kingdom) and used without further purification. Copper(II) hydroxide was synthesised according to a literature procedure,¹ and arsenic acid was generated from arsenic pentoxide by dissolution in water. Water used in these experiments was triply distilled.

6.1.2. Elemental Analysis.

Elemental Analysis was carried out at University College, Dublin by Ms. Ann Connelly using a Carlo Erba 1006 automatic analyser. Expected range C, H, N \pm 0.4% and P \pm 0.5. Values are the average of two runs on the same sample.

6.1.3. Nuclear Magnetic Resonance.

N.M.R spectra were recorded on a Bruker DPX 400 machine operating at 400.14 MHz for ¹H, 100.14 MHz for ¹³C and 162 MHz for ³¹P. Samples were run generally dissolved in deuterated water (D₂O) or deuterated chloroform (CDCl₃). Standard Abbreviations; s, singlet; d, doublet; t, triplet; m, multiplet; br, broad; vbr, very broad.

6.1.4. Infrared Spectroscopy.

Infrared Spectra were recorded in the range 4000-600cm⁻¹ on a Perkin-Elmer 1600 series FTIR or a Mattson Genesis II FTIR. Samples were run as 8mm diameter potassium bromide pellets prepared under vacuum. The following abbreviations were used to describe the intensities: vs, very strong ; s, strong ; m, medium; w, weak, sh, shoulder.

6.1.5. Electrospray Mass Spectroscopy.

Electrospray mass spectroscopy was carried out on the Micromass LCT Electrospray mass spectrometer. Samples were dissolved in triply distilled water at a concentration of ~ 2 ng/ μdm^3 . The spectra were obtained using a mobile phase of triply distilled water with a cone voltage of 50V. Spectra are reported in the following manner; m/z and assignment.

6.1.6. Ultraviolet-Visible Spectroscopy.

UV-vis spectra were obtained on a Shimadzu UV-2401PC spectrophotometer. Spectra were obtained typically as 10^{-4} M solutions. Reference and sample spectra were collected using optically matched 1 cm cuvettes with corrected spectra produced by sample-reference subtraction using the Shimadzu UVPC software program.² Extinction coefficients are not reported or are reported as estimates due to variable degrees of hydration found for some of the complexes reported resulting in inaccurate absorption values.

6.1.7. Magnetic Measurements.

- 1. Room temperature magnetic measurements** were measured using the Evans modified Guoy method on a Sherwood Magnetic Susceptibility balance. The susceptibilities of ligands and anions were calculated from Pascals's constants. The instrument was calibrated using $\text{HgCo}(\text{SCN})_4$. Spin-only contribution was assumed for Cu(II) and magnetic moments are reported per metal ion.
- 2. Variable temperature magnetic measurements** were performed by Professor Miguel Julve and Professor Francesc Lloret (Chemistry Department, University of Valencia, Spain) on a Quantum design SQUID susceptometer in the temperature range 1.9-300K with a an applied magnetic field of $H = 50$ G unless otherwise stated. Crystalline samples (typically 40 mgs) were obtained directly from the reaction mixture, air-dried and powdered in a mortar. In the case of complexes of **(5)**, **(6)** and

(14), which were prepared by thermal treatment, these were transferred directly from the TG-DTA experiment to the susceptometer after being cooled under an inert anhydrous atmosphere. Samples were enclosed in gelatin capsules that were suspended at the middle of a plastic straw, which was rigidly fixed within the sample rod, and lowered into the instrument. The chamber was then Helium purged. The sample was centred between opposing faces of the magnet using computerised DC-centring. Typical $\chi_M T$ value for an isolated Cu(II) spin doublet is $0.40 \text{ cm}^3 \text{ mol}^{-1} \text{ K}$.

6.1.8. Thermal Gravimetric Analysis (TGA).

The thermal behaviour was studied by means of either a simultaneous TG-DTA 111 system (Setaram, France) using an open aluminium crucible, crystalline sample weights of ca.10 mgs, a linear heating rate of 5°C min^{-1} and argon at 1 Lh^{-1} as purge gas for all measurements (Valencia, Spain) or on a Mettler TC 11 system (Trinity College, Dublin), again with open aluminium crucible on samples weights of approximately 10 mgs and a heating rate of 10°C a minute open to air or under nitrogen.

6.1.9. Differential Scanning Calorimetry (DSC).

Differential scanning calorimetry was carried out on a Perkin-Elmer DSC-4 on crystalline samples weighing ~ 3.5 mgs in both a closed and an open pan under nitrogen (Trinity College, Dublin). Dr. Manuel Ruther is thanked for his assistance in the operation of this instrument.

6.1.10. X-ray Powder Diffraction.

X-ray powder diffraction was carried out on a Siemens D500 powder diffractometer in Trinity College, Dublin. Samples were prepared by suspending the powder in acetone and depositing the resulting suspension on an amorphous glass slide. The acetone was then allowed to evaporate resulting in a fine layer of deposited sample. The experiment was run

between 5θ and 60θ using Cu $K\alpha$ radiation (1.54 \AA). The data was manipulated using the Traces version 4, software package.

6.1.11. Single Crystal X-ray Diffraction.

X-ray crystal structure analysis was carried out by Dr. M. Nieuwenhuyzen at the Queen's University of Belfast or in the University of Canterbury, New Zealand on a Siemens P4 four circle diffractometer using Mo- $k\alpha$ radiation or using a Bruker³ CCD SMART system. All samples were transported in sealed sample tubes containing their mother liquors. The structures were solved by direct methods due to Sheldrick⁴ and refined by full-matrix least squares on F^2 using SHELXL-97. All manipulations of the resulting crystal files (*.cif) were carried out using XP⁵ and CeriusTM software at Trinity College, Dublin.

6.1.12. Acid Digestion Bomb - Hydrothermal Synthesis.

Hydrothermal synthesis was carried out using a Parr Instrument Company Series 4760/4765 general purpose digestion Bomb employing a Teflon insert with a capacity 50 mls. (Figure 6.1). Maximum loading of the insert is dependant on reagents used but a maximum volume of 23 mls is recommended.⁶

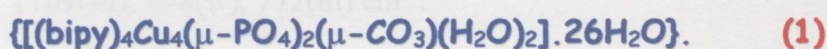


Fig 6.1. Photograph of the working components of the Bomb (Back Row) and the bomb as it appears when sealed (Front row). The Teflon insert is second from the left in the back row. AA Battery is used as scale.

Standard reaction temperatures used were 120° or 180° with a reaction time between 6 and 24hrs. Reactions could be ramped and the temperature controlled to 0.1° using the Carbolite model PF200 oven.

6.2. Experimental.

The description of each experimental procedure follows the order and numbering scheme as applied through the thesis. No distinction between chapters has been made.

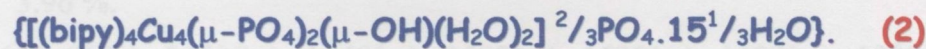


Copper hydroxide (1g; 10.2 mmol) was suspended in 100 mls of distilled water. To this was added an aqueous suspension of 2,2'-bipyridine (1.59 g; 10.2 mmol), followed within five minutes and on generation of a deep blue colour, by the addition of solid ammonium hydrogenphosphate $[(\text{NH}_4)_2\text{HPO}_4]$ (0.676 g; 5.12 mmol). A deep royal blue solution, with traces of unreacted starting material developed and was stirred over 72 hours. After filtration, crystals grew by slow evaporation at ambient temperatures. The crystals lost solvent rapidly on removal from solution and hence it was necessary to conduct single-crystal X-ray data collection at low temperature.

Found: C, 40.9; H, 4.7; N, 9.3; P, 4.6 %. Required for (1) C, 41.2; H, 4.2; N, 8.9; P, 4.9 %. IR (KBr): 3420(vs,br), 1654(m), 1599(m), 1561(m), 1444(w), 1316(m), 1253(w), 1103(sh) 1061(s) 1001(s) 772(m) cm^{-1} .

$\mu_{\text{eff}}(295\text{K}) = 1.78 \text{ B.M.}$

Ultraviolet-visible spectrum (H_2O): 687 nm.



All manipulations were performed under Argon.

Cu(OH)₂ (0.5 g; 5.1 mmol) was suspended in 50 mls of degassed water. To this was added an aqueous suspension of 2,2'-bipyridine (0.795 g, 5.1 mmol). Following the formation of a blue solution, ammonium hydrogen phosphate (0.388g, 2.56mmol) was added and the resulting royal blue solution was stirred over 24 hours. This was then filtered to remove traces of starting material and the filtrate allowed to stand at ambient temperatures.

Found: C, 34.2; H, 4.5; N, 8.1.; P, 4.42 %. Required for **(2)** C, 33.71; H, 4.81; N, 7.68; P, 4.35 %. This result was the best obtained as the sample losses weight. The ratio of C : P however was ~ constant at 7.73 : 1 for each sample analysed. Requires for **(2)** C : P 7.74 : 1. IR (KBr): 3586(s, br), 3564(s), 1654(m), 1507(m), 1493(s), 1444(s), 253(w), 1166(br) 1109(sh), 998(w), 772(m) cm⁻¹.

$\mu_{eff}(295K) = 1.84$ B.M.

Ultraviolet-visible spectrum (H₂O): 691 nm.

ESMS (H₂O) : 533/535, [(bipy)₄Cu₄(μ-PO₄)₂]²⁺.

{[(phen)₄Cu₄(μ-PO₄)₂(μ-CO₃)(H₂O)₂]. 40H₂O}. (3)

Copper hydroxide (1 g;10.2 mmol) was suspended in 100 mls of distilled water. To this was added an aqueous suspension of 1,10-phenanthroline (1.83 g; 10.2 mmol) followed, on generation of a deep blue colour (~ five minutes), by the addition of solid ammonium hydrogenphosphate (0.676 g; 5.12 mmol). A deep royal blue solution developed on vigorous stirring over 48hours. After filtration, crystals grew by slow evaporation of solvent at ambient temperature.

This procedure was used, with the relevant mole changes, for the series of stoichiometric experiments described in Chapter 2 for complex **(3)**.

Found: C, 32.31; H, 6.40 ; N, 6.28 ; P, 3.4 %. Required for **(3)** C, 31.8; H, 6.37; N, 6.70 ; P, 3.96 %.

IR (KBr): 3450(br), 1640(m), 1592(m), 1520(m), 1450(m), 1333(w),1060(sh),1010(w), 724(s), 685(w) cm⁻¹.

Ultraviolet-visible spectrum (H₂O): 685 nm.

$\mu_{eff}(295K) = 1.79$ B.M.

$[[\text{Cu}(\text{bipy})(\text{H}_2\text{O})]_2(\mu\text{-P}_2\text{O}_7)] \cdot 7\text{H}_2\text{O}$. (4)

An aqueous suspension of copper hydroxide (0.5 g; 0.51 mmol) was treated with solid 2-2'-bipyridine (0.79 g; 0.51 mmol) under vigorous stirring at room temperature. After approximately 20 minutes a clear royal blue solution resulted. Tetra-sodium pyrophosphate (0.34 g; 0.255 mmol) was then added directly and the mixture allowed stir for 12 hours, resulting in a clear royal blue solution. Deep blue, parallelepiped shaped crystals, were obtained by slow evaporation over several days.

Found C, 30.80; H, 4.43; N, 7.20 %. Required for (4) C, 30.90; H, 4.42; N, 7.22 %.

IR (KBr): 3378(vs), 3209(vs), 1655(w), 1601.4(m), 1472(w), 1446(m), 1158(s), 1108 (s), 1092(s), 1053(s), 1026(s), 871(m), 783(m), 593(s) cm^{-1} .

Ultraviolet-visible spectrum (H_2O): 657 nm ($1124 \text{ dm}^3 \text{ mol}^{-1} \text{ cm}^{-1}$).

$\mu_{\text{eff}}(295\text{K}) = 1.93 \text{ B.M.}$

$[\text{Cu}(\text{bipy})(\text{H}_2\text{O})]_2(\mu\text{-P}_2\text{O}_7)]$. (5)

Complex (5) was obtained from thermal analysis experiments at a temperature of 65° or by heating a sample of (4) for 1 hour at 65° .

IR of a sample cooled under inert atmosphere (KBr pellet): 3470(vs), 1654(w), 1600(m), 1469(w), 1444(m), 1211(s), 1168(s), 1093(s), 1055(w), 1022(m), 868(m), 792(w), 590 cm^{-1} .

Precise analytical data was not obtained for this complex because it rehydrates on exposure to the atmosphere.

$[\text{Cu}(\text{bipy})]_2(\mu\text{-P}_2\text{O}_7)]$. (6)

Complex (6) was obtained from thermal analysis experiments at a temperature of 120° or by heating a sample of (4) for 1 hour at 120° .

Found C, 36.96; H, 2.95; N, 8.76 %. Required for (6) C, 36.99; H, 3.10; N, 8.63 %.

IR (KBr) of the sample cooled under inert atmosphere: 3399(vs), 1650(sh), 1601(m), 1446(m), 1163(w), 1160(w), 1157(w), 1085(s), 1055(w), 1030(m), 871(m), 768(m), 590(m) cm^{-1} .

$\{[\text{Cu}(\text{bipy})(\text{H}_2\text{O})(\text{Na}_2\text{P}_2\text{O}_7) \cdot 10\text{H}_2\text{O}]\}$. (7)

An aqueous suspension of copper hydroxide (0.5 g; 0.51 mmol) was treated with solid 2-2'-bipyridine (0.79 g; 0.51 mmol) under vigorous stirring at room temperature. A clear royal blue solution resulted after approximately 15 minutes. Tetra-sodium pyrophosphate (0.68 g; 0.51 mmol) was added directly and the mixture allowed to stir for 4 hours. The royal blue solution that resulted was filtered and the filtrate allowed to stand over several days under ambient conditions. Deep blue crystalline needles were obtained.

Found C, 18.60; H, 4.59; N, 4.38 %. Required for (7) C, 18.83; H, 4.74; N, 4.39 %.

IR (KBr); 3424(br), 1654(m), 1608(m), 1570(m), 1449(m), 1184(sh), 1112(br), 1022(sh), 769(w).

Ultraviolet-visible spectrum (H_2O): 663 nm ($560 \text{ dm}^3 \text{ mol}^{-1} \text{ cm}^{-1}$).

$\mu_{\text{eff}}(295\text{K}) = 1.92 \text{ B.M.}$

ESMS: 433/435 m/z, ($\text{M}^- - \text{Na}$)

$\{[\text{Zn}(\text{bipy})_4(\mu\text{-P}_2\text{O}_7)_2(\text{H}_2\text{O})_2] \cdot 7\text{H}_2\text{O}\}$. (8)

Zinc perchlorate hexahydrate (0.477 g; 1.28 mmol) was dissolved in 50 mls of distilled water. To this was added of 2,2'-bipyridine (0.20 g; 1.28 mmol), resulting in a clear solution. Solid tetrasodium pyrophosphate (0.170 g; 0.64 mmol) was then added and after approximately two minutes, a white precipitate was observed. This was collected and dried under vacuum. The white precipitate was re-dissolved by increasing the pH of an aqueous suspension from 7.5 to 9 (0.5 M NaOH). The resultant colourless solution was allowed to stand at ambient temperatures resulting in the formation of white crystalline needles.

Found; Average Carbon to Nitrogen ratio, 4.28 : 1. Required Carbon to Nitrogen ratio for **(8)** 4.28 : 1.

^1H N.M.R: (D_2O , 400MHz) : δ 8.29 (1H, s, br, aromatic-H), 8.01 (2H, s, vbr, aromatic H) and 7.35(1H, s, br, aromatic-H). ^{31}P NMR (D_2O , 162MHz): δ -4.42 (uncoordinated pyrophosphate) and -26.6 (P(1) and P(2)).

IR (KBr); 3400(br), 1654(w), 1598(m), 1475(m), 1443(m), 1159(br), 1100(br), 1019(sh), 776(m).

$\{[(\text{VO})(\text{bipy})]_2(\mu\text{-P}_2\text{O}_7)\cdot 5\text{H}_2\text{O}\}$. (9)

To an aqueous solution of vanadium sulphate (0.5 g; 2.5 mmol) was added an aqueous suspension of 2,2'-bipyridine (0.392 g; 2.5 mmol), with stirring. The solution changed colour from a deep blue to a dark green. Dropwise addition of 0.332g (1.25mmol) of tetrasodium pyrophosphate precipitated, almost immediately, a lime-green solid, which was collected by vacuum filtration and washed with water and diethyl ether. The powder was then dried *in vacuo*. This procedure carried out using argon-degassed solutions and under an argon blanket produced the same result.

Microanalysis returned two sets of results depending on whether the sample was run open to the air or sealed. However, in both cases the carbon to phosphorous ratio was the same. Found C : P, 3.9 : 1. Theoretical C : P ratio for (9) 3.87 : 1.

IR (KBr); 3435(br), 3086(br), 1658(w), 1600(m), 1157(br), 1093(br), 772(m).

$[(\text{bipy})\text{Cu}(\text{H}_2\text{AsO}_4)(\mu\text{-H}_2\text{AsO}_4)]_2$. (10)

All manipulations were performed under Argon.

Copper hydroxide (0.5 g; 5.12 mmol) was suspended in 200 mls of distilled, degassed water. To this was added a degassed, aqueous suspension of 2,2'-bipyridine (0.79 g; 5.12 mmol). An aqueous solution of sodium hydrogen arsenate (2.61 g; 10.24 mmol) was added resulting in a

bright blue solution after 24 hours of vigorous stirring. Deep blue diamond shaped crystals were obtained after several days.

Found: C, 23.88; H, 2.44; N, 5.66 %. Required for **(10)** C, 23.95; H, 2.41; N, 5.58 %.

IR (KBr) : 3396(vs), 1650(m), 1550(m), 1473(m), 1446, 1330(m), 1176(w), 1029(m), 854(s) 771 (s) cm^{-1} .

Ultraviolet-visible spectrum (H_2O): 647 nm.

ESMS (H_2O) : 501/503m/z, $[\text{M}^{2-}]$.



Complex **(11)** was formed after the pH of a solution of complex **(10)** was increased from 11 to 14 following the addition of a 5% aqueous solution of NaOH. A concomitant slight purple colouration was observed. Crystals were grown by slow evaporation of solvent at ambient temperature.

Found: C, 47.44; H, 3.24; N, 10.21 %. Required for **(11)** C, 47.26; H, 3.22; N, 10.33 %.

IR (KBr); 3392(vs, br), 3111(w), 3060(w), 1654(s), 1603(s), 1544(m), 1474(m), 1383(m), 771(w) cm^{-1} .

Ultraviolet-visible spectrum (H_2O): 637 nm.



All manipulations were performed under a blanket of argon.

Copper(II) hydroxide (0.2 g; 2.05 mmol) was placed in 10 mls of degassed distilled water and sealed inside the Teflon insert, which had been previously flushed with Argon. The insert was then sealed within the bomb and heated at 180° over 6 hours. This resulted in the formation of a deep blue solution with a pH recorded as 8. This solution was then allowed to stand at ambient temperatures producing large block blue crystals.

Found: C, 36.32 ; H, 4.52; N, 8.48 %. Required for **(12)** C, 36.42; H, 4.43; N, 8.49 %.

IR (KBr); 3396(s, br), 1652(m), 1547(m), 1471(m), 1451, 1318(m), 877(w).

Ultraviolet-visible spectrum (H₂O): 667 nm.

ESMS (H₂O) : 234/236m/z, [Cu₂(bipy)₂(μ-OH)₂]²⁺



Complex **(13)** is partially dehydrated **(12)** with the four non-coordinated water molecules being lost. This compound was not isolated and is indicated to exist only from Thermal analysis experiments.



Complex **(14)** is the anhydrous form of complex **(12)** and is proposed from thermal analysis data and variable temperature magnetic susceptibility measurements.



The synthesis was performed in air with product manipulation under nitrogen.

Copper(II) hydroxide (0.5 g; 5.1 mmol) was suspended in 50 mls of distilled water. To this was added 0.92 (5.1mmol) of an aqueous suspension of 1,10'-phenanthroline and 0.68g (2.55mmol) of tetrasodium pyrophosphate. On stirring for approximately 15 minutes, a deep royal blue solution began to form. This was stirred for a further 24 hours and then filtered to remove unreacted starting material. The filtrate was then allowed stand under ambient conditions, producing diamond shaped crystals. An identical result is obtained on replacement of the pyrophosphate with 0.63g (2.55mmol) of disodium hydrogen arsenate.

The crystals proved to be extremely unstable and elemental analysis and infrared results are unreliable due to its rapid conversion into **(16)**.

Ultraviolet-visible spectrum (H₂O, blue): 656 nm.

ESMS (H₂O) : 186/188 m/x , [Cu(phen)₂]²⁺.

{[Cu(phen)₂(CO₃)]·7H₂O}. (16)

Complex **(16)** forms rapidly on exposure of complex **(15)** to ambient conditions. In solution the process is slower but occurs over a period of some four weeks. The blue crystals of **(15)** initially become opaque before shattering and producing smaller green crystals which are stable and redissolve to return a blue solution. Over a period of months the solution itself acquires a green coloration.

Found C, 48.96; H, 4.66; N, 9.05 %. Required for **(16)** C, 49.22; H, 4.96; N, 9.18 %.

IR (KBr); 3399(br), 1655(m), 1517(m), 1517(m), 1474(m), 1383(m), 1058(w), 783(m), 692(w) cm⁻¹.

Ultraviolet-visible spectrum (H₂O, Green): 670 nm (250 dm³mol⁻¹cm⁻¹).

ESMS (H₂O) : 186/188 m/z , [Cu(phen)₂]²⁺.

6.3. References.

1. *Handbook of Preparative Inorganic Chemistry*, G. Brauer (Ed.), Academic Press, New York, Vol. 2, 1013, **1963**.
2. *Shimadzu Scientific UVPC Spectroscopic Software*, version 3.9, **1995**.
3. SAINT-NT, Bruker, Madison, WI, **1998**.
4. G.M. Sheldrick, *SHELXL97. Program for the Refinement of Crystal Structures*. University of Göttingen, Germany, **1997**.
5. G.M. Sheldrick, *SHELXP*, version 4.3, Bruker, Analytical X-ray systems, Bruker AXS, Madison, WI, **1992**.
6. Parr Instrument Company, Moline, Illinois, *Safety Manual for Digestion Bomb Series 4760*, No. 239M, **1996**.

Chapter Seven

Future Work

Future Work

During the course of study, the synthesis of a variety of ligands and complexes not discussed within this thesis has also been undertaken. This preliminary work is presented here to give a flavour of how the project may develop and the approaches that may be followed in future work. Throughout the current work, we adopted a three-way approach to synthesis and these approaches may be maintained in any future work.

The first approach involved expansion of the terminal ligand groups (**T**, figure 7.1). The second approach involved expanding our use of bridging oxo-anions (**B**, figure 7.1) to include vanadate (VO_4^{3-}) or longer chain polyphosphates such as tripolyphosphate ($\text{P}_3\text{O}_{10}^{5-}$). A third approach varied the paramagnetic centres (**M**, figure 7.1) to include Co(II), Ni(II) and Mn(II) within homo- and hetero-nuclear (Cu containing) systems.

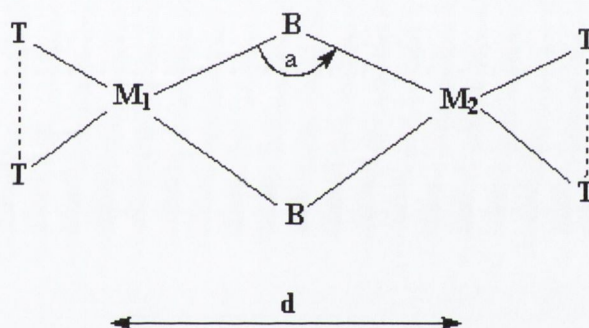
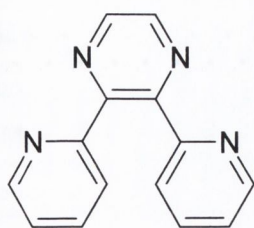
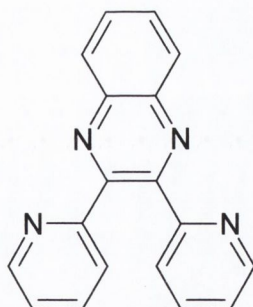


Fig 7.1. Schematic representation of a 'blueprint' for future work.

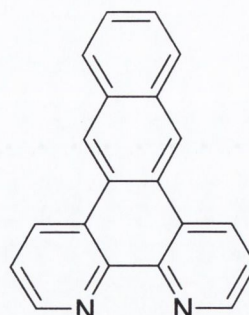
The first avenue may be to alter the terminal chelating ligands in an effort to study the effect of extending the aromatic system beyond 2,2'-bipyridine and 1,10'-phenanthroline. Introducing ligands with greater H-bonding donor/acceptor capability would also be of interest in this regard. Preliminary work employed 2,3-bis(2-pyridyl)pyrazine (DPP)¹, 2,3-bis(2-pyridyl)quinoxaline (DPQ)¹ and naphtha[2,3-*f*][1,*w*]phenanthroline (NP)², these ligands being available through literature synthesis.



DPP

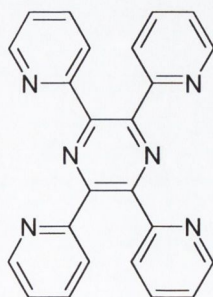


DPQ

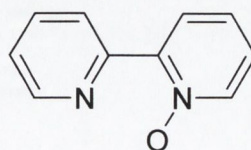


NP

Polypyridyl ligands such as these have received considerable attention as sources of a large delocalised π -system in the search for molecular materials such as electrical conductors,³ molecular magnets,⁴ host-guest molecules⁵ and inorganic-organic composites.⁶ DPP and DPQ offer the possibility of bis(chelating) coordination modes and the ability to potentially form poly-nuclear complexes of greater dimensionality than that offered by bipy, phen or NP. A variety of structural motifs, including chain and framework structures may be produced and these ligands, in combination with phosphate are attractive choices in the preparation of porous materials. Initial attempts to incorporate this ligands with copper(II) and phosphate or pyrophosphate have met with little success however. The compounds returned were either unreacted starting materials (NP) or simple copper(II) complexes, which have precedent in the literature. At no stage was an oxo-anion observed within the systems. Solubility, especially in regard to the NP ligand, is a problem when using this ligands. Future work therefore could involve hydrothermal reaction conditions to overcome these solubility problems and possibly produce an environment conducive to the incorporation of oxo-anions. A collaborative project is also currently underway with the group of Prof. Miguel Julve in Valencia, Spain.⁷ The use of ligands capable of bridging as bis- or tris- bidentate groups has also been attempted using for example, the bis-tridentate 2,3,5,6-tetra(2-pyridyl)pyrazine (TPPZ).⁸



TPPZ



Bipy-N-Oxide

Initial work with TPPZ has produced precursors for the later incorporation of oxo-anions. The first complex returned was the $\text{Cu}_2(\text{TPPZ})\text{Cl}_4$, which proved to be unreactive to addition of oxo-anions such as phosphate and arsenate. The sulphate and triflate salts were then synthesised but so far incorporation of an oxo-anion has not been achieved.

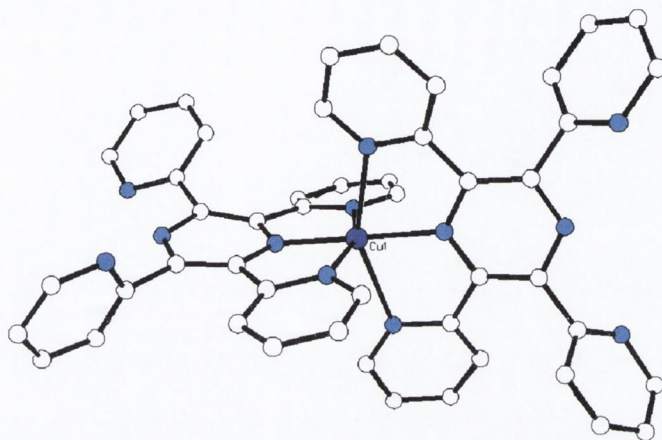


Fig 7.2. $\{[\text{Cu}(\text{TPPZ})_2(\text{OTf})_2] \cdot 6\text{H}_2\text{O}\}$. Triflate counterions and waters of crystallisation are omitted for clarity.

In an effort to increase the donor/acceptor properties of the terminal ligand, the synthesis of 2,2'-bipyridine-N-oxide was achieved through the method of Albright *et al.*⁹ Initial reactions again showed solubility to be a problem with oxo-anion not being incorporated into the systems. Instead, the unusual mononuclear copper-*tetra*-bipy-N-oxide was recovered, where two of the N-oxide ligands are bound through the oxygen atom only and the other two N-oxide ligands coordinated through both the oxygen and nitrogen atom.

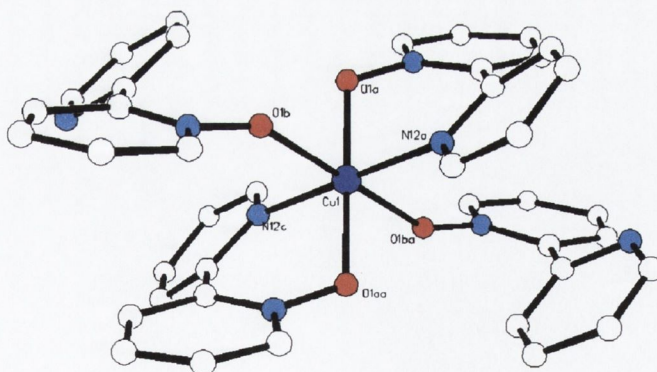


Fig 7.3. The mononuclear copper(II) complex $[\text{Cu}(\text{bpy-N-ox})_4(\text{OH})_2] \cdot 5\text{H}_2\text{O}$. Counterions and waters of crystallisation are omitted for clarity.

There is no precedent for this compound that we have found in the literature¹⁰ and further work is needed to both expand on the properties and characteristics of this compound and return to the initial goal of combining this ligand with oxo-anions.

Initial work with N-nitronyl nitroxide compounds with the aim of combining a radical species with a chelating backbone such as bipy has also been investigated with initial results in the synthesis of the nitronyl nitroxide proving successful.

The second approach of varying the bridging oxo-anions to include both *p*-block and non-*p* block examples is also ongoing. Initial attempts to incorporate tripolyphosphate was found to generate the complex previously reported in this thesis as complex (1), namely the tetranuclear Cu(II) complex with bridging phosphate and carbonate. The tripolyphosphate has therefore undergone hydrolysis. This is a problem that will need to be overcome if successful use of $P_3O_{10}^{5-}$ is to be made.

Finally, our third approach has been to expand the range of paramagnetic metal centres used. The use of cobalt(II) and iron(II) are especially intriguing because of the potential for high-spin/low-spin transitions. This offers the possibility of preparing complexes, which display hysteresis, a phenomenon sometimes associated with high-spin/low-spin transitions.¹¹ The possibility also, of producing heteronuclear systems by the synthesis of the mononuclear copper(II) complex $\{[(bipy)Cu(Na_2P_2P_7)].10H_2O\}$ (7).

Hydrothermal synthesis may also be used to generate new complexes based upon the oxo-anions described throughout. The main advantage of this approach would be the possible formation of metastable phases,¹² which would not normally be observed under ambient conditions. Also simple variation of as reaction parameters such as temperature or time may be enough to alter the morphology of the materials produced offering a strong line of approach to the synthesis of new transition metal complexes incorporating the oxo-anions in which we have an interest. Given the relative dearth of coordination complexes containing phosphate and pyrophosphate for example, more may need to be done to gain a better of understanding of the coordinating ability of these anions in combination with different metal centres and aromatic polypyridyl ligands.

References

1. H.A. Goodwin, F.J. Lions, *J. Am. Chem. Soc.*, **81**, 6415, 1959.
2. G. Albano, P. Belser, L. De Cola and M.T. Gandolfi, *J. Chem. Soc., Chem. Comm.*, 1171, 1999.
3. O. Ermer, *Adv. Mater.*, **3**, 608, 1991.
4. a) J.A. Real, E. Andres, M.C. Munoz, M. Julve, T. Granier, A. Bousseksou and F. Varret, *Science*, **268**, 265, 1995. b) J.A. MacCleverty and M.D. Ward, *Acc. Chem. Res.*, **31**, 842, 1998.
5. a) B.F. Hoskins and R. Robson, *J. Am. Chem. Soc.*, **112**, 1546, 1990.; b) M. Fujita, D. K. Chand and K. Biradha, *Chem. Commun.*, 1652, 2001.
6. O.S. Jung, S.H. Park, D.C. Kim and K.M. Kim, *Inorg. Chem.*, **37**, 610, 1998.
7. a) H. Grove, J. Sletten, M. Julve and F. Lloret, P.E. Kruger, *Inorg. Chim. Acta.*, in press.; b) H. Grove, J. Sletten, M. Julve and F. Lloret, *J. Chem. Soc., Dalton Trans.*, **17**, 2487, 2001.
8. M. Graf, H. Stoeckli-Evans, A. Escuer and R. Vicente, *Inorg. Chim. Acta.*, **257**, 89, 1997.
9. D.B. Moran, G.O. Morton, J.D. Albright, *J. Heterocycl. Chem.*, **23**, 1071, 1986.
10. Cambridge Structural Database, Version 5.22, Oct., **2001**.
11. a) P. Gutlich, A. Hauser and H. Spiering, *Angew. Chem. Int. Ed.*, **33**, 2024, 1994.; b) J. Zarembowitch and O. Kahn, *New. J. Chem.*, **15**, 181, 1991.
12. G. Demazeau, *J. Mater. Chem.*, **9**, 15, 1999.

Appendix A

Solvothermal Synthesis.

Solvothermal processes can be defined as chemical reactions or transformations in a solvent under supercritical conditions or near such a pressure-temperature domain.¹ These processes have been mainly developed in the following scientific areas: -

- (i) the synthesis of new materials,
- (ii) the development of new processes for preparing functional materials, and
- (iii) the shaping of materials (e.g. crystal growth).

Solvothermal processes are therefore a powerful route for materials preparation. The development of this approach for materials synthesis has developed rapidly since the first international conference on solvothermal reactions was held, in Japan, in 1994.² While various solvents have been studied, including alcohols, liquid ammonia and NH_2NH_2 , water has been the real driving force, so much so that the area of solvothermal synthesis is subdivided to include the area of 'Hydrothermal synthesis'. This technique has been very successful in the formation of new materials such as zeolites and aluminophosphates. The process, over the past ten years, has even found use in the production of artificial diamonds.³ Hydrothermal reactions have also been extensively applied to the synthesis of coordination complexes and clusters for the preparation of chemical sensors,⁴ microporous crystals,⁵ and magnetic materials.⁶ Much effort has been focused on the reaction of neutral donor ligands (such as 2,2'-bipyridine, pyrazine) with strictly anionic ligands (such as carbonate, phosphate) in combination with a metal salt. This approach has returned a family of inorganic-organic hybrid materials such as those complexes of formula $[\text{Cu}(\text{L})(\text{VO}_2)(\text{PO}_4)]$ ($\text{L} = 2,2'$ -bipyridine, 4,4'-bipyridine and 1,10'-phenanthroline) reported by Xu *et al.*⁷ In general, solvothermal processes have therefore opened a fruitful route to the synthesis of novel materials as well as improving the synthesis routes to already well-known materials such as oxides and nitrides, by producing these compounds at temperatures and/or pressures much lower than those used in classical solid state chemistry. Knowledge is also gained from comparing the reaction products obtained by reacting identical systems at, for example, both room temperature and under solvothermal conditions. This has led to a better understanding of what is required to generate particular types of materials with specific compositions, structures,

morphologies and, most importantly, properties. Finally, in addition to new materials it is an interesting aside to say that hydrothermal chemistry is currently attracting studies on the origin of life and/or environmental issues. It is hypothesised, for example, that rich hydrothermal reactions occurred in the sea and that all microorganisms have high-temperature ancestors. More and more evidence supports the idea of a hydrothermal origin to life, with micro-organisms found in hydrothermal vents, for example, being archaea on the biological tree.⁸ In summary then, a huge number of new materials have been synthesised from hydrothermal reactions. The increasing interest in hydrothermal synthesis derives from its advantages in terms of high reactivity of reactants and formation of metastable or unique condensed phases.⁹ The new materials it has returned have provoked significant interest in many fields such as photochemistry, catalysis and biology.

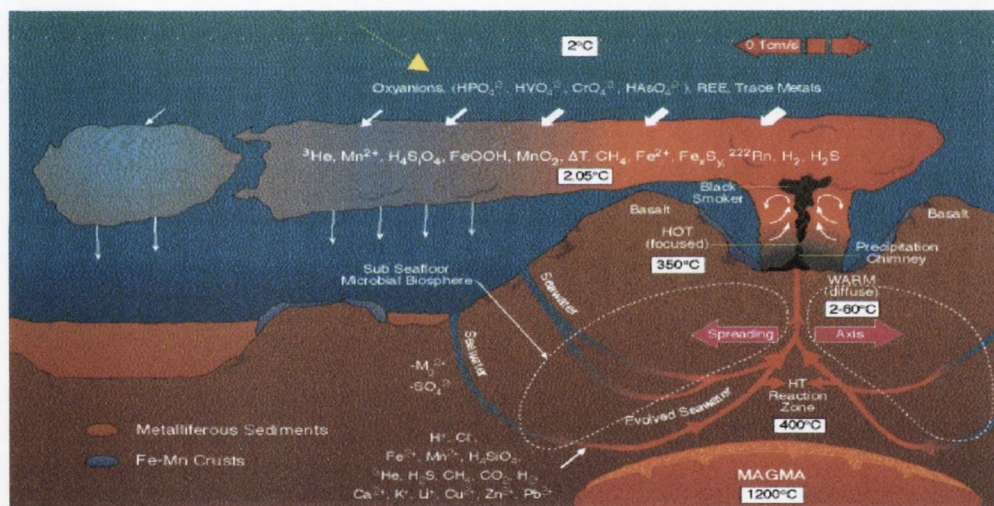


Fig A.1. Diagram of hydrothermal vent chemistry. Note the presence of oxo-anions such as HPO₄²⁻ and HAsO₄²⁻ of which little is known about their hydrothermal chemistry.¹⁰

References

1. G. Demazeau, *J. Mater. Chem.*, 9, 15, 1999.

2. Y. Oka, T. Yao and N. Yamamoto, *Proceedings of the First International Conference on Solvothermal Reactions*, Japan, **1994**.
3. X.Z. Zhao, R. Roy, K.A. Cherian and A. Badzian, *Nature*, 385, 513, **1997** and references therein.
4. S. Feng and M. Greenblatt, *Chem. Mater*, 6, 1257, **1992**.
5. A.K. Cheethan, G. Feray and T. Loiseau, *Angew. Chem. Int. Ed.*, 38, 3268, **1999**.
6. S. Feng, G. Wang, R. Yu and L. Na, *Proceedings of the international Symposium on Solvo-Hydro-Thermal Processes*, Japan, 12, **1997**.
7. R. Xu and S. Feng, *Acc. Chem. Res.*, 34, 239, **2001** and references therein.
8. M. Kates, D.J. Kushner and A.T. Matheson in *The Biochemistry of Archaea*, Elsevier Science, **1993**.
9. Z. Shi, S. Feng, L. Zhang, G. Yang, J. Hua and H. Ding, *Chem. Mater.*, 12, 2930, **2000**.
10. J.C. Alt in *Physical, Chemical, Biological and Geological Interactions in Hydrothermal Systems*, AGU, Monograph, **1994**.

Appendix B

Naturally Occurring Clathrate Structures.




<p>Structure I hydrates contain 46 water molecules per 8 gas molecules. The water molecules form two small dodecahedral voids and six large tetradecahedral voids. These voids can hold only small gas molecules (methane, ethane) with molecular diameters not exceeding 5.2 angstroms.</p>	
<p>Structure II hydrates contain 136 water molecules per 24 gas molecules. The water molecules form 16 small dodecahedral voids and 8 large hexakaidecahedral voids. They may contain gases with molecular dimensions from 5.9 to 6.9, such as propane and isobutane. It was first found in a natural environment in 1983 at a depth of 530 meters.</p>	
<p>Structure H hydrates contain 34 water molecules per 6 gas molecules. This structure is large enough to hold molecules like iso-pentane, Structure H was first found in nature in 1993, at a similar water depth to Structure II, near Jolliet Field, a large oil and gas producing area in the Gulf of Mexico.</p>	

Figure B.1. Both known cubic clathrate structures, I and II, and only tetrahedral clathrate so far discovered. These hydrate inclusion clathrates with "ice-like" structures have been postulated for over 170 years. In the presence of a central "guest" atom at room temperature, the water structure is modified in the direction of greater crystallinity. The rationale is that water is aiming to maintain as many H-bonds as possible resulting in a more rigid network

Appendix C

Crystal Structure Metric Parameters.

Metric Parameters for complex:	(1)
Empirical Formula	C41 H88 Cu4 N8 O37 P2
Formula Weight (AMU)	1601.5
Crystal Colour and Habit	Blue, Plate
Crystal Size (mm)	0.61 x 0.38 x 0.16
Crystal System and Space Group	Orthorhombic, Pnna
Cell Dimensions :: (Å and deg.)	
a : 14.871(3)	
b : 22.146(4)	
c : 19.937(4)	
Cell Volume (Å ³)	6566(2)
Z (formula units/cell)	4
Density (calculated) (g/ml)	1.495
Absorption Coefficient (μ, mm ⁻¹)	1.107
F(000)	3036
Diffractometer	CCD area detector
Radiation Source and Wavelength (Å)	MoKa lambda .7107
Data Collection Temperature (degK)	168(2)
Two-theta range (deg)	5.02 to 55.02
Scan Type and Speed (deg/min)	phi and omega scans : ?
Background Measurements	stationary crystal & counter
Standard Reflections	0 every 0 reflections
Index ranges	18<h<19; -28<k<26; -25<l<17
Reflection Collected	7205
Observed Reflections	3705
Absorption Correction Method	empirical
Max. and Min. Transmission Factors	1.000 to .806
Structure Solution Program	Bruker SHELXTL
Structure Refinement Program	Bruker SHELXTL
Number of l.s. Parameters	419
Residuals (observed data)	R(F) = .0524 : wR(F ²) = .1420
Residuals (all data)	R(F) = .1199 : wR(F ²) = .1601
Goodness-of-fit (all data)	S(F ²) = .8390
Largest and Mean l.s. shifts (delta/sig)	.993 : .016
Largest e- Density Peak and Hole (e/Å ³)	1.006 : -.533

Metric Parameters for complex:	(2)
Empirical Formula	C40 H49.33 Cu4 N8 O28 P2.67
Formula Weight (AMU)	1427.0
Crystal Color and Habit	dark blue, plate
Crystal Size (mm)	0.56 x 0.32 x 0.22
Crystal System and Space Group	Monoclinic, P2/c
Cell Dimensions :: (A and deg.)	
a : 14.250(9)	
b : 18.49(1)	beta : 99.30(2)
c : 21.40(1)	
Cell Volume (A ³)	5564(6)
Z (formula units/cell)	4
Density (calculated) (g/ml)	1.703
Absorption Coefficient (mu, mm ⁻¹)	1.680
F(000)	2901
Diffractometer	CCD area detector
Radiation Source and Wavelength (A)	MoKa lambda .7107
Data Collection Temperature (degK)	153(2)
Two-theta range (deg)	2.20 to 50.00
Background Measurements	stationary crystal & counter
Standard Reflections	0 every 0 reflections
Index ranges	-16<h<16; -21<k<18; -25<l<21
Reflection Collected	9619
Observed Reflections	4225
Absorption Correction Method	Empirical
Max. and Min. Transmission Factors	.709 to .453
Structure Solution Program	SHELXS-97 (Sheldrick, 1990)
Structure Refinement Program	SHELXL-97 (Sheldrick, 1997)
Number of l.s. Parameters	749
Residuals (observed data)	R(F) = .0869; wR(F ²) = .2160
Residuals (all data)	R(F) = .1761; wR(F ²) = .2558
Goodness-of-fit (all data)	S(F ²) = .9720
Largest and Mean l.s. shifts (delta/sig)	.020 : .001
Largest e- Density Peak and Hole (e/A ³)	1.053 : -1.214

Metric Parameters for complex:	(3)
Empirical Formula	C43 H116 Cu4 N8 O37 P2
Formula Weight (AMU)	1653.5
Crystal Colour and Habit	Blue, block
Crystal Size (mm)	0.45 x 0.36 x 0.23
Crystal System and Space Group	Triclinic, P-1
Cell Dimensions :: (A and deg.)	
a : 12.481(2)	alpha : 98.00(1)
b : 14.714(2)	beta : 100.84(1)
c : 20.655(3)	gamma : 114.49(1)
Cell Volume (A ³)	3288.8(8)
Z (formula units/cell)	4
Density (calculated) (g/ml)	1.351
Absorption Coefficient (mu, mm ⁻¹)	.765
F(000)	1384.
Diffractometer	Bruker P4
Radiation Source and Wavelength (A)	MoKa lambda .7107
Data Collection Temperature (degK)	293(2)
Two-theta range (deg)	4.04 to 50.00
Background Measurements	stationary crystal & counter Standard
Reflections	0 every 0 reflections
Index ranges	-14<h<0; -15<k<16; -24<l<24
Reflection Collected	11366
Observed Reflections	6603
Absorption Correction Method	empirical
Max. and Min. Transmission Factors	.945 to .807
Structure Solution Program	SHELXS-97 (Sheldrick, 1990)
Structure Refinement Program	SHELXL-97 (Sheldrick, 1997)
Number of l.s. Parameters	865
Residuals (observed data)	R(F) = .0756 : wR(F ²) = .1651
Residuals (all data)	R(F) = .1456 : wR(F ²) = .1963
Goodness-of-fit (all data)	S(F ²) = 1.0490
Largest and Mean l.s. shifts (delta/sig)	.002 : .000
Largest e- Density Peak and Hole (e/A ³)	1.149 : -.719

Metric Parameters for complex:	(4)
Empirical Formula	$C_{20}H_{34}Cu_2N_4O_{16}P_2$
Formula Weight (AMU)	775.5
Crystal Colour and Habit	blue, parallelepipeds
Crystal Size (mm)	0.47 x 0.34 x 0.18
Crystal System and Space Group	Triclinic, P-1
Cell Dimensions : (A and deg.)	
a : 8.246(1)	alpha : 84.71(2)
b : 9.478(2)	beta : 87.77(1)
c : 20.013(4)	gamma : 74.05(1)
Cell Volume (A ³)	1497.4(5)
Z (formula units/cell)	2
Density (calculated) (g/ml)	1.720
Absorption Coefficient (mu, mm ⁻¹)	1.607
F(000)	796
Diffractionmeter	Siemens P4
Radiation Source and Wavelength (A)	MoKa lambda .7107
Data Collection Temperature (degK)	153(2)
Two-theta range (deg)	4.08 to 45.00
Background Measurements	stationary crystal & counter method
Standard Reflections	0 every 0 reflections
Index ranges	-8 < h < 0 ; -10 < k < 9; -21 < l < 21
Reflection Collected	3884
Observed Reflections	3192
Absorption Correction Method	psi-scans
Max. and Min. Transmission Factors	.941 to .644
Structure Solution Program	SHELXS-86 (Sheldrick, 1990)
Structure Refinement Program	SHELXL-93 (Sheldrick, 1993)
Number of l.s. Parameters	397
Residuals (observed data)	R(F) = .0482 : wR(F ²) = .0000
Residuals (all data)	R(F) = .0631 : wR(F ²) = .1298
Goodness-of-fit (all data)	S(F ²) = .0000
Largest and Mean l.s. shifts (delta/sig)	.000 : .000
Largest e- Density Peak and Hole (e/A ³)	.759 : -.645

Metric parameters for	(7)
Empirical Formula	C10 H30 Cu N2 Na2 O18 P2
Formula Weight (AMU)	637.8
Crystal Colour and Habit	blue, needle
Crystal Size (mm)	0.32 x 0.16 x 0.14
Crystal System and Space Group	Triclinic, P-1
Cell Dimensions :: (A and deg.)	
a : 7.0076(5)	alpha : 91.725(1)
b : 11.0802(8)	beta : 97.820(1)
c : 16.092(1)	gamma : 90.362(1)
Cell Volume (A ³)	1237.2(2)
Z (formula units/cell)	2
Density (calculated) (g/ml)	1.712
Absorption Coefficient (mu, mm ⁻¹)	1.130
F(000)	658
Diffractometer	CCD area detector
Radiation Source and Wavelength (A)	MoKa lambda .7107
Data Collection Temperature (degK)	153(2)
Two-theta range (deg)	2.56 to 57.22
Background Measurements	stationary crystal & counter method
Standard Reflections	0 every 0 reflections
Index ranges	-9 < h < 9 ; -14 < k < 14 ; -21 < l < 21
Reflection Collected	5525
Observed Reflections	4493
Absorption Correction Method	Empirical
Max. and Min. Transmission Factors	.907 to .672
Structure Solution Program	SHELXS-97 (Sheldrick, 1990)
Structure Refinement Program	SHELXL-97 (Sheldrick, 1997)
Number of I.s. Parameters	436
Residuals (observed data)	R(F) = .0386 : wR(F ²) = .0918
Residuals (all data)	R(F) = .0489 : wR(F ²) = .0971
Goodness-of-fit (all data)	S(F ²) = 1.0030
Largest and Mean I.s. shifts (delta/sig)	.001 : .000
Largest e- Density Peak and Hole (e/A ³)	.573 : -.656

Metric Parameters for complex:	(8)
Empirical Formula	C21 H12.50 N4 O11 P2 Zn4
Formula Weight (AMU)	820.3
Crystal Colour and Habit	colourless, Plate
Crystal Size (mm)	0.42 x 0.20 x 0.13
Crystal System and Space Group	Monoclinic, P2(1)/c
Cell Dimensions :: (A and deg.)	
a : 10.042(1)	
b : 21.302(2)	beta : 93.074(2)
c : 13.687(2)	
Cell Volume (A ³)	2923.6(6)
Z (formula units/cell)	4
Density (calculated) (g/ml)	1.864
Absorption Coefficient (mu, mm ⁻¹)	3.413
F(000)	1618
Diffractometer	CCD area detector
Radiation Source and Wavelength (A)	MoKa lambda .7107
Data Collection Temperature (degK)	153(2)
Two-theta range (deg)	3.54 to 57.18
Scan Type and Speed (deg/min)	phi and omega scans : ?
Background Measurements	stationary crystal & counter method
Standard Reflections	0 every 0 reflections
Index ranges	-13<h< 12 ; -27<k<27 ; -18<l< 17
Reflection Collected	6821
Observed Reflections	4680
Absorption Correction Method	empirical
Max. and Min. Transmission Factors	1.000 to .688
Structure Solution Program	Bruker SHELXTL
Structure Refinement Program	Bruker SHELXTL
Number of I.s. Parameters	388
Residuals (observed data)	R(F) = .0347 : wR(F ²) = .0931
Residuals (all data)	R(F) = .0625 : wR(F ²) = .1114
Goodness-of-fit (all data)	S(F ²) = .6810
Largest and Mean I.s. shifts (delta/sig)	.040 : .004
Largest e- Density Peak and Hole (e/A ³)	.821 : -.617

Metric Parameters for complex:	(10)
Empirical Formula	C20 H24 As4 Cu2 N4 O16
Formula Weight (AMU)	1003.2
Crystal Colour and Habit	blue, block
Crystal Size (mm)	0.48 x 0.30 x 0.22
Crystal System and Space Group	Triclinic, P-1
Cell Dimensions :: (A and deg.)	
a : 8.5303(7)	alpha : 88.951(1)
b : 9.4703(8)	beta : 65.375(1)
c : 10.1087(8)	gamma : 71.843(1)
Cell Volume (A ³)	699.5(1)
Z (formula units/cell)	1
Density (calculated) (g/ml)	2.382
Absorption Coefficient (mu, mm ⁻¹)	6.302
F(000)	490
Diffractometer	CCD area detector
Radiation Source and Wavelength (A)	MoKa lambda .7107
Data Collection Temperature (degK)	153(2)
Two-theta range (deg)	4.46 to 52.80
Scan Type and Speed (deg/min)	phi and omega scans : ?
Background Measurements	stationary crystal & counter method
Standard Reflections	0 every 0 reflections
Index ranges	-10<h<10 ; -11<k<11 ; -12<l<10
Reflection Collected	2855
Observed Reflections	2673
Absorption Correction Method	Empirical
Max. and Min. Transmission Factors	1.000 to .359
Structure Solution Program	SHELXS-97 (Sheldrick, 1990)
Structure Refinement Program	SHELXL-97 (Sheldrick, 1997)
Number of l.s. Parameters	212
Residuals (observed data)	R(F) = .0462 : wR(F ²) = .1204
Residuals (all data)	R(F) = .0478 : wR(F ²) = .1219
Goodness-of-fit (all data)	S(F ²) = 1.0470
Largest and Mean l.s. shifts (delta/sig)	.218 : .006
Largest e- Density Peak and Hole (e/A ³)	1.289 : -1.626

Metric Parameters for complex:	(11)
Empirical Formula	C32 H48 Cu3 N6 O19
Formula Weight (AMU)	1011.4
Crystal Colour and Habit	Blue, Plate
Crystal Size (mm)	0.76 x 0.72 x 0.09
Crystal System and Space Group	Triclinic, P-1
Cell Dimensions :: (A and deg.)	
a : 8.739(1)	alpha : 95.74(1)
b : 13.455(1)	beta : 97.55(1)
c : 18.443(1)	gamma : 106.71(1)
Cell Volume (A ³)	2037.2(3)
Z (formula units/cell)	2
Density (calculated) (g/ml)	1.649
Absorption Coefficient (mu, mm ⁻¹)	1.637
F(000)	1042
Diffractometer	Bruker P4
Radiation Source and Wavelength (A)	MoKa lambda .7107
Data Collection Temperature (degK)	153(2)
Two-theta range (deg)	4.16 to 50.00
Scan Type and Speed (deg/min)	\w scans : ?
Background Measurements	stationary crystal & counter method
Standard Reflections	0 every 0 reflections
Index ranges	0<h<10 ; -15<k<15 ; -21<l<21
Reflection Collected	7169
Observed Reflections	6246
Absorption Correction Method	empirical
Max. and Min. Transmission Factors	.867 to .369
Structure Solution Program	SHELXS-97 (Sheldrick, 1990)
Structure Refinement Program	SHELXL-97 (Sheldrick, 1997)
Number of I.s. Parameters	547
Residuals (observed data)	R(F) = .0409 : wR(F ²) = .1031
Residuals (all data)	R(F) = .0488 : wR(F ²) = .1084
Goodness-of-fit (all data)	S(F ²) = 1.0400
Largest and Mean I.s. shifts (delta/sig)	.001 : .000
Largest e- Density Peak and Hole (e/A ³)	1.183 : -.988

Metric Parameters for complex:	(12)
Empirical Formula	C ₂₀ H ₂₉ Cu ₂ N ₄ O ₁₁ P
Formula Weight (AMU)	659.5
Crystal Colour and Habit	Blue, Plate
Crystal System and Space Group	Monoclinic, P2(1)/c
Cell Dimensions :: (A and deg.)	
a : 9.6485(6)	
b : 34.413(2)	beta : 103.300(1)
c : 7.7810(5)	
Cell Volume (A ³)	2514.3(3)
Z (formula units/cell)	4
Density (calculated) (g/ml)	1.742
Absorption Coefficient (mu, mm ⁻¹)	1.822
F(000)	1352
Diffractometer	CCD area detector
Radiation Source and Wavelength (A)	MoKa lambda .7107
Data Collection Temperature (degK)	153(2)
Two-theta range (deg)	2.36 to 56.96
Scan Type and Speed (deg/min)	phi and omega scans : ?
Background Measurements	stationary crystal & counter method
Standard Reflections	0 every 0 reflections
Index ranges	-12 < h < 12; -32 < k < 45 ; -10 < l < 10
Reflection Collected	5718
Observed Reflections	4475
Absorption Correction Method	none
Structure Solution Program	SHELXS-97 (Sheldrick, 1990)
Structure Refinement Program	SHELXL-97 (Sheldrick, 1997)
Number of l.s. Parameters	455
Residuals (observed data)	R(F) = .0375 : wR(F ²) = .0773
Residuals (all data)	R(F) = .0500 : wR(F ²) = .0821
Goodness-of-fit (all data)	S(F ²) = .9810
Largest and Mean l.s. shifts (delta/sig)	.002 : .000
Largest e- Density Peak and Hole (e/A ³)	.542 : -.596

Metric Parameters for complex:	(15)
Empirical Formula	C ₂₅ H ₃₈ Cu N ₄ O ₁₄
Formula Weight (AMU)	682.1
Crystal Colour and Habit	blue, block
Crystal Size (mm)	0.46 x 0.24 x 0.12
Crystal System and Space Group	Triclinic, P-1
Cell Dimensions :: (A and deg.)	
a : 10.873(2)	alpha : 77.732(9)
b : 11.598(2)	beta : 77.628(5)
c : 13.394(3)	gamma : 70.025(5)
Cell Volume (A ³)	1532.7(6)
Z (formula units/cell)	2
Density (calculated) (g/ml)	1.478
Absorption Coefficient (mu, mm ⁻¹)	.786
F(000)	714
Diffractometer	CCD area detector
Radiation Source and Wavelength (A)	MoKa lambda .7107
Data Collection Temperature (degK)	153(2)
Two-theta range (deg)	3.14 to 56.84
Scan Type and Speed (deg/min)	phi and omega scans : ?
Background Measurements	stationary crystal & counter method
Standard Reflections	0 every 0 reflections
Index ranges	-14 < h < 14 ; -15 < k < 14 ; -17 < l < 17
Reflection Collected	6678
Observed Reflections	4529
Absorption Correction Method	none
Max. and Min. Transmission Factors	.912 to .714
Structure Solution Program	SHELXS-97 (Sheldrick, 1990)
Structure Refinement Program	SHELXL-97 (Sheldrick, 1997)
Number of I.s. Parameters	427
Residuals (observed data)	R(F) = .0625 : wR(F ²) = .1659
Residuals (all data)	R(F) = .0919 : wR(F ²) = .1844
Goodness-of-fit (all data)	S(F ²) = 1.0690
Largest and Mean I.s. shifts (delta/sig)	.001 : .000
Largest e- Density Peak and Hole (e/A ³)	.880 : -.913

Metric Parameters for complex:	(16)
Empirical Formula	C ₂₅ H ₃₀ Cu N ₄ O ₁₀
Formula Weight (AMU)	610.1
Crystal Colour and Habit	green, block
Crystal Size (mm)	0.28 x 0.16 x 0.14
Crystal System and Space Group	Monoclinic, P2(1)/c
Cell Dimensions :: (A and deg.)	
a : 9.8564(6)	
b : 26.150(1)	beta : 105.948(5)
c : 10.4712(7)	
Cell Volume (A ³)	2595.1(3)
Z (formula units/cell)	4
Density (calculated) (g/ml)	1.562
Absorption Coefficient (mu, mm ⁻¹)	.908
F(000)	1268.
Diffractometer	CCD area detector
Radiation Source and Wavelength (A)	MoKa lambda .7107
Data Collection Temperature (degK)	153(2)
Two-theta range (deg)	3.12 to 52.94
Scan Type and Speed (deg/min)	phi and omega scans : ?
Background Measurements	stationary crystal & counter method
Standard Reflections	0 every 0 reflections
Index ranges	-12<h<7; -18<k<30 ; -12<l<11
Reflection Collected	4664
Observed Reflections	2020
Absorption Correction Method	Empirical
Max. and Min. Transmission Factors	.928 to .823
Structure Solution Program	SHELXS-97 (Sheldrick, 1990)
Structure Refinement Program	SHELXL-97 (Sheldrick, 1997)
Number of l.s. Parameters	361
Residuals (observed data)	R(F) = .0913 : wR(F ²) = .2187
Residuals (all data)	R(F) = .1834 : wR(F ²) = .3136
Goodness-of-fit (all data)	S(F ²) = .9230
Largest and Mean l.s. shifts (delta/sig)	.003 : .000
Largest e- Density Peak and Hole (e/A ³)	1.063 : -1.35

Publications

- 'Phenazine-2,3-diamine', R.P. Doyle, P.E. Kruger, P.R. Mackie and M. Nieuwenhuyzen, *Acta. Cryst.*, C57, 104, **2001**.
- 'Structure and Magnetic Properties of a pyrophosphate-bridged copper(II) complex', R.P. Doyle, P.E. Kruger, M. Julve, F. Lloret and M. Nieuwenhuyzen, *Inorg. Chem.*, 40, 1726, **2001**.
- 'Structural aspects of the crystal phase transition in $[(\text{phen})_2\text{Cu}(\text{CO}_3)]_n(\text{H}_2\text{O})$, ($n = 11, 7$)', R.P. Doyle, P.E. Kruger, M. Julve, F. Lloret and M. Nieuwenhuyzen, *J. Am. Chem. Soc.*, in preparation.
- 'Dihydrogen arsenate as a hydrogen bonded supramolecular synthon: Crystal structure and magnetic properties of $\{[(\text{bipy})\text{Cu}(\mu\text{-H}_2\text{AsO}_4)(\text{H}_2\text{AsO}_4)]_2\}_n$ ', R.P. Doyle, P.E. Kruger, M. Julve, F. Lloret and M. Nieuwenhuyzen, *Cryst. Eng. Comm.*, submitted December 2001.
- 'Supramolecular dimerisation in a tetranuclear Cu(II) phosphate complex', R.P. Doyle, P.E. Kruger, M. Nieuwenhuyzen and K.S. Murray, *Angew. Chem. Int. Ed.*, in preparation.

Phenazine-2,3-diamine

Robert P. Doyle,^a Paul E. Kruger,^{a*} Philip R. Mackie^a and
Mark Nieuwenhuyzen^b^aDepartment of Chemistry, University of Dublin, Trinity College, Dublin 2, Ireland, and ^bSchool of Chemistry, The Queens University of Belfast, Belfast BT9 5AG, Northern Ireland

Correspondence e-mail: paul.kruger@tcd.ie

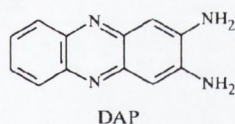
Received 21 August 2000

Accepted 19 October 2000

The planar electron-rich heterocyclic diamine 2,3-diaminophenazine (DAP), C₁₂H₁₀N₄, is of particular interest to both chemists and biochemists because of its rich organic chemistry and intense luminescence. In this paper, we report the first structure of DAP in its non-protonated form and describe the intriguing crystal packing, which features π - π , hydrogen- and T-bonded interactions.

Comment

The planar electron-rich heterocyclic diamine 2,3-diaminophenazine (DAP) is a compound which has long been of interest, initially because of its chemical and physical properties and more recently because of its mutagenic and genotoxic behaviour. The fact that DAP has a rich and varied chemistry is demonstrated by the vast number of organic transformations that have been published in the literature. In addition, the compound has been well characterized spectroscopically by NMR, absorption and most notably by emission techniques, where the remarkable luminescence of DAP has been intensively studied and exploited in analytical and biochemical applications.



DAP is known to luminesce strongly both in polar organic solvents (Zheng *et al.*, 1997) and in aqueous buffer solutions, especially when embedded within a micelle structure (Mekler & Bystryak, 1992). Indeed, it is the luminescence of DAP that sparked our interest in the molecule, especially as probes containing phenazine have shown potential in the exploration of nucleic acid structure. Further, DAP has been shown to damage DNA (Watanabe *et al.*, 1996) and so may have some role to play as a chemotherapeutic agent. The compound has found useful application in analytical chemistry as a catalytic marker in fluorimetric determinations of laccase activity (Huang *et al.*, 1998) and in immunoassay determination of enzyme-catalysed reactions

such as the oxidation of 1,2-phenylenediamine (*o*-PD) by horseradish peroxidase (Jiao *et al.*, 1998).

Synthetically, DAP is prepared by the catalysed auto-sensitized or photochemical oxidation cyclization of *o*-PD. The oxidation has been catalysed by various oxidants, including silver oxide, lead(IV) oxide, ferric chloride, cupric chloride and perchlorate and by cobalt perchlorate (Crank & Makin, 1989). The oxidation takes place in two one-electron transfer steps, a mechanism which may have relevance when studying the biological functions of metal-containing proteins (Loveless *et al.*, 1981). The fact that the heterocycle is produced in high yield in neutral or acid conditions, but not under basic conditions, perhaps explains why only structures of the protonated molecule (as its chloride or perchlorate salts) have been published previously (Brownstein & Enright, 1995; Peng & Liaw, 1986). These studies have shown that the heterocycle is protonated at the phenazine nitrogen although spectroscopic evidence suggests that the more basic amine N atoms are protonated in solution. When one of the phenazine N atoms is protonated the cation may exist in six resonance forms which, when the individual π bond strengths are considered, explains the lack of symmetry of the bond lengths in the structures of protonated DAP. In contrast, the structure of DAP (Fig. 1) shows a high degree of symmetry both in bond lengths and angles on each side of the molecular C₂ axis (Table 1). In the solid state, the structure of DAP is essentially planar, however a small degree of bending is discernible. This curvature may be attributed to the geometry of the central pyrazine ring which displays some distortions from that of an ideal aromatic ring (Table 1).

The crystal packing of DAP (Fig. 2) is particularly interesting and as the molecule is replete with numerous π -bonding and hydrogen-bond donor and acceptor sites it may be expected that it can act as a particularly versatile supramolecular tecton. Indeed, it is found that DAP forms infinite π - π stacks in the *x* and *z* directions, a feature which is a consequence of the orthorhombic crystal system. The average arene-arene non-bonded distance is 3.64 Å. The infinite π stacks are connected in three dimensions by way of intermolecular hydrogen bonds (Table 2). The hydrogen bonds connect the amine H1A and H16A and the aromatic H3 and H14 atoms of one molecule and the pyrazine N atoms (N5 and N12) of its nearest neighbour. In addition, there are T-bonded interactions which feature the terminal benzene ring

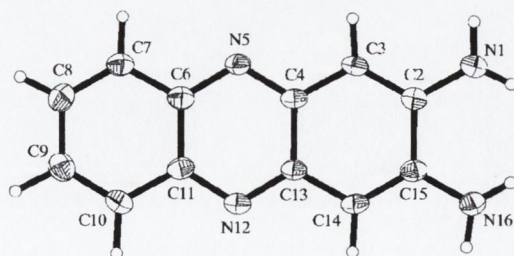


Figure 1
The molecular structure of DAP showing 50% probability displacement ellipsoids.

(C6–C11) of one molecule and the amine H atoms (H1B and H16B) of its nearest neighbour. The typical NH– π distance is 2.71 Å. The cumulative effect of these intermolecular interactions is to create a particularly attractive three-dimensional supramolecular network.

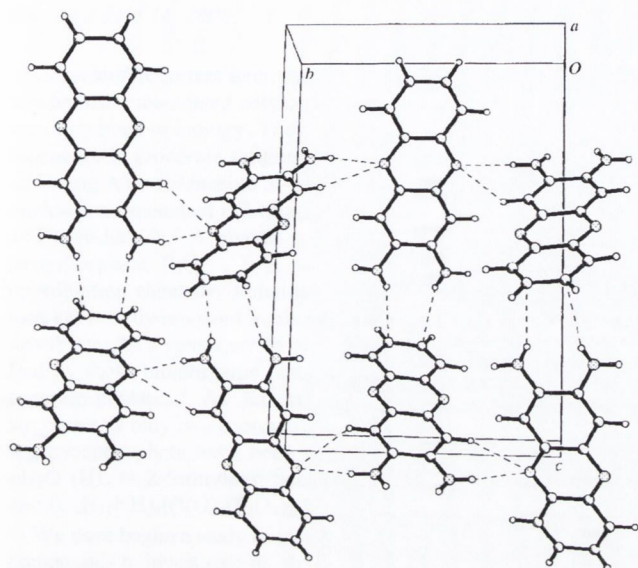


Figure 2
Diagram demonstrating the hydrogen- and T-bonding interactions within the crystal packing of DAP.

Experimental

2,3-Diaminophenazine was prepared by addition of a stoichiometric quantity of copper(II) hydroxide to an aqueous suspension of 1,2-phenylenediamine. The resultant brown precipitate was collected by filtration and subsequently crystallized by slow diffusion of acetonitrile vapour into a methanolic solution of the title compound.

Crystal data

$C_{12}H_{10}N_4$
 $M_r = 210.24$
Orthorhombic, $P2_12_12_1$
 $a = 4.8355$ (8) Å
 $b = 11.583$ (2) Å
 $c = 17.304$ (3) Å
 $V = 969.2$ (3) Å³
 $Z = 4$
 $D_x = 1.442$ Mg m⁻³

Mo $K\alpha$ radiation
Cell parameters from 1452 reflections
 $\theta = 2.12$ – 26.35°
 $\mu = 0.092$ mm⁻¹
 $T = 293$ (2) K
Trigonal prism, brown
 $0.30 \times 0.25 \times 0.20$ mm

Table 1
Selected geometric parameters (Å, °).

N1–C2	1.372 (3)	C11–N12	1.357 (3)
C4–N5	1.342 (3)	N12–C13	1.335 (3)
N5–C6	1.352 (3)	C15–N16	1.371 (3)
C3–C2–N1	122.0 (2)	C13–N12–C11	117.37 (19)
N1–C2–C15	118.9 (2)	C14–C15–N16	121.7 (2)
C4–N5–C6	117.59 (18)	N16–C15–C2	118.7 (2)

Data collection

Bruker AXS SMART CCD area-detector diffractometer
 ω – 2θ scans
3272 measured reflections
1182 independent reflections
985 reflections with $I > 2\sigma(I)$

$R_{int} = 0.032$
 $\theta_{max} = 26.37^\circ$
 $h = -4 \rightarrow 6$
 $k = -14 \rightarrow 13$
 $l = -21 \rightarrow 8$
Intensity decay: none

Refinement

Refinement on F^2
 $R(F) = 0.041$
 $wR(F^2) = 0.115$
 $S = 1.046$
1182 reflections
145 parameters
H-atom parameters constrained

$w = 1/[\sigma^2(F_o^2) + (0.0785P)^2 + 0.0252P]$
where $P = (F_o^2 + 2F_c^2)/3$
 $(\Delta/\sigma)_{max} < 0.001$
 $\Delta\rho_{max} = 0.19$ e Å⁻³
 $\Delta\rho_{min} = -0.19$ e Å⁻³

Table 2
Hydrogen-bonding geometry (Å, °).

D–H...A	D–H	H...A	D...A	D–H...A
N1–H1A...N5 ⁱ	0.86	2.39	3.154 (3)	148
N1–H1B...C9 ⁱⁱ	0.86	2.79	3.586 (3)	154
N16–H16A...N12 ⁱⁱⁱ	0.86	2.29	3.119 (3)	163
N16–H16B...C8 ⁱ	0.86	2.68	3.474 (3)	154
C3–H3...N5 ⁱ	0.93	2.63	3.371 (3)	137
C14–H14...N12 ⁱⁱⁱ	0.93	2.82	3.578 (3)	139

Symmetry codes: (i) $x - \frac{1}{2}, \frac{1}{2} - y, 1 - z$; (ii) $-\frac{1}{2} - x, 1 - y, \frac{1}{2} + z$; (iii) $x - \frac{1}{2}, \frac{3}{2} - y, 1 - z$.

H atoms were placed geometrically with C–H and N–H distances of 0.93 and 0.86 Å, respectively, and $U_{iso}(H) = 1.2U_{eq}(C, N)$.

Data collection: *SMART* (Bruker, 1999); cell refinement: *SAINT* (Bruker, 1999); data reduction: *SAINT*; program(s) used to solve structure: *SHELXTL* (Sheldrick, 1997); program(s) used to refine structure: *SHELXTL*; molecular graphics: *SHELXTL*.

We are grateful to the EC (contract ERBMRXCT98-0226), HEA Strategic Research Initiative and Trinity College Academic Development Fund for financial support.

Supplementary data for this paper are available from the IUCr electronic archives (Reference: BM1429). Services for accessing these data are described at the back of the journal.

References

- Brownstein, S. K. & Enright, G. D. (1995). *Acta Cryst.* **C51**, 1579–1581.
Bruker (1999). *SMART* and *SAINT*. Version 6.01. Bruker AXS Inc., Madison, Wisconsin, USA.
Crank, G. & Makin, M. I. H. (1989). *J. Heterocycl. Chem.* **26**, 1163.
Huang, Z. Y., Huang, H. P., Cai, R. X. & Zeng, Y. E. (1998). *Anal. Chim. Acta*, **374**, 99–103.
Jiao, K., Sun, G. & Zhang, S. S. (1998). *Sci. China Ser. B (Engl.)*, **41**, 345–352.
Loveless, N. P., Brown, K. C. & Horrocks, R. H. (1981). *J. Org. Chem.* **46**, 1182–1185.
Mekler, V. M. & Bystryak, S. M. (1992). *Anal. Chim. Acta*, **264**, 359–363.
Peng, S.-M. & Liaw, D.-S. (1986). *Inorg. Chim. Acta*, **113**, L11–12.
Sheldrick, G. M. (1997). *SHELXTL*. Version 5.1. University of Göttingen, Germany.
Watanabe, T., Kasai, T., Arima, M., Okumura, K., Kawabe, N. & Hirayama, T. (1996). *Mutat. Res. Genet. Toxicol.* **369**, 75–80.
Zheng, O., Huang, H. P. & Cai, R. X. (1997). *Chem. J. Chin. Univ.* **18**, 368–371.

Structure and Magnetic Properties of a Pyrophosphate-Bridged Cu(II) Complex

Paul E. Kruger,^{*,†} Robert P. Doyle,[‡] Miguel Julve,^{*,‡} Francesc Lloret,[‡] and Mark Nieuwenhuyzen[§]

Department of Chemistry, Trinity College Dublin, Dublin 2, Ireland, Department de Química Inorgànica, Facultat de Química, Universitat de València, Dr. Moliner 50, E-46100 Burjassot, València, Spain, and the Chemistry Department, Queen's University, Belfast, U.K. BT9 5AG

Received July 14, 2000

Considerable current interest revolves around the chemistry and biochemistry associated with polyphosphate anions because they are ubiquitous in biology. They participate in a diverse series of bioenergetic processes ranging from oxidative phosphorylation including ATP (adenosine 5'-triphosphate) production,¹ through nucleic acid mediated information processing, to energy storage and transduction.² A pivotal intermediate within this family is pyrophosphate, $P_2O_7^{4-}$. It is somewhat surprising then that its coordination chemistry remains practically unexplored as metal ions are heavily involved in phosphate metabolism.³ This relative dearth may be a consequence of its ready hydrolysis as exemplified by those bioinorganic reactions catalyzed by the inorganic pyrophosphatases.⁴ As far as we are aware, the molecular structures of only two coordination compounds containing bridging pyrophosphate have been reported, namely, $[(CuL)_4P_2O_7] \cdot nH_2O$ (HL = 2-formylpyridinethiosemicarbazone; $n = 9-12$)⁵ and $(C_8H_{11}NH)_4(VO)_4(P_2O_7)_2(OCH_3)_4$.⁶

We have begun a study of pyrophosphate-bridged coordination compounds to investigate its ability to mediate electronic interactions between paramagnetic metal centers. We present here our initial magnetostructural investigations concerning the novel compounds $\{[(bipy)Cu(H_2O)]_2(\mu-P_2O_7) \cdot 7H_2O\}$ (**1**) and its related dehydrated products $\{[(bipy)Cu(H_2O)]_2(\mu-P_2O_7)\}$ (**2**) and $\{[(bipy)Cu]_2(\mu-P_2O_7)\}$ (**3**).

Compound **1** is obtained in good yield (ca. 90%) as sky blue parallelepipeds by slow evaporation of concentrated aqueous solutions containing stoichiometric amounts of $Cu(NO_3)_2 \cdot 3H_2O$, 2,2'-bipyridine, and $Na_4P_2O_7 \cdot 4H_2O$. The structure⁷ of **1** consists of neutral $\{[(bipy)Cu(H_2O)]_2(\mu-P_2O_7)\}$ dinuclear copper(II) units and seven waters of crystallization linked by an extensive network of hydrogen bonding, Figure 1. The geometry of the copper atoms is distorted square pyramidal with two bipy nitrogens and two pyrophosphate oxygen atoms building the basal plane. They are shifted by 0.226 [Cu(1)] and 0.190 Å [Cu(2)] from the mean basal plane toward the axially coordinated water molecules O(1w) and O(2w), respectively. Hydrogen bonds involving the cis-coordi-

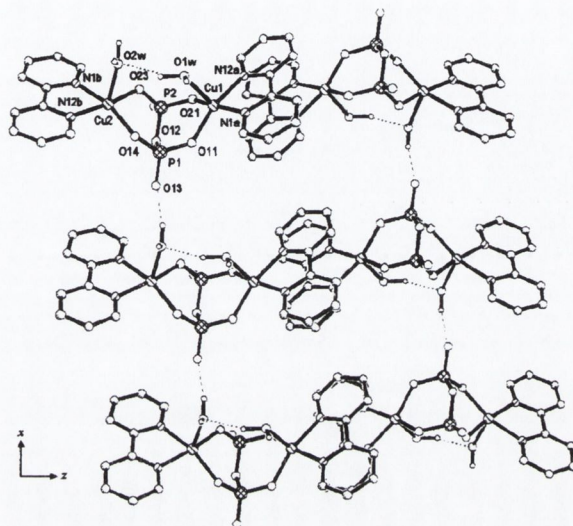


Figure 1. Packing diagram of complex **1** showing the 3-D intermolecular H-bonding and π - π interactions; waters of crystallization have been omitted for clarity.

nated O(1w) and O(2w) water molecules [2.913 Å and 154.1° , for O(1w)···O(2w) and O(1w)-H(1w1)···O(2w), respectively] and O(2w) and O(13p) [2.767 Å and 169.0° for O(2w)···O(13p) and O(2w)-H(2w2)···O(13p); $p = 1 - x, 1 - y, -z$] are highlighted in Figure 1. The pyrophosphate group acts as a bis-bidentate ligand forming two six-membered chelate rings with an envelope conformation. The Cu(1)···Cu(2) distance is 4.646 Å whereas the shortest interdimer Cu···Cu separations are 5.899 [Cu(2)···Cu(2p)] and 6.057 Å [Cu(1)···Cu(1q); $q = 1 - x, 1 - y, 1 - z$]. Intermolecular π - π interactions from adjacent H-bonded chains (interplanar distance between adjacent bipy's is 3.5 Å) through an interleaving of bipy ligands in the yz plane leads to a layer containing Cu(II) dimers. Further π - π interactions are also present along the y -axis (Figure 1), which results in the formation of a three-dimensional network.

[†] Trinity College Dublin.

[‡] Universitat de València.

[§] Queen's University.

- (1) (a) Walker, J. E. *Angew. Chem.* **1998**, *110*, 2438; *Angew. Chem., Int. Ed.* **1998**, *37*, 2308. (b) Boyer, P. D. *Angew. Chem.* **1998**, *110*, 2424; *Angew. Chem., Int. Ed.* **1998**, *37*, 2296.
- (2) (a) *The Biochemistry of Nucleic Acids*, 10th ed.; Adams, R. L. P., Knowler, J. T., Leader, D. P., Eds.; Chapman and Hall: New York, 1986. (b) *Nucleic Acids in Chemistry and Biology*, 2nd ed.; Blackburn, G. M., Gait, M. J., Eds.; Oxford University Press: 1996.
- (3) Lipscomb, W. N.; Sträter, N. *Chem. Rev.* **1996**, *96*, 2375 and references therein.
- (4) (a) Wilcox, D. E. *Chem. Rev.* **1996**, *96*, 2435. (b) Welsh, K. M.; Cooperman, B. S. *Biochemistry* **1983**, *22*, 2243. (c) Heikinheimo, P.; Pohjanjoki, P.; Helminen, A.; Tasanen, M.; Cooperman, B. S.; Goldman, A.; Lahti, R. *Eur. J. Biochem.* **1996**, *239*, 138.
- (5) Ainscough, E. W.; Brodie, A. M.; Ranford, J. D.; Waters, J. M.; Murray, K. S. *Inorg. Chim. Acta* **1992**, *197*, 107.
- (6) Herron, N.; Thorn, D. L.; Harlow, R. L.; Coulston, G. W. *J. Am. Chem. Soc.* **1997**, *119*, 7149.

- (7) Crystal data for **1**: $C_{20}H_{34}Cu_2N_4O_{16}P_2$, $M_w = 775.53$, triclinic, space group $P1$, $a = 8.246(1)$ Å, $b = 9.478(2)$ Å, $c = 20.013(4)$ Å, $\alpha = 84.71(2)^\circ$, $\beta = 87.77(1)^\circ$, $\gamma = 74.05(1)^\circ$, $V = 1497.4(5)$ Å³, $Z = 2$, $D_c = 1.720$, $g\ cm^{-3}$, $F(000) = 796$, $\mu = 1.607\ mm^{-1}$, $T = 293\ K$, crystal size $0.47 \times 0.34 \times 0.18\ mm$, total reflections 4210, independent reflections 3884, ($R_{int} = 0.0282$) with [$I > 2\sigma(I)$] 3192 observed data and 397 parameters. Siemens P4 four-circle diffractometer using graphite-monochromated Mo K α radiation, data collection in the range $4^\circ > 2\theta > 50^\circ$ ($-8 \leq h \leq 0$, $-10 \leq k \leq 9$, $-21 \leq l \leq 21$), corrected for Lorentz, polarization, and absorption effects (max, min transmission = 0.941, 0.644). The structure was solved by direct methods due to Shelldrick and refined by full-matrix least squares on F^2 using SHELXL-97 (Sheldrick, G. M., University of Göttingen). Non-hydrogen atoms were refined anisotropically, and hydrogen atoms were located from a difference Fourier map and refined using a riding model with $U_{ij} = 1.2U_{eq}$. Refinement converged with $wR2 = 0.1298$ for all data and $R1 = 0.0482$ for $2\sigma(I)$ data. CCDC 136177.

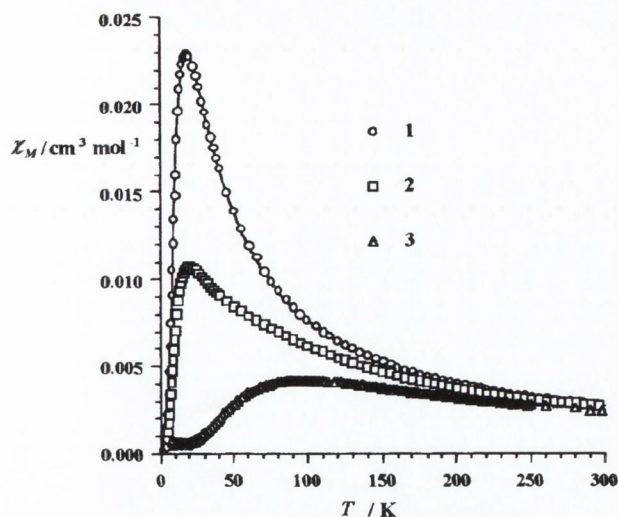


Figure 2. Thermal dependence of χ_M for the compounds 1–3 [χ_M being the magnetic susceptibility per two copper(II) ions]. The solid lines are the best fit (see text).

The thermal decomposition of **1** shows that it loses the seven lattice water molecules in the temperature range 25–68 °C, the resulting dihydrated phase (**2**) being stable for 68° < T < 86 °C. The loss of the two coordinated water molecules starts at 86 °C, giving the fully anhydrous compound (**3**) at T > 120 °C, which decomposes at T > 250 °C.⁸

The magnetic behavior⁹ of **1**–**3** is shown in Figure 2. The χ_M versus T curves are characteristic of antiferromagnetic coupling with susceptibility maxima at 19 K for **1** and **2**, and 90 K for **3**. From a magnetic point of view, **1** can be described to a first approximation as a Cu(II) chain with regular alternation of two kinds of bridges (pyrophosphato and hydrogen-bonded pathways). The analysis of the susceptibility data of **1** through the Hamiltonian $H = -J \sum_i (\hat{S}_{i-1} \cdot \hat{S}_i - \alpha \hat{S}_{i-1} \cdot \hat{S}_{i+1})$ (α being the alternating parameter and \hat{S}_i the local spin) leads to value of α practically equal to zero. In other words, **1** behaves magnetically as an isolated copper(II) dimer with $J = -20 \text{ cm}^{-1}$, $g = 2.09$, and $R = 1.2 \times 10^{-6}$.¹⁰ Inspection of the structure shows that the magnetic orbital on each copper atom is of the $d_{x^2-y^2}$ type with the x and y axes being roughly defined by the bonds from copper to bipy nitrogen. The poor overlap between the two non-coplanar copper centered magnetic orbitals through the equatorial O(11)–P(1)–O(14) and O(21)–P(2)–O(23) bridging networks accounts for the weak antiferromagnetic coupling observed. Although there is possibly an additional exchange pathway in **1**, that involving the axially coordinated waters through hydrogen bonding, it would be expected to be much less efficient than the bis-chelating pyrophosphate in mediating exchange interactions. The loss of seven lattice water molecules from **1** to yield **2** (Scheme S1, Supporting Information) causes a decrease in the height of the susceptibility curve while leaving the temperature at which the maximum occurs unchanged. These features are typical of a higher magnetic dimensionality in **2**, indicating that α is now nonzero. It is likely that the loss of lattice water molecules makes easier

the approximation of the adjacent pyrophosphate-bridged dinuclear units, reinforcing the π – π overlap and introducing additional H-bonding to give an alternating two-dimensional magnetic system. The pyrophosphate-bridged copper(II) fragment would remain essentially unchanged (indeed the temperature at which the maximum occurs remains the same), so the magnetic coupling through this bridge is maintained and the additional weaker coupling is assigned to the hydrogen-bonded pathway. Further dehydration leads to compound **3**. Its susceptibility curve exhibits a maximum at 90 K indicating that a stronger antiferromagnetic coupling occurs in **3** and suggesting the formation of a polymeric compound upon dehydration (Scheme S1). This conclusion is further supported by a shift toward lower frequencies of the strongest P–O stretching vibration (ca. 20 cm^{-1}) in the IR spectrum¹¹ when going from **1** to **2** to **3**. The exchange coupling through the “oxo” bridge (P–O) would be expected to be dominant and strongly antiferromagnetic in nature. Consequently, the magnetic behavior of **3** would be typical of a relatively strongly coupled copper(II) dimer, and this is consistent with the shift of the susceptibility maximum from 19 (**1**) to 90 K (**3**). The analysis of the magnetic behavior of **3** through a simple Bleaney–Bowers expression leads to an excellent fit with $J = -110 \text{ cm}^{-1}$, $g = 2.08$, and $R = 5.0 \times 10^{-5}$. This relatively strong coupling is in agreement with the proposed “oxo”-bridging pathway (Scheme S1). We recall here that strong antiferromagnetic coupling of up to -300 cm^{-1} has been reported for singly hydroxo bridged copper(II) complexes.¹²

The present work illustrates for the first time the profound influence of pyrophosphate-assisted water loss on magnetic properties and demonstrates that controlled dehydration leads to an increase in magnetic dimensionality.¹³ Similar examples of spectacular magnetostructural effects caused by carboxylate-assisted water loss in polynuclear compounds have been reported previously.¹⁴ Extension of this work to incorporate bridging pyrophosphate ligands into other polynuclear assemblies is currently underway.

Acknowledgment. We acknowledge financial support from the Trinity College Academic Development Fund, the HEA Strategic Research Initiative, and the Spanish Dirección General de Investigación Científica y Técnica (DGICYT) (Project PB-97-1397).

Supporting Information Available: Thermal ellipsoid plots of **1** with numbering scheme (Figure S1) and packing diagrams (Figure S2). X-ray crystallographic file in CIF format. Magnetic susceptibility (Figures S3 and S4) and TG-DTA plots (Figure S5). Scheme S1. This material is available free of charge via the Internet at <http://pubs.acs.org>.

IC000782X

- (8) See Figure S5, Supporting Information. Satisfactory elemental analyses (C, H, N) were obtained for **1**–**3**.
- (9) Magnetic measurements for **1**–**3** were performed on a Quantum Design SQUID susceptometer in the temperature range 1.9–300 K under an applied field $H = 50 \text{ G}$.
- (10) R is the agreement factor defined as $\sum_i [\chi_M^{\text{obs}}(i) - \chi_M^{\text{calc}}(i)]^2 / \sum_i [\chi_M^{\text{obs}}(i)]^2$.
- (11) (a) Nakamoto, K. *Infrared and Raman Spectra of Inorganic and Coordination Compounds: Part B: Applications in Coordination, Organometallic and Bioinorganic Chemistry*, 5th ed.; Wiley: Chichester, 1997. (b) Corbridge, D. E. C.; Lowe, E. J. *J. Chem. Soc.* **1954**, 493. (c) Hezel, A.; Ross, S. D. *Spectrochimica Acta* **1967**, *23A*, 1583.
- (12) Castro, I.; Faus, J.; Julve, M.; Lloret, F.; Verdager, M.; Kahn, O.; Jeannin, S.; Jeannin, Y.; Vaisserman, J. *J. Chem. Soc., Dalton Trans.* **1990**, 2207 and references therein.
- (13) (a) Kahn, O.; Larionova, J.; Yakhmi, J. V. *Chem.—Eur. J.* **1999**, *5*, 3443. (b) Pei, Y.; Kahn, O.; Nakatani, K.; Codjovi, E.; Mathoniere, C.; Sletten, J. *J. Am. Chem. Soc.* **1991**, *113*, 6558.
- (14) (a) Nakatani, K.; Carriat, J. Y.; Journaux, Y.; Kahn, O.; Lloret, F.; Renard, J. P.; Pei, Y.; Sletten, J.; Verdager, M. *J. Am. Chem. Soc.* **1989**, *111*, 5739. (b) Lloret, F.; Julve, M.; Ruiz, R.; Journaux, Y.; Nakatani, K.; Kahn, O.; Sletten, J.; *Inorg. Chem.* **1993**, *32*, 27. (c) Cano, J.; De Munno, G.; Sanz, J. L.; Ruiz, R.; Faus, J.; Lloret, F.; Julve, M.; Caneschi, A. *J. Chem. Soc., Dalton Trans.* **1997**, 1915.